The sinking mega-delta

Present and future subsidence of the Vietnamese Mekong delta

Philip S.J. Minderhoud

The sinking mega-delta

Present and future subsidence of the Vietnamese Mekong delta

De zinkende mega-delta

Huidige en toekomstige bodemdaling in de Vietnamese Mekong delta
(met een samenvatting in Nederlands)

Sụt lún đồng bằng

Hiện trạng lún và dự báo tương lai ở vùng Đồng bằng sông Cửu Long, Việt Nam
(tóm tắt bằng tiếng Việt)

PROEFSCHRIFT

ter verkrijging van de graad van doctor aan de Universiteit Utrecht
op gezag van de rector magnificus, prof.dr. H.R.B.M. Kummeling,
ingevolge het besluit van het college voor promoties in het openbaar te verdedigen
op vrijdag 15 februari 2019 des middags te 2.30 uur

door

Philip Simon Johannes Minderhoud

geboren op 23 oktober 1986 te Hengelo (O)

Promotor:
Prof. dr. H. Middelkoop

Copromotoren:
Dr. E. Stouthamer
Dr. G. Erkens

This work is part of the Urbanizing Deltas of the World (UDW): "Rise and Fall" research project, which is financially supported by the Netherlands Organization for Scientific Research (NWO), grant: W 07.69.105 and co-financed by Deltares Research Institute and TNO-Geological Survey of the Netherlands.

Utrecht Studies in Earth Sciences 168

The sinking mega-delta

Present and future subsidence of the Vietnamese Mekong delta

Philip S.J. Minderhoud

Utrecht 2019

Promotor:
Prof. dr. H. Middelkoop

Copromotoren:
Dr. E. Stouthamer
Dr. G. Erkens

Examination committee:
Prof. dr. M.F.P. Bierkens
University of Utrecht, The Netherlands

Prof. dr. T.J. Burbey
Virginia Tech, USA

Prof. dr. J.C.J. Kwadijk
University of Twente / Deltares, The Netherlands

Prof. dr. R.J. Nicholls
University of Southampton, UK

Dr. P. Teatini
University of Padova, Italy

ISBN 978-90-6266-520-4
Published by the Faculty of Geosciences of Utrecht University, The Netherlands in:
Utrecht Studies in Earth Sciences (ISSN: 2211-4335)
Printed by Ridderprint BV, Ridderkerk, The Netherlands

Correspondence to Philip Minderhoud, P.S.J.Minderhoud@uu.nl, Philip.Minderhoud@Deltares.nl, mail@philipminderhoud.nl.

On the cover: Inundated rice field during sunset in the Mekong delta, Vietnam

Copyright © 2019 Philip S.J. Minderhoud

This work is licensed under Creative Commons Atrribution-NonCommercial-NoDerivatives 4.0 International (CC BY-NC-ND 4.0), https://creativecommons.org/licenses/by-nc-nd/4.0/.
Chapters 2 to 6 and Appendices are either unpublished submitted articles or last-author versions of previously published articles. More information and citation suggestions are provided at the beginning of these chapters.

Contents

Summary

River deltas worldwide host over 500 million people living in or close to them and provide global food security as they are amongst the most productive areas for agriculture and aquaculture on Earth. Their low elevation above sea level makes deltas extremely vulnerable to sea-level rise. At present, many major river deltas in the world are sinking relatively to sea level due to a combination of reduced sedimentation, absolute sea-level rise and subsidence. One of those deltas is the Mekong delta, largely situated in Vietnam in southeast Asia. It is the world's third largest delta plain, inhabited by nearly 18 million people and responsible for 50% of Vietnam's total food production. The delta is impacted by decreased fluvial sediment supply, salinization, coastal erosion and global sea-level rise. On top of that, annual subsidence rates up to several centimeters per year cause the Mekong delta to rapidly lose elevation, which increases its vulnerability to flooding, salinization, storm surges, coastal erosion and, ultimately, threatens the delta with permanent inundation.

Land subsidence in deltas can be caused by a range of natural and human-induced mechanisms. Examples of natural processes are natural compaction of unconsolidated sediment, tectonics and isostasy. Human activities in deltas can enhance natural subsidence or create additional anthropogenic subsidence. Human-induced drivers of subsidence are, for example, artificial loading by infrastructure and buildings, phreatic groundwater table lowering and fluid and hydrocarbon extraction from the deeper subsurface (e.g., groundwater, oil or gas). All these drivers result in subsidence of the delta surface. To create projections of future subsidence and support the development of mitigation and adaptation strategies for sinking deltas, it is a prerequisite to understand driving mechanisms and processes of subsidence and to quantify their individual contribution. The main objective of the research of this thesis is to understand and quantify the main natural and human-induced drivers and processes causing subsidence, and its impact on current and future surface elevation of the Vietnamese Mekong delta.

To reach this objective, the research was subdivided into three steps: 1) determine the present elevation of the delta above local mean sea level, 2) quantify the individual contribution of main subsidence mechanisms and 3) assess future subsidence and the impact of consequent relative sea-level rise. The results from this thesis aim to provide a knowledge base on delta subsidence that may facilitate well-informed decision-making and development of sustainable and effective mitigation and adaptation strategies in the Mekong delta and deltas elsewhere in the world facing accelerating rates of relative sea-level rise.

Like many major deltas, the Mekong delta is located in a data-sparse region. As a result, previous assessments of the delta's elevation above sea level and the impact of sea-level rise were based on global spaceborne elevation data with vertical accuracies of several meters. A newly created elevation model based on topographical map elevations of the Mekong delta reveals that the delta has an extremely low mean elevation of ~0.8 m above local geodetic level, which referenced to Vietnamese mean sea level (MSL). This is much lower than previously (erroneously) concluded based on global, spaceborne elevation models (~2.6 m to ~3.3 m). This mismatch is caused by not accounting for vertical inaccuracy of spaceborne elevation models, elevation differences between vertical datum used in global elevation models and local geodetic datum, and potential difference between zero datum and local MSL in the Mekong delta. This implies major uncertainties in

previous sea-level rise impact assessments for the Mekong delta, and for deltas elsewhere in the world. Furthermore, the Mekong delta is more prone to relative sea-level rise, the combination between absolute sea-level rise and subsidence, than previously anticipated.

The Mekong Delta was formed by rapid transgression during the second half of the Holocene by deposition of mainly unconsolidated, fine- grained sediments. These shallow sediments are prone to high rates of natural compaction. Using a novel numerical model capable of simulating sediment accretion and natural consolidation the formation and evolution of the Mekong delta over the past 4000 years was simulated. This showed that present-day rates of natural compaction of the shallow Holocene deposits can reach annual rates up to several centimeters (~35 mm yr^{-1}) at the coastline. This identified natural compaction as a major subsidence driver in the coastal zone of the Mekong delta, which has large implications, for example reducing the designed service life of flood defense structures along the coast, as this natural process cannot be mitigated.

During past decades, following the transformation of Vietnam to an open-market economy in 1986 (*Doi Moi*), the Mekong delta experienced large-scale anthropogenic land-use changes as a result of increased agricultural production, population growth and urbanization. As land-use changes can alter the hydrological system or increase loading of the delta surface, they may amplify natural subsidence processes or create new anthropogenic subsidence. With a new, optical remote sensing-based, time series of land use, combined with InSAR-derived subsidence rates estimates, land-use specific subsidence rates, resulting from current and historical land-use practices, were quantified for the Mekong delta. Lowest mean subsidence rates were found for less-human impacted land-use classes, like marshland and wetland forest (~6-7 mm yr^{-1}), and highest rates for areas with mixed-crop agriculture and cities (~18-20 mm yr^{-1}). The strength of the relationship between current land use, land-use history and subsidence was assessed by the ability to predict subsidence rates during the measurement period solely by land-use history, after initial training of all land-use sequences with InSAR-derived subsidence rates. The land-use-based approach predicted 65-92% of the spatially varying subsidence rates. This means that the spatial patterns of the InSAR-derived subsidence rates can largely be explained by land use-related drivers, revealing the role of human activities on subsidence in the Mekong delta.

Urbanization and intensification of agriculture and aquaculture led to a strong increase in groundwater use. Since the 1990's, groundwater exploitation has increased drastically, transforming the delta's subsurface from an almost undisturbed hydrogeological state to a situation with increasing aquifer depletion. As groundwater levels drop, subsidence is induced through aquifer-system compaction. By creating the first delta-wide numerical model of an entire mega delta, comprising a 3D hydrogeological model coupled to a 1D geotechnical module, the impact of past groundwater exploitation on subsidence in the Mekong delta was modeled. This provides a quantitative spatially-explicit assessment of groundwater extraction-induced subsidence for the entire Mekong delta since the start of widespread overexploitation until present. Extraction-induced subsidence in the Mekong delta has steadily increased over the past decades towards the highest sinking rates at present. During the past 25 years, the delta sank on average ~170 mm as a consequence of groundwater withdrawal. Current average subsidence rate due to groundwater extraction in our best estimate model amounts to ~9 mm yr^{-1}, with areas subsiding over 25 mm yr^{-1}, outpacing absolute sea-level rise almost by an order of magnitude.

As groundwater extraction-induced subsidence is the dominant – anthropogenic – cause of subsidence in the Mekong delta, projections of consequent future extractions and extraction-induced subsidence are a prerequisite to evaluate the impact of future relative sea-level rise. Using six mitigation and non-mitigation scenarios in which the delta follows different groundwater

extraction pathways until 2100, future groundwater dynamics and consequent aquifer-system compaction of the Mekong delta were modeled. The results revealed that when groundwater extraction is allowed to increase continuously, as it did in the past decades, extraction-induced subsidence could potentially drown almost the entire Mekong delta. Reducing future groundwater extraction will also reduce extraction-induced subsidence, however, even when groundwater extractions are completely stopped, subsidence will continue to happen as aquifer-compaction continues afterwards. Still, the quantitative estimates of extraction-induced subsidence disclose the large mitigation potential to reduce extraction-induced subsidence and limit future elevation loss by reducing groundwater extraction and stimulating recharge.

Two dominant mechanisms are responsible for causing subsidence and subsequent elevation loss at the scale of the entire Mekong delta: 1) compaction of shallow Holocene sediments by natural sediment loading, enhanced by human loading and drainage, and predominantly causing high subsidence rates near the coast and 2) extraction-induced subsidence following groundwater overexploitation from the deeper subsurface. Locally, other human-induced drivers, such as loading, and increased drainage or additional groundwater exploitation, cause additional subsidence. Though these last mechanisms may locally result in damage to infrastructure and increase nuasance floodings in urban areas, they do not have a large impact on the overall elevation of the delta plain. Tectonics, natural compaction of pre-Holocene deposits and isotatic adjustment do not seem to play a major role in the present subsidence rates of the Mekong delta.

The present accelerating rates of subsidence in the Mekong delta, in combination with absolute sea-level rise cause the delta to rapidly lose elevation to local sea level. A calculation of the present sediment balance of the delta, including the quantifications in this thesis, reveals the tremendous sediment deficit of the delta. Assuming that all suspended sediment in the Mekong river is added to the delta plain, 35% (best case) to 6% (worst case) of the relative elevation loss to sea-level rise could be compensated. However, given that presently the majority of the Mekong river sediment is not reaching the delta plain, the actual percentages are even lower.

When compared to other deltas in the world, the Mekong delta is in a critical position due to its low elevation and accelerating rate of relative sea-level rise. It is almost inevitable that large parts of the Mekong delta will fall below sea level during this coming century. The best chance for the Mekong delta to sustain itself in the future is through mitigation measures to reduce groundwater use and stimulate groundwater recharge, re-enable sedimentation on the delta plain, and by implementing a smart combination of both hard and soft adaptive measures. Changing the view on delta elevation: valuating it as a precious natural resource which is exploitable and can be depleted, will help to integrate the effects of human-induced subsidence and accelerated relative sea-level rise in strategic delta planning. As a result, exploiting delta elevation by human-induced subsidence becomes a conscious choice rather than an unfortunate and uncontrolled effect of delta development.

Samenvatting

Wereldwijd wonen er meer dan 500 miljoen mensen in of rondom rivierdelta's. Rivierdelta's behoren tot de meest productieve gebieden voor landbouw en aquacultuur op aarde en dragen zo bij aan de wereldwijde voedselzekerheid. Delta's zijn laaggelegen gebieden dichtbij zeeniveau en dit maakt ze uiterst kwetsbaar voor zeespiegelstijging. Op dit moment verliezen veel grote rivierdelta's in de wereld hoogte ten opzichte van de zeespiegel als gevolg van een combinatie van verminderde sedimentatie, absolute zeespiegelstijging en bodemdaling. Een van die delta's is de Mekongdelta, grotendeels gelegen in Vietnam in Zuidoost-Azië. Het is 's werelds derde grootste rivierdelta, bewoond door bijna 18 miljoen mensen en verantwoordelijk voor 50% van de totale voedselproductie in Vietnam. De delta wordt beïnvloed door verminderde aanvoer van riviersedimenten, verzilting, kusterosie en wereldwijde zeespiegelstijging. Daarbovenop zinkt de Mekongdelta door bodemdaling met snelheden tot enkele centimeters per jaar, wat de kwetsbaarheid voor overstromingen, verzilting, stormvloeden en kusterosie verder verhoogt en de delta bedreigt met verdrinking.

Bodemdaling in delta's kan worden veroorzaakt door een reeks natuurlijke en door de mens veroorzaakte mechanismen. Voorbeelden van natuurlijke processen zijn natuurlijke samendrukking van sedimenten, tektonische bewegingen en isostasie. Menselijke activiteiten in delta's kunnen de natuurlijke bodemdaling versterken of extra antropogene bodemdaling veroorzaken. Door mensen geïnduceerde oorzaken van bodemdaling zijn bijvoorbeeld kunstmatige belasting door infrastructuur en gebouwen, freatisch grondwaterspiegelverlaging en vloeistof- en koolwaterstofextractie uit de diepere ondergrond (bijvoorbeeld grondwater, olie of gas). Al deze aandrijfmechanismen kunnen resulteren in daling van het delta-oppervlak. Om voorspellingen van toekomstige bodemdaling te maken ter ondersteuning van de ontwikkeling van mitigatie- en aanpassingsstrategieën voor zinkende delta's, is het een vereiste om de verschillende aandrijfmechanismen en bodemdalingsprocessen te begrijpen en hun individuele bijdrage te kwantificeren. Het hoofddoel van het onderzoek van dit proefschrift is het begrijpen en kwantificeren van de belangrijkste natuurlijke en door de mens veroorzaakte mechanismen en processen die bodemdaling veroorzaken, en de impact ervan op de huidige en toekomstige bodemhoogte van de Vietnamese Mekongdelta. Om dit doel te bereiken, werd het onderzoek onderverdeeld in drie stappen: 1) het bepalen van de huidige hoogte van de delta boven het lokale gemiddelde zeeniveau, 2) het kwantificeren van de individuele bijdrage van de belangrijkste bodemdalingsmechanismen en 3) het voorspellen van mogelijke toekomstige bodemdaling en de impact van de daaruit voortvloeiende relatieve zeespiegelstijging op de delta. De resultaten van dit proefschrift zijn gericht op het creëren van een kennisbasis over bodemdaling ter ondersteuning van besluitvorming en ontwikkeling van duurzame en effectieve mitigatie- en aanpassingsstrategieën in de Mekongdelta en delta's elders in de wereld beïnvloed door toenemende relatieve zeespiegelstijging.

Net als voor veel andere grote delta's zijn er relatief weinig meetdata beschikbaar voor de Mekongdelta. Hierdoor waren eerdere inschattingen van de hoogte van de delta boven de zeespiegel en de invloed van zeespiegelstijging gebaseerd op mondiaal beschikbare hoogtemodellen afkomstig van satellietmetingen. Deze metingen hebben een verticale nauwkeurigheid van enkele meters.

Een nieuw gecreëerd hoogtemodel op basis van topografische kaarthoogtes van de Mekongdelta laat zien dat de delta gemiddeld een hoogte heeft van ~ 0,8 m boven het lokale geodetische niveau, wat overeenkomst met Vietnamees gemiddeld zeeniveau. Dit is veel lager dan voorheen (ten onrechte) geconcludeerd was op basis van mondiale hoogtemodellen (~ 2,6 m tot ~ 3,3 m). Dit verschil wordt veroorzaakt door de verticale onnauwkeurigheid van de mondiale hoogtemodellen, verticale verschillen tussen wereldwijde en lokaal geodetisch datums en verschil tussen nul hoogte en lokaal gemiddeld zeeniveau in de Mekongdelta. Dit impliceert grote onzekerheden in eerdere voorspellingen op basis van mondiale hoogtemodellen over de impact van zeespiegelstijging voor de Mekongdelta en voor delta's elders in de wereld. Het laat ook zien dat de Mekongdelta meer kwetsbaar is voor relatieve zeespiegelstijging: de combinatie tussen absolute zeespiegelstijging en bodemdaling, dan eerder werd verwacht.

De Mekongdelta werd gevormd tijdens de tweede helft van het Holoceen door depositie van hoofdzakelijk fijnkorrelige sedimenten. Deze ondiepe sedimenten zijn zeer gevoelig voor natuurlijke samendrukking. Met behulp van een nieuw numeriek model, dat in staat is sedimentdepositie en natuurlijke samendrukking te simuleren, werd de vorming en evolutie van de Mekongdelta in de afgelopen 4000 jaar gesimuleerd. Dit toonde aan dat de huidige niveaus van natuurlijke samendrukking van de ondiepe afzettingen jaarlijkse kunnen oplopen tot enkele centimeters (~ 35 mm yr^{-1}), met name in jongste gebieden dicht bij de kust. Deze studie identificeerde natuurlijke samendrukking als een belangrijk aandrijfmechanisme van bodemdaling in het kustgebied van de Mekongdelta. Doordat dit natuurlijke proces niet kan worden gestopt, heeft dit grote gevolgen voor bijvoorbeeld de levensduur van dijken en waterkeringen in de kustgebieden van de Mekongdelta.

Sinds de transformatie van Vietnam naar een markteconomie in 1986 (genaamd de '*Doi Moi*') heeft de Mekongdelta in de afgelopen decennia grootschalige antropogene veranderingen in landgebruik meegemaakt als gevolg van toegenomen landbouwproductie, bevolkingsgroei en verstedelijking. Veranderingen in landgebruik kunnen het hydrologische systeem veranderen of de belasting van de ondergrond verhogen. Dit kan natuurlijke bodemdalingsprocessen versterken of nieuwe antropogene bodemdaling creëren. Met behulp van een nieuwe tijdserie van landgebruikskaarten, verkregen door interpretatie van satellietbeelden, gecombineerd met satelliet-afgeleide kwantificering van bodemdaling, werden landgebruik-specifieke bodemdalingssnelheden gekwantificeerd voor de Mekongdelta. De laagste bodemdalingssnelheden werden gevonden voor landgebruik klassen die de minste menselijke invloed kennen, zoals moerassen (~ 6-7 mm yr^{-1}), en de hoogste snelheden voor stedelijke gebieden en gebieden met gemengde landbouw (~ 18-20 mm yr^{-1}). De sterkte van de relatie tussen huidig landgebruik, landgebruiksgeschiedenis en bodemdaling werd beoordeeld door het vermogen om bodemdaling tijdens de meetperiode te voorspellen op basis van uitsluitend de landsgebruiksgeschiedenis. De benadering op basis van landgebruik voorspelde 65-92% van de ruimtelijk bodemdalingspatronen. Dit betekent dat de ruimtelijke patronen van bodemdaling grotendeels te verklaren zijn door factoren gerelateerd aan landgebruik en dit toont de rol aan van menselijke activiteiten op bodemdaling in de Mekongdelta.

Verstedelijking en intensivering van landbouw en aquacultuur leidde tot een sterke toename van het grondwatergebruik. Sinds de jaren negentig van de vorige eeuw is de exploitatie van grondwater drastisch toegenomen, waardoor de ondergrond van de delta veranderde van een bijna onverstoorde staat naar een situatie met toenemende uitputting van de watervoerende lagen. Naarmate de druk van het grondwater afneemt, wordt bodemdaling veroorzaakt door samendrukking van de watervoerende lagen in de ondergrond. Door het creëren van het eerste numerieke model van een hele mega-delta, bestaande uit een 3D-hydrogeologisch model gekoppeld aan een 1D

geotechnische module, is de impact van de grondwaterexploitatie van de afgelopen decennia op bodemdaling in de Mekongdelta berekend. Dit leverde een kwantitatieve, ruimtelijk expliciete inschatting van bodemdaling, veroorzaakt door grondwaterwinning, voor de hele Mekongdelta sinds het begin van wijdverspreide overexploitatie tot op heden. In de afgelopen decennia is de door grondwaterextractie veroorzaakte bodemdaling in de Mekongdelta gestaag toegenomen tot de hoge bodemdalingssnelheden die op dit moment plaatsvinden. In de afgelopen 25 jaar is de delta gemiddeld ~ 170 mm gezakt als gevolg van de grondwateronttrekking. Gemiddeld is de huidige snelheid van bodemdaling door grondwateronttrekking ~ 9 mm yr^{-1} en bepaalde gebieden in de delta zinken zelfs met snelheden van meer dan 25 mm yr^{-1}, bijna een orde groter dan de absolute zeespiegelstijging.

Omdat door grondwateronttrekking veroorzaakte bodemdaling de dominante, antropogene oorzaak is van bodemdaling in de Mekongdelta, zijn projecties van toekomstige grondwateronttrekkingen en de bijbehorende bodemdaling van groot belang om de impact van toekomstige relatieve zeespiegelstijging te evalueren. Met behulp van zes mitigatie- en niet-mitigatiescenario's waarin de delta tot 2100 verschillende paden van grondwateronttrekking volgt, zijn toekomstige grondwaterdynamica en daaruit voortvloeiende samendrukking van de ondergrond van de Mekongdelta gemodelleerd. De resultaten toonden aan dat, wanneer grondwateronttrekking continu toeneemt, zoals het geval was in de afgelopen decennia, bodemdaling mogelijk bijna de hele Mekongdelta kan laten zinken onder zeeniveau. Verminderen van grondwaterwinning in de toekomst zal ook de bodemdaling verminderen, maar zelfs wanneer de grondwaterwinningen volledig worden gestopt, zal bodemdaling blijven plaatsvinden omdat de samendrukking van de ondergrond nog steeds door zal gaan. De voorspellingen van bodemdaling, veroorzaakt door grondwaterwinning, laten de potentie zien van het verminderen van toekomstige bodemdaling door grondwateronttrekking te verminderen en aanvulling van het grondwater te stimuleren. Op deze manier kan het hoogteverlies van de delta in de toekomst worden beperken,

Twee dominante mechanismen zijn hoofdzakelijk verantwoordelijk voor het veroorzaken van bodemdaling, en het daarop volgend hoogteverlies, op de gehele Mekongdelta: 1) samendrukking van ondiepe Holocene sedimenten door natuurlijke sedimentbelasting, versterkt door menselijke belasting en drainage. Dit veroorzaakt overwegend hoge bodemdalingssnelheden nabij de kust en 2) door grondwateronttrekking veroorzaakte bodemdaling na overexploitatie van het grondwater uit de diepere ondergrond. Lokaal veroorzaken ook andere antropogene activiteiten extra bodemdaling, zoals belasting van de ondergrond, toenemende drainage van het oppervlakte water of extra exploitatie van grondwater. Hoewel deze laatste genoemde mechanismen lokaal kunnen resulteren in schade aan de infrastructuur en toename van overstromingen in stedelijke gebieden, hebben ze geen grote invloed op de algemene hoogte van de deltavlakte. Tektoniek, natuurlijke samendrukking van pre-Holocene afzettingen en isostasie lijken geen grote rol te spelen bij de huidige bodemdalingssnelheden van de Mekongdelta.

De recente versnelling van bodemdaling in de Mekongdelta, in combinatie met absolute zeespiegelstijging, zorgt ervoor dat de delta in een rap tempo hoogte verliest t.o.v. het lokale zeeniveau. Een berekening van de huidige sedimentbalans van de delta, inclusief de berekeningen van bodemdaling in dit proefschrift, onthult het enorme sedimenttekort van de delta. Ervan uitgaande dat alle gesuspendeerde sedimenten in de Mekong rivier aan de deltavlakte worden toegevoegd, zou 35% (beste geval) tot 6% (slechtste geval) van het relatieve hoogteverlies tot de stijgende zeespiegel kunnen worden gecompenseerd. Gezien het feit dat de meerderheid van het Mekong riviersediment echter niet de deltavlakte bereikt, zijn de werkelijke percentages zelfs lager.

In vergelijking met andere delta's in de wereld bevindt de Mekongdelta zich in een kritieke positie vanwege zijn geringe hoogte boven zeeniveau en de versnellende relatieve zeespiegelstijging. Het is bijna onvermijdelijk dat grote delen van de Mekongdelta de komende eeuw onder zeeniveau zullen vallen. De beste kans voor de Mekongdelta om zich in de toekomst te handhaven, is door mitigatiemaatregelen om het grondwatergebruik te verminderen en de aanvulling van het grondwater te stimuleren, sedimentatie op de deltavlakte mogelijk te maken en door een slimme combinatie van zowel harde als zachte adaptieve maatregelen te implementeren. Het is nodig om de manier waarop men naar de hoogteligging van een delta kijkt te veranderen naar het waarderen van hoogte als waardevolle natuurlijke 'grondstof' die kan worden geëxploiteerd en uitgeput. Op deze manier kunnen de effecten van, door de mens veroorzaakte, bodemdaling en de versnelde relatieve zeespiegelstijging op een strategische manier worden geïntegreerd in deltaplanning. Zodoende wordt het 'exploiteren' van deltahoogteligging door bodemdaling een bewuste keuze in plaats van een vervelend en ongecontroleerd effect van ontwikkelingen in een delta.

Tóm tắt bằng tiếng Việt

Translation by Trung Phan, Tri Van Pham Dang, Hung Pham Van

Các đồng bằng châu thổ cung cấp nơi ở cho hơn 500 triệu người và góp phần đảm bảo an ninh lương thực toàn cầu bởi đây là khu vực sản xuất nông nghiệp và thuỷ sản lớn nhất trên thế giới. Với cao trình thấp so với mực nước biển, những đồng bằng này rất dễ bị tổn thương khi nước biển dâng. Hiện tại, nhiều đồng bằng lớn trên thế giới đang lún dần (so với mực nước biển) do tác động tổng hợp từ việc suy giảm bồi tụ trầm tích, nước biển dâng và sụt lún đất. Đồng bằng sông Cửu Long (ĐBSCL), với phần lớn diện tích thuộc Việt Nam ở khu vực Đông Nam Á, là một trong những điển hình cho vấn đề này. ĐBSCL là vùng châu thổ lớn thứ ba toàn cầu, là nơi sinh sống của gần 18 triệu người và đang đóng góp 50% tổng sản lượng lương thực cho Việt Nam. Tương tự như ở các vùng đồng bằng khác, ĐBSCL đang chịu tác động bởi sự suy giảm lượng bùn cát từ thượng nguồn, xâm nhập mặn, sạt lở vùng ven biển và nước biển dâng. Ngoài ra, sụt lún đất có thể lên đến vài cen-ti-met mỗi năm đã làm cho cao trình ĐBSCL sụt giảm nhanh hơn, dẫn đến nguy cơ tăng rủi ro về lũ, xâm nhập mặn, sạt lở vùng ven biển, và nguy hiểm hơn là nguy cơ ngập vĩnh viễn đồng bằng.

Sụt lún đất ở ĐBSCL là hệ quả của các quá trình vận động tự nhiên cũng như tác động của con người. Một trong những yếu tố tự nhiên dẫn đến tình trạng sụt lún là quá trình cố kết tự nhiên của các trầm tích đệ tứ và hoạt động kiến tạo. Bên cạnh đó, các hoạt động của con người có thể làm cho quá trình sụt lún tự nhiên trở nên nghiêm trọng hơn; ví dụ: hoạt động xây dựng hạ tầng và công trình, sự sụt giảm mực nước dưới đất, khai thác hydrocacbon từ các tầng địa chất sâu (nước dưới đất, dầu hoặc khí đốt). Tất cả các tác nhân này dẫn đến sự sụt lún bề mặt của đồng bằng. Để theo dõi sự sụt lún trong tương lai và hỗ trợ cho việc xây dựng các chiến lược thích ứng và giảm nhẹ quá trình chìm dần của đồng bằng, việc hiểu rõ các tác nhân, tiến trình sụt lún và lượng hoá mức độ tác động tổng hợp của các tác nhân là điều kiện tiên quyết. Mục tiêu chính của luận án này nhằm tìm hiểu và định lượng các tác nhân tự nhiên và con người gây ra sự sụt lún cũng như tiến trình dẫn đến sụt lún và tác động của nó đến cao trình bề mặt hiện tại và tương lai của ĐBSCL. Để đạt được mục tiêu này, đề tài được chia thành ba hợp phần: 1) xác định cao trình hiện tại của đồng bằng dựa trên mực nước biển trung bình tại vùng nghiên cứu, 2) Định lượng các mức độ tác động từ từng tác nhân thành phần và 3) đánh giá khả năng sụt lún trong tương lai kết hợp xem xét tác động của sự gia tăng mực nước biển. Kết quả của đề tài hướng đến việc cung cấp thông tin và sự hiểu biết về vấn đề sụt lún của đồng bằng, từ đó tạo điều kiện cho các nhà ra quyết định phát triển các chính sách khả thi cho việc thích ứng và giảm nhẹ không chỉ tại ĐBSCL mà còn những đồng bằng tương đồng khác trên thế giới hiện đang phải đối mặt với các tác động tích luỹ từ gia tăng mực nước biển.

Như các đồng bằng lớn khác, dữ liệu có sẵn liên quan đến đề tài nghiên cứu tại ĐBSCL rất hạn chế. Các nghiên cứu trước đây về cao trình của đồng bằng dựa vào mực nước biển cũng như đánh giá tác động của nước biển dâng chủ yếu dựa trên số liệu cao trình bề mặt từ vệ tinh với độ chính xác theo chiều thẳng đứng đạt vài met. Một mô hình cao trình mặt đất mới được xây dựng dựa trên bản đồ cao độ địa hình của ĐBSCL cho thấy cao độ bề mặt trung bình của đồng bằng rất thấp, chỉ đạt khoảng 0.8 m so với mức trắc địa vùng nghiên cứu, thấp hơn nhiều so với kết qủa nghiên cứu trước đây (kết quả không chính xác) được kết luận dựa trên mô hình cao độ toàn cầu (cao độ trung bình từ 2.6 m đến 3.3 m). Sự không trùng khớp này là do các nghiên cứu trước không xem xét và tính toán mức độ không chính xác theo chiều thẳng đứng của mô hình cao độ với số liệu từ vệ tinh, sự khác biệt về cao độ bề mặt giữa mốc theo chiều thẳng đứng được sử dụng trong mô hình cao độ toàn cầu và mốc trắc địa tại vùng nghiên cứu cũng như sự khác biệt giữa mốc chuẩn (mốc không) và mực nước

biển trung bình tại Việt Nam. Điều này dẫn đến nhiều vấn đề không chắc chắn trong các nghiên cứu về tác động của nước biển dâng trước đây tại ĐBSCL, và tương tự với các đồng bằng khác trên thế giới. Hơn nữa, ĐBSCL ngày càng dễ bị tác động bởi nước biển dâng, và các tác động này cũng đang diễn ra nhanh hơn so với dự đoán trước đây bởi sự tích hợp giữa mực nước biển tuyệt đối và sụt lún đất.

ĐBSCL được hình thành trong thời kỳ biển lùi nhanh vào nửa sau trong giai đoạn Holocen bởi sự tích tụ chủ yếu của các hạt trầm tích mịn và không dính kết. Những trầm tích tại các tầng nông này dễ bị tác động mạnh bởi mức độ nén tự nhiên. Việc sử dụng một mô hình toán giả định có thể mô phỏng sự bồi tụ trầm tích và kết dính tự nhiên trong quá trình hình thành và phát triển của ĐBSCL qua 4000 năm. Kết quả tính toán cho thấy mức độ nén tự nhiên đến thời điểm hiện tại của sự bồi tụ Holocen tầng nông có thể đạt trong khoảng vài cen-ti-met hằng năm (35 mm/năm) tại vùng ven bờ. Yếu tố nén tự nhiên này là tác nhân chính dẫn đến sự sụt lún tại vùng ven biển của ĐBSCL, với nhiều hệ quả nghiêm trọng, ví dụ như làm giảm các lợi ích từ hệ thống chắn sóng ven biển, trong khi quá trình nén tự nhiên này không thể làm giảm nhẹ được.

Từ 1986, Chính sách Đổi Mới đã làm thay đổi cơ cấu phát triển kinh tế - xã hội của Việt Nam theo hướng đẩy mạnh kinh tế thị trường. Cơ chế mở cửa này đã làm hệ thống sử dụng đất của ĐBSCL trải qua sự chuyển dịch trên diện rộng để thúc đẩy sản xuất nông nghiệp, kéo theo vấn đề gia tăng dân số và đô thị hoá. Và do việc chuyển đổi sử dụng đất có thể làm thay đổi điều kiện địa chất thuỷ văn và gia tăng chất tải lên bề mặt đồng bằng, quá trình sụt lún tự nhiên đã và đang diễn ra nhanh hơn do có các yếu tố do con người tác động vào. Với công cụ viễn thám mới, số liệu chuỗi thời gian về sử dụng đất, kết hợp với ước tính mức độ sụt lún lấy được từ ảnh vệ tinh InSAR, độ lún cụ thể do sử dụng đất (có được từ quá trình canh tác từ quá khứ đến hiện tại) đã được tính toán cho ĐBSCL. Mức độ sụt lún trung bình thấp nhất được tìm thấy ứng với nhóm đất ít được sử dụng cho canh tác nhất, như đất đầm lầy và đất ngập nước (độ lún từ 6 – 7 mm/năm) và mức độ lún trung bình cao nhất tại các khu vực có sự xáo trộn giữa canh tác nông nghiệp và các đô thị (18 – 20 mm/năm). Mối tương quan chặt chẽ giữa sử dụng đất hiện tại và lược sử quá trình canh tác với quá trình sụt lún đã được phân tích từ kết quả tính mức độ lún trong giai đoạn quan trắc độc lập yếu tố sử dụng đất, sau khi xem xét toàn bộ tiến trình thay đổi sử dụng đất với kết quả về tính toán sụt lún từ giải đoán ảnh InSAR. Việc tiếp cận dựa vào quá trình sử dụng đất đã dự đoán 65 – 92 % các vùng có sụt lún. Như vậy từ kết quả giải đoán ảnh InSAR, những vùng được ghi nhận bị sụt lún phần lớn có liên quan đến yếu tố sử dụng đất, và đây cũng là minh chứng cho thấy tác động từ các hoạt động của con người đến quá trình sụt lún ĐBSCL.

Bên cạnh đó, đô thị hoá cùng với thâm canh nông nghiệp và thuỷ sản gây ra sự gia tăng việc sử dụng nguồn nước dưới đất (NDĐ). Từ những năm 1990, nguồn NDĐ được khai thác ồ ạt, làm cho cấu trúc dưới bề mặt của đồng bằng thay đổi từ trạng thái địa chất thuỷ văn hầu như không bị xáo trộn sang bối cảnh các tầng nước bị suy giảm đi một cách nhanh chóng. Và sự suy giảm này chính là tiền đề cho quá trình sụt lún diễn ra thông qua sự cố kết của các tầng chứa nước. Một mô hình toán tích hợp đầu tiên cho toàn đồng bằng, bao gồm cặp mô hình địa chất thuỷ văn 3D và mô hình địa kỹ thuật 1D, thông tin về tác động của quá trình khai thác NDĐ đến sự sụt lún ĐBSCL đã được tính toán và mô phỏng. Mô hình cung cấp góc nhìn rõ ràng về mặt không gian kết hợp với khả năng định lượng mức độ sụt lún do khai thác NDĐ ở ĐBSCL kể từ lúc bắt đầu quá trình khai thác NDĐ một cách tập trung và trên diện rộng cho đến nay. Độ lún do khai thác NDĐ tại ĐBSCL không ngừng tăng lên kể từ những năm 1990 dẫn đến hệ quả là đến thời điểm hiện tại, khả năng chìm xuống của đồng bằng đang ở mức độ báo động. Trong khoảng 25 năm trở lại đây, đồng bằng đã chìm xuống khoảng 170 mm do sự giảm đi lượng nước của các tầng chứa nước. Mức độ lún trung bình hiện tại do khai thác NDĐ thông qua ước tính từ mô hình toán vào khoảng 9 mm/năm, với một số vùng có độ lún lên đến 25 mm/năm, vượt xa so với nước biển dâng đã và đang tác động đến đồng bằng.

Khai thác NDĐ là một hoạt động của con người chi phối và trực tiếp gây ra hiện tượng sụt lún ở ĐBSCL, là yếu tố dùng để đối chiếu cho các hậu quả trong thời gian tới khi tiếp tục khai thác NDĐ, đồng thời cũng là là điều kiện tiên quyết để xem xét và đánh giá mức độ tác động của nước biển dâng. Việc sử dụng sáu kịch bản giảm nhẹ và không giảm nhẹ trong đó cho phép ĐBSCL áp dụng các cách khai thác NDĐ khác nhau cho đến 2100, động thái nguồn NDĐ và sự nén xuống của các tầng nước nhạt kèm theo đó đã được tính toán và mô hình hoá. Kết quả đã cho thấy khi mà việc khai thác nguồn NDĐ còn được cho phép và không ngừng tăng lên, như những gì đã diễn ra trong những thập niên trở lại đây, thì lúc đó mức độ sụt lún còn sẽ nghiêm trọng đến mức có thể nhấn chìm gần như toàn bộ vùng ĐBSCL. Việc cắt giảm lượng khai thác NDĐ trong thời gian tới phần nào làm giảm tiến trình sụt lún, tuy nhiên, có một sự thật rằng cho dù NDĐ có ngừng bị khai thác, quá trình sụt lún vẫn sẽ tiếp tục xảy ra do sự nén các tầng nước nhạt vẫn còn duy trì sau đó. Tuy vậy, kết quả tính toán mức độ sụt lún do khai thác NDĐ đã mở ra một phương hướng khả thi nhằm hạn chế sự lún và suy giảm cao trình trong tương lai đó là cắt giảm khai thác cũng như tăng cường bổ cập nguồn NDĐ.

Hai cơ chế chủ yếu gây ra sự sụt lún kéo theo sự suy giảm cao trình tại ĐBSCL là: 1) sự cố kết trầm tích Holocen tầng nông bởi chất tải trầm tích tự nhiên, gia tăng chất tải của con người, với khu vực bị sụt lún chủ yếu là tại khu vực ven biển; và 2) sụt lún do sự khai thác quá mức nguồn NDĐ tại các tầng nước sâu. Tại các địa phương, các tác nhân khác từ con người, có thể kể đến như xây dựng cơ sở hạ tầng bề mặt, gia tăng cấp nước hoặc khai thác NDĐ, dẫn đến sự sụt lún càng nhiều thêm. Dù những tác nhân này có thể dẫn đến các hệ quả như đe doạ đến hệ thống hạ tầng và tăng thiệt hại do ngập lũ tại các khu vực đô thị, chúng hầu như chỉ mang tính cục bộ và không gây ảnh hưởng lớn đến cao trình chung của ĐBSCL. Các hoạt động kiến tạo, sự nén tự nhiên của trầm tích tiền Holocen và thay đổi trong quá trình biển lấn cũng gần như không có nhiều tác động lớn đến sự sụt lún hiện tại ở ĐBSCL.

Sự tích hợp từ tiến trình sụt lún hiện tại ở ĐBSCL, kết hợp với nước biển dâng làm cao trình của đồng bằng giảm đi nhanh hơn. Một nghiên cứu về sự cân bằng trầm tích hiện tại ở ĐBSCL, cho thấy đã có sự suy giảm lớn về lượng trầm tích được bồi tụ ở đồng bằng. Giả thuyết đặt ra rằng nếu như toàn bộ lượng trầm tích lơ lửng của sông Mekong được bồi tụ về ĐBSCL, thì sẽ có khoảng từ 35% (trong trường hợp cao nhất) đến 6% (trong trường hợp thấp nhất) cao trình đã bị sụt giảm đi của ĐBSCL sẽ được củng cố lại. Tuy nhiên, trên thực tế thì tỷ lệ cao trình bề mặt có thể được củng cố lại sẽ thấp hơn giả định rất nhiều vì theo các nghiên cứu gần đây, lượng trầm tích từ sông Mekong hầu như không thể về đến ĐBSCL do các phát triển ở thượng nguồn.

Khi so sánh với các đồng bằng khác trên thế giới, ĐBSCL nằm ở vị trí rất đáng quan ngại do cao trình bề mặt vốn đã thấp lại chịu tác động sự tăng nhanh chóng của nước biển dâng. Một điều gần như chắc chắn sẽ xảy ra là phần lớn ĐBSCL sẽ thấp hơn mực nước biển trong thế kỷ này. Cơ hội tốt nhất để sự tồn tại của ĐBSCL có thể được duy trì trong tương lai chính là thông qua các giải pháp giảm nhẹ để cắt giảm các vấn đề liên quan đến sử dụng nguồn NDĐ và khuyến khích tăng cường bổ cập nguồn NDĐ, tạo điều kiện để tối đa hoá lượng trầm tích bồi tụ ở đồng bằng, và thực hiện kết hợp hợp lý các giải pháp thích ứng tích hợp cả về nhóm giải pháp cứng và giải pháp mềm. Đồng thời, cách nhìn nhận và những hiểu biết về yếu tố cao trình của đồng bằng cũng cần được thay đổi: hãy xem cao trình bề mặt như một nguồn tài nguyên quý giá mà chúng ta có thể khai thác được và cũng có thể bị cạn kiệt, từ đó tích hợp với các tác động từ hiện tượng sụt lún do chính con người gây ra trong bối cảnh gia tăng liên tục của mực nước biển vào kế hoạch hành động chiến lược của đồng bằng. Như vậy, sự suy giảm cao trình đồng bằng bởi các tác nhân nhân tạo sẽ được nhìn nhận từ góc độ khách quan hơn thay vì trong hiện tại, quá trình suy giảm này được cho rằng chỉ là hệ quả từ các tác động không mong muốn và không kiểm soát được từ thiên nhiên trong tiến trình phát triển đồng bằng.

1 Introduction

Deltas are baptized after the Greek letter delta by Herodotus (484-425 BC) because of the deltoid-shape of the Nile river mouth. Herodotus already recognized their fluvial origin as a result of flooding: "*But the delta, as the Egyptians affirm, and as I myself am persuaded, is formed of the deposits of the river*" (Herodotus in The Histories 440 BC). Deltas form where rivers flow into a body of water and deposit fluvial sediments. In a pristine and natural state, deltas are dynamic landforms, characterized by shifting channels and a changing sediment supply by floods and storms. The deposition of ample new sediments counterbalances subsidence and results in delta growth. Most modern river deltas are geologically young landforms that began to form 8500 to 6500 years ago, when global sea-level rise, resulting from deglaciation after the last glacial period, ceased (Stanley and Warne, 1994). The deltas' fertile soils, reliable water supply, aquatic food sources and the ease to travel and trade via their distributary channels made and still make them attractive for humans to live. Today, deltas are amongst the most densely populated areas in the world and host over 500 million people living in or close to them (Ericson et al., 2006; Tessler et al., 2015; Higgins, 2016). Deltas accommodate vast areas with agriculture and aquaculture and they host unique ecosystems. Altogether, deltas are among the most ecologically valuable and economically important areas on our planet.

Being low-lying landforms, only slightly elevated above sea level, renders nature deltas sensitive to environmental change. During the last century, humans have dramatically modified the natural dynamics of deltas, and put additional pressures on them (Fig. 1.1). Today, most major river deltas are sinking relatively to sea level, due to the combination of absolute sea-level rise, reduced fluvial sediment supply and accelerated subsidence (Ericson et al., 2006; Syvitski et al., 2009; Giosan et al., 2014; Dunn, 2017). Sea level globally rises as a result of climate change. Ocean warming causes thermal expansion of sea water, and additional water is added to the oceans from land ice melt and land water reservoirs. Sea-level projections range from ~28-98 cm by the end of the century (RCP 2.6-8.5)(Church et al., 2013) and potentially even higher in case of a collapse of the Antarctic Ice Sheet (DeConto and Pollard, 2016). Although highly uncertain, sea-level rise is hard to stop and could continue for centuries, potentially rising multiple meters. This is presenting challenges to coastal regions worldwide (Nicholls and Cazenave, 2010; Day et al., 2016). Also, the amount of sediment carried by the rivers, feeding deltas worldwide, has been strongly reduced due to the construction of upstream reservoir dams (Woodroffe et al., 2006; Syvitski et al., 2009; Giosan et al., 2014). This limits the natural ability of deltas to gain elevation through sediment accumulation and cope with sea-level rise. Within deltas, embankment and channel engineering has protected the land from flooding, but at the same time has ceased the natural accretion by overbank sedimentation. Moreover, a range of subsidence processes in the subsurface causes the delta surface to subside. The sum of land movement (e.g. subsidence) and sea-level change is referred to as relative sea-level rise. Currently, many deltas experience relative sea-level rise. As a result, deltas are becoming increasingly vulnerable to natural hazards such as flooding, storm surges, coastal erosion, salt water intrusion into surface and groundwater, and are ultimately threatened with permanent inundation (Wolters and Kuenzer, 2015).

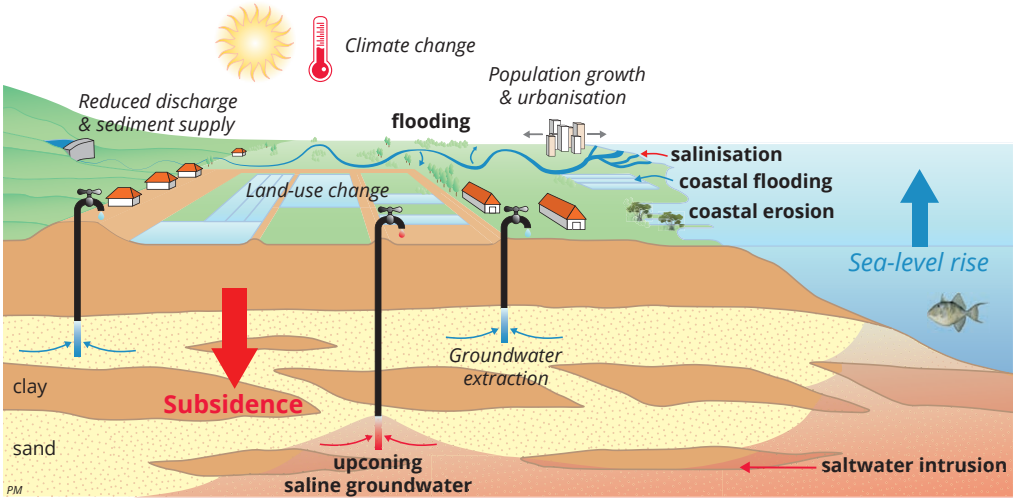

Fig. 1.1 | *Changes (italic) and consequences (**bold**) in modern urbanizing deltas.*

For decades, research towards relative sea-level rise has been focused on global sea-level rise (a.o. Douglas, 1991; Nicholls and Leatherman, 1995). More recently, reduced sediment supply to deltas from their upstream river basins (a.o. Ericson et al., 2006, Syvitski et al., 2009) draw much attention as a major factor leading to delta drowning. Although land subsidence has been acknowledged as key issue in some well-known cases, such as the Po delta and the Venice Lagoon (Teatini et al., 2005; Tosi et al., 2009; Teatini et al., 2011), the Rhine-Meuse delta (Van Asselen, 2010; Erkens et al., 2016; Koster, 2017), and Mississippi delta (e.g. Törnqvist et al., 2008), still little attention has been given to quantify regional and local processes driving land subsidence within deltas worldwide. As local subsidence rates can exceed absolute sea-level rise by an order of magnitude, it is presently the main driver of relative sea-level rise in many coastal mega-cities around the world (e.g. Holzer and Jonhson 1985; Gambolati and Teatini, 2015), and therefore has potentially far-reaching consequences for future delta livability. Quantitative estimates of subsidence and understanding of its underlying drivers and mechanisms are of primary importance to assess the impacts of contemporary and future rates of relative sea-level rise on low-lying deltas around the world. Moreover, when aiming to mitigate relative sea-level rise in a delta, subsidence lies within the sphere of influence of delta managers, in contract to the amount of upstream sediment supply, often due to the transboundary character of most major rivers, let alone global sea-level rise.

For many large delta systems in the world, amounts and rates of land subsidence have yet to be determined; measuring and monitoring present-day subsidence is only the first step to deal with delta subsidence. To effectively integrate subsidence in delta management policy and support the development of adequate mitigation and adaptation strategies, projections of subsidence are needed (Erkens et al., 2015), together with assessments of the impact on future delta elevation and relative sea-level rise. Subsidence in a delta is a single expression of the cumulative effect arising from a variety of processes, steered by a range of driving mechanisms, active at different depths and time scales in the subsurface (Tosi et al., 2009; Galloway et al., 2016). Therefore, it is important to understand the functioning of each of these processes and drivers, and to quantify their individual contribution to delta subsidence to create projections of future subsidence. Achieving this for an entire delta system is a major challenge, as subsidence can be highly variable, both in space and time, due to subsurface heterogeneity, differences in variety and intensity of driving mechanisms and variable response times and time lags of subsidence processes.

1.1 Land subsidence processes in deltas

Natural subsidence drivers and processes

Subsidence can result from a variety of natural processes associated with Earth's crust dynamics, such as tectonic movement, isostatic adjustment, and compaction of unconsolidated sediments under natural loading (by e.g. sediments, biomass, water or ice) (Fig 1.2). It is no coincidence that large delta systems are often located in tectonically subsiding basins at the fringes of continents. On geological timescales, tectonic subsidence creates the accommodation space that allows the deposition of a sequence of delta deposits stacked on top of each other, such as occurred during the Quaternary glacial cycles. Tectonic activity can occur at large regional or local scale. Isostatic adjustment is the viscoelastic response of the Earth's crust to the weight of sediment, water or ice. Glacial isotatic adjustment (GIA) is the associated response of the melting of ice sheets and can cause uplift in regions that were previously covered by land ice masses (Peltier and Andrews, 1976, Yuill et a., 2009). Loading by water of the continental shelves following Holocene sea-level rise (Jouet et al., 2008) and sediment loading by prograding delta systems (Ferrier et al., 2015) can also cause isostatic deformation.

The shallow subsurface of deltas consists of soft unconsolidated sediments, which are recently deposited during Holocene delta formation. Especially fine-grained deposits can be highly compressible and experience compaction during deposition and subsequent soil formation. When stress on unconsolidated sediments in the delta subsurface increases, for example through loading by addition of overburden material (driver), the intergranular skeletal matrix of the sediments compresses (process). In sand layers (aquifers), this deformation is typically elastic (reversible) and results in only small ground displacements. Fine-grained deposits (e.g. silt, clay and peat) are far more compressible and experience, next to elastic, also inelastic (i.e. viscous) compression when stress exceeds critical levels. The viscous compression of fine-grained deposits can be much larger than elastic compression and therefore, much of the experience subsidence in these deposits, once happened, is irreversible and permanent. For the sediments to consolidate, the pore-water trapped in the spaces between the sediment particles needs to escape. However, especially in low-permeable, fine-grained deposits, the weight of the overburden may increase faster than pore-water pressure can dissipate, creating a time lag in the consolidation response of the sediments. Furthermore, the restructuring of sediment particles, a process described as 'creep' (Buisman, 1936; Šuklje 1957; Bjerrum, 1967; Den Haan, 1994), causes additional time-dependent consolidation response. As a result consolidation can continue to happen long after the initial increase in overburden.

Natural compaction of a delta's subsurface leads to volume reduction expressed as subsidence of the delta surface and creates accommodation that, under natural circumstances with abundant sediment supply, is filled by new clastic and/or organic sediments. In turn, these new sediments increase the overburden of the underlying sediments and drive further compaction. The subsurface composition of shallow, unconsolidated sediments has a demonstrated relation with shallow subsidence rate, with higher rates associated with more and younger fine-grained material (e.g. Törnqvist et al., 2008; Van Asselen et al., 2009; Teatini et al., 2011; Higgins et al., 2014, Koster et al., 2018).

Human-induced subsidence drivers and processes

Human activities in deltas can enhance natural subsidence processes or create additional anthropogenic subsidence (Fig. 1.2). Shallow compaction processes can be accelerated by increasing load at the delta surface by infrastructure and buildings or by phreatic groundwater table lowering

through excessive drainage. Also, the lowering of the groundwater table causes aeration of the soil, which triggers decomposition of organic material (oxidation), and in turn leads to additional volume reduction and shallow consolidation (e.g. Schothorst, 1977; Van Asselen et al., 2009; Erkens et al., 2016; Koster et al., 2018). In the deeper subsurface, extraction of fluids, such as groundwater or hydrocarbons, can cause consolidation when it decreases the pore pressure within the subsurface reservoir layers (e.g. Pratt and Johnson, 1926; Poland and Davis, 1969; Tosi et al., 2009, Galloway et al., 2016). Groundwater overexploitation, when extraction volumes exceed recharge volumes by infiltrating surface or sea water (*driver*), is well-known to trigger aquifer-system compaction (process) which results in subsidence of the delta surface (*consequence*) (a.o. Poland and Davis, 1969; Galloway and Burbey, 2011; Gambolati and Teatini, 2015).

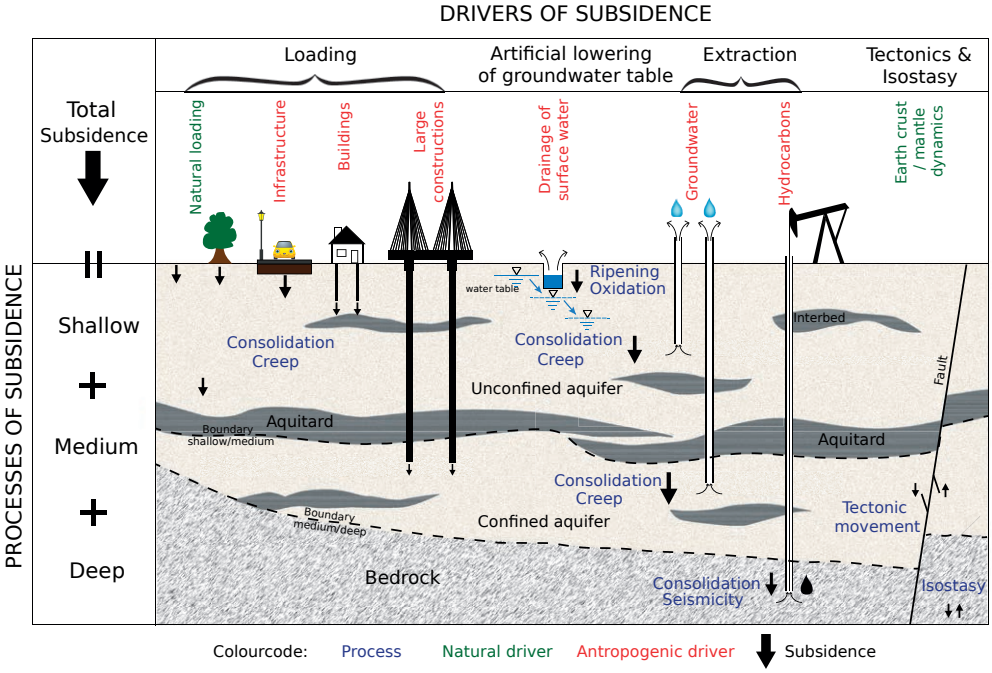

***Fig. 1.2** | Main drivers and processes of subsidence in a deltaic system. Subsidence drivers and processes act at different depths and time intervals. Generally, subsidence processes in the shallow subsurface cause local subsidence, while deeper processes can affect much larger areas.*

Deltas worldwide are experiencing rapid changes and become increasingly cultivated, populated and urbanized. With these changes, human-induced subsidence in deltas likely increases and as a result an increasing number of deltas is struggling to stay elevated above sea level (e.g. Syvitski et al., 2009). The Mekong delta is no exception to this: it is an example of a large, densely-populated and increasingly urbanizing mega-delta that is intensely cultivated for agriculture and aquaculture practices. It is facing the full range of typical issues related to relative sea-level rise in deltas, and experiences rates of subsidence exceeding those of absolute sea-level rise (Erban et al., 2014). However, the contribution to present delta subsidence of different drivers and processes is still unclear, and so are the potential impacts of future subsidence and associated relative sea-level rise on the sustainable livability of this delta in the coming century and beyond.

1.2 The Mekong delta

The Mekong delta, also known as C- u Long, '*Nine dragons*' in Vietnamese, named after the nine distributary channels of the Mekong river in the delta, is largely located in the south of Vietnam in South-East Asia (Fig. 1.3). The delta was formed during the second part of the Holocene, when global sea level reached its high stand after the last ice age. The combination of high sediment supply by the Mekong river, its wave-sheltered location (Anthony, 2015), and a relatively shallow Pleistocene substrate (~20 meter below present sea level) allowed the delta to prograde rapidly into the South China Sea (Nguyen et al., 2000; Ta et al., 2002; Tamura et al., 2012) and form the third largest delta plain on Earth (Coleman and Roberts, 1989), covering an area of 48.900 km^2 (Tessler et al., 2015). Underlying the shallow Holocene sediments, the subsurface of the Mekong delta consists of a sequence of stacked delta deposits from glacial cycles up to 500 meters depth till bedrock is reached, dating back to Miocene age (DGMS, 2004; Wagner et al., 2012). The Mekong delta's climate is tropical monsoonal and its natural vegetation consists of wetlands, swamps and, along the coastline, mangrove forests. Its flat delta plain is cross-cut by river branches and tidal creeks (Fig. 1.4).

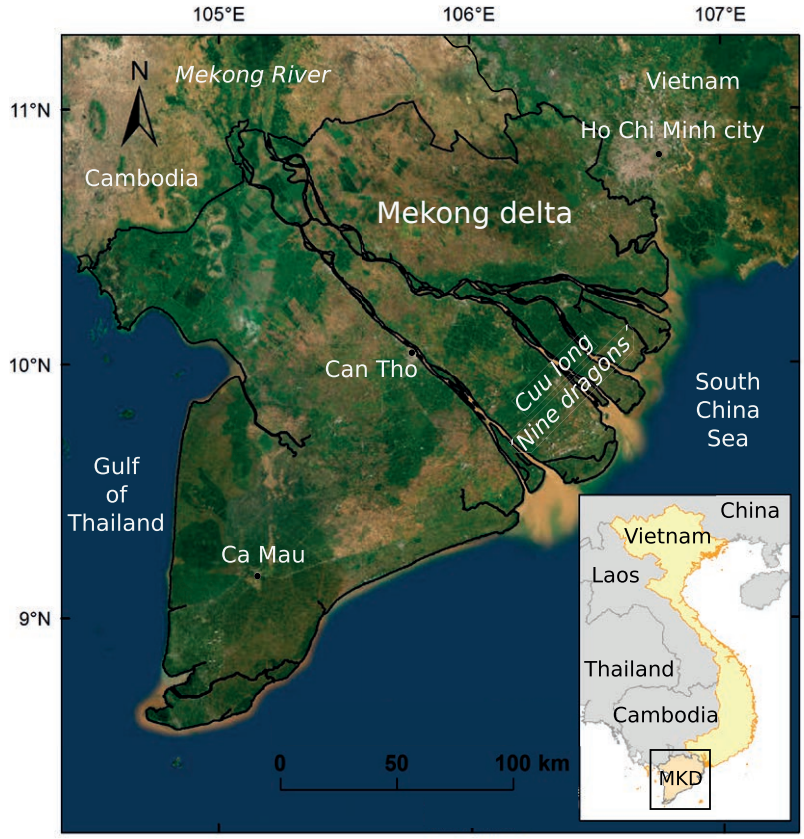

Fig. 1.3 | *Satelite image of the Mekong delta in the Vietnam in South-East Asia. Source satellite imagery: ESRI, DigitalGlobe, GeoEye, Earthstar Geographics, CNES/Airbus DS, USDA, USGS, AeroGRID, IGN, and the GIS User Community*

Fig. 1.4 *| Natural landscapes in the Mekong delta. A&B) Swamp and wetland forest in Tra Su Cajuput Forest in An Giang province. C) Mangroves at Dat Mui, the most southwest point of Ca Mau province. Tidal river channel connected to the Bassac river, Soc Trang province.*

Fig. 1.5 | *Rice production in the Mekong delta that earned the delta its nickname: 'Rice bowl' of Vietnam. A) Inundated rice fields in Kien Giang province. B&C) Rice fields, mixed with maize (B) in An Giang province.*

Presently, the Vietnamese Mekong delta is populated by nearly 18 million people (Renaud and Kuenzer, 2012), and the delta plain is intersected by numerous rivers, creeks and man-made channels and waterways, many of which date back to the French colonial period in the 19th and 20th century (Hung et al., 2012). Large-scale land-use changes, aiming to develop the agricultural and aquacultural potential of the delta, took place after the Vietnam War in 1975 (Nguyen and Viet, 2013). Vietnam's transformation to an open-market economy in 1986 (called 'Doi Moi') stimulated land-use change further and boasted agricultural and economical activities in the delta (Irvin, 1995; Funkenberg et al., 2014; Tran et al., 2015). In addition, the delta has become progressively urbanized, with an ever-densifying and expanding network of roads connecting the fast growing settlements, cities and urban areas (Karila et al., 2014).

The Mekong delta produces mainly rice (Fig. 1.5), but also substantial amounts of fruit, vegetables and aquaculture products, such as fish and shrimp (Fig. 1.6). The delta is one of world's most productive agricultural areas and provides income and food for over 60 million people, making it of vital importance to national and international food security (Renaud and Kuenzer, 2012).

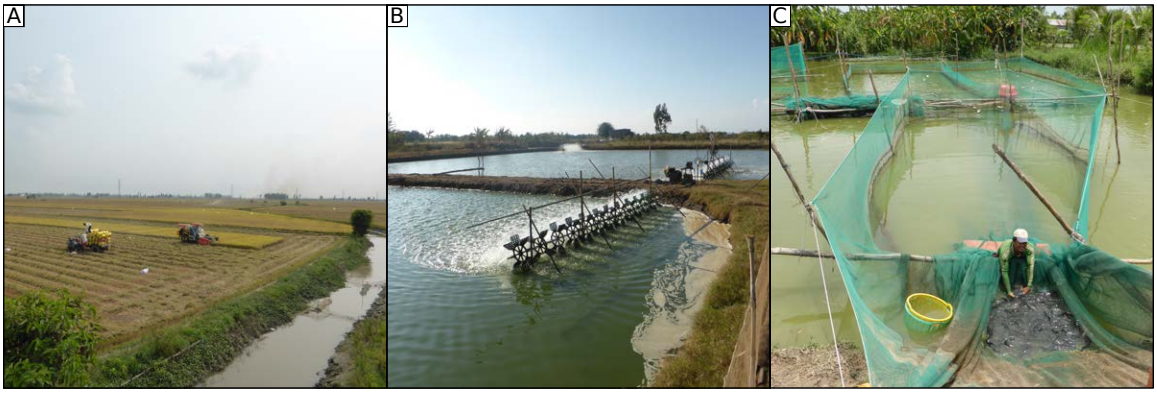

***Fig. 1.6** | Agricultural and aquaculture practices in the Mekong delta. A) Rice fields being harvested, An Giang Province. B) Shrimp farms, Bac Lieu province. C) Fish farms, An Giang province.*

Delta under pressure

The increased agricultural development and urbanization during the recent decades has increased anthropogenic pressure on the Mekong delta. At present only a very small part of the original land cover and vegetation remains, as the majority of the delta has been converted to agricultural and aquaculture area (Tran et al., 2015). The development and intensification of agricultural practice were partly fueled by easy access to untaxed, high-quality fresh groundwater, which led to a strong increase in the amount of groundwater used over the past decades (Wagner et al., 2012). Groundwater overexploitation resulted in depletion of the aquifer systems, and whereas hydraulic heads (i.e. water pressure) in the aquifers were previously reported as being artesian (Anderson, 1978), they have presently dropped to levels well below the delta plain surface (Wagner et al., 2012). This increasingly leads to salinization of the groundwater system, as fresh groundwater is replaced by salt water. The surface water system of the Mekong delta is also experiencing increased salt-water intrusion (Renaud et al., 2015; Smaglj et al., 2015). In the upstream catchment of the Mekong river the construction of hydropower dams have caused sediment trapping, resulting in a decreasing fluvial sediment supply to the delta (a.o. Kummu and Varis, 2007; Kondolf et al., 2014, 2018; Manh et al., 2015; Allison et al., 2017; Li et al., 2017), on top of the natural decrease in sediment supply cause by reduced hurricane activity (Darby et al., 2016). Within the delta itself, flood control through an extensive dyke system also hampers sedimentation by preventing seasonal flooding and overbank deposition (Triet et al., 2017; Tran et al., 2018). Extensive sand mining in the river branches is accelerating river-bank erosion (Brunier et al., 2014), and adds to a sediment deficit at the delta coast, which presently experiences increased rates of coastal erosion (Anthony et al., 2015; Li et al., 2017).

Like all coastal areas in the world, the Mekong delta faces accelerating global sea-level rise (Wassmann et al., 2004) and, on top of that, the delta itself is subsiding at rates up to several centimeters per year (Erban et al., 2014). For these reasons, the Mekong delta has been classified as 'delta in peril' (Syvitski et al., 2009), with a considerable risk to tip towards a 'collapsed' state if

construction of upstream dams significantly alters water and sediment fluxes (Renaud et al., 2013). Awareness in the Mekong delta is increasing and much effort is undertaken by the Vietnamese government, with intergovernmental cooperation, e.g. Mekong Delta Master Plan (1993) and Mekong delta plan (MDP, 2013), and through large World Bank loans to ensure a sustainable development of the Mekong delta. However, as the effects of subsidence in the Mekong delta is still largely '*terra incognita*', this requires serious attention as it poses uncharted risks.

1.3 Subsidence in the Mekong delta

Evidence of past subsidence can be witnessed in many places across the Mekong delta (Fig. 1.7). In recent years, the awareness of subsidence in the Mekong delta has grown, and measurements of subsidence have become available. At several locations in the delta shallow subsidence of Holocene deposits and sediment accretion is measured using Surface Elevation Tables (SETs) combined with marker horizons (Giao et al., 2014). At three locations in mangrove forests at the coast, average subsidence rates ranging from 25-41 mm yr^{-1} have been measured by SET since 2014 (Lovelock et al., 2015). More inland within the Mekong delta plain, SETs measured lowering between 5.5 and 7.8 mm yr^{-1}, and at the apex of the delta near the Cambodian border 5.8 mm yr^{-1} was measured (Nguyen et al., 2015). Additionally, Fujihara et al (2015) used river stage measurements from 1987-2006 to determine an average subsidence rate of 6 mm yr^{-1} for the central part of the delta around the main river channels of the Mekong river and a similar analysis by Takagi et al. (2016) on river stage measurements in Can Tho city from 1993-2013 revealed an average subsidence rate of 17 mm yr^{-1}. In the south of the Mekong delta in the province of Ca Mau, three extensometers, registering subsidence for the top 100 meters of the delta subsurface, have recently been installed and first measurements reveal rates of respectively 6, 15 and 22 mm yr^{-1} (NGI, 2017; Karlsrud and Vangelsten, 2017). Beside these ground measurements of subsidence, Erban et al. (2013; 2014) provided a first map based on satellite-based Interferometric Synthetic Aperture Radar (InSAR) measurements during the period 2006-2010 showing subsidence rates estimates ranging from 10-40 mm yr^{-1} for a large part of the Mekong delta.

***Fig. 1.7** | Evidence of subsidence in the Mekong delta. A) Cracks in a bridge ramp caused by shallow subsidence. B) Protruding groundwater well evident by the cracked concrete floor and bended pipe. C) Abandoned protruding groundwater well. The original delta surface when the well was installed is indicated by the author's right hand.*

Proposed drivers of subsidence

Several processes have been proposed to be causing subsidence in the Mekong delta, but conflicting opinions exist on the main driver. Based on the InSAR-derived subsidence estimates in combination with measurements of hydraulic head drawdown, hydrogeological modeling and 1D consolidation computations, Erban et al. (2013, 2014) suggested groundwater extraction as a major driver of subsidence. Whereas Nguyen et al. (2015) concluded from SET measurements of shallow subsidence in coastal mangrove forests and hydrogeological computations on deeper sediments that groundwater extraction '*plays a very small role*' and that consolidation of the shallow clay layer is the main cause of subsidence in the Mekong delta. The Department of Geology and Minerals of Vietnam (DGMV, unpublished internal report) reached the conclusion that neo-tectonic movement is the primary source of subsidence in the delta. Each of these drivers may thus potentially be a main contributor to subsidence in the Mekong delta, and their contribution may also differ spatially and temporally across the delta.

Showcase of a global challenge

The Mekong delta provides a pre-eminent opportunity to unravel and quantify different driving mechanisms of subsidence, as large changes like high population growth, intensification of land-use practices and urbanization happened only relatively recently and hydrogeological observations cover almost the entire period of human disturbance of the groundwater system in the subsurface. Also because future subsidence and consequent relative sea-level rise may have far-reaching consequences for this exemplar mega-delta.

To target these delta issues, the research project: '*Rise and Fall: strategies for the subsiding and urbanizing Mekong Delta (Vietnam) facing increasing salt water intrusion*' of which the research of this thesis was part of, was established. The Rise and Fall research project is part of the Dutch "Urbanizing Deltas of the World" (UDW) research programme funded by the Dutch Scientific organization (NWO, grant: W 07.69.105) and co-financed by Deltares Research Institute and TNO-Geological Survey of the Netherlands. The project was carried out by Utrecht University in collaboration with Dutch partners: Deltares and TNO, and Vietnamese partners: Can Tho University, Division of Water Resources Planning and Investigation for the South of Vietnam (DWRPIS), Southern Institute of Water Resources Research (SIWRR) and Southern Institute of Water Resources Planning (SIWRP). The main objective of the Rise and Fall project was to enhance the capabilities of individuals and organizations to develop sustainable strategies to deal with land subsidence and salt water intrusion in the increasingly urbanizing Mekong delta.

The research reported in this thesis focuses mainly on two driving mechanisms that are known to have the potential to cause *delta-wide* subsidence at rates that can largely exceed absolute sea-level rise: 1) Compaction of shallow subsurface sediments and 2) aquifer-system compaction as a result of groundwater extraction. The presence of both mechanisms is indicated for the Mekong delta as SET measurements reveal high rates of shallow sediment compaction (Lovelock et al., 2015) and the hydraulic heads drops witnessed in the Mekong delta's aquifer-system (Wagner et al., 2012) are known to potentially drive high rates of aquifer-compaction. The quantification of the relative contribution of these two drivers at delta-scale is a prerequisite to enable the development of sustainable and effective mitigation and adaptation strategies to deal with future relative sea-level rise.

1.4 Research objectives and approach

This research aimed to enhance the quantitative understanding of drivers, mechanisms and processes causing land subsidence in deltas, and building on these insights, to predict future subsidence rates to improve assessments of relative sea-level. This thesis focuses on the Mekong delta in Vietnam, as an exemplar mega-delta to serve as a model for deltas elsewhere in the world. The main objective of this research was:

- *To understand and quantify the main natural and human-induced drivers and processes causing subsidence, and its impact on current and future surface elevation of the Vietnamese Mekong delta.*

To reach this objective, the research was subdivided into different steps, each with separate research objectives, reported in different parts of this thesis. In the first step, the current elevation of the Mekong delta to local sea level is quantified as this determines the vulnerability of a delta system to relative sea-level rise and the relative impact of delta subsidence (Chapter 2). The second step consists of a quantification of the contribution of potential causes of delta subsidence (Chapter 3-5, 7). The third step is to evaluate future delta subsidence following different groundwater management scenarios and the impact of consequent relative sea-level rise on the Mekong delta (Chapter 6-7). The following sub-questions are addressed in this thesis:

Step 1: Determining the current elevation of the delta

1. How high is the Mekong delta surface presently elevated above local mean sea level?

Step 2: Quantifying the individual contribution of main subsidence mechanisms

2. How much natural compaction occurs at present in the Holocene deposits of the Mekong delta following delta progradation?
3. Is land subsidence related to land use in the Mekong delta? Is there a spatial correlation, and which are the causal mechanisms?
4. How much land subsidence in the Mekong delta has been caused by increased groundwater extraction during the past decades?
5. Which drivers and processes are predominantly causing present-day subsidence in the Mekong delta?

Step 3: Future subsidence of the delta and the impact of relative sea-level rise

6. By how much may the Mekong delta subside in the coming century as a result of groundwater extraction, and how much of this subsidence can be mitigated?
7. Can restoring natural deposition of Mekong river sediment compensate the elevation loss by subsidence of the delta?
8. When will certain parts of the delta fall below sea level in the coming century?

To determine the present-day elevation of the Mekong delta above sea level, different digital elevation models, both spaceborne and interpolated from elevation points from a detailed topographical map, were compared. Their accuracy and overall quality in terms of absolute and relative elevation were validated using elevation benchmarks and comparison with elevations of geomorphological features and occurrences of tide-dominated inundation (Chapter 2).

To determine present and potential future rates of natural compaction of young sediments in the Mekong delta, data on the age and rates of Holocene delta progradation, lithological borelogs, geotechnical data and measurements of present shallow compaction were used to build a novel 2D numerical model to simulate the Holocene delta evolution for the southern Mekong delta (Chapter 3).

To assess the impact of land use on subsidence in the Mekong delta, a time series of land-use maps (1988-2009) was created for a large part of the delta using satellite images, providing insight on land use and land-use history over the past ~30 years. The land-use map time series was spatially compared to a dataset of subsidence rate estimates derived by InSAR to quantify the impact of different land use practices and land-use history on subsidence rate in the Mekong delta. Subsequently, by assessing the ability to predict subsidence rates based solely on land use and land-use history, the strength of the relationship was tested, and underlying potential causal mechanisms were evaluated (Chapter 4).

The impact of past, present and future groundwater extraction in the Mekong delta was assessed by creating the first 3D hydrogeological numerical model of an entire mega-delta which could resolve both the hydrogeological and geotechnical response of the multi-aquifer system, using a 1D subsidence module. The model was based on large datasets containing hydrogeological, geological, lithological, geotechnical information on the multi-aquifer system in the subsurface of the delta. Measured time series of hydraulic heads together with databases on groundwater extraction provided data that enables the simulation of the hydrogeological development of the Mekong delta and consequent aquifer-system compaction during the past decades until the preset (Chapter 5). Furthermore, the numerical model was used to calculate future extraction-induced subsidence based on different scenarios of future groundwater use (Chapter 6).

The quantifications of natural compaction and extraction-induced subsidence for the Mekong delta were used in combination with InSAR-derived estimates of subsidence to assess their ability to explain observed subsidence in the Mekong delta and evaluate the potential impact of other driving mechanisms and processes. Their impact on delta-wide elevation loss were quantified and combined with information from literature on Mekong river sediment volumes and absolute-sea level rise to create a sediment balance for the delta. Lastly, by combining delta elevation with rates of future relative sea-level rise, the impact on future delta elevation and the timing of potential permanent inundation were subsequently quantified (Chapter 7).

2 What is the elevation of the Mekong delta? Accurate elevation data crucial to sea-level rise impact assessments in deltas

Submitted manuscript: Minderhoud, P.S.J., Coumou, L., Erkens, G., Middelkoop, H., Stouthamer, E. **What is the elevation of the Mekong delta? Accurate elevation data crucial to sea-level rise impact assessments in deltas.** *(in review)*

2.1 Introduction

Worldwide over 500 million people living in deltaic areas are increasingly exposed to flood hazards arising from climate extremes and relative sea-level rise (Giosan et al., 2014; Tessler et al., 2015). The combined effect of relative sea-level rise (RSLS), the result of absolute sea-level rise and land subsidence, and reduced sediment aggradation on the delta surface causes many deltas to lose elevation relative to sea level (Syvitski et al., 2009; Higgins, 2015). Elevation loss increases the vulnerability to floods and storm surges and ultimately threatens deltas with permanent inundation. Impact assessments of relative sea-level rise are valuable sources of information for policy makers. The quality of aforementioned assessments primarily relies on the accuracy of available elevation data. To date, various types of elevation datasets exist with different spatial coverages, and horizontal and vertical resolutions, derived from space-borne or air-borne remote sensing surveys, photogrammetric surveys, or direct geodetic surface measurements. The accuracy of these different data types is highly variable, so are the inherent assessments of potential delta drowning.

Digital elevation models (DEMs) have been the subject of numerous studies, focusing on DEM accuracy and comparison between different DEMs (Vaze et al., 2010; Mukherjee et al., 2012), implications of DEM inaccuracy for river flood mapping (Cook and Merware, 2009; Schumann et al., 2008) and required DEM corrections for hydrodynamic modelling (Jarihani et al., 2015; Yamazaki et al., 2012). Still few studies specifically focused on the effect of DEM accuracy on assessments of impacts of sea-level rise on flat coastal areas that are only slightly elevated above sea level (Kulp and Strauss, 2016). Global, spaceborne DEMs, like the Shuttle Radar Topography Mission (SRTM) DEM (Farr et al., 2007) or the TanDEM-X WorldDEM (Krieger et al., 2007), have a typical vertical accuracy of several meters, while the vertical resolution is too coarse to capture the subtle elevation differences in the order of decimeters required for accurate SLR impact assessments of flat delta regions (Keunzer et al., 2013; Schumann et al., 2014). Clearly, these global satellite-borne DEM-products were not designed for such purpose. In contrast, airborne LiDAR measurements or surface leveled elevation data (e.g. obtained from detailed topographical maps) can be used to create DEMs that do capture these low-gradient elevation differences (Cook et al., 2009; Schumann et al., 2008). A comparison between SRTM-based DEMs with high-accuracy LiDAR data in the United States showed the tendency of SRTM-based estimates to underestimate sea-level rise impacts for lower elevated coastal areas due to DEM errors (Kulp and Strauss, 2016). Unfortunately, as many deltas around the world are located in data sparse regions, high-accuracy elevation data is often

not available, or - when existing - not publicly accessible. Consequently, global DEMs derived from space-borne surveys are generally the only available elevation models and, in spite of their low vertical accuracy, many delta studies use these as a basis for assessments of delta elevation above sea level (e.g. Syvitski et al., 2009), flood risk and impacts of e.g. relative sea-level rise or storm surges (Woodruff et al., 2013; Muis et al., 2016). The lack of alternative elevation data makes it very hard to determine the spaceborne DEM inaccuracy locally, and hence to quantify the uncertainty in the impact assessments. Here we aim to address this issue by comparing DEMs derived from SRTM data to a DEM derived from geodetic survey and photogrammetric data represented on topographic maps for the Vietnamese Mekong delta. Our findings for this exemplar mega-delta demonstrate the potential effects of DEM inaccuracy on impact assessments of sea-level rise for large data-sparse deltas, and demonstrates the need of accurate DEMs for this purpose.

The Mekong delta has one of the largest and seemingly lowest elevated delta plains in the world (Syvitski et al., 2009). While ongoing land subsidence increases the rates of RSLR in the delta (Erban et al., 2014, this thesis) the sediment load of the Mekong river to counterbalance RSLR with sediment accretion on the delta plain is dwindling due to upstream dam construction (Kondolf et al., 2014; Manh et al., 2015) and decreased hurricane activity in the Mekong catchment (Darby et al., 2016). In spite of the awareness of their low vertical accuracy and resolution of global DEMs within a large scientific community (Kuenzer et al., 2013; Schumann et al., 2014), several studies did use SRTM elevation data (Carey-Reid, 2008; Warner et al., 2010; Kondolf et al., 2018) to assess potential impacts of RSLR for the Mekong delta (Fig. 2.1). Resulting products from such studies, such as inundation maps, have been adopted in policy advisory reports (MRC, 2009; WWF, 2009; ADB, 2013; MDP, 2013; Warner et al., 2009) (Fig. 2.1B & 2.1C). Remarkably, resulting flood zone maps reflect the NE-SW-orientated striping pattern present in the underlying SRTM DEM, obviously showing inaccuracies in the SRTM DEM rather than the actual delta elevation differences. Hence, the use of such SRTM DEM-derived flood maps in policy advisory reports can potentially have far-reaching negative consequences as they may misinform delta policymakers.

Recently, the MERIT (Multi-Error-Removed Improved-Terrain) DEM was developed, in which multiple height errors existing in global DEMs, a.o. the SRTM DEM, have been removed in a consistent way (Yamazaki et al., 2017). The authors report an improvement of vertical accuracy (from 39% to 58% of the land areas mapped with ±2 m or better), and the MERIT DEM was presented as especially helpful for flood inundation modeling since it significantly improved landscape representation for flat regions. The MERIT DEM thus might improve future sea-level rise assessments for the Mekong delta, although its vertical accuracy remains low when compared to magnitudes of sea-level rise over the coming century (typically ranging between 0.2 and 1 m).

For our study we have acquired a large dataset of elevation points from a detailed topographical map of the Vietnamese Mekong delta; these elevation data were previously unavailable for users outside Vietnamese government institutes. We created a new elevation model for the delta based on the topographical map elevations (Topo DEM) and compared this with the SRTM and the MERIT DEMs of the Mekong delta. We performed three independent analyses to evaluate the elevation accuracy of all DEMs. For these analyses, we used an independent dataset of elevation points providing absolute elevation to Vietnamese geodetic datum. Besides, we analyzed the relative elevation patterns by comparing the DEMs to a geomorphological map and a dataset of tide-dominant flood occurrences. Subsequently, we quantified the influence of using different DEMs on relative sea-level rise impact assessments by comparing the results in terms of affected area and amount of inhabitants to underscore the large uncertainties associated with the use of spaceborne DEMs.

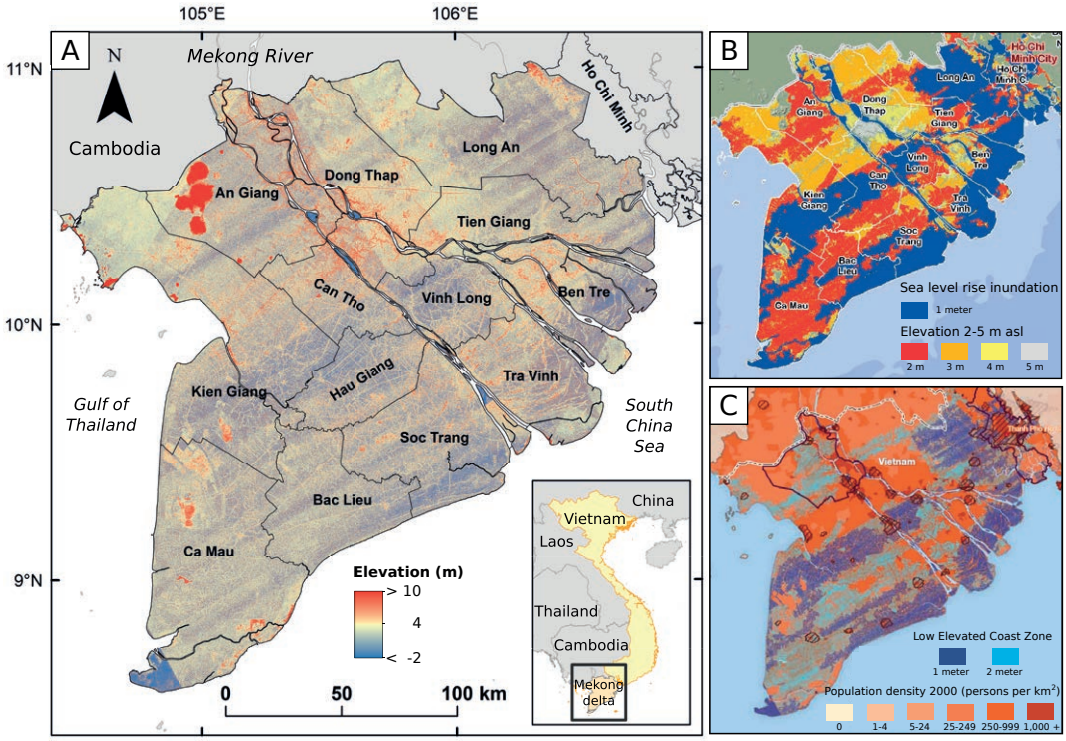

Figure 2.1 *| A) Shuttle Radar Topography Mission (SRTM) Digital Elevation Model (DEM) of the Mekong delta in Vietnam and B-C) inundation maps following sea-level rise based on the SRTM DEM containing effects of striping and other height errors. B) Inundation zones with meters sea-level rise (Carew-Reid, 2008). This map was included in several policy documents a.o. Asian Development Bank (ADB, 2013), Mekong River commission technical paper (MRC, 2014); World Wildlife fund risk assessment Mekong (WWF, 2009) and the Dutch-Vietnamese Mekong Delta Plan (MDP, 2013) which is now a leading document for major Worldbank projects in the delta. C) Low elevated coast zone with population density (Warner et al., 2009, 2010), copyright by 2008 CARE International and UN University. Used by permission. This map was included in o.a. the risk assessment Mekong by the World Wildlife Fund (WWF, 2009).*

2.2 Data and Methods

2.2.1 Spaceborne elevation model: SRTM DEM

The Shuttle Radar Topography Mission (SRTM) Digital Elevation Model (DEM) was created from phase-difference measurements of interferometric synthetic aperture radar (InSAR) collected in February 2000 and was the first near-global topography product for the Earth acquired in a consistent way (Farr et al., 2007). The SRTM was designed to create a DEM with an absolute vertical accuracy of 16 m and this goal was met as 90% of the absolute height errors is <9 m (Rodriguez et al., 2005, 2006). The SRTM DEM is a digital surface model, describing the elevation of the Earth's surface including objects at the surface, like buildings and vegetation. Therefore, the SRTM DEM has a tendency to overestimate actual ground surface elevation. There are different versions of the

SRTM DEM available and efforts have been made to optimize the SRTM DEM, for example through vegetation removal (Su and Guo, 2014; O'Loughlin et al., 2016). Previously published SLR impact assessments for the Mekong delta used basic versions of the SRTM DEM, readily available through online portals, and no post-processing steps were performed to optimize the SRTM DEM for the studied area (Carew-Reid, 2008; Warner et al., 2010; Warner et al., 2009). As this paper aims to assess the effect of using a basic version of the SRTM DEM for SLR assessments, we also selected a readily downloadable and widely-used version of the SRTM DEM without performing post-processing corrections. We used the SRTM Plus (or void-filled) DEM version 3.0 with an one-arc second grid, approximately ~30 x 30 m and a vertical resolution of 1 meter (DEM available through: lpdaac.usgs.gov/data_access/data_pool).

2.2.2 Spaceborne elevation model: MERIT DEM

The high-accuracy global MERIT DEM (Multi-Error-Removed Improved-Terrain DEM)(Yamazaki et al., 2017) was developed by removing major error components, i.e. absolute bias, stripe noise, speckle noise, and tree height bias from existing DEMs. For the Mekong delta region, the MERIT DEM uses the SRTM DEM as baseline, and unobserved areas were filled with the Viewfinder Panoramas DEM. To portray the improvements of the MERIT DEM, the Mekong delta was used as example on the data portal website (http://hydro.iis.u-tokyo.ac.jp/~yamadai/MERIT_DEM/). We acquired the MERIT DEM for the Mekong delta from the data portal.

Both the SRTM and the MERIT DEMs contain an obvious elevation error in the southwest corner of the delta where the elevation is <-1 m below MSL (Appendix A, Fig. A.1a). This part of the SRTM and MERIT DEM was therefore omitted in the DEM quality assessments in this study.

2.2.3 Topographical elevation model: Topo DEM

Elevation points from topographic map

We acquired a dataset with almost 20.000 elevation points located in the Vietnamese Mekong delta from the Division of Water Resources Planning and Investigation of the South of Vietnam derived from the national topographical map of 2014 (scale 1:200,000) made by the Department of Survey and Mapping of Vietnam, part of Vietnam's Ministry of Natural Resources and Environment (Fig. 2.2). The data is projected in the VN-2000 coordinate reference system and vertically referenced to the Vietnam's geodetic Hon Dau datum, which has its elevation origin at mean sea level (MSL) of the Hon Dau tide gauge, an island offshore of Hai Phong in North Vietnam. The applied measurement technique of the elevation points present in the topographical map is not documented, limiting accuracy assessment of the provided elevations. Furthermore, a potential offset between mean sea level at the Hon Dau tide gauge (defining its zero datum level) and mean sea level in the Mekong delta cannot be excluded. These uncertainties in the provided elevation relative to local sea level along the Mekong delta reduces the suitability of the dataset for SLR impact assessments. Still, this topographical dataset is presently the only available local elevation data for the Mekong delta, apart from the global DEMs.

The dataset has an average point density of 0.51 points per km^2. The precision of the elevation indicated on the maps is 0.1 m for elevation points up to +2 m. Between +2 m and +3 m the elevations are given at 0.5 m intervals, elevations higher than +3 m are documented with intervals of 1 m.

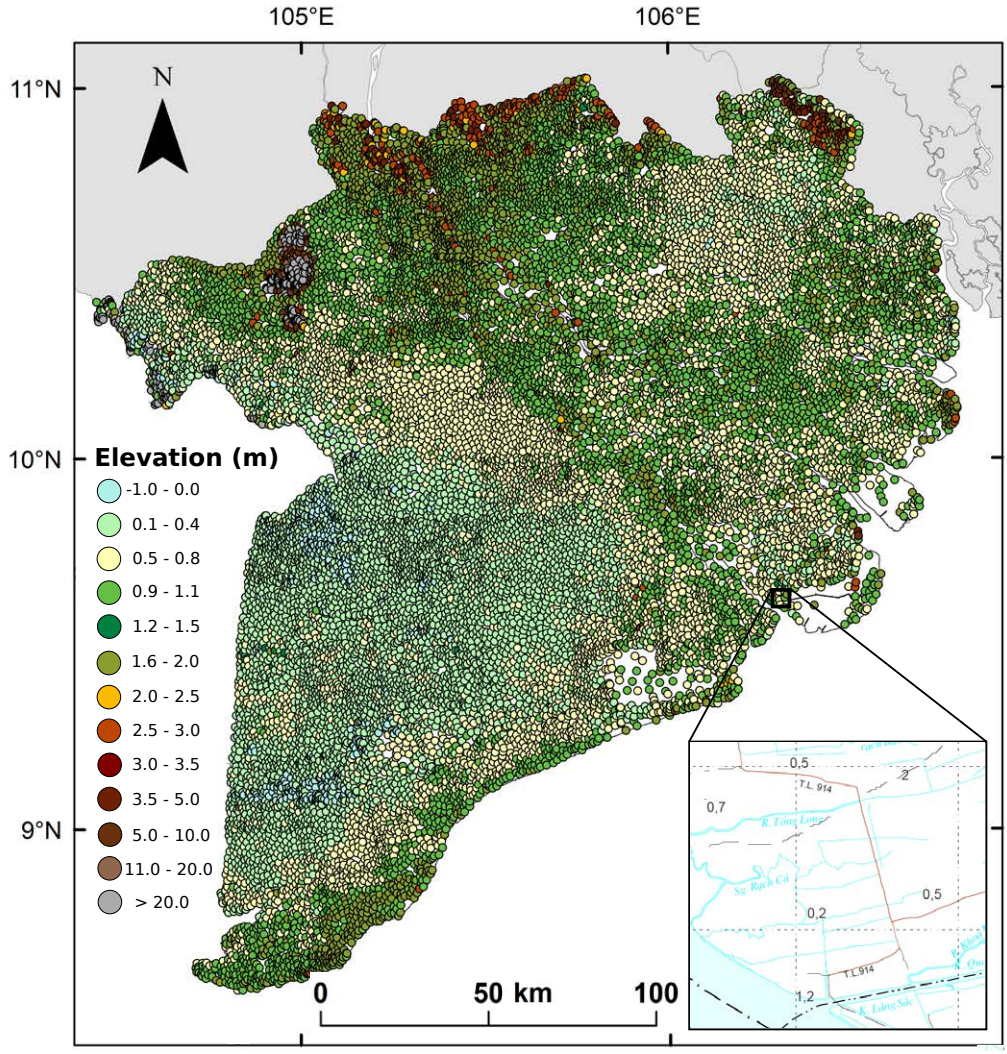

Figure 2.2 | *Elevation points used to create the topographic (Topo) DEM. The dataset contains almost 20.000 points derived from a national digital topographical map by the Department of Survey and Mapping of Vietnam (2014).*

Topographical DEM interpolation

We interpolated the elevation points to create a smooth, delta-wide, topographical (Topo) DEM. A grid cell size of 500 x 500 m is appropriate based on the optimal points per grid cell (Aguilar et al., 2006) and the point density of the dataset (0.51 m km^{-1}). A larger cell size would result in an increased RMSE, while a smaller cell size would result in an unfounded higher resolution. The Topo DEM resulting from the interpolation has an average root mean square error (RMSE) of 0.16 m that spatially increases with decreasing elevation point density and increasing local elevation variation (see RMSE map in the supplementary information (Appendix A, Fig. A.1)).

We tested several interpolation methods available in the 3D analyst and geostatistical analyst toolbox of ArcMap v.10.3.1., i.e. Inverse distance weighting, ordinary kriging, empirical Bayesian kriging, nearest neighbor, spline and ANUDEM. We compared the resulting DEMs based on a statistical analysis using 120 randomly distributed control points (a subset from the elevation points excluded from the interpolation) and inspection of interpolation correctness in areas with large elevation differences (e.g. spline interpolation created erroneous negative elevations around higher elevated bed rock outcrops). The DEM interpolated using empirical Bayesian kriging employing empirical data transformation and an exponential model produced the lowest mean absolute deviation of all control points (0.22 m) and interpolated realistically between points with larger elevation differences. As a result, this method was selected to interpolate the Topo DEM. Before interpolation, all elevation points exceeding individual elevations of +10 m were removed from the dataset. These points are located on highly elevated limestone outcrops towering above the otherwise flat delta plain and including them in the interpolation would inevitably introduce errors to the elevation of the flat delta plain in the immediate surroundings. After interpolation, these areas with elevated limestone bedrock outcrops were excluded from further analyses using a shapefile delineating them based on Google Earth imagery. Furthermore, the large Mekong river branches were removed from the Topo DEM, which is also the case for the SRTM DEM.

2.2.4 DEM quality assessment

To evaluate and validate the SRTM, the MERIT and the new Topo DEM, we performed three analyses, one to evaluate the absolute elevation using an independent dataset of absolute surface elevation measurements referenced to Vietnam's geodetic datum, and two tests to evaluate relative elevation correctness.

Absolute elevation validation

We evaluated the absolute elevation of the DEMs relative to Vietnam's geodetic datum using an independent dataset of 69 national benchmark elevation measurements throughout the delta managed by the Department of Survey and Mapping of Vietnam (see Appendix A for benchmark locations, Fig. A.4 and values, Table A.1). The dataset provides coordinates (VN-2000) and vertical elevation at mm precision referenced to Vietnam 2000 geodetic Hon Dau datum (origin at MSL at Hon Dau tide gauge). The geodetic network of national benchmarks in South Vietnam was built by radio-positioning and traverse measurement techniques connected to stable points with known elevation at bedrock outcrops at the edge of the delta plain (Dang & Le, ND). Vertical elevation accuracy of the measurements is not publicly documented. Benchmarks are reportedly located ~30 cm below terrain surface for protection (see Appendix A, Fig. A.3), however it is uncertain whether this is the case for all benchmarks in the dataset. As we compare the elevation of point locations to the average elevation of an entire grid cell (30 m x 30 m for the STRM DEM, 94 m x 94 m for the MERIT DEM and 500 m x 500 m for the Topo DEM), we do expect differences between individual elevation points and the elevation models cells. If the overall elevation of the DEM is in agreement with the overall benchmark elevation, the residuals are expected to show a narrow, non-skewed normal distribution centered at zero.

Validation of spatial patterns of relative elevation

We assessed the correctness of the spatial distribution of relative elevation of the DEMs by using two datasets that function as proxy for relative elevation: i) a geomorphological map (Nguyen et al., 2000) and ii) a flood occurrence map (Kuenzer et al., 2013).

Geomorphological map

The geomorphological map of the Vietnamese Mekong delta (Nguyen et al., 2000) was mapped using aerial photographs and satellite images combined with field surveys, cored sediment samples and paleoenvironmental assessment using microfossils. It shows the presence and distribution of different geomorphological regions and features throughout the delta (Fig. 2.3). In a natural setting, each geomorphological unit is characterized by a certain elevation relative to other geomorphological units because on differences in depositional environment (Fig. 2.4). For example, natural levees and beach ridges are higher elevated than adjacent flood basins and coastal plains. Therefore, the geomorphological map can serve as proxy for spatial relative elevation distribution. A correct DEM should provide a similar logical elevation pattern, correctly reflecting the relative elevation of the different geomorphological units. We digitized the geomorphological map into a polygon shapefile in ArcMap and extracted the DEMs statistics per geomorphological unit.

We grouped the geomorphological units in three categories that characterize depositional environments with a typical elevation distribution. The first category consists of the Pleistocene geomorphological units, which are mainly found in the N and NW of the Vietnamese Mekong delta. We expect all Pleistocene deposits to be higher elevated than the younger Holocene deposits, because, otherwise, they would have been buried by Holocene onlap deposits. Within the Holocene deposits, we distinguish between the higher elevated, alluvial landscape in the Upper delta plain and the lower elevated coastal plain in the Lower delta plain (Ta et al., 2005) (Fig. 2.3).

Within each category, we estimated the expected elevation of a geomorphological unit relative to the other units based on typical landscape geomorphology (Fig. 2.4A; Table 2.1). For the alluvial landscape of the Upper delta plain, we based our expected relative elevation on typical channel belt and floodplain morphology in lowlands (Bridge, 2003). Natural levees are the highest elevated units, followed by channel bars and abandoned channel belts, which are in turn elevated higher than flood basins (partly as a result of post-depositional subsidence of soft flood basin soils). Swamps, requiring frequent flooded and waterlogged conditions, are located in the lowest parts of the landscape. For the coastal environments, we based the expected relative elevation on typical coastal morphology, with mangroves and relict sandy beach ridges separating the tidal flats from the back barrier salt marshes and coastal plain with fresh water marshes in the hinterland (Fig. 2.4B). The elevation of tidal flats at the coastline are expected to match high tide levels. Sand spits and especially relict beach ridges are generally elevated higher than the tidal flats. The near-coastal mangrove and salt marshes are expected to have a similar elevation as the tidal flats as they trap sediments during high tide. The back barrier coastal plain is expected to have a lower elevation, as a result of the combination of ongoing compaction of the Holocene strata (Chapter 3) and reduced sediment supply with progradation of the coastline. Inland marshes within the coastal plain are expected to have the lowest relative elevation, as they are located furthest away from the coastline and active tidal channels, which reduces sediment delivery even further. At delta scale, the coastal plain in the western part of the delta is expected to be lower elevated than the coastal plain in the east, as the nearby Gulf of Thailand only has a tidal range of 40 cm and no direct sediment delivery by rivers.

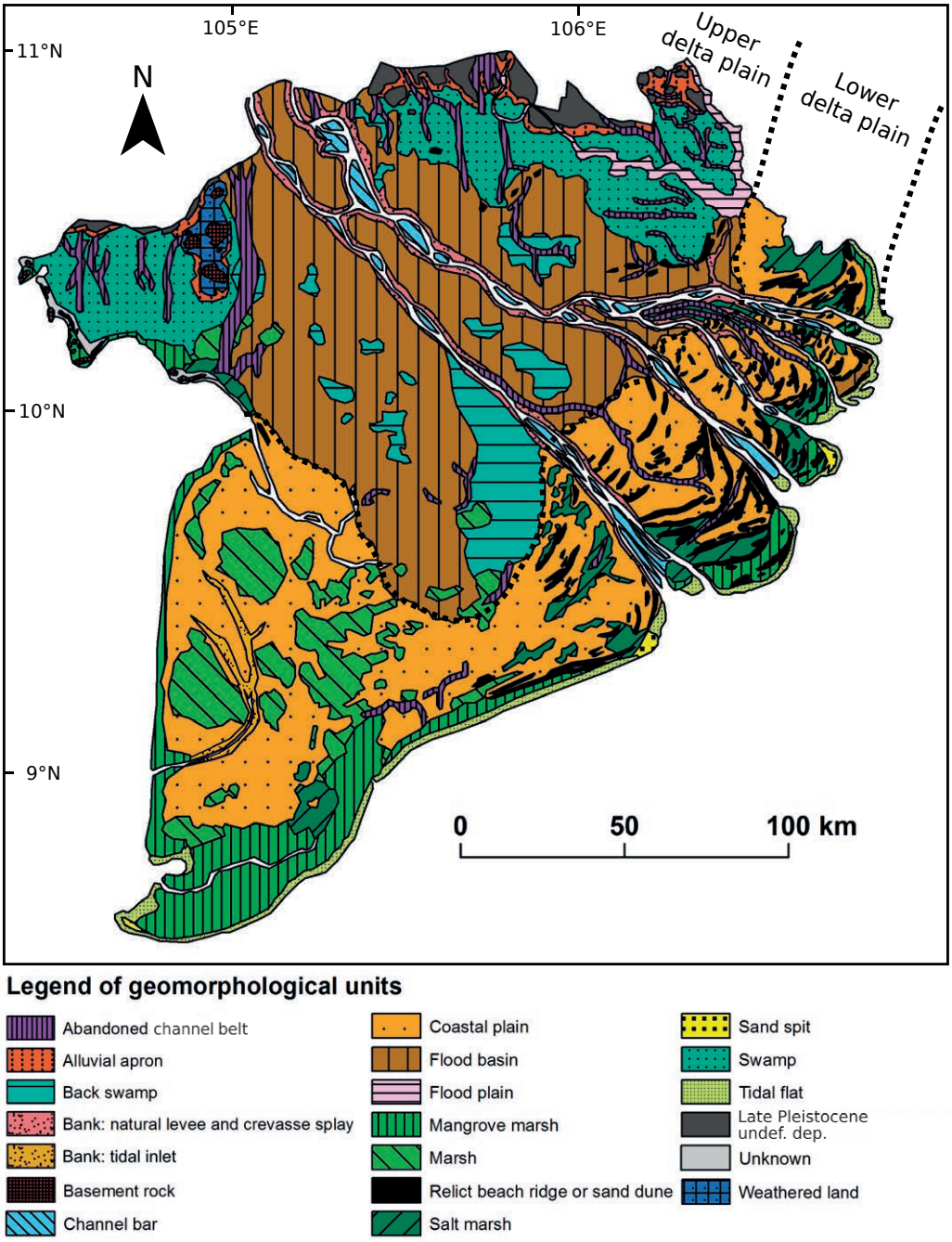

Figure 2.3 | *Geomorphological map of the Vietnamese Mekong delta based on Nguyen et al. (2000). The upper and lower Holocene delta plain delineate the separation between the predominantly alluvial and coastal depositional environment (Ta et al., 2005).*

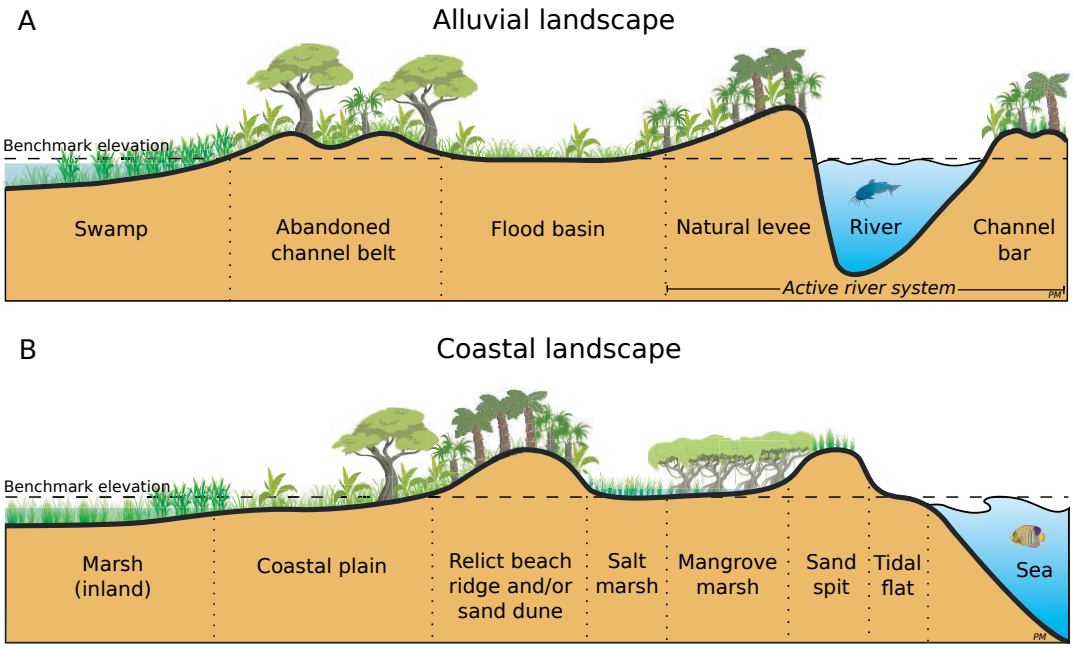

Figure 2.4 | *Schematic profiles with geomorphological units of the alluvial and coastal landscapes in the Mekong delta showing their relative elevation. The alluvial landscape (A) is representative for the Upper delta plain and the coastal landscape (B) for the Lower delta plain of the delta. The dashed horizontal line represents a benchmark elevation of the flood basin and the tidal flat for the relative elevation comparison of each geomorphological unit.*

Table 2.1 | *Relative elevation of geomorphological units in the Mekong delta.*

Category and age	Geomorphological unit	Relative elevation
Pleistocene (and older) deposits	Weathered land, bed rock outcrops	Very high, hills
	Late Pleistocene undifferentiated deposits	Higher than Holocene deposits
	Alluvial apron	Higher than Holocene deposits
Upper delta plain Holocene alluvial deposits	Flood basin	Benchmark [1]
	Bank: natural levees and crevasse splay	Highest (++)
	Channel bar	Higher (+)
	Abandoned channel belt	Higher (+)
	Swamp	Lower (-)
	Back swamp	Lower (-)
Lower delta plain Holocene coastal deposits	Tidal flat	Benchmark [1]
	Sand spit	Higher (+)
	Relict beach ridge or sand dune	Higher (+)
	Mangrove marsh	Equal (+/-)
	Salt marsh	Equal (+/-)
	Coastal plain	Lower (-)
	Marsh (inland)	Lowest (- -)

[1] *Benchmark of relative elevation for geomorphological units within its category*

Inundation occurrence

The second method to validate the spatial distribution of the relative elevation is based on the assumption that lower areas in the flat coastal zone are more often inundated than higher areas, either naturally-induced by flooding or human-induced for agri- and aquaculture purposes. Kuenzer et al. (2013) created 128 maps of the extent of floods in the Mekong delta from 2007 to 2011 based on Envisat ASAR-WSM (Advanced Synthetic Aperture Radar Wide Swath Mode) satellite images. Combing these maps resulted in a cumulative inundation map showing the number in which an area was inundated during this four year period with a grid cell size of 150 m (Fig. 2.5).

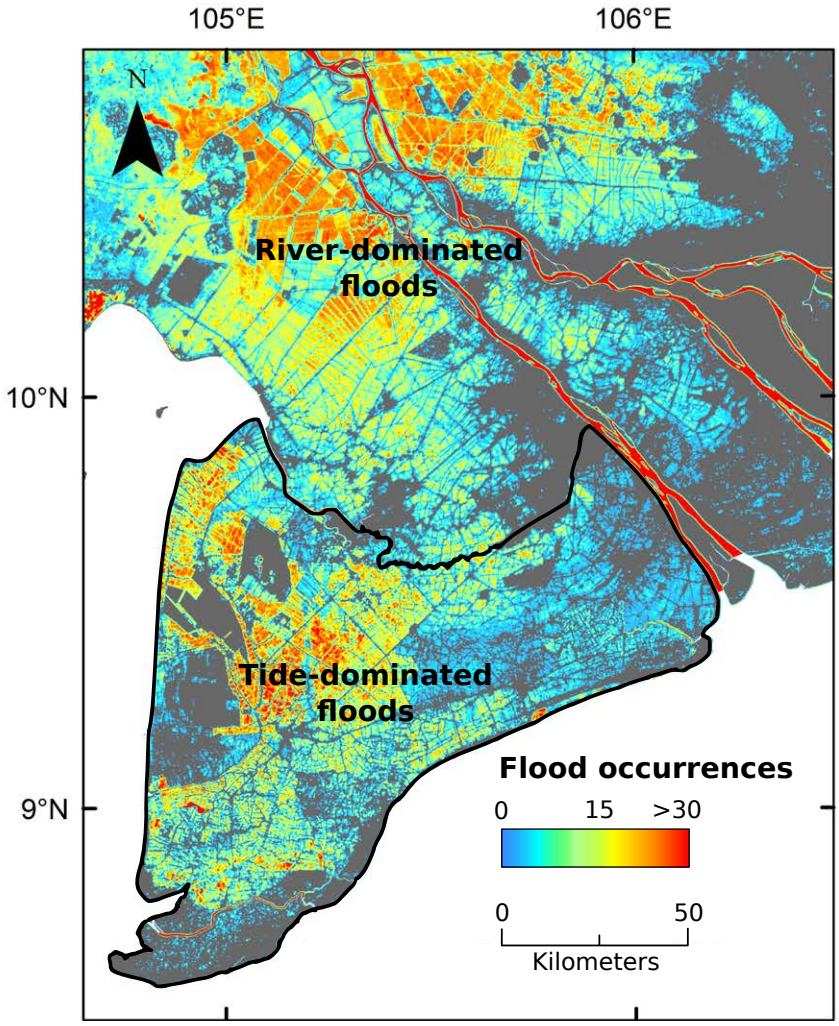

Figure 2.5 | *Inundation occurrences in the Mekong delta in the period 2007-2011 derived from ENVISAT ASAR WSM data (Kuenzer et al., 2013). Floods in the upstream part of the Mekong delta are river-dominated and in the southern part tide-dominated. The black line demarcates the tide-dominated flood area used to compare inundation occurrences to elevation of the digital elevation models.*

The authors distinguished four influencing factors for inundation in the Mekong delta: 1) natural floods of the Mekong river and overland flow, 2) artificial floodwater distributed by canals and controlled by dykes and sluice gates, 3) extreme local precipitation events and 4) floods related to high tides (Kuenzer et al., 2013; Hung et al., 2012). Inundations resulting from the first three factors do not solely correlate to lowly elevated areas, as they also occur in elevated areas. For example, river floodwater and overland flow happens mostly in the higher, upstream areas as dikes and canals block and retain the floodwater, preventing it to reach the lowest, more distal parts of the delta plain. Extreme precipitation events can occur anywhere in the delta, as the flat topography of the region does not cause orographic lift which would induce increased precipitation at a certain location. However, inundations following tidal flooding are expected to negatively correlate to elevation in terms of extent and duration, as tidal floodwater inundates the lowest topographical areas first and longest. In general, inundation in the northern and middle part of the Mekong delta is predominantly caused by river-induced floods, overland flow and human floodwater control and retention, whereas in the southwestern part of the delta, flooding is induced by both high tides and human action (Fig. 2.5).

We compared the spatial pattern of tide-dominated flood occurrences (which is related to the elevation relative to sea level) to the relative elevation of the DEMs. We only considered those areas where floods are determined by sea water level and tides, which include the provinces of Ca Mau, Bac Lieu, Soc Trang and the southern part of Kien Giang (Fig. 2.5). Part of the area in the southwestern tip of the Mekong delta experience very long, up to year-round, inundation to accommodate aquaculture, mainly shrimp farms (Kuenzer et al., 2015). Although inundation of such aquaculture areas is human controlled, e.g. by opening/closing of sluices (Vo et al., 2013), they are located in the lowest parts in the landscape, to facilitate water circulation and management. Therefore, the presence of aquaculture does not obstruct the correlation between inundated area and elevation.

The analysis was performed by sampling the elevation of the DEMs at the center of each inundation-map raster cell and calculating the elevation statistics per inundation occurrence. Less than one percent of the total area is inundated more than 25 out of 128 times. As the areas per inundation occurrence >25 became too small to derive a representative mean elevation from the DEMs, they were excluded from the analysis.

2.2.5 Estimation of the area below sea level following sea-level rise

To evaluate the effect of using the SRTM, the MERIT or the Topo DEM for sea-level rise (hereafter: SLR) impact assessments, we estimated the area below sea level after future SLR for each DEM. Both the SRTM and the MERIT DEM are referenced to WGS84 and EGM96, of which the zero level does not represent local MSL. Moreover, a comparison between the newer EGM08 geoid and Vietnam's Hon Dau datum revealed a mean elevation bias of +0.890 m (Hoa, 2017). Still, some previous studies directly used the SRTM DEM for SLR impact assessments, erroneously assuming zero meter elevation in the SRTM DEM to be the elevation of local mean sea level (Carey-Reid, 2008; Warner et al., 2009, 2010). To evaluate to what extent such assumption would lead to errors in SLR impact assessments, we purposely assumed zero meter elevation in both STRM and MERIT DEMs to represent mean sea level, thereby mimicking previous studies. Although MSL at the Mekong delta might have a different value, in the absence of additional data, we assumed the zero level in the Topo DEM to represent MSL in the Mekong delta. To directly compare the Topo DEM to the MERIT DEM, the latter was vertically shifted to match the Topo DEM's mean elevation by subtraction the absolute difference in mean elevation of the two DEM, in this case 2.5 m.

The vertical resolution of both the MERIT and the Topo DEMs allowed detailed quantification of the affected area under rising sea level. We quantified areas falling below sea level for SLR scenarios of 20, 50, 80 and 100 cm. In case of the SRTM DEM with a vertical resolution of 1 meter, we determined the area falling below sea level for a SLR of 1 meter, similar to analyses done in previous studies (Carey-Reid, 2008; Warner et al., 2009, 2010). We also estimated the number of people living in the area below sea level for each scenario by using provincial population statistics of 2016 (people per km^2; General Statistics Office of Vietnam available at www.gso.gov.vn; Appendix A, Table A.2). As spatial data on the population distribution within provinces were not available, we assumed an even distribution excluding rivers and steep bedrock outcrops. Additionally, a detailed analysis of delta surface and people impacted for each province individually was done for the Topo DEM.

2.3 Results

2.3.1 Elevation models

The Topo DEM (Fig. 2.6) shows remarkable differences in elevation of the Mekong delta when compared to the space-borne SRTM and MERIT DEMs (Fig. 2.7). The average elevation of the delta plain (excluding areas with bedrock outcrops) is 2.6 m according to the SRTM DEM, 3.3 m according to the MERIT DEM and 0.82 m according to the Topo DEM. A clearly visible NE-SW oriented striping pattern dominates the SRTM DEM; in MERIT DEM this noisy striping has been largely removed, but some remains of major banding in elevation are still present. The Topo DEM does not show these features.

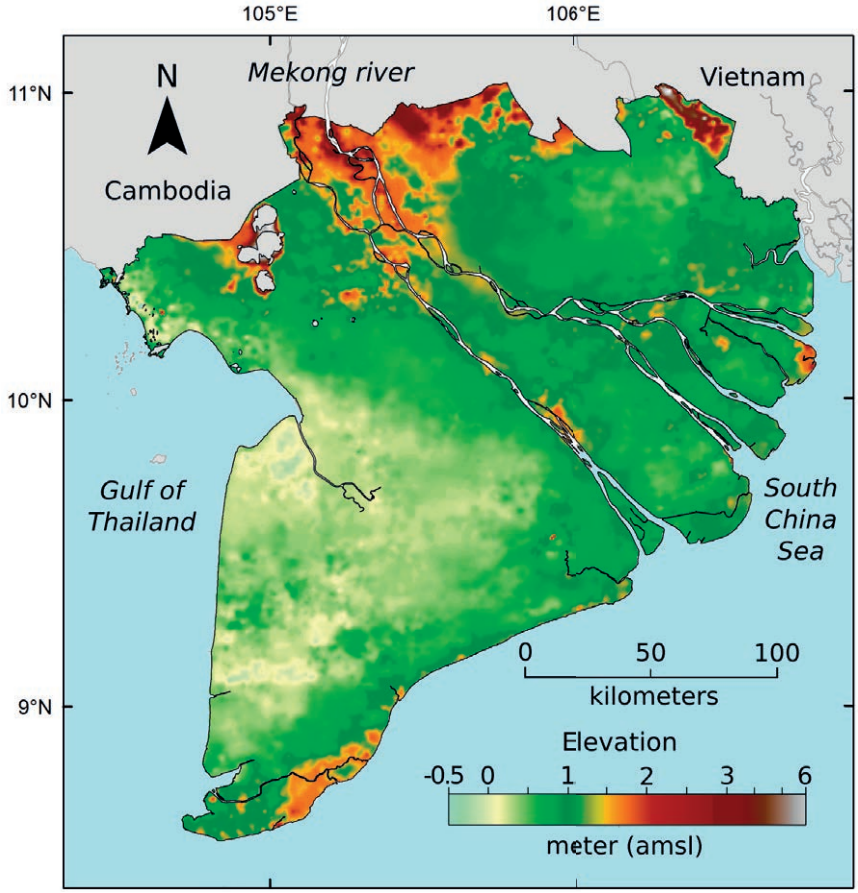

Figure 2.6 *| New elevation model (Topo DEM) of the Vietnamese Mekong delta based on topographical elevation points. The DEM is gridded at 500 m x 500 m.*

Because of the high horizontal resolution (30 x 30 m) of the SRTM DEM, and to a lesser extend also the MERIT DEM (94 x 94 m), small-scale topographical features, such as natural levees and beach ridge remnants, elevated roads and cities, can be distinguished. This detail is not present in the Topo DEM as the spatial resolution is too coarse (500 x 500 m). Instead, the Topo DEM shows

the larger scale topography of the delta surface, which is poorly visible in the MERIT DEM and not visible in the SRTM DEM. The Topo DEM displays higher elevated areas in the NW, the upstream part of the delta, along the Mekong river branches and along the coastline in the SE. Lower elevated areas are found towards the west coast and at distal locations in the delta plain away from the river system and the SE coastline. A large area in the SW part of the Mekong delta lies only several decimeters above MSL according to the Topo DEM.

Two elevation profiles through the delta allow a detailed visual comparison of the DEMs. One cross-section runs parallel to the main Mekong river branches spanning from the upstream river apex in the NW to the coastline in the SE (Fig. 2.7, profile A-A') and the other cross-section is NE-SW orientated, perpendicular to the river branches (Fig. 2.7, profile B-B'). The SRTM and MERIT elevation data is averaged in bins of 500 m to match the Topo DEMs spatial resolution. The elevation profiles of the SRTM DEM show an erratic topography with excursions high above the average delta plain elevation to several meters below sea level. The elevation profiles of the MERIT DEM show a more smoothed pattern with less excursions in both directions. Especially the lower end excursions present in the SRTM DEM are no longer present, resulting in higher mean elevations in the MERIT DEM. Compared to both spaceborne DEMS, the elevation profiles of the Topo DEM are smoother and much less erratic and show a, generally, much lower elevation of the delta surface.

Apart from the apparent, NE-SW orientated striping in the SRTM DEM, a remarkable elevation anomaly in the SW corner of the delta is present in both SRTM and MERIT DEM (Appendix A, Fig. A.2a), which clearly visible in the elevation profile (Fig. 2.7, left side profile B-B'). Elevation values change with a sharp, geomorphological unrelated boundary up to several meters below sea level. Although in absolute value much smaller, the Topo DEM also contains an inconsistency in elevation. In the southern part of the delta along a horizontal line the elevation abruptly changes about 30 cm (Appendix A, Fig. A.2b). This systematic offset in elevation is also present in the topographical elevation point dataset on which the Topo DEM is based and may stem from a measurement error. However, this seems to be a local error, as the offset is not present in the eastern part of the delta plain on the same latitude.

Province	Topo DEM	SRTM DEM	MERIT DEM
An Giang	**1.42**	3.3	3.8
Đồng Tháp	1.41	**3.7**	**4.4**
Long An	1.07	2.4	3.9
Bến Tre	0.95	2.6	3.1
Vĩnh Long	0.94	2.1	2.6
Tiền Giang	0.85	2.8	3.6
Trà Vinh	0.79	2.5	2.8
Cần Thơ	0.72	2.9	3.9
Sóc Trăng	0.68	2	3.5
Cà Mau	0.59	2.3	***2.4***
Bạc Liêu	0.5	2	2.9
Kiên Giang	0.39	2.5	3.1
Hậu Giang	***0.38***	***1.9***	*3.4*
Entire Mekong delta	**0.82**	**2.6**	**3.3**

Table 2.2 | *Mean elevation of each province and the entire Vietnamese Mekong delta plain according to the Topo, SRTM and MERIT DEMs. Elevation is color ranked from green (highest) to blue (lowest). Bedrock outcrops, rivers and islands were excluded from this analysis. Province boundaries in Fig. 2.1a.*

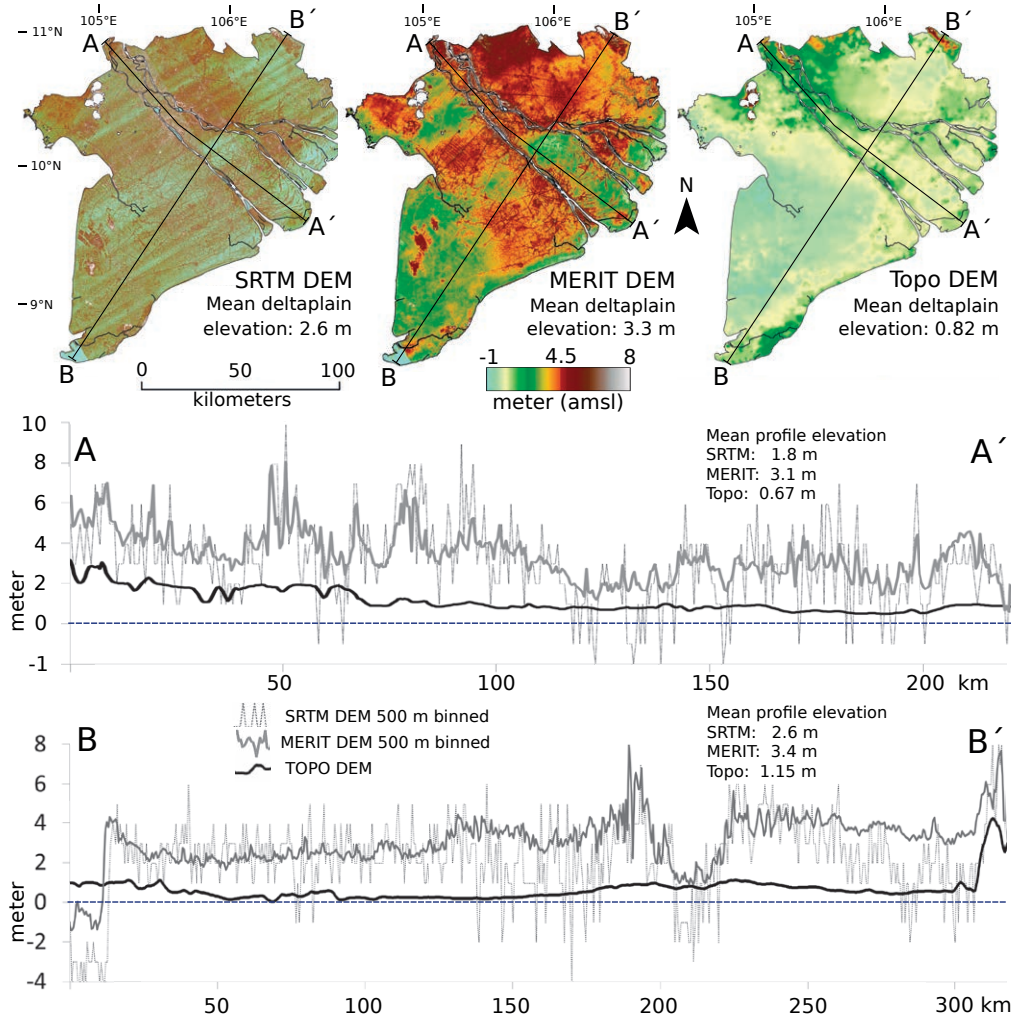

Figure 2.7 | *SRTM, MERIT and Topo Digital Elevation Models (DEM) of the Mekong delta with two elevation profiles. The SRTM and MERIT elevation was binned (mean elevation) in 500 meter segments to match the spatial resolution of the Topo DEM to allow visual comparison. Mean elevation of the DEMs was calculated for the delta plain only, excluding the higher elevated bedrock outcrops in the northwest of the delta.*

The elevation statistics at provincial level are given in Table 2.2. In both the Topo DEM and the SRTM DEM, the province Hau Giang has the lowest land surface, closely followed by Kien Giang, Bac Lieu and Ca Mau for the Topo DEM and Bac Lieu, Soc trang and Vinh Long for the SRTM DEM. In the MERIT DEM Ca Mau is lowest elevated, followed by Vinh Long and Tra Vinh and Bac Lieu. The upstream-located provinces are generally higher in all DEMs. Average elevation of An Giang and Dong Thap is highest in the Topo DEM; Dong Thap is also highest in both the SRTM and MERIT DEM.

2.3.2 DEM elevation validation

Absolute validation using benchmarks

The absolute elevations of 69 national benchmarks (referenced to Vietnam's Hon Dau geodetic datum) located in the delta were compared to the corresponding elevation given by the DEMs (Fig. 2.8; Appendix A, Fig. A.4). In the SRTM DEM the mean elevation at the benchmark locations deviates by +2.0 m from the mean elevation of the benchmarks. The residuals of the MERIT DEM show an even larger mean deviation of +3.0 m; however the residuals are more clustered, with a standard deviation (SD) of 1.3 m, when compared to a SD of 2.9 m for the SRTM DEM residuals. The large mean deviation may indicate a structural overestimation of the geodetic surface elevation by the SRTM and MERIT DEMs. The residuals of the Topo DEM have a much smaller mean deviation of +0.2 m and their distribution resembles a normal distribution with 57% confidence (Anderson-Darling normality test). The offset of 0.2 m may well be the result of the elevation difference (~-0.3 m, Appendix A, Fig. A.3) between the benchmarks and actual surface elevation as presented by the Topo DEM, but also falls within the interpolation error (standard deviation = 0.16 m) of the Topo DEM. The individual deviations in elevation between the benchmarks and the Topo DEM are in the order of decimeters up to 2 m (mean absolute deviation is 0.6 m) (Fig. 2.8). The residuals do not show a specific spatial pattern and, therefore, might stem from comparing elevation of point locations to average grid cell elevation (500 x 500 m). For the SRTM and the MERIT DEM, the individual absolute deviations are much larger (mean absolute deviation of 2.6 m and 3.0 m). Whereas the SRTM and the MERIT DEM seem to systematically overestimate actual benchmark elevation by 2 and 3 meters respectively, the Topo DEM appears to represent the geodetic elevation of the delta surface at the national benchmarks quite well.

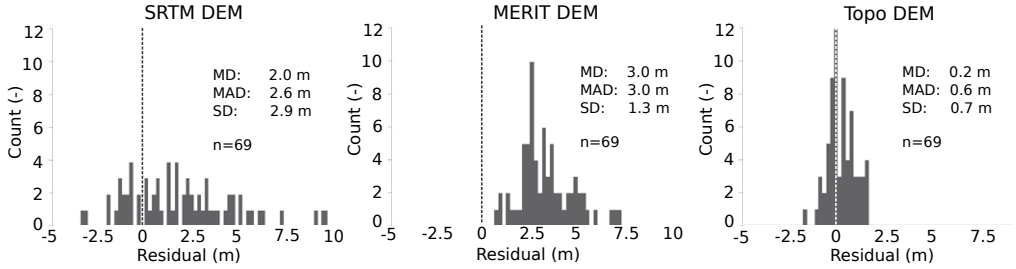

Figure 2.8 *| Histograms of differences between elevation of the SRTM (left), MERIT (center) and the Topo (right) DEMs and national benchmarks in the Mekong delta. A positive residual means DEM elevation exceeds benchmark elevation. MD = mean deviation (difference in means), MAD = mean absolute deviation (mean of individual differences), SD = standard deviation of residuals.*

Relative elevation validation: geomorphology

We used the principle that by nature geomorphological units are characterized by a typical relative elevation compared to adjacent geomorphological units, as a result of their specific depositional environments (Fig. 2.4). As such, the geomorphological map of the Mekong delta (Nguyen et al., 2000) (Fig. 2.3) serves as a proxy for relative elevation. Table 2.3 shows the mean elevation of each geomorphological unit in the delta for each DEM, and the qualitative expected elevation of each unit relative to other units within the same category. In all DEMs, the expected relative elevation differences between the three main categories is present, with the older Pleistocene deposits having

the highest mean elevation, followed by the Holocene upper alluvial delta plain and, subsequently, the lower coastal delta plain with the lowest average elevation.

Table 2.3 | *Elevation of geomorphological units in the Mekong delta, according to the Topo, SRTM and MERIT DEMs. The relative elevation of the Pleistocene deposits is given in comparison with the Holocene deposits; within the Holocene deposits relative elevation is given compared to the elevation of the benchmark geomorphological unit, respectively flood basin for the upper delta plain and tidal flat for the lower delta plain. Expected relative elevation was based on typical elevation characteristics of the depositional environment corresponding to the geomorphological unit (see Fig. 2.4) and is color ranked from green (higher) to white (equal) to blue (lower).*

Category and age	Geomorphological unit	Expected relative elevation	Mean elevation (m)		
			Topo DEM	SRTM DEM	MERIT DEM
Pleistocene (and older) deposits	Weathered land	Very high	3.27	6.37	6.87
	Undifferentiated deposits	Higher	1.84	3.11	4.67
	Alluvial apron	Higher	1.38	2.84	4.19
Upper delta plain Holocene alluvial deposits	Flood basin	*Benchmark*	*0.85*	*2.83*	*3.54*
	Bank: natural levees and crevasse splay	Highest (++)	1.38	4.11	4.67
	Channel bar	Higher (+)	1.41	3.17	5.06
	Abandoned channel	Higher (+)	0.91	2.65	3.48
	Swamp	Lower (-)	0.85	2.57	3.73
	Back swamp	Lower (-)	0.66	2.44	3.49
Lower delta plain Holocene coastal deposits	Tidal flat	*Benchmark*	*0.99*	*2.20*	*1.47*
	Sand spit	Higher (+)	1.14	2.67	2.78
	Relict beach ridge or sand dune	Higher (+)	0.84	2.19	1.58
	Mangrove marsh	Equal (+/-)	0.97	2.35	2.29
	Salt marsh	Equal (+/-)	0.83	2.14	3.13
	Coastal plain	Lower (-)	0.53	2.15	2.87
	Marsh (inland)	Lowest (- -)	0.34	2.65	2.69

The expected relative elevation of the different geomorphological units within each of the main classes is, in most cases, present in the elevation of the Topo DEM. Within the upper alluvial delta plain, the natural levees and channel bars are highest elevated units, while the flood basin and the swamps are correctly located in the lowest elevated areas. The reason that channel bars are elevated as high as natural levees is probably because they actually represent large vegetated islands within river branches, which feature a similar depositional environment as natural levees. In the lower coastal delta plain, inland marshes are the lowest elevated unit, with an average elevation of 0.34 m above sea level. The coastal plain is the second lowest elevated around half a meter above sea level. Sand spits are, as expected, the highest geomorphological unit in the coastal zone. A notable exception is the elevation of 'relict beach ridge or sand dune', which is lower than expected. Reasons for this could be that the spatial resolution of the Topo DEM (500 m x 500 m) and the input data is too coarse to capture these relatively small geomorphological features. Furthermore, a comparison with aerial photographs revealed that the delineation of the beach ridges in the geomorphological map does not always match their exact location and has a tendency to overestimate their spatial extent.

In case of the SRTM and the MERIT DEM, the geomorphological units that were expected to have the highest relative elevation within each main class, which are weathered land, natural levees and sand spits, do so indeed. However, the expected order of relative elevation among the lower elevated geomorphological units is absent, and all classes have a similar mean elevation. Especially

for the lower delta plain, the SRTM DEM hardly shows any elevation differentiation between the geomorphological units. In the MERIT DEM the expected order in the lower delta plain is even reversed, with the geomorphological units expected to have the lowest relative elevation, having higher mean elevation (see Appendix A, Table A.4 & A.5 and Fig. A.5 for elevation statistics for each geomorphological unit in each DEM).

Relative elevation validation: tide-dominated flood occurrence

The second method used to validate relative elevation was based on the assumption that tide-dominated floods occur more often in lower areas. Tidal flooding is the dominant factor controlling the number of inundations and therefore, when an elevation model is correct, increasing flood occurrence is expected to correlate with decreasing elevation. Therefore for each DEM the mean elevation of the delta surface was determined for all flood occurrences during the period 2007-2011 (Kuenzer et al., 2013) in the coastal zone of the southwest part of the Mekong delta (Fig. 2.9). Total inundated areas and boxplots showing the distribution of elevation points per flood occurrence are given in Appendix A (Fig. A.6). The elevations of both the MERIT and the Topo DEM show the expected correlation of decreasing elevation with increasing flood occurrence with a continuous trend, while the elevations in the SRTM DEM only weakly show this correlation.

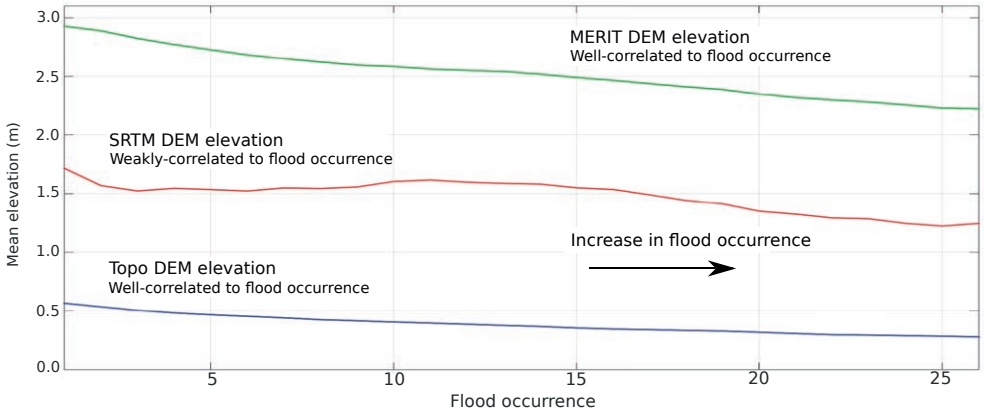

Figure 2.9 | *Mean MERIT, SRTM and Topo DEM elevation arranged according to increasing tide-dominated flood occurrence in the southwestern part of the Mekong delta. Flood occurrences were derived from satellite imagery for the period 2007-2011 (Kuenzer et al., 2013) (Fig. 2.5).*

In addition to a relative elevation validation, this analysis also contributes to the absolute elevation validation of the DEMs. Tide-dominated floods in the delta occur when the average high tide level is exceeded as a result of spring tides and storm tides. Most of the coastal flooding occurs in the southwest of the Mekong delta plain towards the Gulf of Thailand, where the tidal range is 40 cm. The absolute elevations of the Topo DEM of areas that experience regular tide-dominated floods are within decimeters of the average tidal range and MSL, which is realistic. The MERIT and SRTM DEM provide absolute elevation values that are at least one meter higher, and such elevations are unlikely to experience regular coastal flooding considering the small tidal range.

2.3.3 Evaluating area below sea level following relative sea-level rise

The high vertical precision of the novel Topo DEM and the transposed MERIT DEM (original MERIT DEM minus 2.5 m, see methods) allowed for impact analyses of relative sea-level rise (hereafter: SLR) at decimeter scale. The area below sea level for SLR scenarios of 20, 50 and 80 cm above mean sea level (MSL) based on the Topo and the transposed MERIT DEM is shown in Fig. 2.10. Based on the Topo DEM, 20 cm SLR results in 6% of the total delta plain area below sea level. This area progressively increases to 29% and 54% of the total delta plain after a SLR of 50 and 80 cm respectively. Based on the transposed MERIT DEM, 32%, 41% and 51% of the total delta plain area falls below sea level under 20 ,50 and 80 cm SLR.

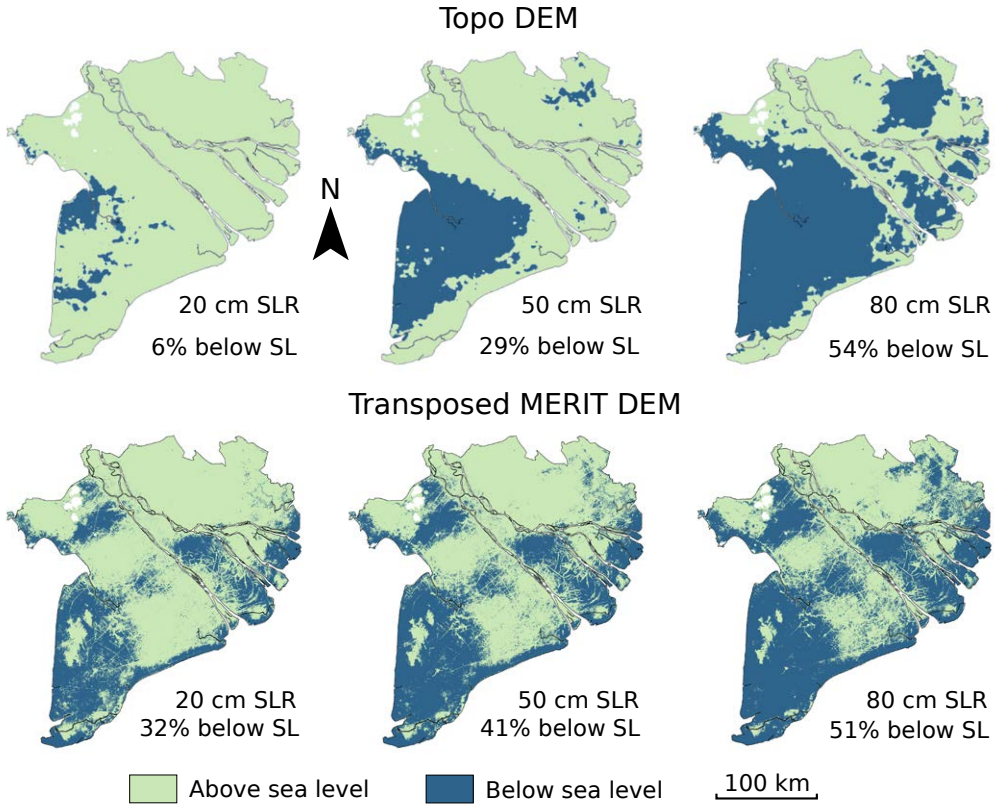

Figure 2.10 | *Area below sea level (SL) with relative sea-level rise (SLR) scenarios of 20, 50 and 80 cm based on the Topo DEM and the transposed MERIT DEM. The transposed MERIT DEM matches the mean delta elevation of the Topo DEM and was created by subtracting 2.5 m from the original MERIT DEM. The percentages give the area of the delta plain below sea level (excluding bed rock outcrops).*

The estimated number of affected people per province affected by flooding under sea level rise based on the Topo DEM is shown in Fig. 2.11A (See Appendix A, Table A.3 for elevation statistics per province). Based on the results, the provinces can be divided into two main groups. The first group comprises the four provinces most prone to SLR: Bac Lieu, Ca Mau, Hau Giang, Kien Giang, which are all located in the southwest part of the Mekong delta. Where a SLR of 20 cm already moderately affects the provinces of Ca Mau and Kien Giang, the largest impact occurs under a

SLR of 20 to 60 cm. Half a meter of SLR will result in over 50% of the delta area of each of these provinces to fall below sea level. The second group consists of provinces located in the middle and NE part of the delta, which become mostly affected when SRL reaches 60-90 cm. The province of Soc Trang is an exception that lies between both groups and this province is most affected by a SLR of 30-90 cm. The estimates of the number of people affected in the Mekong delta by SLR show a similar pattern (Fig 2.11B). With a SLR of 20 cm, an area inhabited by ~1 million people (6% of the total population) falls below sea level (mainly located in the first group of provinces) and following a SLR of 50 cm this area increases to an area habituated by approximately ~4.7 million people (27% of the total population).

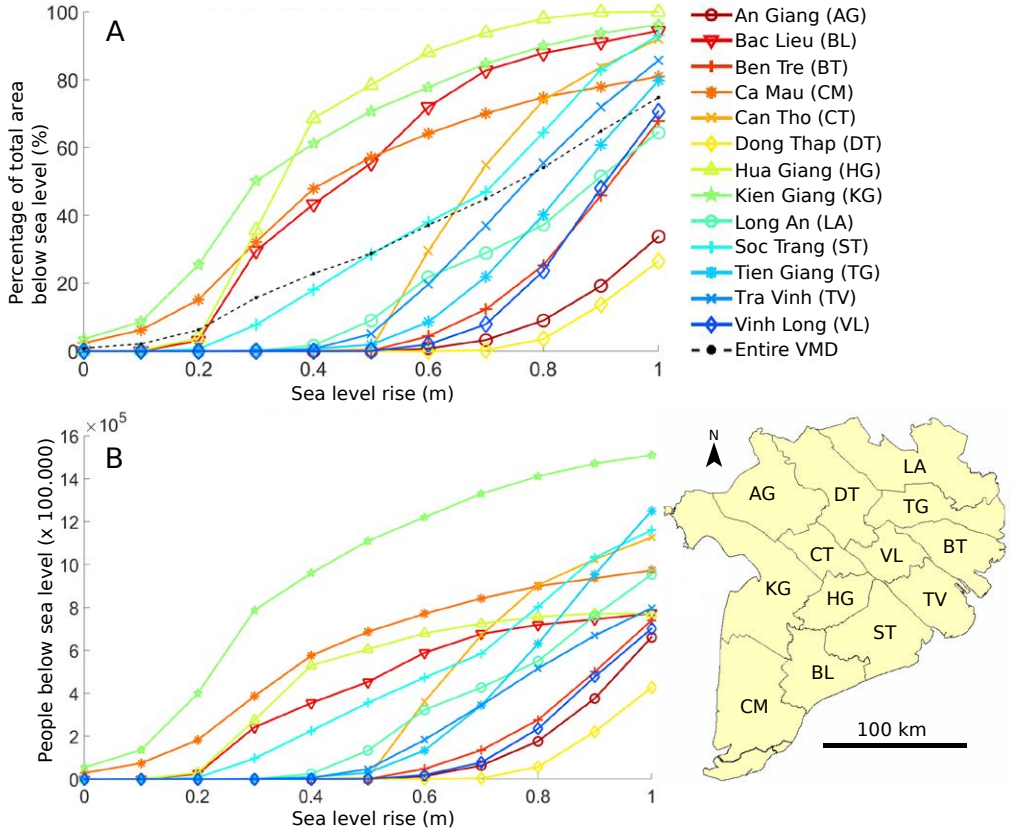

***Figure 2.11** | Delta surface (A) and estimated number of inhabitants (B) below sea level following sea-level rise up to 1 meter based on the Topo DEM.*

Where according to the SRTM DEM, a one-meter SLR causes 31% of the Mekong delta plain to fall below sea level, this area is only 2% in the MERIT DEM, 59% in the transposed MERIT DEM and 75% according to the Topo DEM (Fig 2.12). This corresponds to an estimated number of affected people of 5.1 million (29% of total population) based on the SRTM DEM, 0.3 and 9.7 million (2% and 55% of the total population) based on the MERIT and transposed MERIT DEM, and 12.3 million (70% of the total population) based on the Topo DEM (Table 2.4). Spatially, the affected area also differs between the SRTM, MERIT and the Topo DEM.

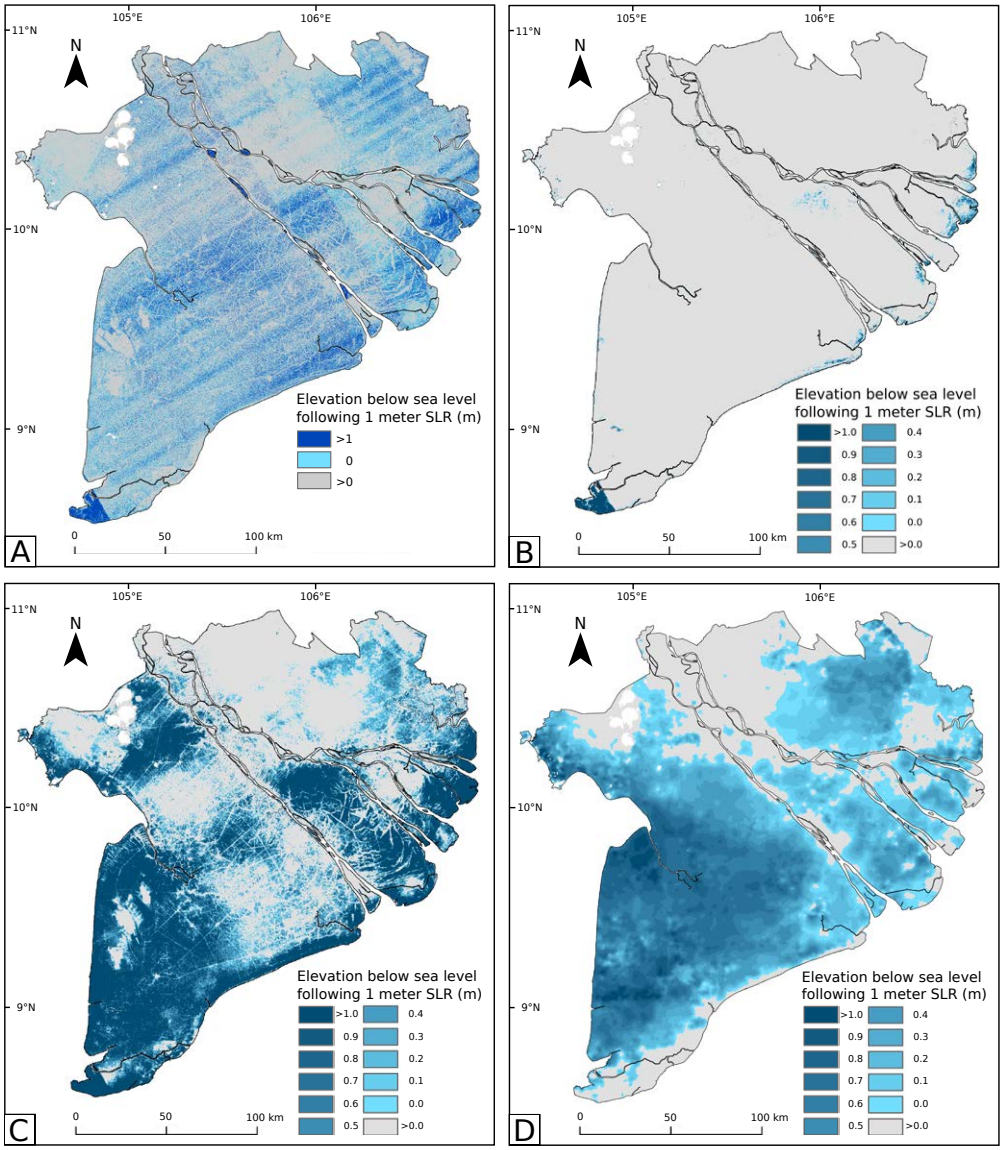

Figure 2.12 *| Area below sea level with sea-level rise (SLR) up to 1 meter based on the A) SRTM DEM, B) the MERIT DEM, C) the transposed MERIT DEM and the D) Topo DEM. The transposed MERIT DEM matches the mean delta elevation of the Topo DEM and was created by subtracting 2.5 m from the original MERIT DEM. Total area of the delta plain below sea level with 1 meter SLR is 31% for the SRTM DEM, 2% for the MERIT DEM, 59% for the transposed MERIT DEM, and 75% for the Topo DEM.*

***Table 2.4** | Delta plain and estimated number of people below mean sea level (MSL) for 0 and 1 meter sea-level rise (SLR) using different DEMs for the Vietnamese Mekong delta. Total delta plain area is based on the area of the flat, deltaic surface excluding high bedrock outcrops.*

	SRTM DEM		MERIT DEM		Transposed MERIT DEM		Topo DEM	
	0 m SLR	1 m SLR	0 m SLR	1 m SLR	0 m SLR	1 m SLR	0 m SLR	1 m SLR
Delta plain area below MSL (x 1.000 km^2)	5.5	11.9	0.2	0.8	10.2	23.9	0.3	28.5
Delta plain area below MSL (% of total area)	14%	31%	1%	2%	25%	59%	1%	75%
Estimated number of people below MSL (x 10^{-6})	2.4	5.1	0.1	0.3	4.1	9.7	0.1	12.3
Estimated number of people below MSL (% of total population)	14%	29%	1%	2%	23%	55%	1%	70%

2.4 Discussion

Performance of the DEMs

In each elevation validation analysis, the Topo DEM performed superior to both spaceborne DEMs. Whereas the SRTM and MERIT DEM overestimate the absolute surface elevation at the national benchmarks on average by 2 and 3 m, the Topo DEM shows almost no absolute elevation overestimation (0.2 m). A fundamental explanation for this can be found in the difference in geodetic datum. The Topo DEM and national benchmarks are referenced to Hon Dau datum, while both the SRTM and the MERIT DEM are reference to the global EGM96 geoid. This analysis clearly illustrates the large difference that can exist between global geoid models and local geodetic datum based on mean sea level. Since elevation referenced to a global geoid is not intended to represent terrain elevation above local sea level, major errors arise when studies on deltas directly use global spaceborne DEM elevations in assessment of sea level impacts. Still, in the absence of other elevation data for large deltas, this direct use of STRM elevation was done in many delta studies in the Mekong delta (Carey-Reid, 2008; Warner et al., 2010; Kondolf et al., 2018) and other deltas worldwide (e.g. Syvitski et al., 2009). Clearly such assessments should at least include local elevation data to correct vertical offsets of such DEMS for specific coastal regions or deltas. These results confirm the observation of Kulp & Strauss (2016) that, even when converted to local tidal datum, spaceborne DEMs have the tendency to underestimate coastal vulnerability.

In terms of relative elevation, the Topo DEM shows the expected relative elevation differences between geomorphological units. Both SRTM and MERIT DEMs fail to represent the expected elevation differences based on terrain geomorphology. In contrast to the SRTM DEM, both the MERIT and the Topo DEM correlate well with tide-dominated flood occurrence. The high horizontal resolution of the SRTM and the MERIT DEMs does allow distinguishing small, individual topographical features such as dikes, roads and natural levees, which are not present in the Topo DEM. However, at delta scale, the Topo DEM seems to represent the actual delta plain elevation relative to local sea level far better than the SRTM and the MERIT DEM, both in terms of absolute elevation and relative elevation.

Mekong delta lower than global studies suggest

Analysis of the Topo DEM shows that apparently the Mekong delta plain is much lower above local sea level than previously (erroneously) concluded based on SRTM elevation data (Syvitski et al., 2009; Carey-Reid, 2008; Kondolf et al., 2018; MDP, 2013; Schmitt et al., 2017). According to the Topo DEM, the Mekong delta plain has a mean elevation of 0.82 m to Hon Dau datum, which is only one third of the SRTM DEM's mean elevation of 2.6 m, and even less compared to the MERIT DEM's mean elevation of 3.3 m. Hence the Mekong delta plain might well be the lowest elevated of all mega deltas in the world. This means that the delta is actually even more vulnerable to sea-level rise than previously foreseen, and moderate estimates of absolute sea-level rise (~40 cm by 2100 (Church et al., 2013)) may already result in a quarter of the delta falling below sea level by the end of the century. Moreover, as the delta itself is subsiding at increasing rates following groundwater overexploitation16, with present delta-average rates exceeding 1.1 cm yr^{-1}, large parts of the delta may face submersion already during the coming decades.

The impact of elevation data on SLR impact assessments

Elevation above sea level is a key factor to assess the vulnerability of deltas to risks arising from sea-level rise and land subsidence, which both decrease the relative elevation of a delta. The superior vertical accuracy of the Topo DEM over the SRTM DEM enables more reliable sea-level rise impact assessments for the Mekong delta. The cumulative area that falls below sea level following a SLR of 1 meter is a factor two larger according to the Topo DEM compared to the SRTM DEM, respectively 75% versus 31% of the total delta plain (Table 2.4). Also the spatial patterns of the affected area are completely different between the two elevation models (Fig. 2.12). In spite of the improvements of the MERIT DEM when compared to the STRM (Yamazaki et al., 2017), direct (and incorrect) use of the MERIT DEM as a measure of elevation above sea level would wrongly suggest that 1 meter SLR only inundates 2% of the total Mekong delta plain, as the mean elevation of MERIT DEM is even higher than the SRTM DEM. The vertically transposed MERIT DEM by -2.5 m to match the average elevation of the Topo DEM still results in large differences in terms of delta area inundated and number of people impacted, when compared to using the Topo DEM. According to the Topo DEM over 12 million people (>70% of the total population of the delta) live in areas which will fall below sea level following a SLR of 1 meter, which doubles the number of earlier analyses using the SRTM DEM (Carey-Reid, 2008)(~5 million people, 29% of the total). The above numbers reveal the large differences between sea-level rise impact assessments of a single delta and their strong dependency on the quality, accuracy and vertical datum of the used elevation model.

Timing of drowning of the Mekong delta

With rising sea level, present and future land surface elevation of a delta above sea level in a way determines time remaining before delta drowning. The apparent much lower elevation of the Mekong delta above local sea level means that there is much less time to implement mitigation or adaptation strategies than previously realized by the international research community. The southwestern part of the delta with the provinces of Bac Lieu, Ca Mau, Kien Giang and Hua Giang is the lowest and therefore most vulnerable part of the delta. However, it is hard to predict when and where exactly in the delta the surface elevation will fall below sea level as this does not depend solely on present elevation, but also on the combined effect of eustatic SLR and subsidence. Furthermore, sedimentation of clastic and organic sediments at the delta surface, in turn, increases elevation of the delta plain and must also be considered. The sum of these factors determines when a certain part of the delta plain will lose it's elevation above sea level. Present rates of local

eustatic SLR in the Mekong are ~3.3 mm yr^{-1} (Hak et al., 2016). Land subsidence in the Mekong delta is the result of the cumulative effect of various subsidence drivers (Chapter 1). Groundwater extraction causes subsidence rates to exceed 25 mm yr^{-1} in certain areas (Chapter 5), while natural compaction of young Holocene sediments contributes up to 20 mm yr^{-1} to subsidence rates in the coastal zone (Chapter 3). Conversely, sedimentation in some coastal mangrove forests with ample sediment supply amounts to rates of ~36 to ~67 mm yr^{-1} (Lovelock et al., 2015), while the average sedimentation rate on the Mekong floodplains amounts ~6 mm yr^{-1} (Hung et al., 2014). Both subsidence and sedimentation can spatially be highly variable and, as not all processes are yet mapped for the entire delta, a more detailed assessment of the timing of complete elevation loss in the delta as a result of sea-level rise is currently not possible. Nevertheless, given the above numbers, it is likely that within the next generations large parts of the Mekong delta will fall below sea level. Whether or not this also means permanent inundation also depends on the level of flood protection and ability to manage surface water through a polder system, like in the Dutch Rhine-Meuse delta. However, given its large extent, it will likely be an impossible task to protect the entire Mekong delta plain against drowning, and thus difficult choices will arise: what to protect and what not.

Collecting and disclosing high-accurate elevation data is crucial to protect our deltas

This study clearly reveals the importance of accurate elevation data, such as DEMs derived from detailed topographical elevation data or LIDAR campaigns, and correctly referencing to local geodetic datum and local sea level for SLR assessments in low-lying deltas and coastal plains worldwide. Such assessments are crucial to the development of sustainable delta management strategies. In Vietnam, the government is aware of the delta's low elevation; Vietnamese SLR assessments following climate change scenarios in internal governmental reports show inundation patterns and magnitudes similar to our analyses using the Topo DEM (Tran et al., 2016). Unfortunately, neither such internal documents nor the important underlying elevation data have sufficiently found their way into the global climate adaptation studies.

Using presently available spaceborne DEMs as alternative source of information for delta elevation for SLR assessments, suffers from accuracy problems in the order of meters, and will lead to major errors in assessments of coastal drowning (Kulp & Strauss, 2016). Remarkably, the MERIT DEM shows a less noisy and banded elevation when compared to the SRTM DEM, but yields no improved estimate of the Mekong delta elevation. Whenever available, elevation data from local geodetic surveys, and the relation between the used reference datum and mean sea level should be obtained, for direct use, or to vertically adjust the MERIT DEM and relate it to local sea level as a first-order estimate.

When high-accuracy elevation datasets are available, they should not be kept confidential within governmental bodies but made publically accessible for the scientific community and NGOs. An open-data strategy will undoubtedly improve SLR impact assessments, but also river flood modelling and storm surges risk assessments. This will lead to better informed delta policy decision-making and this way governments benefit in turn from disclosing elevation data. Otherwise researchers may continue to settle for 'best available', but potentially highly inaccurate, spaceborne DEMs which are in essence unsuitable to use in SLR impact assessments for low-lying, flat deltas.

For this reason, the acquisition of accurate elevation datasets based on ground measurements or LIDAR campaigns should be top priority for governments and intergovernmental organizations responsible for the management of deltaic and near-coastal regions. And evenly important, this elevation data, including all metadata, should be made publicly accessible for the international research community. Only then the next step towards improved SLR impact assessments for

low-lying deltas and coastal plains can be made. And these assessments are crucial in directing adaptation and mitigation policies to safeguard world's deltas for future generations.

Acknowledgements
The Division of Water Resources Planning and Investigation of the South of Vietnam (DWRPIS) is thanked for providing the dataset of the topographical elevation points used to create the Topo DEM and the independent elevation benchmarks in the Mekong delta. Dr. Lau Nhuyen Ngoc from the Ho Chi Minh City University of Technology is thanked for sharing documentation and discussions on coordinate reference systems and geodetic datums used in Vietnam.

3 The role of sedimentation and natural compaction in a prograding delta: insights from the mega Mekong delta, Vietnam

The Vietnamese Mekong Delta was formed by rapid transgression during the second half of the Holocene by deposition of mainly unconsolidated, fine-grained (clayey) sediments undergoing high compaction rates. The natural subsidence can seriously impact the already vulnerable delta plain as its low elevation exposes the delta to global sea level rise, flooding, salinization. Human activities such as groundwater pumping, infrastructural loading, sand mining and dam construction have exacerbated the effects of natural consolidation. Here we present a novel modeling study that has allowed to reproduce the formation and evolution of the Mekong delta over the past 4000 years. Using an adaptive finite-element mesh, the model properly simulates accretion and natural consolidation characterizing the delta evolution. Large soil grain motion and the delayed dissipation of pore-water overpressure are accounted for. We find that natural compaction of Holocene deposits following delta evolution exceeds predicted values of absolute sea level rise. The unprecedented high rates (up to ~20 mm yr^{-1}) threaten the lower delta plain with permanent inundation and inevitably reduce the designed service life of flood defense structures along the coast. Total subsidence and sediment delivery to the delta plain will determine its future elevation and vulnerability to relative sea level rise.

Published as: Zoccarato, C., Minderhoud, P.S.J., Teatini, P. (2018). **The role of sedimentation and natural compaction in a prograding delta: insights from the mega Mekong delta, Vietnam.** *Scientific Reports*. doi:10.1038/s41598-018-29734-7

3.1 Introduction

The populous Vietnamese Mekong Delta (VMD) hosts a thriving agricultural and industrial economy (Renaud & Kuenzer, 2012). Like many deltas in the world (Syvitski et al., 2009), its current delta plain has only been formed recently by deposition of sediments during the last several thousand years (Nguyen et al., 2000). Its low elevation makes the VMD vulnerable to global sea level rise (Wassmann et al., 2004; Ericson et al., 2006), river flooding (Kuenzer et al., 2013), and salinization (Renaud et al,. 2015). Moreover, fluvial sediment supply of the Mekong river is diminishing due to upstream dams (Milliman & Farnsworth, 2011; Kondolf et al., 2014; Kummu & Varis, 2007) and decreased activity of tropical cyclones over the Mekong river basin (Darby et al., 2016). Within the delta, sediment delivery to the flood plains is decreasing due to dykes (Triet et al., 2017) and sand mining (Brunier et al., 2014; Anthony et al., 2015).

In addition, the delta is subsiding (Erban et al.,2014) and the rates are accelerating due to the strong increase in groundwater extraction during the past decades (Chapter 5). Although human

activities, like groundwater extraction and infrastructural loading, can increase land subsidence, sediment compaction in deltas is a natural process inherently related to delta evolution. As deltas evolve and prograde, new sediments are deposited on top of older, earlier deposits. The gravitational load of overlying sediments (overburden) causes the underlying sediments to compact (reduction in sediment volume and increase in bulk density), as a result of pore collapse (mechanical grain reorganization) and fluid expulsion (Teatini et al., 2011). Delayed dissipation of excess pore water pressure can result in ongoing compaction long after sedimentation has ceased. This process is especially apparent in fine-grained soils (i.e., peat and clay). The factors that determine the rate of natural compaction, and possibly land subsidence, are sediment type (hydrological and geotechnical properties) and the specific depositional history that has resulted in the present stratigraphy. Secondarily, compaction can be influenced by chemical or biological processes like dissolution, cementation, and decay of organic matter. As such, natural compaction can spatially be variable and characterized by high rates; in the Mississippi delta for example, compaction of Holocene sediments is identified as the main cause for delta subsidence, with multi-decadal rates exceeding 10 mm per year (Meckel et al., 2006; Törnqvist et al., 2008; Jankowski et al., 2017). Determining compaction rates in modern transitional environments is difficult and direct observations and monitoring efforts are expensive and time consuming. Calculation of natural compaction is often complicated by the lack of data on sediment properties and incomplete knowledge of the depositional history (Meckel et al.,2007).

In VMD, very high compaction rates of Holocene strata between 25 and 41 mm per year are measured at three locations in coastal mangrove areas by surface elevation tables (SET) combined with marker horizons that register accretion at the surface (Lovelock et al., 2015). Although sediment accretion for these locations exceeds compaction rate, which results in a net elevation gain of the surface, these numbers reveal the potential of the Holocene deltaic sediments to contribute to VMD subsidence through natural consolidation. This holds especially in cases where sediment accretion is reduced by natural causes, dyke development or following cultivation (Chapter 4). With subsidence posing an increasing threat to the VMD, it is essential to quantify the contribution of each specific driver to the delta subsidence to create an action perspective for sustainable delta management (Chapter 5).

In this chapter, we aim to address and quantify natural compaction of the Holocene strata in the VMD as a result of the sedimentation history following delta evolution. We present a novel modeling approach that allows us to reproduce the VMD evolution and quantify the corresponding compaction over the past 4000 years. The model represents the most low-lying and vulnerable part of the delta, mainly consisting of fine-grained Holocene material (clays). Due to the extremely high porosity of newly deposited soil, the medium is deformable with large solid grain movements. Therefore, we use a two-dimensional (2D) groundwater flow model coupled to a one-dimensional (1D) compaction module where the assumption of infinitesimal displacements is relaxed to account for large deformations (Zoccarato & Teatini, 2017). This implies the recast of Darcy's law in term of relative velocity of the soil grains to the fluid velocity. We do not incorporate chemical or biological processes as they represent secondary factors contributing to compaction because of general waterlogged conditions (Zanello et al., 2011; Hooijer et al., 2012). This approach may serve as a model to investigate natural compaction in other deltas and prograding coastal environments elsewhere in the world.

3.2 Materials and Methods

3.2.1 Site evolution over the Holocene

With an area of 50,000 km^2, the Mekong delta, largely situated in the southwest of Vietnam, is the third largest delta plain in the world and it is characterized by the largest areal extent elevated less than 2 m above mean sea level (Syvitski et al., 2009), i.e. more than 20,000 km^2 (Fig. 3.1).

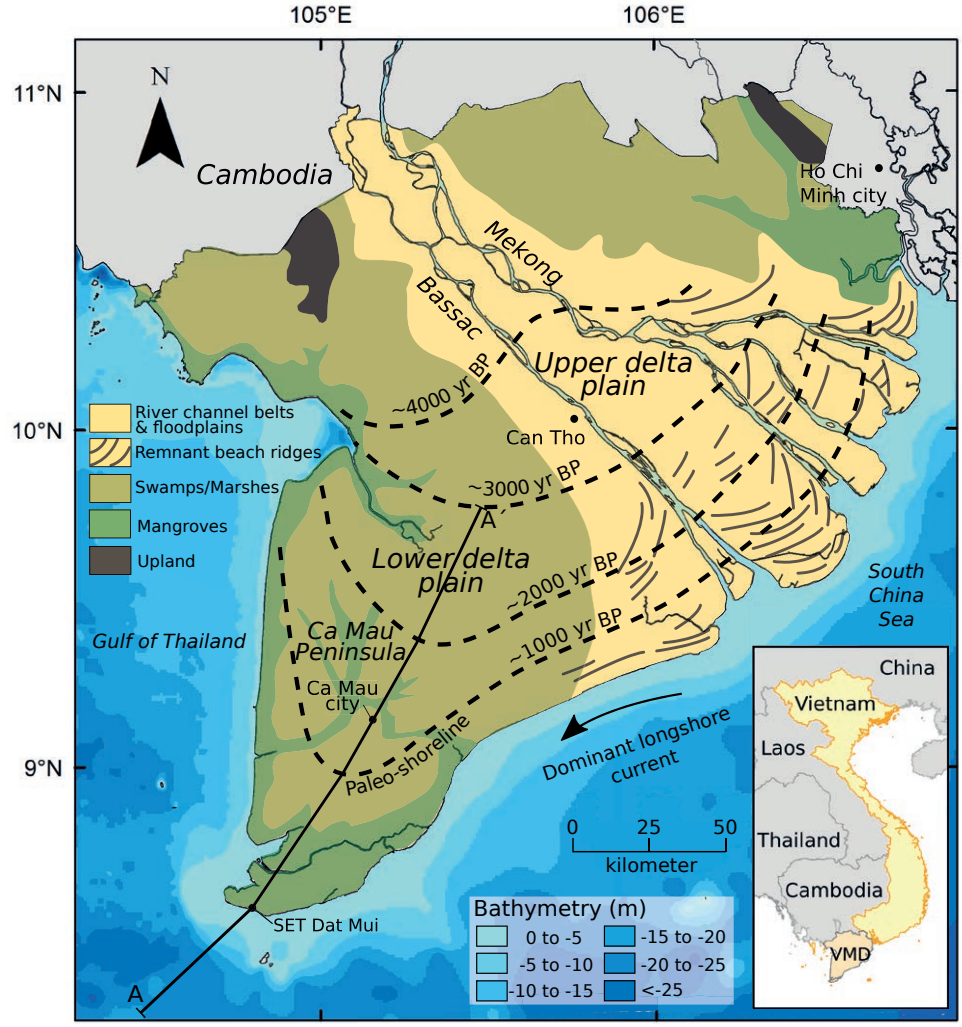

Figure 3.1 | *Map of the Vietnamese Mekong Delta (VMD) in Southeast Asia showing the main depositional paleoenvironments (modified after Anthony, 2015). Dashed lines represent the approximated paleo-coastlines based on a combination of data (Nguyen et al, 2000; Ta et al., 2002; Tamura et al., 2012). The 3000 yr BP shoreline demarcates the boundary between the upper and lower delta plain. The A-A' profile is the selected representative transect along which the 2D model is applied for the simulation of the delta progradation. Ocean bathymetry 'World Ocean Base' map from NOAA and Esri.*

The combination of high sediment supply, wave-sheltered position and relatively shallow sea favored a very rapid growth of the delta over the last 6000 years (Ta et al., 2002). Around ~3000 yrs BP, the delta changed from a tide dominated delta to a wave-tide dominated delta with increased long-shore sediment transport (Ta et al., 2005). On entering the flat delta plain, the Mekong river branched out in eastward direction, forming a river landscape with large channel belts and floodplains. Sand transported by the river was deposited in sequences of wave-formed beach ridges between the different river mouths (Tamura et al., 2012). The impressive muddy load of the Mekong river was transported by wave-induced longshore currents towards the south-western part of the delta. The accumulation of fine-grained sediments filled the space between the coarser-grained Pleistocene surface and the present day delta surface. This resulted in the rapid progradation of the so-called Ca Mau peninsula (Fig. 3.1), and the formation of vast swamp, marsh and mangroves areas (Anthony et al., 2015).

3.2.2 Available data to constrain the sedimentation and consolidation model

The prodelta moved seaward approximately 200 km during the past 4000 years (Nguyen et al., 2000; Ta et al., 2002). This results in an average progradation rate of 50 m yr^{-1} for the Ca Mau peninsula. Fig. 3.1 shows a map of the present Vietnamese Mekong delta and its evolution in time. The model simulates the delta formation and progradation along the A-A' section (Fig. 3.1 & 3.2) over the 4000 yrs-interval. Note that the 200 km delta includes 50 km of prodelta.

The information on the sedimentation rates over the delta is available from the literature. In particular, the bay and prodelta sediments are found to accumulate at a rate up to 32 – 63.7 mm yr^{-1} (Ta et al., 2002; Ta et al., 2005). Sedimentation rates up to 36.8 ± 3.1 mm yr^{-1} and 67.8 ± 6.6 mm yr^{-1}, respectively, at Dat Mui and the Bassac river mouth, have been quantified using marker horizon measurements at SET sites (Lovelock et al., 2015). These data allow constraining the model input in term of prodelta sedimentation rates. An average sedimentation rate (ω) of 35 mm yr^{-1} over a 1000-yr time interval roughly corresponds to a prodelta progradation of 50 km.

For the lower delta plain we assume a dynamic balance between natural compaction and sedimentation, meaning that accommodation is filled through sedimentation but sedimentation rate does not exceed compaction rate. An average subsidence rate of 30-35 mm yr^{-1} is derived from 12 SET stations established at 4 locations in mangrove areas along the coast (Lovelock et al., 2015). Thus, sedimentation rates of 30-40 mm yr^{-1} represent a likely estimate of the amount of sediment required at the coastal front to balance subsidence. Notice that these SET combined with marker horizon data are not representative of most of the peninsula which is nowadays predominantly agricultural. Therefore, a reduced value is prescribed at the upper delta plain with an average floodplain sedimentation of ~6 mm yr^{-1} (Hung et al., 2014). This results in a flat and lowly elevated surface in agreement with the present setting of the VMD lower delta plain. Sedimentation likely decreases gradually away from the coastline towards the upper delta plain. Following this principle and data to constrain on past coastline progradation, a consistent behavior of sedimentation rate, $\omega(x,t)$, for the prodelta and the delta plain was determined (Fig. 3.3).

Surely, we are aware that the sediment deposition and its spatial variability as provided in Fig. 3.3a is a simplification of a much more complex process of sediment re-distribution, starting from the sources (the Mekong river and its mouth) to the dispersal work carried out by dominant longshore currents and river floodings in the delta plain. However, an accurate representation of these processes is beyond the scope of our study and it cannot be captured in a 2D modeling framework as the one used in the proposed analysis.

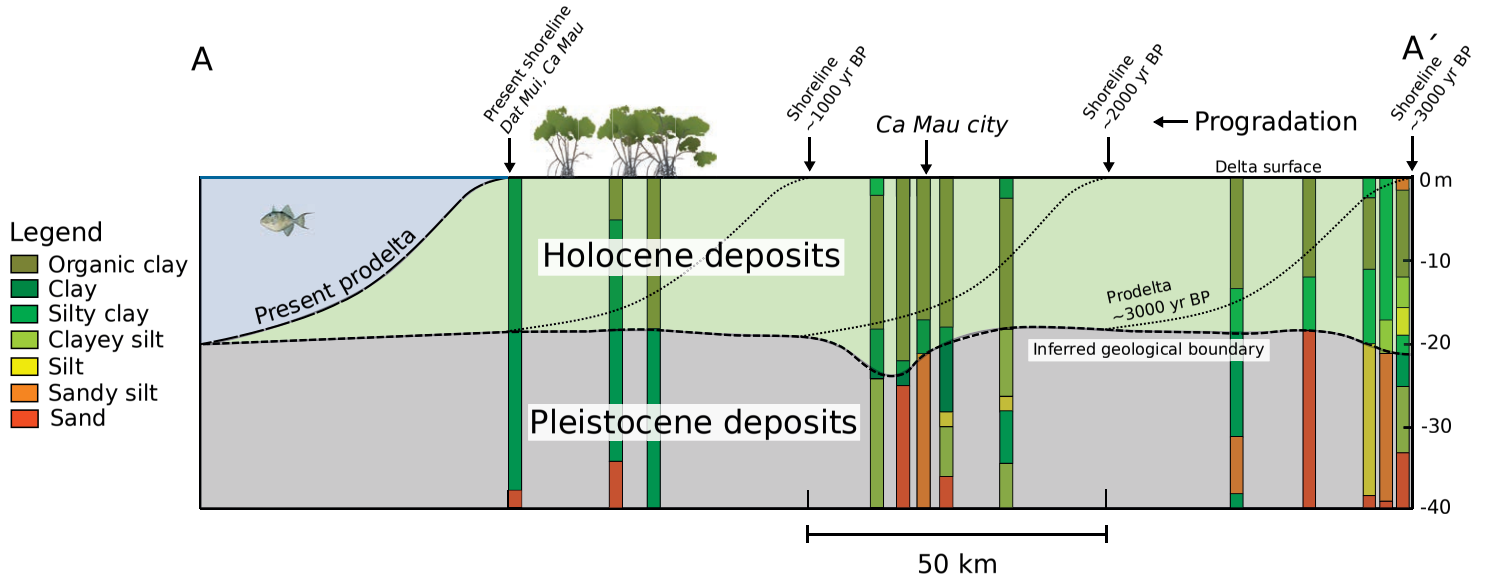

Figure 3.2 | *Lithological borelogs of the Division of Water Resources Planning and Investigation for the South (DWRPIS) of Vietnam and Division for Geological Mapping for the South (DGMS) of Vietnam along the transect A-A'. The boundary between the Holocene deposits, mainly consisting of organic clays (clays with high organic matter content), clays and silty clays and the underlying coarser and stiffer Pleistocene deposits is highlighted. The prodelta gradient is determined by profile measurements of the submarine delta front at the west side of the present VMD. The north part of the section A-A' demarcates the present boundary between the lower and the upper delta plain (Ta et al., 2005). The lithological profile at Dat Mui has been obtained from Surface Elevation Table (SET) (Giao et al., 2014).*

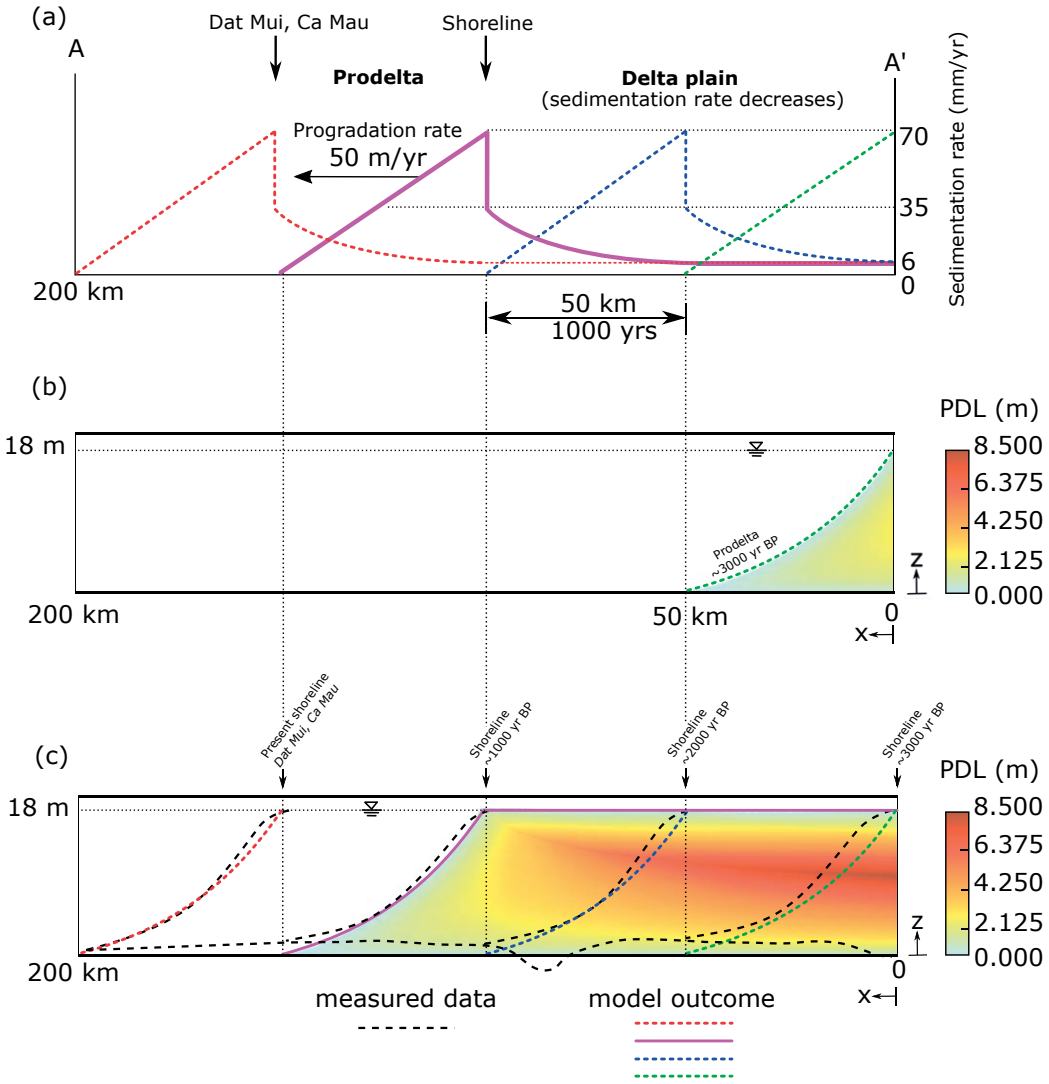

Figure 3.3 | *Prodelta formation, progradation and evolution of the delta plain. (a) Profiles of the sedimentation rate at 3000, 2000, 1000 yrs BP and present. The information on the sedimentation rates are available from literature data (Lovelock et al., 2015; Ta et al., 2002; Ta et al., 2005; Hung et al., 2014). (b) and (c) PDL distribution after the prodelta formation at 3000 yrs BP and during the delta plain evolution at 1000 yrs BP, respectively, resulting from sediment accretion and compaction. The PDL value at any z-coordinate represents the compaction of the sediment column underlying z from time of deposition to the actual time. In subpanel (c), the prodelta profiles at 3000, 2000, 1000 yrs BP and present from the model outcome are depicted by colored lines whereas dashed-black lines represent the reconstructed profiles (Fig. 3.2). The prodelta evolution is the consequence of the sedimentation rates given in subpanel (a).*

3.2.3 Hydro-geomechanical data and model set-up

The main input parameters of the model are the hydro-geomechanical properties of the Holocene deposits. These features have been quantified using datasets from the geotechnical measurements summarized in Table 3.1. Lithological boreholes and geotechnical profiles in Ca Mau revealed the presence of very soft organic clays overlying soft mineral clays in the upper 20 m-depth (Giao et al., 2014; DWRPIS, 2017). Based on the available lithological information (Fig. 3.2), these two sediment types, which prevail within the Holocene sequence, are accounted for in the model.

Table 3.1 | *Measured ranges and values of the hydro-geomechanical parameters used in the simulations. The number of available measurements is indicated with n. [a]DWRPIS (2017); [b]NGI (2017); [c]Clennell et al., (1991).*

Parameter	Measured values	Modeled values
Organic clay		
Initial void ratio (e_0)	2.52[a]	2.50
Compressibility index $C_c/(1+e_0)$	0.21-0.43 (n=10)[b]	0.30
Clay / Silty clay		
Initial void ratio (e_0)	1.55-2.63 (n=133)[a]	1.89
Compressibility index C_c	0.52-2.63 (n=133)[a]	0.57
Organic clay & Clay / Silty clay		
Initial permeability ($k_{z,0}$)	2.2 x 10^{-9} m s^{-1} [b]	2.2*10^{-9} m s^{-1}
Anistropy k_x/k_z	2.0[c]	

The behavior of the vertical oedometric compressibility c_b versus the vertical effective intergranular stress σ_z represents the fundamental constitutive relationship implemented in our modeling approach. This law is obtained by integrating the relation:

$$\frac{-1}{(1+e(\sigma_z))}de = c_b d\sigma_z \tag{3.1}$$

with e the void ratio and $e\ (\sigma_z) = e_0 - C_c\ log\ \sigma_z$. The void index e is representative of the porosity of the newly deposited sediments on the delta surface. An initial void index e_0 = 2.5 has been obtained by geotechnical analyses on shallow organic clay samples collected in Ca Mau (DWRPIS, 2017). A corresponding C_c = 1.05 is computed using the relationship $C_c/(1+e_0)$ = 0.3 experimentally derived from the geotechnical surveys carried out by NGI (NGI, 2017). These values are supported by empirical relationships(Moayed et al., 2016; Higashi et al., 2002) and measurements on similar, shallow very-soft clays in Ho Chi Minh city where C_c = 1.01 with $e_{0\ =}$ 2.23 (Thoang et al., 2015). Different values of e_0 and C_c are measured for the mineral clays underlying the organic clays. An average value C_c = 0.57 is derived using a liquid-limit relationship (Moayed et al., 2016) based on the analyses of 133 soil samples collected at Ca Mau city with e_0 = 1.89. Notice that in the proposed model the geomechanical properties depend on the lithotype and vary with the vertical effective stress differently for each sediment type. Moreover, it has been assumed that the properties of each element shift from organic to mineral clay for an effective stress larger than 5 KPa, i.e., when the element is buried at depth approximately larger than 1 m. Oedometer tests carried out by the NGI

at zero-volume change provide a vertical hydraulic conductivity $k_{z,0}$ = 2.2 x 10^{-9} m s^{-1} (NGI, 2017). This value is considered representative for the unconsolidated soil at the delta surface. Moreover, the same tests also define the following relationship between k_z and the volumetric change ε_{vol} of the porous media due to compaction:

$$\frac{\log k_{z,0} - \log k_z}{\varepsilon_{vol}} = 4.0 \tag{3.2}$$

Since ε_{vol} is provided by the numerical model as described below, Equation 3.2 allows reproducing the change of k_z during the delta evolution. Finally, an anisotropic hydraulic conductivity with a ratio between the horizontal value k_x and k_z equal to 2.0 is assumed for shallow clay material (Clennell et al., 1999).

3.2.3 Governing equations

The formation and evolution of the VMD is described with the aid of a numerical model (NATSUB-2D) by coupling a 2D groundwater flow model over a cross-section of the delta and a 1D geomechanical module. The model allows describing the spatio-temporal evolution of the consolidation process within the forming delta system, depending on the overpressure evolution. The rigorous equations of the 1D flow in an elastic saturated compacting porous medium was originally developed in the late 70s (Gambolati, 1973a; Gambolati, 1973b), where the hypothesis of infinitesimal displacement of the grains is relaxed and large soil deformations are accounted for introducing a geometric non-linearity. In a 2D vertical cross-section, the governing equations of the groundwater flow can be written as (Zoccarato & Teatini, 2017)

$$\frac{\partial}{\partial x}\left(\frac{k_x}{\gamma}\frac{\partial p}{\partial x}\right) + \frac{\partial}{\partial z}\left(\frac{k_z}{\gamma}\frac{\partial p}{\partial z}\right) = (c_b + \phi\beta)\,Dp - 2\beta k_z \frac{\partial p}{\partial z} - \beta\frac{k_x}{\gamma}\left(\frac{\partial p}{\partial x}\right)^2 - \beta\frac{k_z}{\gamma}\left(\frac{\partial p}{\partial z}\right)^2 \tag{3.3}$$

where k_x and k_z are the horizontal and vertical hydraulic conductivities, γ is the specific weight of water, c_b is the soil oedometric compressibility, φ is the soil matrix porosity, β is the volumetric water compressibility, p is the incremental pore pressure with reference to the hydrostatic condition (overpressure), x and z are the horizontal and vertical coordinates. Dp refers to the total or Eulerian derivative, which can be treated as a partial time derivative dp/dt by using a Lagrangian approach (Zoccarato & Teatini, 2017) with a dynamic mesh where the grid nodes follow the grains in their consolidation movements. In this case, the second term of $Dp = dp/dt + v_{g,z} \cdot dp/dt$ vanishes and the mesh nodes move accordingly to the vertical grain velocity $v_{g,z}$ *as* (Gambolati et al., 1998)

$$v_{g,z}(z,t) = (1 - \alpha\sigma_z)\int_0^z \frac{(\alpha + \sigma_z\frac{\partial p}{\partial t})}{(1-\alpha\sigma_z)^2}dz \tag{3.4}$$

In Equation 3.4, α is the classical compressibility defined as $\alpha = d\varepsilon_z/d\sigma_z$ with ε_z the vertical deformation, and linked to c_b by the relationship $c_b = (pd\alpha/pd + \alpha)/(1 + \alpha p)$ follows that the compaction $u(z,t)$ (and hence the volumetric change) of the mesh elements can be computed as

$$u(z,t) = -\int_0^z \frac{\alpha\sigma_z}{1-\alpha\sigma_z}dz \tag{3.5}$$

Equation 3.3 holds under the following expression of the relative Darcy's lay

$$\phi(v_{w,i} - v_{g,i}) = -k_i \frac{\partial \psi}{\partial i} \quad i = x, z \tag{3.6}$$

with $v_{g,i}$ and $v_{w,i}$ the (absolute) velocity of solid grains and water along the i direction, respectively, and the hydraulic potential expressed as $\psi = z + \int_0^p dp/\gamma$. Notice that for the specific process of interest $v_{g,x}$ is negligible and only vertical compaction is considered. Moreover, it is assumed incompressible solid grains and constant total stress expressed by Terzaghi's principle in the form $\sigma_t = \sigma_z,0 + \sigma_z + p_0 + p$, with $\sigma_z,0$ and σ_z the initial and incremental intergranular effective stress, respectively, and p_0 the initial reference value for p.

To account for the delta progradation due to sediment accumulation, a sedimentation rate $\omega(x,t)$ is admitted and Equation 3.3 turns into (Zoccarato & Teatini, 2017):

$$\frac{\partial}{\partial x}\left(\frac{k_x}{\gamma}\frac{\partial p}{\partial x}\right) + \frac{\partial}{\partial z}\left(\frac{k_z}{\gamma}\frac{\partial p}{\partial z}\right) = \left(\frac{\sigma_z \frac{d\alpha}{d\sigma_z} + \alpha}{1 - \alpha\sigma_z} + \phi\beta\right) Dp - \frac{\sigma_z \frac{d\alpha}{d\sigma_z} + \alpha}{1 - \alpha\sigma_z} D\sigma_t \tag{3.7}$$

In natural conditions, the variation of the total stress, $D\sigma_t$, is due to the change of load by new sediment deposition on the delta surface, thus $D\sigma_t = \omega(x,t)\ (1 - \varphi_0)(\gamma_s - \gamma)$ with γ_s the specific weight of the grains and φ_0 the initial porosity at $\sigma_{z,0}$. The material properties such as porosity, compressibility, and hydraulic conductivity are functions of the intergranular effective stress to account for their variability with the progressive deformation of the soil matrix. Indeed, c_b, k_z, φ diminish at increasing values of σ_z. The numerical solution of Equations 3.5 and 3.7 is implemented in NATSUB-2D by a Finite Element discretization, using a back Euler method for the time integration and a fixed-point iteration scheme to solve the material and geometric non-linearities. A constant time step equal to 1 year has been adopted. Fig. 3.4 shows the evolution of the computing mesh in time. The increasing number of triangular elements is provided to point out the spatio-temporal evolution of the computing grid following the delta formation and progradation.

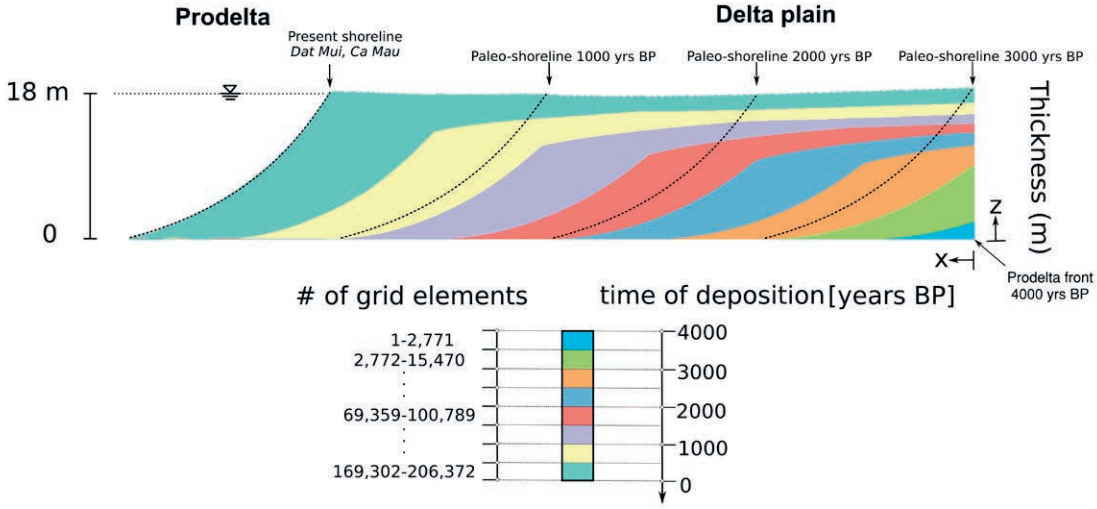

Figure 3.4 *| Evolution of the finite element mesh. The number of triangular elements in each temporal interval is provided. Note that the mesh size increases in time to account for deposition. The age of the grid elements is highlighted by colors.*

3.3 Results

The present study focuses on the simulation of the VMD evolution over the past 4000 yrs during which the prodelta moved 200 km in seaward direction along the alignment A-A' traced in Fig. 3.1. Large amounts of fine-grained material from the Mekong river mouths entered the sea and were subsequently transported by dominant longshore currents in southwest direction. Accumulation of these sediments resulted in a shoreline migration of about 150 km seaward during the past 3000 yrs at an average progradation rate of 50 m yr^{-1} (Ta et al., 2002), creating the Ca Mau peninsula. The Holocene sediments mainly consist of clay and organic clay and accumulated to a total thickness varying between 18 and 25 m on top of the older Pleistocene deposits (Fig. 3.2). We assess spatio-temporal compaction and deformation of the Holocene sediments following delta progradation for both the prodelta and the lower delta plain. The northern part of section A-A' demarcates the boundary between the marine dominated deposits of the lower delta plain and the fluvial dominated deposits of the upper delta plain (Ta et al., 2005) (Fig. 3.1).

3.3.1 Prodelta formation and progradation

The large accumulation of clayey sediments on the prodelta caused the rapid progradation of the delta in the direction of profile A-A'. The prodelta migration of 50 m yr^{-1} is simulated by a spatio-temporal evolution of the sedimentation rate properly constrained by available data. The modeling approach enabled the dynamical simulation of the prograding delta employing an adaptive mesh. New grid elements were progressively added at increasing time steps to account for the accumulation of new material, burying the underlying sediments. The mesh initially consisted of 1000 nodes and 998 triangular elements, which increased during the simulation to the final values of 103,799 nodes and 206,372 triangles. The initial thickness of a new-deposited element equaled 0.2 m, whereas a 400 m-discretization was used along the x-axis with a 1:1000 x-scaling factor. The mesh elements deformed accordingly to the occurring consolidation process and their thickness decreased as the load of the overlying sediments increased. The deformations were obtained through the computation of the movement of the soil grains, which are represented by the grid nodes, by using a 1D geomechanical model (Zoccarato & Teatini, 2017).

Prodelta formation was simulated with a sedimentation rate (ω) ranging from 0 to 70 mm yr^{-1} with shoreline proximity, accounting for increasing near-coastal sedimentation. This sedimentation evolved over the distance of 50 km in 1000 yrs (Fig. 3.3a). After 1000 yrs, i.e. at 3000 yrs BP, the prodelta was completely formed. At this stage, the accumulated sediments became elevated above sea level and the depositional environment changed from prodelta to lower delta plain. The simulated thickness of compacting sediments at the coastline reached 18 m (Fig. 3.3b). This value is in line with the 18-20 m-thick Holocene clays on top of stiffer Pleistocene silty clays to silty sands reported for the Ca Mau peninsula (Fig. 3.2) (Ta et al., 2005; Giao et al., 2014). A detailed description of the data used to derive the ω behavior is provided in Materials and Methods section.

Fig. 3.3b shows the post-depositional lowering (PDL) of the delta sediments occurred in the interval between 4000 and 3000 yrs BP. The PDL value at any z-coordinate represents the compaction of the sediment column underlying z from time of deposition to 3000 yrs BP and its integral over z gives the total compaction of the soil column. The highest PDL equal to ~2.3 m is experienced by sediments at the shoreline and approximately in the middle of the column thickness. As the cumulative amount of unconsolidated sediments deposited at the shoreline is 35 m (average sedimentation rate over 1000 yrs is 35 mm yr^{-1}), the total compaction taking place during prodelta formation is 17 m, corresponding to an average rate of 17 mm yr^{-1}. After 3000 yrs BP, the prodelta

successively advanced along the delta progradation-direction at a constant speed of 50 m yr^{-1} until it reached the present 200 km-length. Fig. 3.3c shows the profiles of delta progradation at 3000, 2000, and 1000 yrs BP, and at present. The model outcomes agree with: i) data from corings that reveal the southward evolution of the delta and approximate locations of the shoreline in the past (Fig. 3.2); and ii) high-resolution, offshore seismic profiles of the low-gradient prodelta surrounding the modern VMD with a maximum thickness of ~20 m at the shoreline (Xue et al., 2010, Liu et al., 2017).

3.3.2 Lower and upper delta plain evolution

During delta evolution over the past 3000 yrs, the lower delta plain remained about constantly elevated at the sea level or slightly above as it is at present, with wetlands forests and marshes being the main eco-morphological features (Nguyen et al., 2000). This is the result of a dynamic balance of sediment accumulation and compaction. Accommodation created by ongoing compaction following delayed overpressure dissipation was filled by new, clastic, and organic sediments. As a result, the delta plain sustained its elevation and the total thickness of Holocene sediments remained constant, while becoming more compact. Simulated sedimentation rates are based on available data. The maximum sedimentation rate equals 35 mm yr^{-1} just behind the shoreline, corresponding to the location of Dat Mui at the present day coastline (Ca Mau peninsula, see Fig. 3.2). The sedimentation rate decreases progressively moving inland along the cross-section A-A' (Fig. 3.3a) as, with the gradual decrease in overpressure (Fig. 3.5a), compaction rate decreases and less sediment is needed to fill the accommodation. On the upper delta plain, a constant sedimentation rate of 6 mm yr^{-1} suffices to counterbalance the consolidation (Fig. 3.3a).

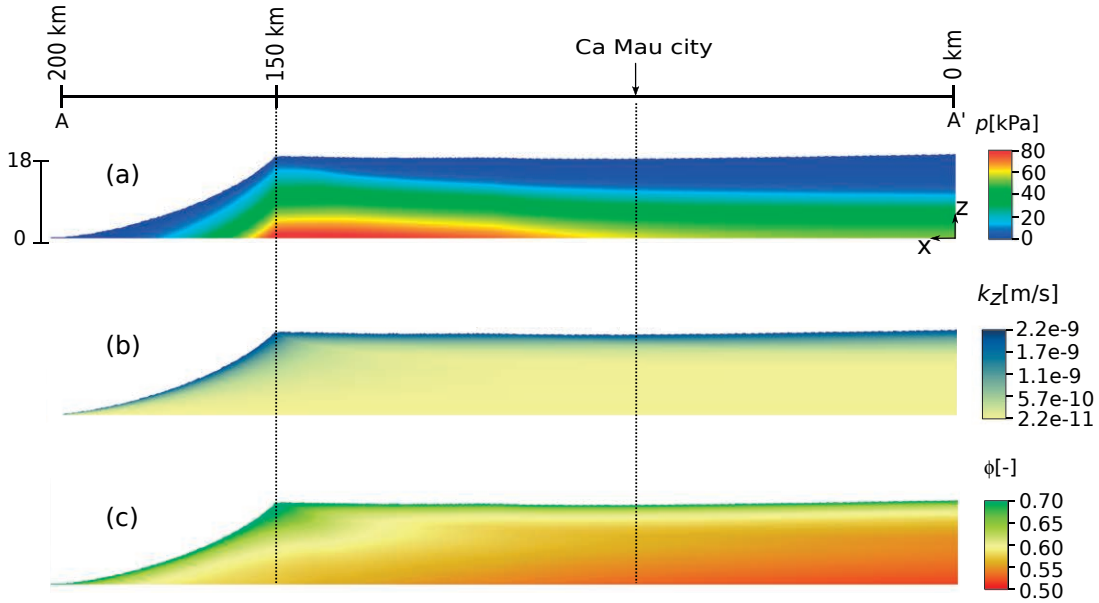

Figure 3.5 *| Distribution of (a) overpressure, (b) permeability, and (c) porosity within the cross-section A-A' (see Fig. 3.1) at present after calibration with available data of sedimentation rates and hydro-geomechanical properties of the Holocene deposits.*

At 1000 yrs BP (Fig. 3.3a, magenta line), the total compaction is equal to 17 m at shoreline location (x=100 km) and 37 m at the edge of the lower delta plain (x=0 km), where the total thickness of the deposited material (before consolidation) is 35 m and 55 m, respectively (Fig. 3.3c). The maximum PDL at 1000 yrs BP amounts up to 8.5 m (x=0 km, location of the shoreline 3000 yrs BP) (Fig. 3.3c), meaning that these sediments are now buried 8.5 m below their elevation at time of deposition. This value increases to 9.3 m at present, i.e., at the end of the model simulation.

The overpressure (p) in the present condition (t=0 yrs BP) is shown in Fig. 3.5a. The maximum value (p=80 kPa) is located at the bottom of the Holocene column at the shoreline (x=150 km) where sedimentation rate assumes the largest value. Overpressure is lower seaward as there is less overburden and inward as partial dissipation of overpressure has already taken place. At the edge of the lower delta plain(x=0 km) the remaining overpressure at the bottom of the sediment column amount to p=53 kPa. Obviously, there is no overpressure at the delta surface. At Ca Mau city (Fig 3.4), the simulated maximum overpressure is equal to ~60 kPa and the maximum PDL to ~7.8 m, suggesting that natural compaction is an ongoing process. The modeled overpressure values are within the range of values measured in shallow VMD clays using cone penetration tests (overpressures up to 200 kPa are reported) (NGI, 2017; Hoang et al., 2016). Fig. 3.5b and 3.5c show the vertical permeability (k_z) and porosity (φ) distribution within the domain, respectively. Porosity decreases with depth due to the increase of the intergranular effective stress (σ_z), see Materials and Methods for the φ-σ_z relationship. An empirical relationship is used to relate permeability to soil deformation and, in turn, to porosity distribution. The permeability reduction of about two orders of magnitude from the shallowest to the deepest deposits strongly delays overpressure dissipation and, consequently, consolidation dynamics.

3.3.3 Sensitivity analysis

The model is calibrated using the available datasets of sedimentation rates, geotechnical soil properties and lithology of the Holocene sediments. Although the model results provide a satisfactorily match with observations, we present a sensitivity analysis of the model output to the main input data and parameters to evaluate the variability range of the system dynamics due to different factors. The sensitivity analysis refers to the prodelta formation phase, i.e., the time interval between 4000 and 3000 yrs BP. The investigated range of model parameter (m_p) variability is 20% ($m_p \pm 20\% m_p$), which is probably a somewhat narrow range due to the large uncertainty associated with the hydraulic permeability and deposition rate. Fig. 3.6a shows the changes in total elevation of Holocene deposits due to variations of permeability and sedimentation rate. A smaller vertical permeability implies a slower overpressure dissipation in time, thus lower consolidation rate and higher elevations. A variation in the total elevation of 12-15% is found for $k_z \pm 20\% k_z$. On the other hand, keeping permeability fixed, the sedimentation rate affects the thickness of deposited sediments, causing an approximate 22% difference in elevation from the calibrated value.

The relation between sediment deformation and the geomechanical properties of the soil is also investigated, with the results presented in Fig. 3.6b. The geomechanical characteristics are described through the coefficient of compression, C_c, with organic clays having higher compressibility than mineral clays. C_c is kept constant for each lithological unit. A smaller C_c yields lower deformations of the porous matrix, which, in turn, influences the permeability distribution within the soil column. Following the relationship between permeability and vertical deformation ε_v provided in section 3.2, a 50% decrease of vertical deformation results in a 23% higher permeability. As such overpressure dissipation is higher, subsequently larger consolidation rates are computed. This complex behavior is summarized in Fig. 3.6b where the total deformation of the soil column ε_{tot} at x = 0 km and t =

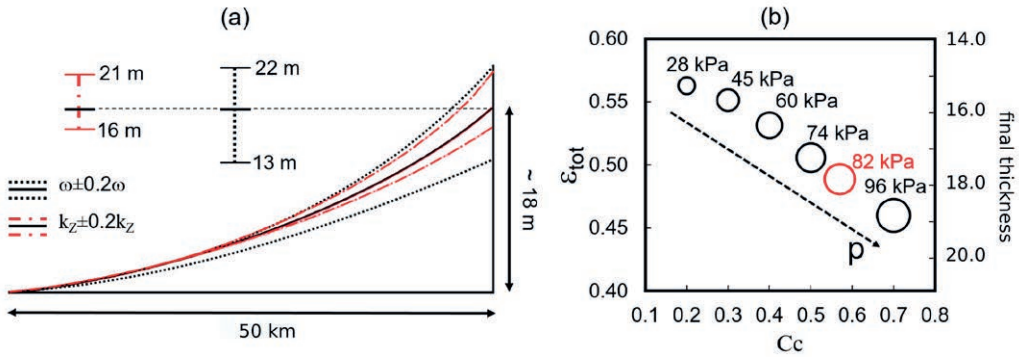

Figure 3.6 | *Influence of model parameters on the total elevation of the Holocene sediments at t=3000 yrs BP. (a) A 20% variation of sedimentation rate, ω, and the vertical permeability, k_z is investigated. The black solid line represents the shoreline computed through the calibration values used in the model, whereas the black dot-dot and red dot-dashed lines show the variability of the model outcome. (b) Total deformation, ε_{tot} , of the soil column at position x=0 m for different values of the compression index, C_c. The overpressure p increases at increasing C_c. The red circle refers to the calibrated scenario.*

3000 yrs BP is plotted against C_c. ε_{tot} is computed as $\varepsilon_{tot} = (T_{tot} - T_{3000})/T_{tot}$ with T_{3000} the thickness of the Holocene column at t = 3000 yrs BP and T_{tot} the thickness of the deposited, unconsolidated material between t = 4000 yrs BP and t = 3000 yrs BP. Overpressure drops of about 70 kPa follow the reduction of C_c from 0.7 to 0.2. This implies a 20% variation of ε_{tot}, corresponding to 3.6 m-difference in elevation.

3.3.4 Future delta evolution

In the past, natural compaction of the delta plain was counterbalanced by clastic and organic sedimentation, allowing the delta to maintain its elevation above sea level. However, cultivation (Chapter 4), dyke development on the delta plain (Triet et al., 2017), and reduction of upstream sediment supply have disturbed this natural balance. As a result, Ca Mau peninsula is receiving a decreasing amount of sediments both at the prodelta and on the delta plain. The feedback of this new condition on land subsidence is not straightforward because a dynamic coupling between accretion and overpressure dissipation, and therefore land subsidence, exists. Moreover, the coupling is governed by the intrinsic hydro-geomechanical properties of the accreting and underlying deposits.

To understand this complex mechanism the proposed model has been applied. We simulated two scenarios of delta evolution over the next 100 yrs. The first scenario (scenario A) investigates the situation in which the sediment supply is halved compared to the present values for which compaction and sedimentation are in equilibrium. The model results are provided in Fig. 3.7. With a 50% reduction of sedimentation rate, we can reasonably assume that the delta is still prograding at halved speed of 25 m yr^{-1}. The consequence is a net aggradation at the prodelta up to 6 mm . However, on the delta plain, sedimentation is no longer enough to counterbalance the consolidation of the underlying deposited sediments. At the present shoreline location (Dat Mui) this results in an average subsidence rate of 12 mm yr^{-1}, amounting to ~1.2 m by the end of the century (Fig. 3.7b). Subsidence rates decrease gradually inland to 0.8 mm yr^{-1} towards the upper delta plain.

In the worst case (scenario B) sediment deposition is assumed to cease completely (ω=0 mm yr^{-1}). Land subsidence is no longer counterbalanced by sedimentation and, because of the ongoing overpressure dissipation, subsidence is expected along the entire prodelta and delta plain. The results presented in Fig. 3.7c show a maximum loss of land elevation equal to ~2.0 m at the present shoreline, which means an average subsidence rate of 20 mm yr^{-1}. This rate gradually decreases toward the upper delta plain, where the subsidence rate drops to 2.4 mm yr^{-1}. Progradation of the VMD completely stops in this scenario and a large part of the lower delta plain will sink below sea level before the end of the century.

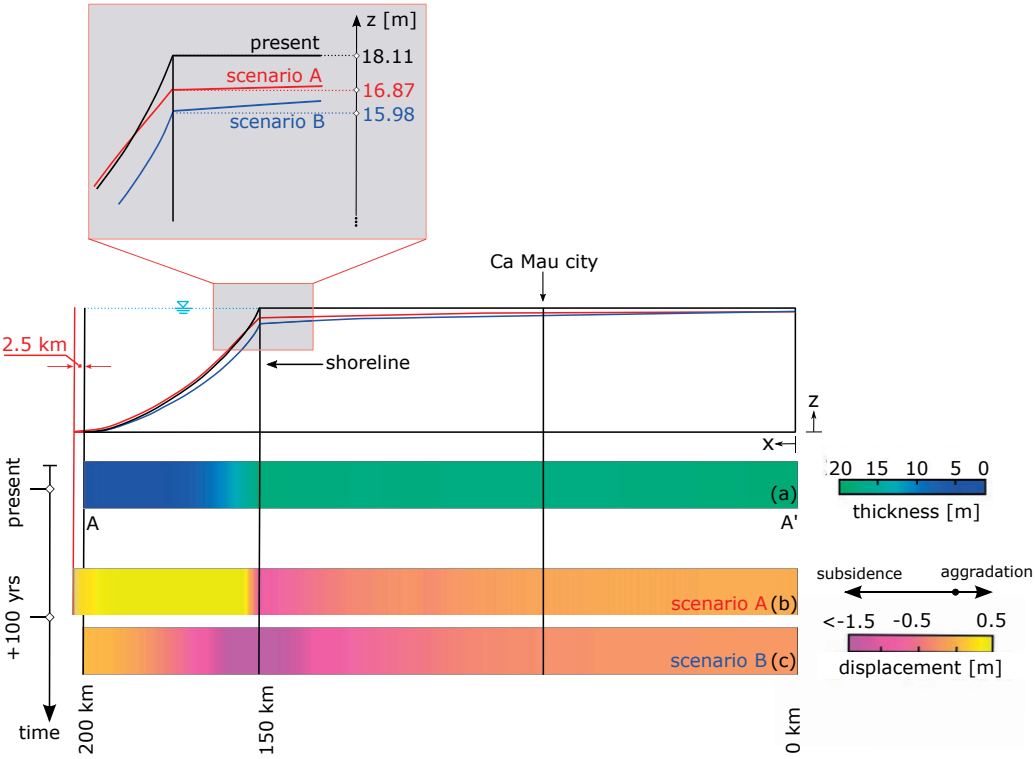

Figure 3.7 | *(a) Present thickness of the Holocene deposits along the transect A-A' as obtained by the numerical model. (b)-(c) Land displacements along the A-A' transect as computed by the model over the next 100 years for two sedimentation scenarios. In scenario A, sedimentation rates are halved (50%) compared to the calibrated distribution (Fig. 3.3b). In scenario B, sedimentation has completely stopped. Negative values mean land subsidence, positive aggradation.*

3.4 Discussion

The main processes controlling delta progradation are sediment aggradation and natural compaction of Holocene sediments. Here natural compaction involves the volume reduction of the deposited material due to the loading exerted by the overlying, more recent deposits following the consequent overpressure dissipation. Our novel model allowed for the first time to simulate the spatio-temporal formation and evolution of the VMD along a representative 2D vertical section (Fig. 3.1) by using an adaptive mesh, with changing element shape and number following new sediment deposition and consolidation over time. The modeling application is properly supported by geomorphological and geotechnical information.

We estimate rates of natural compaction of the Holocene sediment sequence at the coastline equal to ~20 mm yr^{-1} as a result of thousands of years of VMD delta evolution. These high rates were previously unaccounted for (Erban et al., 2014) and pose a serious threat to the Mekong delta as these rates cannot be mitigated. Moreover, such natural compaction rates directly affect unfounded structures and inevitably reduce the designed service life of coastal defense structures that are currently being build. As a result, if not taken into account, natural compaction seriously threatens Vietnam's investments in a hard coastal protection system of the VMD coastline. Such measures should be considered carefully, also because the construction of a coastal dyke system decreases sedimentation on the hinterland, accelerating delta plain subsidence further.

Land subsidence in modern deltas is partly related to the decrease of sediment availability (Syvitski et al., 2009). It is reported that the VMD has experienced a decrease of sediment supply by 12% in the 20th century. Larger reduction are expected in the coming decades. Dam development in the Mekong drainage basin may potentially cause major changes in the amount of sediment transported to the delta (Allison et al., 2017). Major dam construction began in the Mekong basin in 1993; by April 2016, 35 dams had been commissioned for hydropower, irrigation reservoirs, and drinking water supply. A further 226 dams are under construction and even more are planned (WLE, 2016). A recent study predicts that the cumulative suspended sediment in the Mekong river decreased to 51% following the construction of the current dams, and that this value goes up to 96% in case all planned dams are constructed (Kondolf et al., 2014). Changing global climate may also affect the future water and sediment supply to the Mekong Delta (Xue et al. 2011), as a large fraction of the suspended sediment load reaching the delta is associated with rainfall from tropical cyclones. Climate models suggest the locations of cyclone tracts to shift away from the latitude of the Mekong Basin, which may also lead to additional suspended sediment reduction (Darby et al., 2016).

We estimate that a sediment reduction of 50% over the 21st century results in a loss of elevation amounting to ~1.2 m at the present coastline due to ongoing natural compaction of the Holocene sequence. The prediction worsens if sedimentation on the delta surface is completely prevented, leading to an elevation loss of ~2.0 m by the end of the century. More inland, towards the upper delta plain, the elevation loss reduces to ~10 cm and ~20 cm for a sediment reduction of 50% and 100%, respectively. Our estimates suggest that Ca Mau city will subside ~34 cm as a result of natural compaction of Holocene sediments during the next century as flood sedimentation in the city has completely ceases.

Other natural and human-induced drivers and processes may also contribute to subsidence and the future evolution of deltaic regions. Examples of natural subsidence drivers are tectonics, natural compaction of Quaternary units, and glacial isostatic adjustment. In the VMD their contribution to subsidence has been quantified in the order of a few mm yr^{-1} over the late-Holocene (Nguyen et al., 2000; Hanebuth et al., 2011). Therefore, they have played a secondary role on the recent

delta evolution and have been neglected in our analysis. The effect of biological and chemical processes, which may trigger additional subsidence, have been negligible in the past as a result of the general waterlogged conditions and were therefore not included in this study. However, they should be accounted for in future modeling as drained conditions may be established in deltaic-plain sediments for agricultural purposes. Aeration triggers oxidation of the organic matter, which represents a large fraction of the top soils, and consequently enhances the ongoing natural compaction as experienced for example in the Rhine-Meuse (The Netherlands)(Asselen et al., 2009; Koster et al., 2016) and Po (Italy)(Zanello et al., 2011) river deltas. Concerning anthropogenic subsidence, groundwater pumping from the deep multi-aquifer system has significantly contributed, in the range of 10 to 25 mm yr^{-1}(Chapter 5), to the present land subsidence in the VMD over the last few decades. Oil and gas activities are also on the rise offshore of the VMD with areas undergoing seismic exploration and some initial drilling by the Vietnam National Oil and Gas Group (PetroVietnam) and international partners (Allison et al., 2017). Future hydrocarbon explorations may contribute as well to subsidence of the delta.

Finally, also sea level rise contributes, although secondarily, to the relative loss of land elevation with respect to the sea level. Estimates of absolute sea level rise for the VMD are ~3.5 mm yr^{-1} (Nicholls & Cazenave, 2010), which are small compared to the land subsidence the delta may experience in the coming decades. Our study reveals that natural compaction of the Holocene sediments alone can create subsidence rate up to one order of magnitude larger than absolute sea level rise. As the VMD is only elevated ~1-2 m above sea level, the anticipated subsidence rates seriously threaten the lower delta plain with permanent inundation. Therefore, sediment supply to the delta plain and a proper management of surface water and groundwater resources are key factors for the VMD survival. The model presented here represents a valuable tool for understanding the natural compaction dynamics of the VMD and, more generally, of coastal environments at risk of submersion. It can be used to identify areas vulnerable to high compaction rates and hereby contribute to improve coastal protection plans.

Acknowledgements
We thank the Division of Water Resources Planning and Investigation for the South (DWRPIS) of Vietnam and Division for Geological Mapping for the South (DGMS) of Vietnam for supplying lithological and geotechnical data. Kjell Karlsrud of the Norwegian Geotechnical Institude (NGI) is thanked for discussions on the subject and sharing geotechnical data from three subsidence monitoring sites in Ca Mau. Simon van Laarhoven (former MSc. student of PM) is thanked for building the digital geotechnical database of this data. CZ and PT are supported by the Flagship Project RITMARE - The Italian Research for the Sea, CNR-MIUR, National Research Program 2011-2013, "Linea SOLVE".

Author contributions statement
P.M. and P.T. conceived the experiments. P.M. built-up the dataset. C.Z. developed the model and conducted the experiments. All authors analyzed the results and prepared the manuscript.

4 The relation between land use and subsidence in the Vietnamese Mekong delta

The Vietnamese Mekong delta is subsiding due to a combination of natural and human-induced causes. Over the past several decades, large-scale anthropogenic land-use changes have taken place as a result of increased agricultural production, population growth and urbanization in the delta. Land-use changes can alter the hydrological system or increase loading of the delta surface, amplifying natural subsidence processes or creating new anthropogenic subsidence. The relationships between land use histories and current rates of land subsidence have so far not been studied in the Mekong delta. We quantified InSAR-derived subsidence rates for the various land-use classes and past land-use changes using a new, optical remote sensing-based, 20-year time series of land use. Lowest mean subsidence rates were found for undeveloped land-use classes, like marshland and wetland forest (~6-7 mm yr^{-1}), and highest rates for areas with mixed-crop agriculture and cities (~18-20 mm yr^{-1}). We assessed the relationship strength between current land use, land-use history and subsidence by predicting subsidence rates during the measurement period solely based on land-use history. After initial training of all land-use sequences with InSAR-derived subsidence rates, the land-use-based approach predicted 65-92% of the spatially varying subsidence rates within the measurement error range of the InSAR observations (RMSE = 5.8 mm). As a result, the spatial patterns visible in the observed subsidence can largely be explained by land use. We discuss in detail the dominant land-use change pathways and their indirect, causal relationships with subsidence. Our spatially explicit evaluation of these pathways provides valuable insights for policymakers concerned with land-use planning in both subsiding and currently stable areas of the Mekong delta and similar systems.

Published as: Minderhoud, P.S.J., Coumou, L., Erban, L.E., Middelkoop, H., Stouthamer, E., Addink, E.A. (2018). **The relation between land use and subsidence in the Vietnamese Mekong delta.** *Science of the Total Environment,* 634, 715–726. doi:10.1016/j.scitotenv.2018.03.372

4.1 Introduction

Many of the world's major deltas have experienced significant anthropogenic change during the past decades. Within Southeast Asia, the Vietnamese Mekong delta stands out as hotspot of anthropogenic land-use change (Giri et al., 2003). Following Vietnam's transition towards an open-market economy in 1986, the vast majority of natural wetlands and forested areas in the delta have been converted to agricultural lands dominated by rice paddies (Funkenberg et al., 2014; Tran et al., 2015). Along the Mekong river branches, orchards and fish farms have been created, and in the coastal zone vegetables farms sprouted on the higher elevated beach ridges. Furthermore, mangroves have been cut to make place for shrimp farms and other aquaculture (a.o. Binh et al., 2005; Sakamoto et al., 2009; Tong et al., 2004). Over the years, rice production in the delta

has increased as intensified irrigation allowed for more crops per year (Sakamoto et al., 2006). Moreover, the delta has become progressively urbanized, with an ever-densifying and expanding network of roads connecting the fast-growing settlements, cities and industrial areas (Karila et al., 2014; Tran et al., 2015). Other large-scale alterations of the delta system include increased flood control through extensive dike systems (Triet et al., 2017), sand mining activities in the river branches (Brunier et al., 2014), and wide-spread exploitation of groundwater resources (Wagner et al., 2012). The Vietnamese Mekong delta is further impacted by reduced sediment supply due to upstream dams (Kummu et al., 2007; Kondolf et al., 2014), decreased hurricane activity (Darby et al., 2016), salinization (Renaud et al., 2015), coastal erosion (Anthony et al., 2015) and global sea-level rise in response to climate change (Wassmann et al., 2004). On top of that, the delta is subsiding at rates up to several centimeters a year, exceeding current absolute sea-level rise by up to a magnitude (Erban et al., 2014; Minderhoud et al., 2017).

Land subsidence is a natural phenomenon in delta systems. Deltaic sediments are highly compressible and susceptible to significant natural compaction during deposition and subsequent soil formation. Enhanced land subsidence in deltas due to human activities is widely recognized (e.g. Syvitski et al., 2009; Giosan et al., 2014). Human use of land and groundwater resources can amplify natural subsidence processes or initiate new anthropogenic subsidence in different ways (Galloway et al., 2016). Firstly, subsidence can be enhanced by direct loading of the delta surface, both by natural material, such as water and sediment, and by anthropogenic artifacts, such as buildings and infrastructure. Secondly, drainage of wetlands to prepare for agricultural use leads to a lowering of the phreatic water table, causing compaction and aeration of the subsoil. Consequent decomposition of organic material (oxidation) causes additional volume reduction (e.g. Van Asselen et al., 2009). Additionally, the extraction of groundwater from deeper aquifers (water-bearing sediment layers), to meet the increasing freshwater demands of rapidly urbanizing areas, agriculture and aquaculture, can trigger aquifer-system compaction (e.g. Galloway & Burbey, 2011; Gambolati & Teatini, 2015). In the Vietnamese Mekong delta evidence of widespread absolute subsidence was recently revealed by InSAR (Interferometric Synthetic Aperture Radar) (Erban et al., 2013; 2014). Minderhoud et al. (2017) demonstrated that a steady increase of groundwater use and excessive pumping over the past decades has dramatically accelerated subsidence in this area. Together, these land-use developments of the past decades in the Vietnamese Mekong delta have affected the natural environment, and introduced anthropogenic drivers, enhancing subsidence rates.

Subsidence is a sluggish process that may show a remarkably slow but pertinent response to a change in land use, due to time-dependent effects of both subsidence *drivers* and *processes*. For example, the amount of groundwater extraction (*driver*) might grow gradually over the years following a change in land use. The consequent aquifer-system compaction (*process*) increases even more slowly, as it takes time for overpressure to dissipate from clay-rich sediments which than start to compact and due to time-dependent secondary consolidation. This process can continue up to decades after initiation. This implies that groundwater extractions under past land use still can affect present-day subsidence rates; hence land use and land use history might be important indicators of present-day subsidence rates in a delta.

In this study, we aim to quantify the relationship between land use and land subsidence rates and to determine the effect of past land-use changes in the Vietnamese Mekong delta. We hypothesize that land use and land-use history correlate to subsidence in two ways: 1) by affecting subsidence drivers and processes as described above, and, 2) through location preference of certain land-use types for a geomorphological setting with specific subsidence characteristics, e.g. orchards prefer higher elevated, sandy natural levees, which are less prone to shallow compaction. Thus, land

use could potentially explain part of the spatial patterns of observed subsidence rate and may serve as an indirect proxy for subsidence rate. We used optical remote sensing-based products to map land use and land-use change, together with InSAR-derived subsidence rates for a representative part of the Mekong delta. We created a time series of land use from Landsat TM5 images and determined subsidence rates for specific land-use sequences both for areas with unchanged land use in the period 1988-2006, and for areas in which land-use changes occurred during this period. Subsequently, we assessed the impact of land use and land-use changes on subsidence rates and derive time-dependent effects of subsidence. Moreover, we evaluate the strength of the relationship between land use and subsidence rate by predicting and mapping subsidence rate solely based on land use and land-use history. The ability to predict subsidence rates based on land use and land-use history, after the initial training of individual land-use change sequences with observed subsidence rates, reveals the relation between land use and subsidence in the Mekong delta.

4.2 Data and methods

4.2.1 Consistent land-use time series

A consistent land-use time series of the Mekong delta over the past decades is required to study the relation between land use, land-use change and subsidence rates. The Vietnamese government produces land-use maps every five years (Dijk et al., 2013; Phuong & Catacutan, 2014), but they are not publicly accessible and, if available, lack metadata on data sources and used methods. Besides these national maps, many land-use maps exist for the Mekong delta, however they all vary in terms of *subject* (e.g. rice cropping system: Bouvet & Le Toan., 2011; Karila et al., 2014; Kono, 2001; shrimp farm expansion: Giang & Hoa., 2013; Tong et al., 2004; Vo et al., 2013), *spatial extent* (regional: e.g. Chen et al., 2012; delta-wide: e.g. Sakamoto et al., 2006, 2009, Son et al., 2013 and Xiao et al., 2006), *defined land-use classes* (Kuenzer et al., 2011), *used satellite imagery* (MODIS (e.g. Kuenzer & Knauer, 2013), SPOT (e.g. Nguyen et al., 2012), Landsat (e.g. Funkenberg et al., 2014) or Rapid Eye (e.g. Huth et al., 2012) and *classification method and accuracy* (Kuenzer et al., 2011; Kuenzer & Knauer, 2013). Consequently, no single study or combination of studies provided a consistent land-use time series of the Mekong delta appropriate for our study.

Land-use mapping

We created a new consistent time series of land-use maps using optical remote sensing Landsat Thematic Mapper (TM) 5 images. Landsat TM5 imagery was selected for its long period of available images (1984-2013), the large range of spectral bands, the suitable ground resolution (30 m) for land-use mapping and free of charge availability (see Appendix B, section B.1.1). The Landsat tile with the largest spatial coverage of the delta was selected as study area (WRS path 134, row 053, Fig. 4.1). This area hosts all major land-use types present in the Mekong delta. We selected four images with limited cloud cover acquired during the dry season (January – March) in 1988, 1996, 2006 and 2009 to enable distinction of dry-season irrigation.

For our analyses we defined land-use classes that 1) encompassed all land-use types representative for the entire delta, 2) were identifiable from the Landsat 5 TM images and 3) were potentially related to different subsidence drivers. We considered the characteristics of all land-use classes regarding the following three main human-induced subsidence drivers associated with land-use practices: 1) lowering of the phreatic water table, 2) extracting groundwater and 3) loading of the delta surface by buildings and infrastructure (Table 4.1). Unlike other land-use studies in the

Mekong delta, we did not distinguish rice agriculture based on the number of annual crops, for this could not be determined based on a single, dry-season image. Nevertheless, rice crop phenology patterns (Son et al., 2014) do indicate that our land-use class 'dry-season rice' likely corresponds to two or three annual irrigated rice crops and 'dry season bare field' to one or two annual rain-fed crops.

Table 4.1. | *Land-use classes used for the classification and their estimated characteristics related to subsidence.*

Land-use class	Land-use practices related to subsidence		
	Phreatic water table	Groundwater use	Anthropogenic loading
Marshland/marshes	High, year-round	-	-
Wetland forest [1]	High, year-round	-	-
Mangroves	High, year-round	-	-
Dry-season rice *(irrigated rice; two or three crops yr[-1])*	High, year-round (excl. harvest)	-[2]	-
Dry-season bare field *(rain fed rice; one or two crops yr[-1])*	Wet- and dry-season fluctuation	-	-
Dry-season partly rice (alternation rice and bare field) [3]	Wet- and dry-season fluctuation	-[2]	-
Mixed crops – non-rice	Lowered by drainage	Moderate-High	-
Orchard	Lowered by drainage	Low-Moderate	-
Aquaculture (mainly shrimp farming)	Wet- and dry-season fluctuation	Moderate-High	-
Linear settlements [4]	Wet- and dry-season fluctuation	Low-Moderate	Moderate
Urban dense	Lowered by drainage	High	High
Urban open	Lowered by drainage	High	High
Water: sea, rivers, small channels			
Clouds			

[1] Based on other land-use maps, 'wetland forest' is dominated by melaleuca trees, but other tree species may be present.
[2] Groundwater use for rice irrigation is prohibited by Vietnamese law. Rice is irrigated using surface water.
[3] The classification aims at classifying land-use at delta scale and therefore, relatively small-scale inter-field alternations between the 'dry season rice' and 'dry season bare field' class are merged as one class: 'Dry season partly rice'.
[4] Linear settlements are narrow settlements or groups of buildings stretched along a transport route, like a road or canal. They are the common form of settlement in the rural parts of the Mekong delta.

Object-based image analysis

The Landsat images were classified using object-based image analysis (OBIA) (Addink et al., 2012). This means that neighboring pixels in the images are grouped into objects ('segmentation'), which are subsequently classified based on object characteristics. The large advantage of OBIA over more traditional, pixel-based classification is that not only spectral, but also shape and context characteristics can be used for the classification (Addink et al., 2012). This enables the distinction of different land-use classes with similar land cover and hence spectral behavior in the Landsat images. For example, a shrimp pond and a canal both have the spectral properties of water. However, with OBIA they can be distinguished based on their shape, e.g. rectangular versus a line. As a result, OBIA generally performs better than pixel-based approaches, especially with high-resolution imagery (Blaschke, 2010).

As preprocessing step, we created a shapefile outlining clouds and cloud shadows in each image. In this step, each image was segmented and classified using the seven Landsat 5 TM spectral bands, the enhanced vegetation index (EVI), the normalized difference vegetation index (NDVI) and the normalized difference moisture index (NDMI) (see Appendix B, section B.1.2.1. for detailed description of the process and segmentation settings). The classification result was subsequently used to mask the clouds and cloud shadows in the Landsat images. Subsequently, each cloud-masked Landsat image was segmented using six Landsat 5 TM spectral bands (thermal infra-red was excluded because of its coarser resolution and limited value for land-use discrimination), the EVI and the NDMI. Pixels were grouped based on their spectral resemblance aiming at maximum

within-object spectral similarity (see Appendix B, Section B.1.2.2. for details). After segmentation, a large random selection of objects (n = 1100) was manually labelled to the corresponding land-use class to serve as training and validation datasets.

Land-use classification

We employed a 'random-forest' algorithm to assign the land-use classes to the segments in the Landsat images (Gislason et al., 2006; Rodriguez-Galiano et al., 2012). A random forest is a data-mining or machine learning method that uses an ensemble of decision trees (the 'forest') to 'predict' land-use class using multiple object variables (here spectral, shape and context characteristics of the object). We used the randomForest package v. 4.6-12 in R v 3.3.2 (Breiman & Cutler, 2003). Random forests are insensitive to noisy input data and make no assumptions about the frequency distribution of training samples (Funkenberg et al., 2014). Besides they correct for potential overfitting of a single decision tree (Breiman, 2001).

The randomly selected training-and-validation dataset was split randomly into a training (2/3) and validation set (1/3). The training set was used to train a random forest, containing 10,000 decision trees, with 55 object features as input variables and the land-use classes as output variable (Appendix B, Table B.4). The trained random forest was subsequently used to classify all objects of the image based on their spectral and spatial characteristics. This procedure was repeated for each Landsat image to create four consistent land-use maps. The land-use map of 2009 suffered from extensive cloud cover, which would greatly reduce the size of the area for analysis. Moreover, comparison between the 2006 and 2009 land-use map revealed few differences. Therefore, we excluded the land-use map of 2009 from further analyses and adopted the land-use map of 2006 as representative for the period during which the InSAR-based subsidence rates were estimated (2006-2010). From the three remaining maps, we created maps that indicate the land-use sequence from 1988 to 2006. For complete description of the land-use classification procedure, pre- and post-processing steps and validation, see Appendix B (B.1.2).

4.2.2 InSAR-derived subsidence rates

The InSAR-derived (Interferometric Synthetic Aperture Radar) subsidence rates by Erban et al. (2013, 2014) are the first, and until present only, available estimates of subsidence providing spatial coverage for large parts of the Vietnamese Mekong delta. The subsidence rate estimates are based on the phase shift in radar returns from coherent reflectors at the earth surface or from areas where the surface texture remains largely unchanged during the study period. Examples include roads and rooftops, which are well distributed throughout the delta in urban and rural areas. Subsidence rates are not estimated for pixels with low InSAR correlation. Changes in surface elevation due to flooding and associated sediment aggradation therefore cannot be detected using InSAR, as areas subject to these changes exhibit low InSAR correlation. As a result, the subsidence-rate estimates do not provide continuous spatial coverage. Furthermore, as sediment aggradation is not included, the quantified rates represent subsidence rather than net surface elevation change. The InSAR raster dataset (spatial resolution ~57 x 57 m) represents mean subsidence rates for the period 2006-2010 (in mm yr^{-1}), with an estimated error due to spatio-temporal variability in surface scattering properties of 5-10 mm yr^{-1} (Erban et al., 2013). The rasters were georectified, mosaicked and a subset was created for the extent of the study area (Fig. 4.1).

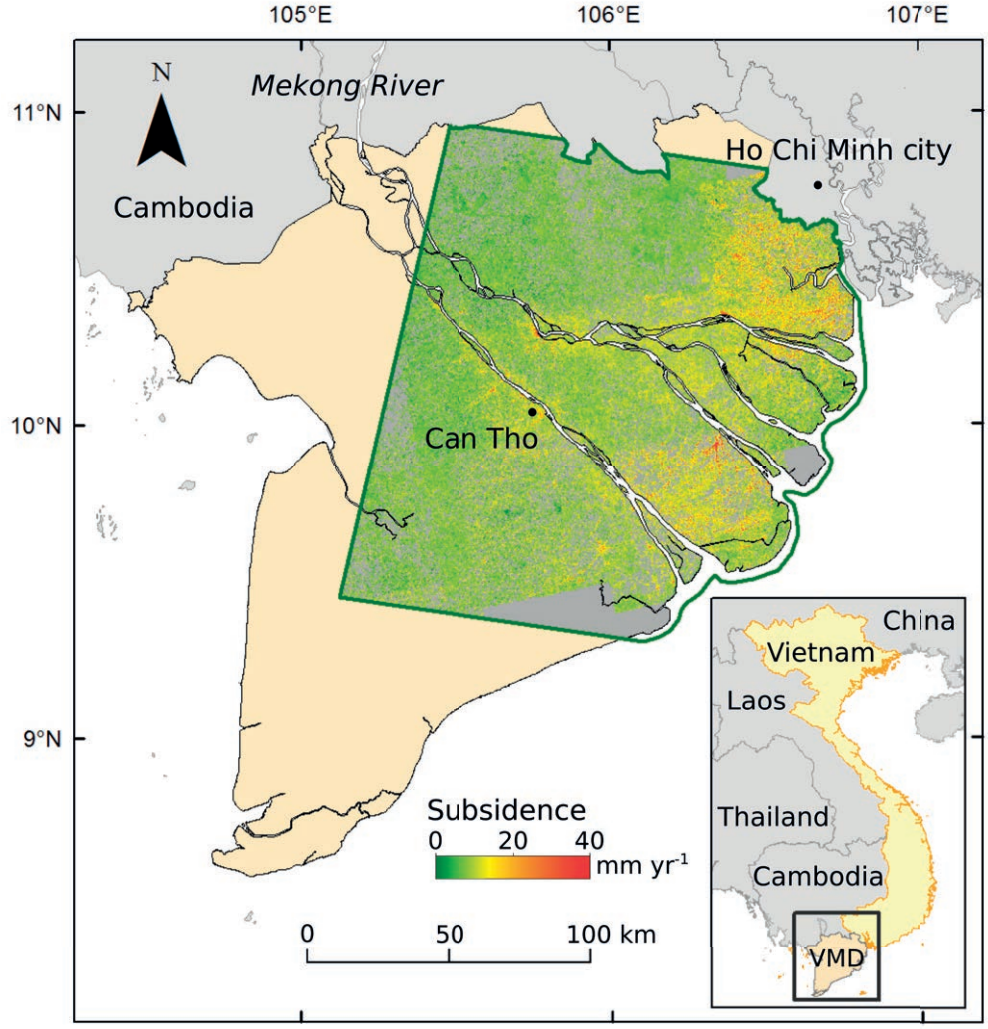

Figure 4.1 | *The location of the study area (outlined in green) with InSAR-derived subsidence rates in the Vietnamese Mekong delta (VMD) in Southeast Asia. The selected area corresponds to the Landsat 5 TM tile: WRS path 134, row 053 (USGS, 2016) and has an area of ~20,000 km^2. Subsidence rates are InSAR-derived annual means for 2006-2010 (Erban et al., 2014).*

4.2.3 Relating land use and land-use change to subsidence

The land-use-sequence maps were combined with the InSAR-based subsidence rates to quantify subsidence rates for individual land-use sequences. First, the InSAR raster dataset was converted to a point dataset with a point in the center of each grid cell. Then, the InSAR points corresponding to each land-use-sequence object were extracted and their median subsidence value was assigned as representative object-subsidence rate.

Four categories of land-use sequences can be distinguished. The first category comprises the constant-land-use sequences, i.e. land use remained the same from 1988 until 2006. The second category comprises the sequences where a land-use conversion occurred between 1988 and 1996, but no conversion took place between 1996 and 2006. The third category is the inverse of the second and in the fourth category during both periods a change occurred. This resulted in a map with segments representing unique sequences of 3 land use types that occurred in the three periods. We focused on the first, second and third category (sequence category 1, 2 and 3), i.e. where the land-use sequences contain at most one change in land-use.

We compared subsidence rates for the first three categories (category 1, 2 and 3) of land-use sequence to determine the relation between land use and subsidence. For each land-use sequence the subsidence rates in all composing objects with this sequence were determined, and the median value of these rates was taken to obtain the characteristic land-use-sequence subsidence rate. The subsidence rates for the sequence category without land use change were considered to represent the primary relation between land use and subsidence rate. By comparing these subsidence rates with those for the other two categories of sequences (with land-use change), we determined a potential time-lag effect in the response of subsidence rate to land-use change. So, for example, we compared subsidence rates for the marshland-changed-to-rice sequences (sequence categories 2 and 3) with those for areas that where marshland and rice fields during the entire period (both first sequence category). For these analyses, we focused on the prominent and characteristic land-use sequences that reflect the developments in the delta, which are: cultivation of previously undeveloped land, changes in agricultural practice, and urbanization.

4.2.4 Predicting subsidence rates based on land-use sequence

We evaluated the strength of the relationship between land use, land-use change and subsidence according to the ability to predict subsidence rates based solely on land-use history. For each unique sequence, two thirds of the objects were assigned to a training set and one third to a validation set. All objects classified as water in any year were excluded. For each unique land-use sequence we determined the median InSAR-based subsidence rate of all comprising objects. Next, a subsidence prediction map was made by assigning the median rate of each land-use sequence to every individual object. From the resulting map the independent validation objects were retrieved and their InSAR-based subsidence observation was compared to the land-use predicted value. To test the added value of including land-use history and not just land use in the analysis, we also created a prediction map based only on the land use map of 2006 for comparison.

4.3 Results

4.3.1 Land-use maps and land-use change

The land-use maps for 1988, 1996, 2006 and 2009 based on the Landsat TM5 images are shown in Fig. 4.2; the areal coverage of each land use class is shown in Appendix B, Fig. B.2. None of the maps is completely cloud-free, but the 2009 land-use map suffers from extensive cloud cover (>26%). The overall accuracies of the land-use maps are 77%, 94%, 92% and 89% for the land-use maps of 1988, 1996, 2006 and 2009 respectively (Appendix B, Table B.5).

Between the years 1988, 1996 and 2006, major changes in land use occurred, and by the year 2006 only 30% of the area land use had remained unchanged since 1988 (Table 4.2). The total area of undeveloped land (i.e. marshland, wetland forest and mangroves) strongly decreased from 18% to 5% between 1988 and 2006. The total area used for rice production (i.e. 'dry-season bare field', 'dry-season partly rice', 'dry-season rice') remained stable throughout this period, and covered over half of the entire study area. The area used for other agricultural practices (orchards and mixed crops) strongly increased between 1988 and 1996, but decreased again towards 2006, while aquaculture and urbanized areas steadily increased in size from the start of the study period until 2006. These developments directly reflect population growth and urbanization of the Mekong delta during the past decades with growing delta cities and more shrimp farms as response to increased salinization.

The transition matrices for the periods 1988-1996 (Table 4.3) and 1996-2006 (Table 4.4) provide a quantitative overview of the land-use changes. The most prominent change that took place is the expansion of irrigated rice culture (class 'dry-season rice') by reclaiming marshland and intensifying rice production that previously were rain-fed ('dry-season partly rice' and 'dry-season bare field'), especially between 1988 and 1996. Along the main river braches, orchards expanded at the expense of 'dry-season rice'. Furthermore, along the coast mangroves were cut to make place for aquaculture. The area of wetland forest strongly increased between 1996 and 2006 at the expense of marshlands, reflecting natural succession or anthropogenic conversion to forested lands. Finally, urban areas expanded, as well as rural settlements that appeared as linear elements throughout the delta.

Table 4.2 | *Total area of main land-use classes in the land-use maps of 1988, 1996 and 2006. Area is color-coded from green (small) to red (large) and given in percentage of the total study area excluding cloud-covered areas.*

	Land-use maps		
Main land-use classes	**1988**	**1996**	**2006**
Undeveloped	18	9	5
Rice	54	50	54
Other agriculture	21	32	23
Aquaculture	4	4	8
Urban	3	5	10

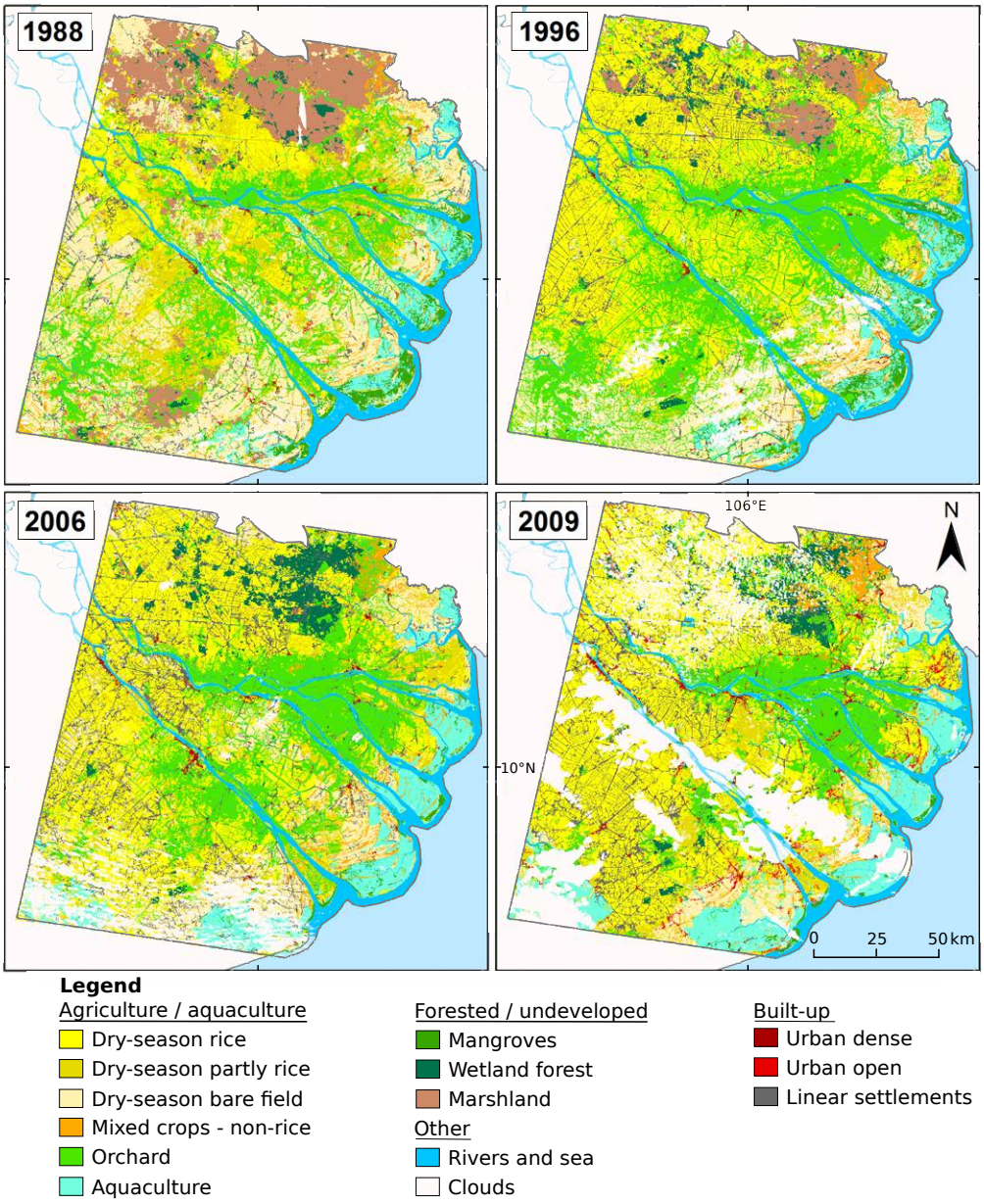

Figure 4.2. *Land-use maps of the northeastern part of the Vietnamese Mekong delta derived from Landsat 5 TM imagery of 1988, 1996, 2006 and 2009. The 'dry-season rice' class represents irrigated rice cultivation producing two or three annual rice crops, while 'dry-season bare field' is rain-fed rice with one or two annual rice crop(s). 'Dry-season partly rice' represents small-scale patchwork of rice crops and bare field.*

Table 4.3 | *Land use and land-use changes: 1988 and 1996. Area is color-coded from green (small) to red (large) and given in percentage of the total study area excluding cloud-covered areas. Land use remained unchanged in 42% of the study area (in italic the percentage of unchanged land-use area). Blank spaces show land-use changes that did not happen.*

Land-use class in 1988	Land-use class in 1996													
	Aqua-culture	Dry-s. rice	Dry-s. p. rice	Dry-s. b. field	Mix c. no rice	Mangro ves	Wet. Forest	Orchard	Urban dense	Urban open	Linear Settle.	Water	Marsh-land	Total in 1988
Aquaculture	*2.4*	0.0	0.0	0.1	0.0	0.6		0.1	0.0		0.0	0.1	0.0	3.4
Dry-season rice	0.0	*7.1*	0.1	0.1		0.0	0.0	1.2	0.0	0.0	0.5	0.0	0.0	9.1
Dry-season partly rice	0.1	6.5	*0.7*	0.6	0.2	0.1	0.2	7.7	0.0	0.1	1.0	0.1	0.2	17.4
Dry-season bare field	0.4	8.6	1.5	*7.3*	0.5	0.3	0.0	3.5	0.1	0.1	0.8	0.1	0.1	23.2
Mix crops - non-rice	0.1	0.1	0.1	0.2	*0.6*	0.1	0.0	0.3			0.1	0.0	0.1	1.6
Mangroves	0.6	0.0	0.0	0.1	0.0	*1.1*		0.2			0.0	0.0		2.1
Wetland forest	0.0	0.2	0.0	0.0	0.0		*0.4*	0.1			0.1	0.0	0.3	1.1
Orchard	0.1	3.8	0.4	0.3	0.2	0.3	0.3	*11.5*	0.0	0.0	0.8	0.2	0.1	17.8
Urban dense		0.0	0.0						*0.0*	0.0	0.0			0.1
Urban open	0.0	0.0	0.0	0.0	0.0			0.1	0.0	*0.0*	0.0	0.0	0.0	0.3
Linear settlement	0.0	0.7	0.1	0.2	0.1	0.0	0.0	0.4	0.0	0.0	*0.5*	0.0	0.0	2.1
Water	0.4	0.1	0.0	0.0	0.0	0.1	0.0	0.3	0.0	0.0	0.1	*7.2*	0.0	8.3
Marshland	0.0	5.5	0.4	0.5	0.3	0.0	0.9	1.6	0.0	0.0	0.7	0.1	*3.4*	13.6
Total in 1996	4.0	32.6	3.4	9.7	1.9	2.5	1.9	27.1	0.2	0.2	4.5	7.9	4.2	100.0

Table 4.4 | *Land use and land-use changes: 1996 and 2006. Area is color-coded from green (small) to red (large) and given in percentage of the total study area excluding cloud-covered areas. Land use remained unchanged in 53% of the study area (in italic the percentage of unchanged land-use area). Blank spaces show land-use changes that did not happen.*

Land-use class in 1996	Land-use class in 2006													
	Aqua-culture	Dry-s. rice	Dry-s. p. rice	Dry-s. b. field	Mix c. no rice	Mangro ves	Wet. Forest	Orchard	Urban dense	Urban open	Linear Settle.	Water	Marsh-land	Total in 1996
Aquaculture	*3.5*				0.1	0.2		0.1			0.1	0.1		4.0
Dry-season rice	0.0	*19.3*	3.9	3.0	0.1	0.0	0.5	3.2	0.0	0.0	2.5	0.0		32.6
Dry-season partly rice	0.1	1.0	*0.7*	0.6	0.1	0.0	0.1	0.5	0.0	0.0	0.4	0.0		3.4
Dry-season bare field	0.8	1.6	1.0	*4.9*	0.3	0.0	0.1	0.4	0.0		0.6	0.0	0.0	9.6
Mix crops - non-rice	0.1	0.1	0.4	0.2	*0.7*		0.0	0.3	0.0	0.0	0.1	0.0		1.9
Mangroves	1.5	0.1	0.2	0.1	0.2	*0.3*		0.2	0.0		0.1	0.0		2.5
Wetland forest	0.0	0.6	0.0	0.0	0.0		*0.8*	0.3			0.2	0.0	0.0	1.9
Orchard	0.6	4.0	3.9	1.1	0.4	0.1	0.4	*13.8*	0.1	0.0	2.5	0.2	0.0	27.1
Urban dense	0.0	0.0	0.0	0.0	0.0		0.0	0.0	*0.1*	0.0	0.0			0.2
Urban open		0.0	0.0	0.0	0.0		0.0	0.0	0.1	*0.0*	0.0	0.0		0.2
Linear settlement	0.0	1.3	0.5	0.2	0.0		0.2	0.4	0.0		*1.7*	0.0	0.0	4.5
Water	0.3	0.1	0.1	0.0	0.0	0.1	0.0	0.1	0.0		0.2	*6.9*		7.9
Marshland	0.0	0.8	0.1	0.1	0.3		2.0	0.5			0.3	0.0	*0.1*	4.2
Total in 2006	6.9	28.9	10.7	10.2	2.2	0.7	4.0	19.7	0.5	0.1	8.7	7.4	0.1	100.0

4.3.2 Subsidence rates per land-use class

InSAR-based subsidence rates (measured by InSAR between 2006-2010) of all points for each land use class that did not change during the period 1988-2006 are shown in Fig. 4.3. Lowest subsidence rates occurred in undeveloped marshland with a mean rate of 6 mm yr^{-1}, closely followed by wetland forest (7 mm yr^{-1}). The highest subsidence rates were found for agricultural areas with mixed crops and urban areas (respectively 18 and 20 mm yr^{-1}). The within-class variability of subsidence rates varies with standard deviations between 4 mm yr^{-1} (marshland and wetland forest) and 7 mm yr^{-1} (several agriculture land-use classes, aquaculture and mangroves) (Appendix B, Table B.10). Differences in median and mean subsidence rates larger than 1 mm yr^{-1} between classes are significant (Appendix B, Section B.3.2).

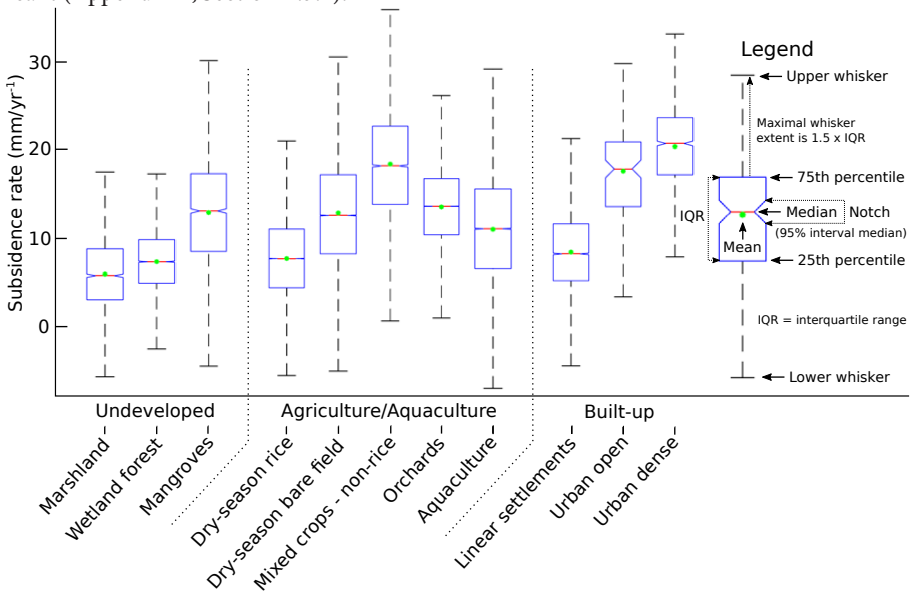

Figure 4.3 | *Subsidence rates (2006-2010) for unchanged land-use sequences during the period 1988-2006. Boxplots summarize the rates for each land-use class. Outliers beyond the whisker range are not shown.*

4.3.3 Relation between land-use change and subsidence rate

The effects of past land-use change on modern subsidence rates were assessed for three typical development groups (Table 4.5), which are 1) cultivation of previously undeveloped land, 2) changes in agricultural practice, and 3) urbanization. Areas where undeveloped land was reclaimed for cultivation, and where urbanisation occurred generally experienced higher subsidence rates. Areas where changes between agricultural practice occurred experienced higher or lower subsidence rates, depending on the specific land-use change. Furthermore, where land use already changed to its current type in the first period (1988-1996) current subsidence rates are closer to those of the unchanged land-use sequence, than where the change occurred in the second period (1996-2006). Remarkably, highest subsidence rates are found in the areas where land use changed into 'urban dense' between 1988-1996, exceeding the rates found for the unchanged 'urban dense' sequence.

Table 4.5 | *Impact of past land-use (LU) changes on the subsidence rates in the Mekong delta. The mean subsidence rates (in mm yr^{-1}) for areas in which LU 1 and LU 2 was unchanged during the period 1988-2006 (columns 'Unchanged LU 1' and 'Unchanged LU 2') and for areas that experienced a transition from LU 1 to LU 2 between 1996-2006 (column 'Transition from LU 1 to LU 2 1996-2006) and 1988-1996 (column 'Transition from LU 1 to LU 2 1988-1996), respectively <10 and 10-18 years before the measurement period (2006-2010). Subsidence rates are color-coded from yellow (low rates) to red (high rates).*

Land use change			Subsidence rate (mm yr^{-1})			
	Original land use	Land use after change	*Unchanged*	*Transition from LU 1 to LU 2*		*Unchanged*
Development	*Land use 1*	*Land use 2*	*LU 1*	1996-2006	1988-1996	*LU 2*
Cultivating undeveloped land	Marshland	Dry-season rice	6	8	8	8
	Marshland	Linear settlement	6	8	8	9
	Marshland	Dry-season bare	6	9	10	13
	Marshland	Orchard	6	9	11	14
	Mangroves	Aquaculture	13	11	11	11
Changing agriculture	Dry-season bare	Dry-season rice	13	10	8	8
	Dry-season rice	Orchard	8	10	12	14
Urbanization	Dry-season rice	Urban dense	8	9	27	20
	Dry-season bare	Urban dense	13	16	23	20
	Orchard	Urban dense	14	16	20	20

4.3.4 Predictions of subsidence rate based on land-use history

The land-use based predictions of land subsidence rates for the period 2006-2010 show spatial patterns similar to those derived from InSAR, with increasing rates from northwest to southeast and aligned along the river branches (Fig. 4.4A&B). The predicted subsidence rates show a strong linear relation with the InSAR rates and no bias (regression equation: slope = 0.99, intercept = 0.02, r^2 = 0.16: Appendix B, Fig. B.4). As the predictions use a single, median subsidence rate for each land-use sequence that is attributed to the objects, the resulting subsidence estimation map is more uniform than the map of InSAR-observed rates. The root mean squared error (RMSE) between observed and estimated rates is 5.8 mm yr^{-1}. If we consider the InSAR estimated error range of the observed subsidence rates (5 to 10 mm yr^{-1}), 65% to 92% of the predictions are within range with the observed InSAR values (Fig. 4.4C). The spatial patterns and trends present in the InSAR and predicted subsidence rate maps are not visible anymore in the residuals (Fig. 4.4C). When the prediction is only based on present land use without including land-use history, the correlation of the predicted subsidence and the observed subsidence decreases (r^2 = 0.09).

4.4 Discussion

4.4.1 Land-use change

Land-use changes show a trend of expansion and intensification of rice agriculture, aquaculture expansion at the expense of mangroves, and urbanization of the Vietnamese Mekong delta. These trends are in agreement with spatial and temporal patterns reported in other studies (e.g., Sakamoto et al., 2009; Tran et al., 2015). The timing of the wide-spread marshland cultivation (1988-1996) coincides with the economic and political reforms following the transition of Vietnam towards an open-market economy in 1986 (Funkenberg et al., 2014). The spatial pattern of the land-use class 'dry-season rice' largely agrees with the extent of irrigated double and triple rice cropping areas, while 'dry-season bare field' agrees with the extent of rain-fed single and double rice crops (e.g. Son et al., 2014; Sakamoto et al., 2009). Furthermore, the rice farming intensification, to enable

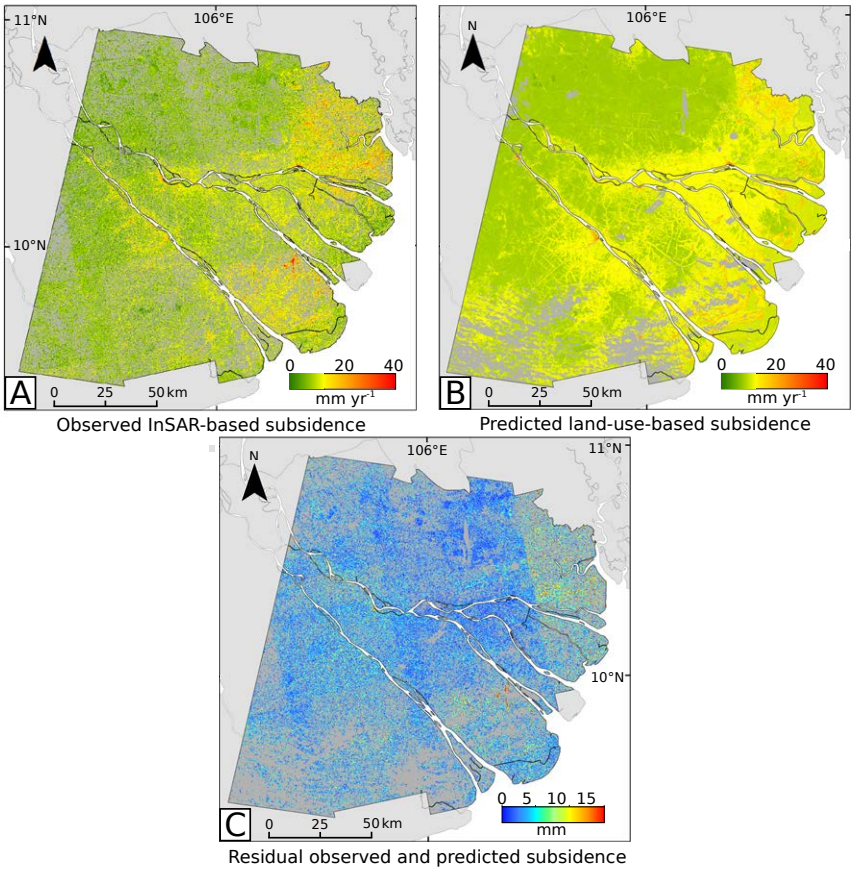

Figure 4.4 *| A) Observed InSAR-based subsidence rate, B) predicted subsidence rates for the period 2006-2010, and C) difference between observed and predicted subsidence. The predicted subsidence over the period 2006-2010 (B) is based on land-use history. Land-use sequence-specific median InSAR-derived subsidence rates were assigned to each individual land-use sequence. Respectively, 66% to 92% of the estimations fall within 5 to 10 mm of the observed values, which corresponds to the error range associated with the InSAR-based subsidence observations (A).*

the growth of an additional rice crop per year, is clearly shown by the consecutive land-use maps characterized by the expansion of the dry-season, hence irrigated rice. This is especially apparent in the upstream part of the delta. The large-scale transition of mangroves to aquaculture in the coastal zone observed between 1996 and 2006 is in line with Binh et al. (2005), Karila et al. (2014), Sakamoto et al. (2009b) and Tran et al. (2015). The steady increase of linear settlements along channels, dikes and roads, as well as urban areas, corresponds with the findings of e.g. Binh et al. (2005) and Tran et al. (2015).

4.4.2 Land-use driven subsidence

The main anthropogenic subsidence drivers associated with land-use practices are lowering of the phreatic water table, groundwater extraction and loading of the delta surface by buildings and infrastructure (e.g. Minderhoud et al., 2015; Galloway et al., 2016). We ranked the land-use classes by their mean observed subsidence rate (Fig. 4.5), and qualitatively estimated the impact of

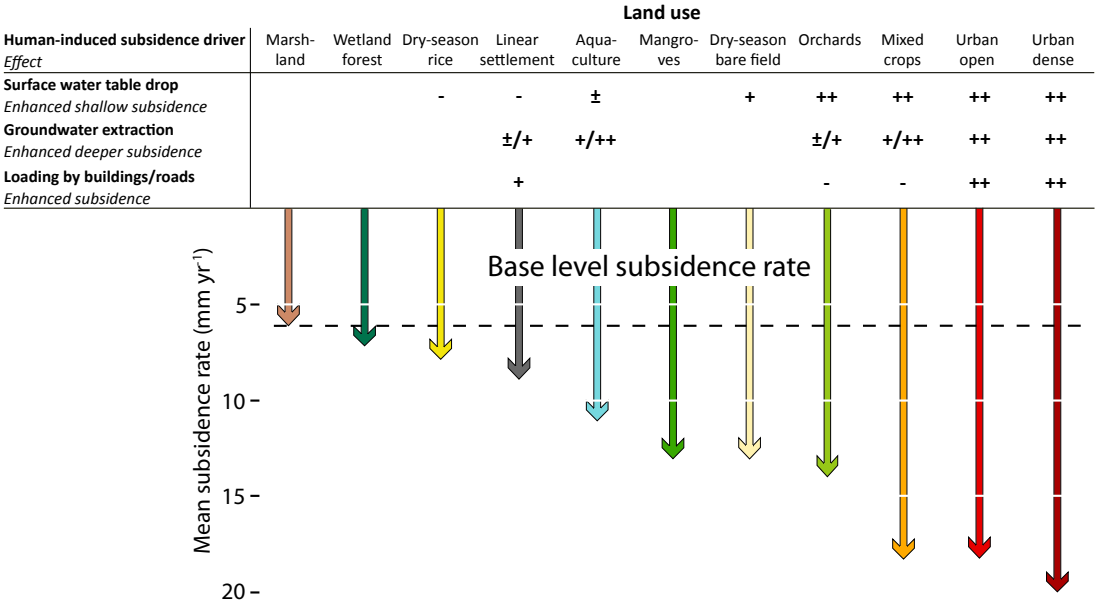

Figure 4.5 | *Estimated impact of subsidence drivers, and mean InSAR-based subsidence rate for the period 2006-2010 per land-use class. Mean subsidence rate is based on areas that sustained the same land use throughout the period of 1988-2006. The estimated impact of each subsidence driver is ranked: minimal (-), low (±), moderate (+) and high (++). All classes experience a subsidence rate of at least 6 mm yr^{-1}. Higher subsidence rates are generally found for land-use classes associated with increased impact of anthropogenic subsidence drivers.*

each subsidence driver for each land-use class based on the characteristics as described in Table 4.1. To exclude the influence of time lags of subsidence following a land-use change in the studied period, the subsidence rate per land-use class was based on areas that sustained the same land use throughout the period of 1988-2006 (Fig. 4.3). A trend is apparent between anthropogenic impact on the natural system and the mean subsidence rate of a land-use class. Lowest mean subsidence rates are found for natural, undeveloped areas, i.e. marshland and wetland forest, and highest rates for areas with high anthropogenic influence, i.e. mixed-crop agriculture and densely urbanized areas. More anthropogenic impact thus results in higher subsidence rates.

The lowest subsidence rate of 6 mm yr^{-1} occurs in undeveloped marshland. As natural marshland experiences no distinct human influence that alters the hydrological situation or loading of the land surface, this value likely reflects the mean natural compaction rate in the Vietnamese Mekong delta. The same value of 6 mm yr^{-1} was measured as mean floodplain sedimentation rate in frequently flooded areas in the delta (Hung et al., 2014). The similarity of these values probably reflects the dynamic equilibrium between natural compaction and sedimentation in the Mekong delta, which enabled the delta to maintain its elevation throughout the thousands of years prior to extensive human impact on the delta.

The subsidence rates presented reflect rates of subsidence of solid surfaces, as InSAR is unable to detect sediment accumulation that might occur in wetland areas. For this reason, the subsidence rates of this study may not necessarily reflect net surface-elevation change in some areas and for some land-use classes. For example, mangrove areas experienced relatively high absolute subsidence rates, but sedimentation in those areas can easily be as high or even higher, resulting in

a net elevation gain. The latter is actually the case in the Mekong delta as Surface Elevation Table (SET) measurements in mangrove areas registered a net elevation gain in healthy mangrove areas (Lovelock et al., 2015). However, the InSAR subsidence data do not represent elevation changes in these natural land surfaces due to detection limitations, as they only include 'hard' reflectors, such as buildings and roads. These are typically objects that likely do not experience elevation gain owing to sediment deposition. Conversely, the effective dike system, which was constructed to retain irrigation water to enable year-round rice cultivation (dry-season rice), likely decreases the amount of river flood-carried sedimentation, in contrast to more traditional rice cultivation practices (dry-season bare field) that continue to receive sediment by flood pulses. Estimates of the actual surface elevation change for a specific land-use class thus should consider the effect of sediment accumulation as well.

In the agricultural areas, subsidence rates are lowest for 'dry-season rice' (irrigated rice). This might be explained by the effect of irrigation during the dry season, resulting in a year-round high phreatic water table. This artificially high phreatic water table prevents soil ripening and organic matter decay in the subsurface, processes that would otherwise induce subsidence during the dry season when the water table normally drops. Other, rain-fed, agricultural land-use types do not have this 'paddy benefit' and show higher subsidence rates. A similar difference was observed in Japan where land subsidence rates in areas with rain-fed upland crops (comparable to our class 'mixed crop – non rice') were much higher than for rice paddies (Miyaji et al., 1995). The large difference in mean subsidence rate between rain-fed and irrigated rice thus suggests a high impact of seasonal water table lowering as driver of shallow subsidence.

Groundwater extraction causes differences in subsidence rates between the various agricultural land-use classes. While Vietnamese law prohibits groundwater extraction for rice irrigation, this seems to be tolerated for the irrigation of mixed crops and orchards. Moreover, rice paddies irrigated by river water potentially increase groundwater recharge to the deeper layers, therefore reducing groundwater extraction-driven subsidence (Wen, 1995), as was observed in Taiwan (Lui et al., 2010). However, we expect this recharging effect to be small in the Mekong delta, due to the thick, clay-rich Holocene top layer, which effectively seals off the underlying, exploited aquifers (Chapter 5).

In densely urbanized areas, subsidence rates are highest. This agrees with observations of rapidly subsiding delta cities elsewhere, such as Bangkok (Phien-wej et al., 2006), Jakarta (Abidin et al., 2011) and Shanghai (Ye et al., 2016). These high subsidence rates are due to the combination of all three main anthropogenic subsidence drivers: effective drainage causing a lowering of the groundwater table, excessive groundwater extraction, and physical loading of the compressible subsurface sediments by city buildings and infrastructure. For rural settlements the subsidence rate is lower, as the above-mentioned drivers are much less intensive. Besides, these settlements often occupy higher elevated terrain, and are often located as linear settlements on natural levees that are less prone to subsidence than flood-basins sediments.

Remarkably high subsidence rates were found for mangrove areas, despite the absence of human interference to accelerate subsidence. Here, the high rates might be attributed to their near-coastal position on the geologically youngest parts of the delta plain (e.g. Ta et al., 2002); these recently deposited, unconsolidated sediments are probably highly susceptible to natural compaction. This observation is in line with the high rates of shallow subsidence measured in the youngest, near-coastal mangrove areas in the Mekong delta (Lovelock et al., 2015).

The relatively low subsidence rates found for areas with aquaculture are remarkable, and contradict observations from other deltas such as the Yellow river delta where groundwater extraction at an

aquaculture-dominated coastline causes local annual subsidence rates of several decimeters per year (Higgins et al., 2013). The low subsidence rates for aquaculture in the study area suggest limited groundwater extraction. This is in line with the relatively small groundwater pressure drop and inherent extraction-induced subsidence, documented for the aquaculture areas in the study area for the InSAR observation period (Minderhoud et al., 2017). Probably, the aquacultures in the study area are partly fed by river water from the nearby Mekong river branches. Still, areas with aquaculture in the south of the Mekong delta, outside our study area, seem to experience more groundwater-extraction-induced subsidence (Chapter 5).

Within-class variation of subsidence rate

The standard deviation of observed subsidence rates varies between 4 and 7 mm yr^{-1} for the different land-use classes (Appendix B, Section B.3). Apart from the contribution of InSAR inaccuracy (5-10 mm yr^{-1}; Erban et al., 2013; 2014) and inaccuracies in the land-use classifications, this variation may reflect actual (spatial) variation of subsidence rates present within a certain land-use class.

Within-class variation of subsidence rates may be attributed to four categories of factors: 1) differences in water use and water management within areas with the same land use; 2) 'transboundary' subsidence resulting from practices in neighboring areas with a different land use, e.g. groundwater extraction at a single location can influence a much larger area; 3) variability in inherited subsidence related to land use and land-use changes prior to 1988; 4) properties of the physical system that are independent of land use, including local subsurface composition and tectonic subsidence. This last factor is captured by a trend in subsidence rates for the linear settlements land-use class that shows increasing rates from the northwest, upstream part, towards the southeast, downstream part of the delta. This trend likely reveals the higher natural compaction rates associated with the younger, shallow sediments in seaward direction.

4.4.3 Land-use change and time-dependent subsidence response

Our results show that most of the investigated land-use changes in the Mekong delta led to an acceleration of subsidence rates. Only the conversion from rain-fed rice to year-round irrigated rice and the conversion from mangroves to aquaculture shows reduced subsidence rates. Furthermore, when the land-use conversion occurred in the first period (1988-1996), the present subsidence rate under the new land use is more similar to the characteristic subsidence rate of the unchanged land-use class than when the conversion occurred in the second period (1996-2006). This delayed change in subsidence rate following a land-use change clearly reveals the delayed response or time-lag of subsidence.

This time-lag in subsidence rate is the result of time-dependent effects of which we distinguish two types. 1) Time-dependent effects can stem from changing boundary conditions and the delayed response of subsidence drivers and processes. Examples are the ongoing drainage of land following the conversion to agricultural land resulting in gradually phreatic water table lowering (driver) which leads to increasing clay and peat compaction and peat oxidation (processes), or, a land use changes to a more groundwater-demanding land-use type with increased groundwater exploitation (driver) which leads to increasing rates of aquifer-system compaction (process). 2) The second type of time-dependent effect that we distinguish can stem from internal mechanisms of subsidence processes. Examples are the decrease of subsidence over time following decomposition of organic matter as organic matter gradually depletes (Yuill et al., 2009), or, in case of aquifer system compaction, the subsidence rate gradually decreases when a new equilibrium between pore pressure and overburden is reached (Isotton et al., 2015). Our results suggest that time-dependent

effects can affect subsidence rates up to at least two decades following a land-use change. This underscores the importance of land-use history, and not just current land use, when studying the land use-subsidence relationship.

Finally, it should be noted that the subsidence rates reported and predicted in this study are based on the InSAR analysis of subsidence acquired between 2006-2010 (Erban et al., 2014). Given the accelerating trend in groundwater extraction-related subsidence in the Mekong delta (Minderhoud et al., 2017), these rates likely underestimate the present-day subsidence rates. This effect will be especially apparent for land-use classes that require large volumes of groundwater use, e.g. mixed crops, aquaculture and urban areas.

4.4.4 Predictions of subsidence rates based on land-use history

The observed InSAR-derived subsidence rates and the land-use-based predicted rates agree well and show similar spatial patterns and magnitudes of rate. These spatial patterns are no longer present in the residuals map, which means that a large part of the spatial variability of the InSAR-observed subsidence across the delta is correlated with land-use history. This confirms the existence of the hypothesized relation between land-use history and subsidence, as 1) land-use practices affect subsidence drivers and processes and/or 2) preference of land-use types for locations with specific subsidence characteristics. The majority (65%-92%) of the predicted rates falls within the error range of the observed, InSAR-derived subsidence rates (5-10 mm yr^{-1}). This confirms the possibility of providing predictions of subsidence rate using land-use history when it can be trained using subsidence-rate observations. Incorporating land-use history, and not just land use, to prediction subsidence rates strongly increased the prediction results. Predictions of subsidence rates based on land-use history should therefore preferably be derived from time series of land use covering the longest possible period.

Subsidence predictions could potentially be improved by including additional factors that influence subsidence unrelated to land use, such as subsurface composition, if spatial data is available. In this study, the data used to derive the median values had the same spatial extent for which we predicted subsidence. However, the method might also be applied to create estimations of land-subsidence for regions larger than the training area, as long as the land-use classes and the corresponding dominant subsidence drivers and processes remain similar. In such cases using land-use history as a proxy for subsidence rates provides a promising approach for data-sparse regions lacking direct subsidence measurements, such as large delta systems, to produce subsidence estimates for the entire region using land-use maps. For instance, this approach could be applied in the Ganges-Brahmaputra delta where InSAR-based subsidence data is currently available for a small region only (Higgins et al., 2014).

4.4.5 Supporting land-use management in subsiding deltas

Our results show a clear link between land use (trajectories) and subsidence in the Mekong delta. These insights may be used to guide sustainable land-use planning that considers delta subsidence and promotes land-use types less prone to subsidence. Additionally, our spatially explicit evaluation can aid policy making and planning around subsidence-mitigation measures. Our approach is further relevant to any area in the world where land-use practices. Using land cover data, which are more readily available than direct or indirect measurements of subsidence, as a proxy for subsidence rates, facilitates such opportunities also in data-sparse deltas and other regions.

4.5 Conclusions

The Vietnamese Mekong delta has experienced major changes in land use over the past decades. The wide-spread cultivation of previously undeveloped lands and expansion of cities strongly altered the hydrological situation in the delta, both at the surface and in the subsurface, and added loading to the delta plain. These anthropogenic drivers triggered and enhanced subsidence processes. Our analysis of land use and InSAR-derived subsidence rates demonstrates that different land uses lead to different subsidence rates, where more anthropogenic influence leads to higher rates.

In general, subsidence rates in the Mekong delta increase after conversion of land use to a type that uses more groundwater or causes land subsidence otherwise. Past land-use changes, between 1988-1996 or 1996-2006, significantly influence subsidence rates observed between 2006-2010. This means that both subsidence drivers and processes can need at least up to two decades to adapt to the new land-use practices. Hence it is important to include the land-use history over several decades rather than current land use in the analysis of subsidence rates.

The predicted subsidence rates for the land-use classes and land-use change sequences agree well with the InSAR-derived subsidence rates. This confirms the strong relation between land-use history and subsidence. It also reveals the ability to predict subsidence rates based on land-use history. Moreover, it could provide a promising proxy-approach for upscaling and producing subsidence estimates for larger regions that lack direct subsidence measurements. The relation between land use, land-use history and subsidence rate reveals their strong interlinkage through subsidence drivers and processes caused by the use of land as well as land-use preference for locations with specific subsurface characteristics. Overall, our spatially explicit evaluation of land-use change pathways provides land-use specific insights for policymakers concerned with land-use planning in both subsiding and currently stable areas of the Mekong delta and similar systems.

Acknowledgements
We thank many people that shared land-use maps with us in the early phase of this project. Pepijn van Elderen is thanked for geo-rectifying the InSAR tiles. We thank the GEO ICT team of the Faculty of Geosciences, Utrecht University for assisting with ICT-related challenges and providing computational facilities. Gilles Erkens is thanked for discussions on land use-subsidence interactions. Luigi Tosi and an anonymous reviewer are thanked for reviewing the manuscript. The views expressed in this article are those of the authors and do not necessarily reflect the views or policies of the U.S. Environmental Protection Agency. The article tracking number is ORD-024109.

Author contributions
P.M., E.S., and E.A. jointly conceived this research as part of the Rise and Fall research project and supervised the MSc graduation research of L.C. L.C. collected the optical remote sensing data and performed the pre-processing. L.E. performed the InSAR analysis. E.A., L.C., and P.M. designed the remote sensing and machine-learning analyses and P.M., L.C., and E.S. the subsidence analyses. L.C. performed all computer analyses and reported the study in a MSc thesis. P.M. drafted the paper, which was then edited by all co-authors.

5 Impacts of 25 years of groundwater extraction on subsidence in the Mekong delta, Vietnam

Many major river deltas in the world are subsiding and consequently become increasingly vulnerable to flooding and storm surges, salinization and permanent inundation. For the Mekong Delta, annual subsidence rates up to several centimetres have been reported. Excessive groundwater extraction is suggested as main driver. As groundwater levels drop, subsidence is induced through aquifer compaction. Over the past 25 years, groundwater exploitation has increased dramatically, transforming the delta from an almost undisturbed hydrogeological state to a situation with increasing aquifer depletion. Yet, the exact contribution of groundwater exploitation to subsidence in the Mekong delta has remained unknown. In this study we deployed a delta-wide modelling approach, comprising a 3D hydrogeological model with an integrated subsidence module. This provides a quantitative spatially-explicit assessment of groundwater extraction-induced subsidence for the entire Mekong delta since the start of widespread overexploitation of the groundwater reserves. We find that subsidence related to groundwater extraction has gradually increased in the past decades with highest sinking rates at present. During the past 25 years, the delta sank on average ~18 cm as a consequence of groundwater withdrawal. Current average subsidence rates due to groundwater extraction in our best estimate model amount to 1.1 cm yr^{-1}, with areas subsiding over 2.5 cm yr^{-1}, outpacing global sea level rise almost by an order of magnitude. Given the increasing trends in groundwater demand in the delta, the current rates are likely to increase in the near future.

Published as: Minderhoud, P.S.J., Erkens, G., Pham, H.V., Bui, V.T., Erban, L., Kooi, H., Stouthamer, E. (2017). **Impacts of 25 years of groundwater extraction on subsidence in the Mekong delta, Vietnam.** *Environmental Research Letters* 12. doi:10.1088/1748-9326/aa7146

5.1 Introduction

The low-lying and densely populated Mekong delta (MKD), largely located in Vietnam, has the third largest delta plain in the world (Coleman and Roberts, 1989). The delta is fertile, intensively cultivated, and responsible for 50% of Vietnam's total food production. As Vietnam is the world's second largest rice exporter, and 90% of all rice is produced in the MKD, over 200 million people rely on the delta for food (GSO, 2016).

By nature, low-lying delta systems are sensitive to environmental change. The MKD is threatened by global sea-level rise (Wassmann *et al.,* 2004), natural decrease in fluvial sediment supply (Darby *et al.,* 2016), enhanced by upstream sediment trapping behind dams (Kondolf *et al.,* 2014; Manh *et al.,* 2015), salinization (Renaud *et al.,* 2015) and coastal erosion (Anthony *et al.,* 2015). On top of that, highly compressible soils make deltas worldwide vulnerable to subsidence

(Syvitski *et al.,* 2009), increasing relative sea-level rise (RSLR). In the MKD subsidence rates seem to exceed global eustatic SLR by an order of magnitude (Erban *et al.,* 2014). As a result, subsidence acts as a catalyst, increasing vulnerability to flooding and storm surges, saltwater intrusion in the channels and risk of permanent inundation of the delta.

Groundwater overexploitation has been proposed to be the main driver of subsidence in the MKD (Erban *et al.,* 2013, 2014), corresponding to observations in other subsiding deltas and coastal areas around the world (Phien-wej *et al.,* 2006; Teatini *et al.,* 2006; Saito *et al.,* 2007; Abidin *et al.,* 2011; Higgins *et al.,* 2013). In the MKD, the demand for fresh water has steadily risen following the ongoing economic growth after Vietnam's transition to a market economy in 1986. This transition stimulated massive cultivation, urbanisation and industrialisation in the MKD (Seto, 2011). With surface water often being polluted or saline, groundwater is the main source to meet this increasing freshwater demand (Wagner *et al.,* 2012). In 1991, when groundwater monitoring in the MKD commenced, piezometric levels in the aquifer system were at more or less natural levels (i.e. at or above delta surface elevation) in most parts of the delta. Over the past 25 years, groundwater exploitation strongly increased, resulting in a persistent drawdown of hydraulic heads (i.e. water pressure) throughout the entire delta subsurface. This process is known to trigger fine-grained sediment consolidation in the subsurface, causing aquifer-system compaction (e.g. Galloway and Burbey, 2011; Gambolati and Teatini, 2015), expressed as land subsidence of the delta surface.

Average subsidence rates for the Mekong delta were determined at 6 mm yr^{-1} from 1987-2006 by surface water level trend analysis (Fujihara *et al.,* 2015), 17.1 mm yr^{-1} from 1993-2013 for Can Tho city (Takagi *et al.,* 2016) and 16 mm yr^{-1} from 2006-2010 at 15 monitoring stations by InSAR (Interferometric Synthetic Aperture Radar) (Erban *et al.,* 2014). For Ho Chi Minh City (HCMC) local extreme rates of 46 mm yr^{-1} (Erban *et al.,* 2014), and 70 mm yr^{-1} (Minh *et al.,* 2015) are reported. As InSAR is unable to measure areas lacking clear reflectors, such as rural areas that constitute most of the MKD, the analyses only cover part of the delta. Local 1D subsidence calculations as a function of measured groundwater drawdown have been performed for point locations in the MKD (Erban *et al.,* 2014), Ca Mau city (Karlsrud and Vangelsten, 2017) and Ho Chi Minh City (Thoang and Giao, 2015). Interpolation maps based on such subsidence calculations from sparse groundwater monitoring well locations fail to reproduce the actual situation, since factors that influence subsidence locally, such as spatial heterogeneity of the delta subsurface and variability in the hydrogeological situation, are unaccounted for. Consequently, a delta-wide cumulative subsidence map of the MKD still does not exist. Furthermore, the relative contribution of 25 years of groundwater extraction to the total observed subsidence rates is unknown, as well as the current *rates* of groundwater extraction-induced subsidence.

In this paper, we present the first delta-wide quantification of groundwater extraction-induced subsidence over the last 25 years in the Mekong delta. Using a newly developed 3D numerical groundwater flow model of the delta subsurface, we simulated groundwater drawdowns based on measured time series of hydraulic heads and an estimate of the extraction history. Subsequently, we calculated the corresponding aquifer system consolidation using a one-way coupled subsidence module. Our approach enables the evaluation of groundwater extraction-induced subsidence at delta scale. The modelling period captures the onset of widespread groundwater drawdown, allowing us to quantify the evolution of subsidence rates and total cumulative subsidence due to groundwater extraction over the past decades, pre-dating measurements, until present. Our process-based modelling approach provides an important step towards disentangling the measured total subsidence signal into the relative contribution of different natural and human-induced drivers to total subsidence for deltaic areas like the MKD. This will greatly benefit thorough and knowledge-

based predictions of delta-wide subsidence for the coming decades, supporting urgently needed decision-making in subsiding deltas (Galloway *et al.,* 2016).

5.2 Model setup and calibration

We created a delta-wide, 3D hydrogeological groundwater model for a physical, process-based interpolation of measured drawdown rates in time and space driven by groundwater extraction. Groundwater flow was modelled using the MODFLOW-based environment iMOD (Vermeulen, 2006; Minnema *et al.,* 2013). The lowering of water pressure in the subsurface was subsequently used to calculate subsidence in the entire aquifer system using a one-way coupled geotechnical subsidence module called SUB-CR. The main focus of the hydrogeological model was to simulate the evolution of relative hydraulic head (i.e. water pressure) changes, driving subsidence. Absolute head levels are therefore less relevant for this study. Vermeulen et al. (2013) built a first quasi-3D, steady-state groundwater model of the MKD in iMOD. To be able to simulate subsidence and meet our model requirements, we built a new transient model in which confining layers are explicitly modelled. The model was based on available geological, hydrological and geotechnical data, supplied by the Division of Water Resources Planning and Investigation for the South of Vietnam (DWRPIS).

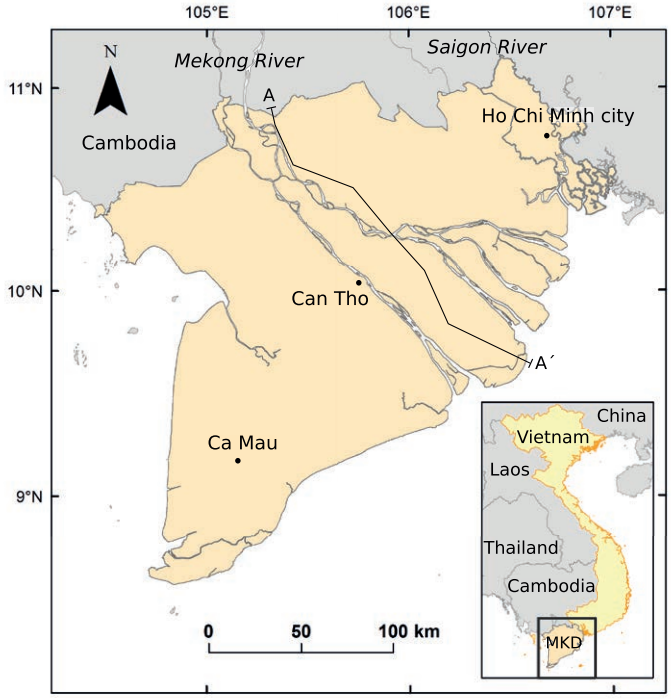

Figure 5.1 *| Location of the Mekong Delta (MKD) and part of the interconnected Saigon River to the northeast, encompassing the province of Ho Chi Minh City, in the south of Vietnam. The map extent corresponds with the model extent. Cross-section line A-A' shows the location of the hydrogeological cross-section in figure 5.2.*

5.2.1 Hydrogeological model

A numerical hydrogeological model of the entire Mekong delta and part of the inter-connected Saigon river delta, hosting HCMC, was constructed (Fig. 5.1). A 3D model of the aquifer-aquitard subsurface was built using the iMOD SolidTool (Vermeulen *et al.,* 2016) by interpolating 95 borehole logs in 10 hydrogeological cross-sections, dividing the delta subsurface into seven main hydrogeological units distinguished by the Division for Geological Mapping for the South of Vietnam (DGMS, 2004; Fig. 5.2). This resulted in a 15 layer, subsurface model, representing 7 aquifers, 7 aquitards and a phreatic top layer. See Appendix C for a more in-depth description of the subsurface model.

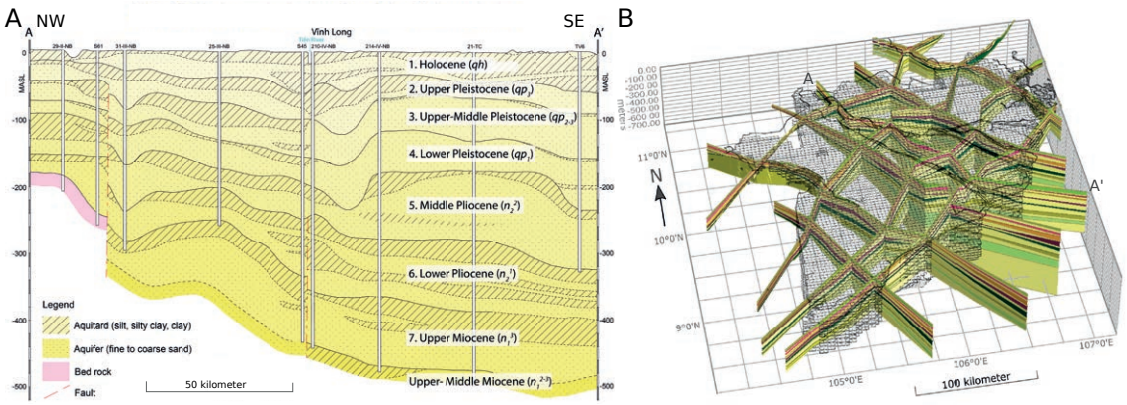

Figure 5.2 *| A) Hydrogeological cross-section with the interpretation of the deltas subsurface aquifer-system identifying the main units according to the Division of Geological Mapping for the South of Vietnam (modified after DGMS, 2004). Each unit consists of a permeable bottom layer (aquifer) and a, occasionally discontinuous, confining top layer (aquitard). B) Ten hydrogeological cross-sections distinguishing aquifers and aquitards used to create the 3D subsurface model, by linear interpolation, of the MKD. The cross-sections are linearly extrapolated into the sea and cross-border to reach the model boundary 50 km offshore and 20 km outside the national border.*

The 3D schematization of the MKD subsurface was used to build a transient hydrogeological model at 1 x 1 km^2 horizontal resolution to simulate groundwater flow and fluctuations in hydraulic head over the past 25 years (1991-2015) with monthly time steps. The boundary of the active model area was positioned 20 km outside the national border and 50 km off-shore to account for lateral groundwater flow in the modelled delta, i.e. transboundary flow from Cambodia (Erban *et al.,* 2016) and off-shore groundwater flow (e.g., Post *et al.,* 2013). Recharge is modelled based on annual amounts of precipitation and evaporation measured from 1999-2010. The amounts were spatially modelled using distribution maps (Luong, 2008), and for each month the average, multi-year, monthly percentage was taken. The average measured values of precipitation and evaporation were assigned for the modelling period beyond the measurement records. The surface water network in the MKD was not explicitly modelled. Recharge from the river system to the aquifers in the downstream part of the MKD is expected to be limited due to the presence of the thick, largely impermeable, Holocene aquitard near the surface effectively sealing off the aquifers below, and therefore was not considered in the model. A model run using a simplified river system of the Mekong river from Vermeulen *et al.* (2013) confirmed this assumption as the inclusion of the river

system only affected calculated subsidence significantly for some model cells located along the river system. Drainage was modelled by a constant drain level 0.5 meter below surface level, simulating the draining effect of the dense network of paddies, surface channels and canals cross-cutting the delta. Initial hydraulic heads followed from a steady-state simulation without groundwater extraction and average recharge values (See Appendix C, section C.3 for a summary of the model setup).

Groundwater extraction during the transient modelling period of the past 25 years was modelled based on an integration of several datasets reporting extracted volumes for the MKD and the HCMC province (DWRPIS, 2010)(Appendix C, section C.3). In total extraction in the MKD was modelled at over 15,000 locations, including large wells and clusters of small household wells, accounting for a daily abstracted volume of over 2.5 million m^3 (Fig. 5.3). For HCMC province more than 1,300 well nests are responsible for extracting over 800,000 m^3 on daily basis. As a result of a water act in HCMC to restrict groundwater exploitation (HCMC, 2007), the extracted volume in HCMC has gradually stabilised in recent years.

Initial hydrogeological model parameterization for the MKD was based on available data of the DWRPIS. The hydraulic conductivity (K_h) and storage coefficient (SS_c) of each model layer were calibrated through an automated parameter estimation (PEST) protocol (following the approach of Olsthoorn (1995), described in Vermeulen *et al.,* 2016) using piezometric head measurements from 91 monitoring wells located throughout the delta and HCMC (see Appendix C, section C.4 for description and calibrated parameter values).

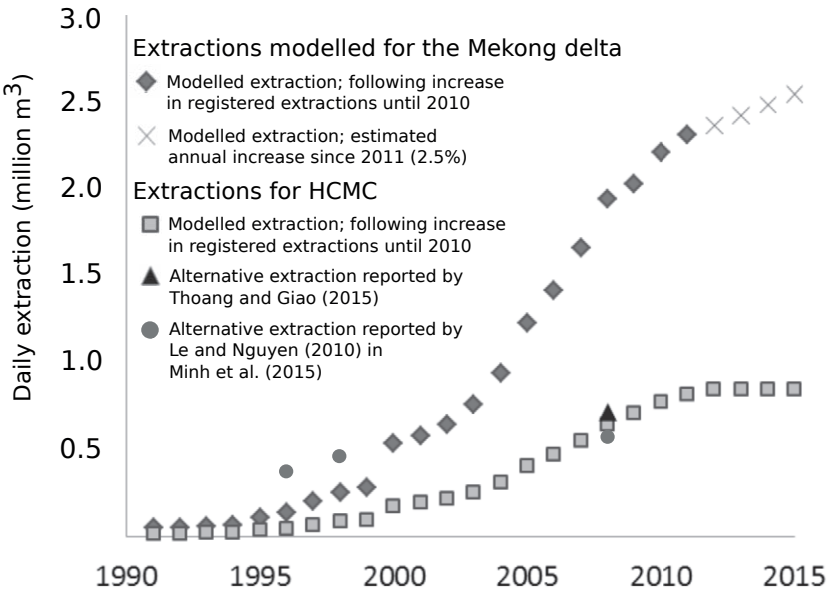

Figure 5.3 | *Annual modelled groundwater extraction in the Mekong delta (MKD) and Ho Chi Minh City (HCMC) province. An annual increase of 2.5% is assumed for extraction in the MKD after 2011. The dots (Trung et al., 2010 in Minh et al., 2015) and triangle (Thoang and Giao, 2015) show alternative values reported for HCMC province.*

5.2.2 Subsidence calculation and parameterization

Subsidence due to aquifer-system compaction following the hydraulic head decline (i.e. decreasing pressure) was calculated using the *abc* model (Den Haan, 1994). This model determines natural strain (i.e. degree of compression) based on the isotach concept first proposed by Šuklje (1957) and extended by Bjerrum (1967). In this model natural strain (ε^H) is described as follows:

$$\varepsilon^H = \int_{m_0}^{m_{final}} \frac{1}{m} dm \tag{5.1}$$

where m is momentary layer thickness. The model decomposes total strain (ε^H) into two components, a direct elastic contribution ($\varepsilon^H{}_d$) and a time-dependent (secular) creep contribution. ($\varepsilon^H{}_s$); $\varepsilon^H = \varepsilon^H{}_d + \varepsilon^H{}_s$. The first component accounts for the elastic (i.e. reversible) response to changes in effective stress, and the latter component for the permanent strain that develops by creep (viscous deformation). Creep, which is widely used in geotechnical models of land surface settlement induced by surface loads, is considered more appropriate to model the deformation of clay and peat than plastic deformation that is more commonly employed in land subsidence models (e.g. SUB-WT; Leake and Galloway, 2007) for secondary consolidation is ignored in these models. Three compression parameters define the system of the *abc* method: a (recompression or swelling constant) accounts for the elastic compression, b (compression constant) and c (secondary compression constant) for the viscoplastic compression. Using these constants, total natural strain is calculated as a function of effective stress and intrinsic time (τ) by the following expression (Den Haan, 1994):

$$\varepsilon^H = a \ln\left(\frac{\sigma'_p}{\sigma'_o}\right) + b \ln\left(\frac{\sigma'}{\sigma'_p}\right) + c \ln\left(\frac{\tau}{\tau_{ref}}\right) \tag{5.2}$$

where σ'_p is the initial pre-consolidation stress, σ'_o the initial effective stress, σ' the momentary effective stress and τ_{ref} the reference time (= 1 *day*). Intrinsic time (τ) is calculated as follows:

$$\tau = \tau_{ref} OCR^{\frac{b-a}{c}} \tag{5.3}$$

where a, b and c are the compression parameters and OCR is overconsolidation ratio which is described by this general relationship:

$$OCR = \sigma'_p / \sigma' \tag{5.4}$$

The incremental vertical strain is calculated for every time step for each layer as a function of effective stress, in this case solely derived from hydraulic head changes. The model only considers vertical deformation. Horizontal displacement is assumed negligible at delta scale (c.f. Ye *et al.,* 2016). The hydrological effect of viscous (creep) compression, which tends to increase pore pressure and therefore hydraulic head, was set to zero, as the model was calibrated without this budget term.

Parameterization for the *abc* compression constants was based on local geotechnical data (Bakr *et al.,* 2013; Thoang and Giao, 2015; Toan and Nu, 2013) combined with general relationships among compression parameters known from other studies (see Appendix C, section C.5 for a detailed description and summary of the used values). Deformation behaviour is strongly determined by the overconsolidation ratio, but only limited data is available to constrain the OCRs for the MKD. Hoang *et al.,* (2016) determined OCRs ranging between 1.0 and 2.7 (average: ~1.6)

for clayey deposits using cone penetration, incremental loading oedometer and constant rate of strain consolidation tests from five boreholes in the MKD. Thoang and Giao (2015) reported an OCR value of 1.6 for medium to stiff clays in HCMC province. OCRs published for comparable delta deposits are within a similar range: Bangkok, Thailand 1.5 (Phien-wej *et al.,* 2006); Belfast, N-Ireland 1.2-1.8 (Crooks and Graham, 1976), 1.6-2.0 (Bell, 1977 in Graham *et al.,* 1983). Based on these values, we established an initial OCR range of 1.2-2. As there is no known trend or consistency on how OCR changes with depth in the MKD (Hoang *et al.,* 2016), a single OCR value was assigned to all model layers. A sensitivity analysis of modelled subsidence to OCR was used to further constrain the range of possible OCR values. Subsequently, the OCR of the model results that shows the highest correlation to the InSAR-measured subsidence (Erban *et al.,* 2014) for the MKD was determined.

5.3 Results

5.3.1 Modelled aquifer drawdown

For the simulated period of 25 years, the calibrated hydrogeological model produces groundwater heads correlating reasonably well with the observed time series of groundwater head in the MKD (r^2 = 0.73). The residuals of the absolute observed versus absolute modelled hydraulic heads are normally distributed with over 75% smaller than 2 meters (See Appendix C, Fig. C.5). For HCMC, the residuals are larger and observed drawdown at the observation wells is consistently underestimated several meters by the model (See Appendix C, Fig. C.6). Despite such systematic offsets, the decrease of head over time matches well (median cross-correlation (r) = 0.94). This provides a good basis for the subsequent subsidence calculations, as they strongly depend on the hydraulic head *change*, rather than absolute values.

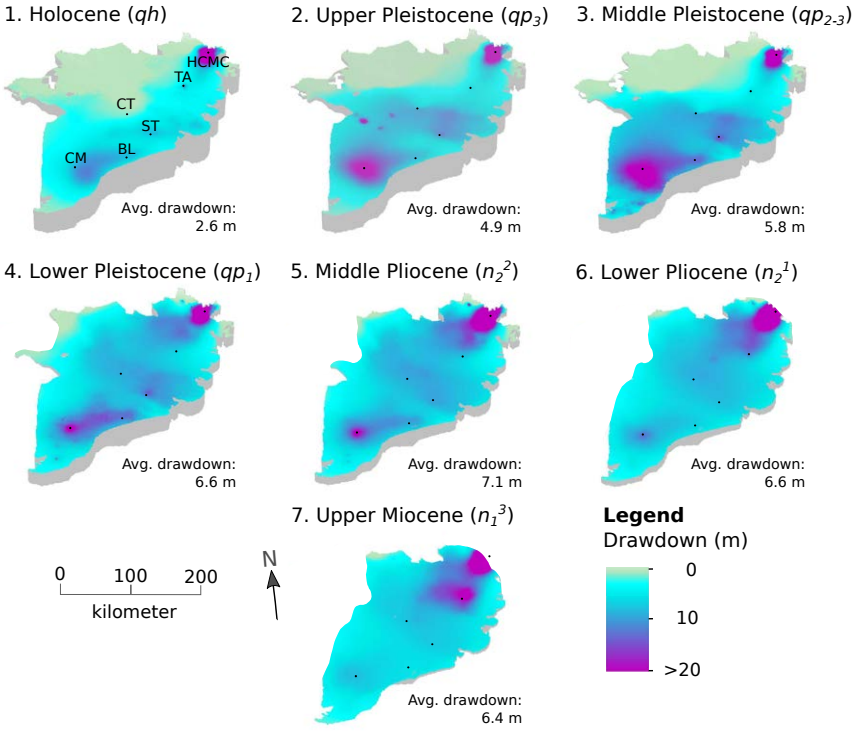

Figure 5.4 *| Modelled aquifer drawdown at the start of 2016 after 25 years of simulated groundwater extraction for in the 7 main aquifers of the Mekong delta (see Fig 5.2A). The deeper aquifers do not extend over the entire delta. Cities located in the figure: BL: Bac Lieu; CM: Ca Mau; CT: Can Tho; HCMC: Ho Chi Minh City; ST: Soc Trang; TA: Tan An.*

Over the past 25 years, large areas in the MKD experienced drawdown in the aquifers exceeding five meters (Fig. 5.4). Modelled average delta-wide drawdown increases with depth and large drawdown areas are located around major cities and industrial areas with extensive groundwater extraction, e.g. Bac Lieu, Ca Mau, Soc Trang and Tan An. HCMC has extensive cones of depression modelled in all aquifers, with local groundwater levels reduced well over 20 m, locally up to 40 m.

5.3.2 Effect of overconsolidation ratio on subsidence modelling

Subsidence modelling of aquifer-system compaction related to hydraulic head drops strongly depends on the overconsolidation ratio attributed to the model. By scrutinising the sensitivity analysis of modelled subsidence to the initial OCR range, the plausible OCR range could be decreased (Fig. 5.5). Low OCR values (< 1.45) result in an unrealistic rapid subsidence response, i.e. very high viscous creep rates, even without groundwater extraction. High OCR values (>1.75) result in very limited to zero viscous response of the aquifer system, which is very unlikely in a delta system. The 1.45-1.75 OCR-range provides a series of subsidence calculations from a least conservative (very weak sediments) to a most conservative model (rigid sediment properties). If no direct measurements of subsidence are available for a delta system, this would be the range in which groundwater extraction related subsidence can be reported. In case of the MKD, we determine the best estimate model by correlating the average model results to the average InSAR-measured subsidence rates for the entire MKD for the period 2006-2010 (Erban *et al.,* 2014). The model parameterized with an OCR of 1.63 provides the best match with the average InSAR-measured subsidence and was consequently used to calculate the reported results. This OCR value approaches the reported average OCR value of 1.6 reported for the MKD (Hoang *et al.,* 2016) and HCMC (Thoang and Giao, 2015). The amount of the total InSAR-measured subsidence reproduced by the model, resulting from a cell-by-cell comparison, was ~75% of the total measured subsidence for the best estimate model (respectively ~50% and ~95% for the most and least conservative model) (Appendix C, Fig. C.7).

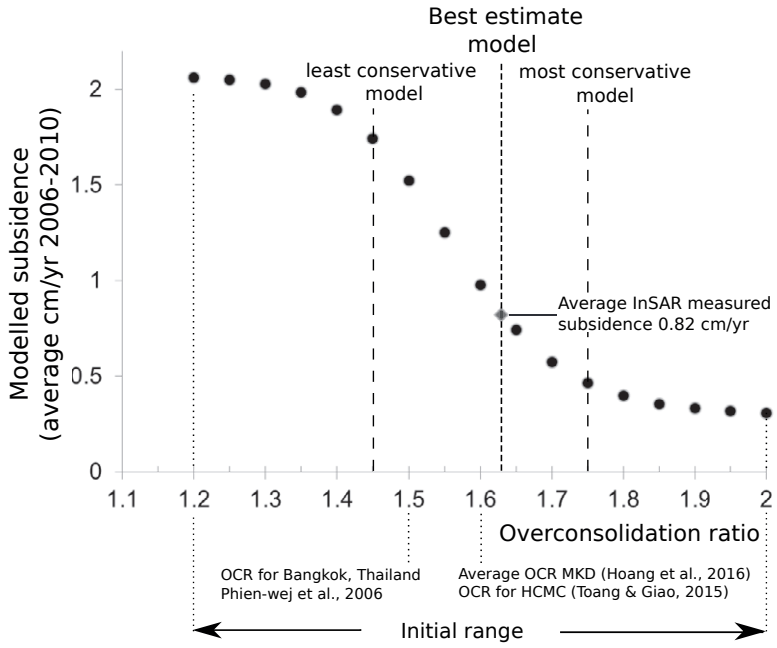

Figure 5.5 *| Sensitivity analysis of modelled subsidence to overconsolidation ratio. The range of OCR values of 1.45-1.75 represents the determined least to most conservative subsidence model. The model using an OCR of 1.63 has the highest correlation with the average InSAR-measured subsidence for the entire MKD (calculated from the Erban et al., 2014) and is selected as the best estimate model. Rates are all average annual value over the period 2006-2010.*

5.3.3 Groundwater extraction-induced subsidence in the Mekong delta

The model indicates that since 1991, 25 years of groundwater exploitation in the MKD has resulted in an average total subsidence of ~18 *(9-53)* cm for the best estimate *(most conservative and least conservative)* model, respectively, with hotspots over 30 *(18-75)* cm (Fig. 6A). Cumulative subsidence values calculated for HCMC well exceed those figures, on average ~115 *(90-150)* cm). The modelled average sinking rate for 2015, solely due to 25 years of groundwater extraction, is 1.1 *(0.7-1.8)* cm yr^{-1}. Cities and major industrial areas particularly stand out with high subsidence rates (up to 2.5 *(1.7-3.3)* cm yr^{-1}) while rates for rural areas with substantial groundwater extraction generally range from 1-2 *(0.6-3.1)* cm yr^{-1} (Fig. 5.6b). Present average modelled subsidence rate for HCMC is ~7.3 *(6.6-7.7)* cm yr^{-1}.

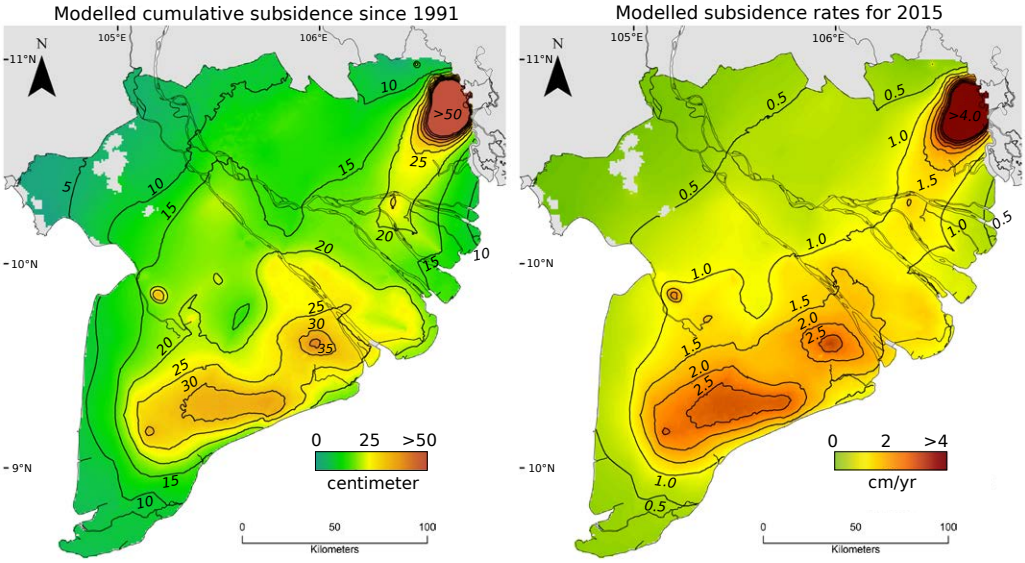

Figure 5.6 *| A) Modelled cumulative subsidence due to groundwater extraction-induced during 25 years of groundwater exploitation from 1991 to 2016. B) Modelled groundwater extraction-induced annual subsidence rates for 2015.*

At the start of the modelling period in 1991, the hydrogeological situation for the vast majority of the Mekong delta was in a natural, undisturbed state. With the exception of Ca Mau city, hydraulic heads were at surface elevation and locally artesian. Groundwater extraction started to exceed aquifer recharge at many locations between 1991 and 1995, initiating widespread hydraulic head decline. As extraction rates continued to increase (Fig. 5.3), hydraulic head declines accelerated throughout the multi-aquifer system (Fig. 5.7A-H). The modelled heads follow the measured hydraulic heads in this period, although during the middle part of the modelling period, the modelled head decline is lagging behind the observed head decline. Substantial subsidence commenced during the 1990s as a result of groundwater pumping-induced aquifer compaction in large parts of the delta (Fig. 5.7I-V). Annual rates steadily increased towards the present as aquifer depletion persisted. For the MKD, the highest subsidence rates are found at the end of the modelling period. In HCMC a slight decrease in subsidence rate is visible towards the present, following the recent decrease in aquifer depletion (Fig. 5.7D).

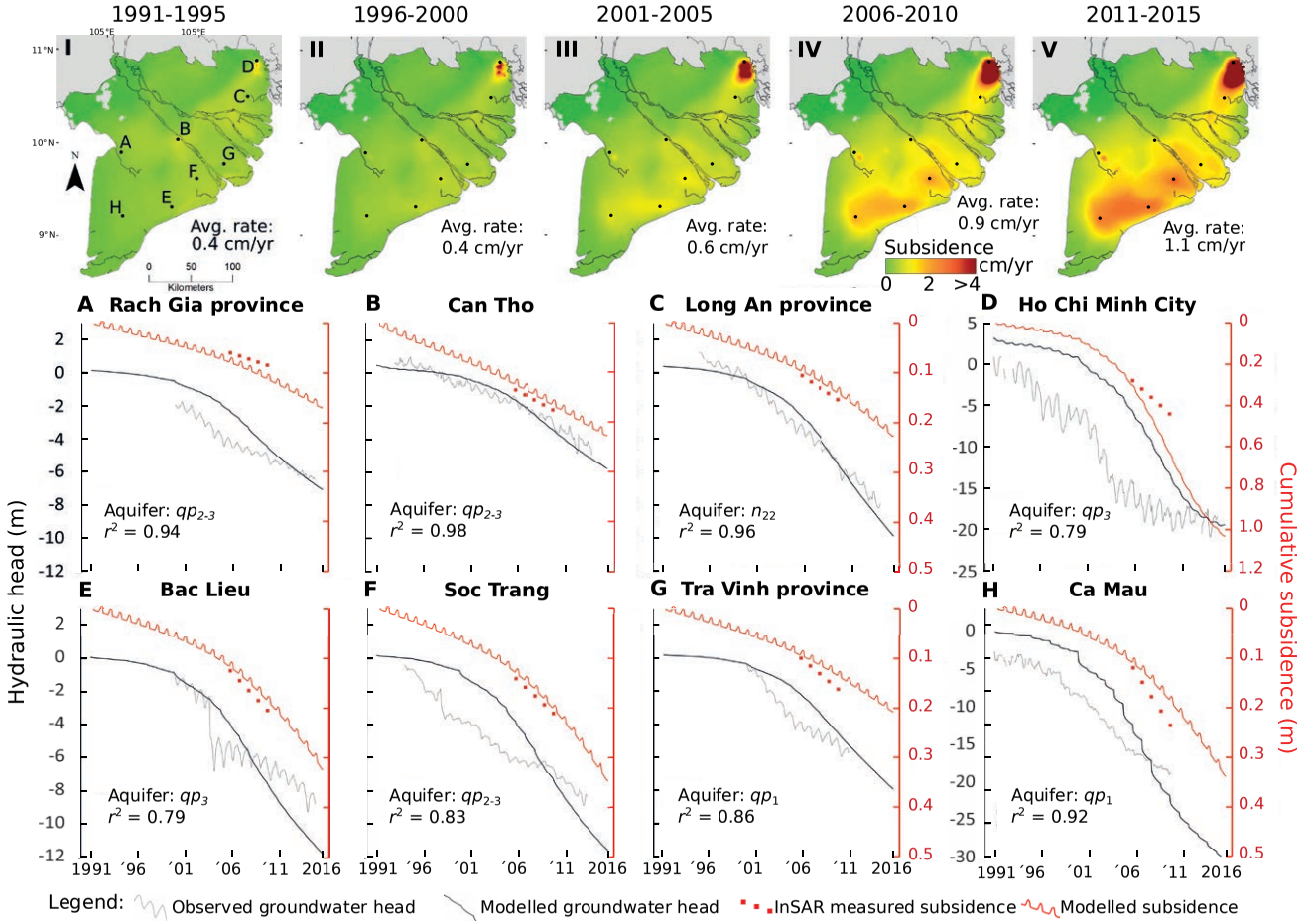

Figure 5.7: *I-V) Annual groundwater extraction-induced subsidence rates for each five year period. Monitoring well locations are marked alphabetically. A-H) Modelled and measured hydraulic head time series at monitoring well locations. Cumulative calculated subsidence is shown in red. The periodic fluctuations in the subsidence graphs reflect the elastic response up to 2 cm to seasonal wetting and drying as the aquifer system expands and shrinks. The red dots represent InSAR-measured subsidence rates over 2006-2010 by Erban et al., (2014) for visual comparison.*

5.4 Discussion

5.4.1 Contribution of groundwater extraction to total subsidence in the Mekong delta

Our model calculates subsidence resulting from aquifer-system deformation when subjected to groundwater over-extraction. In general, subsidence includes contributions by other drivers (e.g. Tosi *et al.,* 2009). Apart from groundwater extraction, these include (e.g. Galloway *et al.,* 2016): 1) shallow subsidence in the unsaturated zone triggered by phreatic groundwater level lowering, 2) natural and anthropogenic loading by for example buildings and infrastructure and 3) deeper-rooted tectonics. For the MKD, in ~75% of the cases the InSAR-measured subsidence is at least matched by the best estimated modelled subsidence, respectively ~50% to ~95% for the most conservative to the least conservative model (Appendix C, Fig. C.7). These numbers provide an estimate of how much of the InSAR-measured subsidence might be caused by groundwater extraction. Even though groundwater extraction seems to explain a large part of the measured subsidence, a large part of the InSAR-measured subsidence is unaccounted for by the model results. In addition, InSAR measurements may underestimate total subsidence in a delta, as InSAR measurements are relative measurements within individual satellite imaging swaths (~50-100 km) and can miss additional regional-scale subsidence unless calibrated with ground-based GPS.

Locally, underestimation by InSAR of total subsidence may occur where the InSAR signal was reflected from objects (e.g. buildings) founded on deeper sediment layers, and thus not register any shallow subsidence occurring between the foundation and the delta surface. Groundwater extraction is but one component of the entire InSAR-measured subsidence signal, which may include other factors such as young sediment consolidation or motion along faults. Other subsidence drivers are likely contributing to the total subsidence in the MKD and to the InSAR measurements of surface deformation.

The estimates of groundwater extraction-induced subsidence resulting from this studysuggest groundwater extraction as a dominant driver of subsidence in the MKD, supporting previous indications (Erban *et al.,* 2013, 2014). This is in line with observations from other subsiding deltas, such as the Yellow river delta (Higgins *et al.,* 2013) and delta cities e.g. Bangkok (Chao Phraya delta, Phien-wej *et al.,* 2006), Suzhou (Yangtze delta, Shi *et al.,* 2012), Jakarta (Abidin *et al.,* 2011), numerous Indonesian cities (Chaussard *et al.,* 2013), Shanghai (Wu *et al.,* 2010, Ye *et al.,* 2016) and many more (e.g. Holzer and Johnson, 1985; Gambolati and Teatini, 2015). Where the above-mentioned studies often focused on a single city or a relatively small part of a delta, our work now provides quantitative estimates for nearly the entire delta system, including all its cities and rural areas, and demonstrates spatial differences in subsidence due to groundwater extraction.

Overall, groundwater extraction-induced subsidence in the MKD seems to be highest in urban and industrial areas, where high, concentrated groundwater usage creates local subsidence hotspots. In the rural parts of the delta subsidence rates are slightly lower. Still, as most of the delta comprises rural areas, the collective extractions by millions of local people for domestic and agricultural use are responsible for ~80% of the total extracted volume in the MKD (DWRPIS, 2010), and therefore they are the largest contributor to groundwater extraction-induced subsidence at the delta scale.

5.4.2 Robustness of modelling results

Our best estimate model produces a subsidence pattern for the MKD that shows similarities to the subsidence portrayed by the InSAR measurements, with a large, subsiding region extending from HCMC (in the northeast) to Ca Mau province (in the south-west)(Fig. 5.8a-b). For a more detailed comparison, we selected twelve subsets in the MKD with 1) a clear InSAR signal and 2)

substantial groundwater extraction. The areas cover major cities as well as rural parts of the delta. Almost all average measured and modelled subsidence values within the comparison windows fall within 0.5 cm yr^{-1} of the linear fit for the best estimate model (Fig. 5.8c). This value is similar to the average uncertainty range reported for the InSAR derived subsidence rates (Erban *et al.,* 2013). Furthermore, all average subset values fall within the apriori defined least to most conservative model range, underscoring the potential to determine an acceptable subsidence model parameterization range (i.e. OCR) even when validation data is lacking. The least to most conservative models produce annual subsidence rates of respectively ~160% and ~60% of the best estimate model. As such, this range is taken as uncertainty range for the reported modelling results.

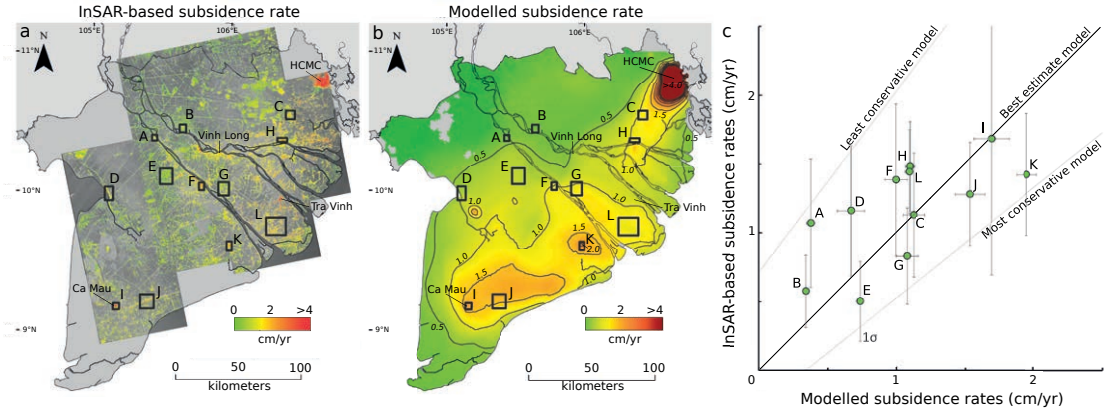

Figure 5.8. *a) InSAR-measured subsidence (after Erban et al., 2014, data © JAXA, METI 2011). Rectangles show selected subsets for comparison. A: Long Xuyen; B: Cao Lahn C: Tan An; D: Rach Gia; E: Can Tho province; F: Can Tho; G: Vinh Long province; H: My Tho; I: Ca Mau; J: Bac Lieu province; K: Soc Trang; L: Tra Vinh province. b) Modelled subsidence of the best estimate model (OCR: 1.63). c) Fit between modelled subsidence rates and InSAR measurements for the selected subsets showing average values (green dots) with 1 standard deviation (σ). The linear fit trend line (y=1.0x) of the best estimate model and respectively the least and most conservative models are shown (data points are not shown). All rates are in annual averages over the period 2006-2010.*

5.4.3 Subsidence in the Mekong delta

At several locations in the delta the InSAR-measured subsidence rates do not match well with the modelled subsidence. For example, modelled subsidence is appreciably lower for the cities of Tra Vinh and Vinh Long and the rural area south of HCMC. In addition to the aforementioned uncertainties associated with each method, we have three possible explanations. Firstly, the observed subsidence is largely caused by shallow subsidence, unrelated to groundwater extraction and therefore unaccounted for by the model. This effect may be especially important in coastal areas with young, recently deposited, superficial sediments with high consolidation potential. Surface elevation table (SET) measurements in three coastal mangrove areas in the MKD indeed reveal fairly high near-surface consolidation rates, ranging from 1.4-4.1 cm yr^{-1}, (Giao *et al.,* 2014; Lovelock *et al.,* 2015). Secondly, as subsidence rates can vary over relatively short distances associated with differences in subsurface conditions, as has been observed in the Rhine-Meuse delta (Asselen *et al.,* 2009; Koster *et al.,* 2016), the Mississippi delta (Törnqvist *et al.,* 2008) and the Ganges-Brahmaputra delta (Higgins *et al.,* 2014), the model is unable to reproduce local subsidence

resulting from subsurface heterogeneity beyond the resolution of the subsurface discretization but captured by high-resolution InSAR measurements. Thirdly, groundwater extraction in the model is based on officially registered and estimated extractions by the DWRPIS, which is at present the best available source of data on groundwater use. However, uncertainty and/or deficits of groundwater extraction in the records, for example due to unregistered extractions, likely influence model results locally (Further discussed in Appendix C, C3.3).

5.4.4 Subsidence in Ho Chi Minh City

Modelled subsidence rates for HCMC exceed the InSAR-measured subsidence (Erban *et al.,* 2014) in both spatial extent and magnitude. A detailed InSAR analysis of HCMC by Minh *et al.* (2015) shows annual subsidence rates up to 7 cm, matching the average modelling results for the city, but spatial patterns differ. Minh *et al.* (2015) attribute spatial subsidence variations in HCMC to subsurface heterogeneity that cannot be captured by the 3D spatial resolution of our current delta-wide subsurface model. Additionally, at several locations in the city with high extraction well density, modelled drawdown rates greatly exceed head declines monitored at the fringes of the city. This leads to questionable annual subsidence rates go up to several decimetres. Possible explanations for overestimated drawdown include underestimation of local aquifer connectivity and the absence of the Saigon river system (not modelled), resulting in lower recharge values. For this reason, we reported only average simulated subsidence values for HCMC, as the current model and available data does not permit more detail.

Nonetheless, all estimates suggest the HCMC law to limit groundwater use (HCMC, 2007) seems to have had an effect. Extraction figures have stabilised since 2007 and decelerating drawdown rates over the past years are both measured and modelled. Consequently, the associated subsidence also shows a slight deceleration towards the present (Fig. 5.7D). However, as subsidence is a slow responsive process and with hydraulic heads still well below initial levels, subsidence is on-going.

5.4.5 Future outlook for the Mekong delta

As the MKD continues to develop and industrialise, groundwater exploitation is likely to increase further in the decades to come. In rural areas, conversion of land use practice to more groundwater-intensive businesses, e.g. from two to three rice crops, or paddy to shrimp ponds, is on-going (e.g. Renaud *et al.,* 2015). Our modelling results indicate that pumping-induced subsidence rates in the MKD continuously increased over the past 25 years, with present rates (delta-wide average of 11 *(7-18)* mm yr^{-1}, with areas surpassing 25 *(17-33)* mm yr^{-1}) exceeding local rates of absolute sea level rise by an order of magnitude (~3 mm yr^{-1}; Church *et al.,* 2013). These rates are alarming given that the majority of the MKD land surface is less than 2 meters above mean sea level, while subsidence rates may increase further.

Elevation loss resulting from subsidence increases flood and storm surge vulnerability. The MKD and its cities are likely to experience more frequent and prolonged inundation periods. This trend is already apparent in the cities of Can Tho (Huong and Pathirana, 2013; Tagaki *et al.,* 2016) and HCMC (Phi, 2008). Moreover, subsidence increases salt water intrusion in the estuaries and the delta's dense network of surface waterways, in turn increasing the pressure on groundwater reserves.

5.5. Conclusions

Our process-based approach, employing the first delta-wide, one-way coupled 3D hydrogeological and subsidence numerical model of the MKD, enabled us to compare groundwater extraction-related subsidence to total InSAR-measured subsidence at delta scale. This is an important step towards disentangling the total, measured subsidence signal for a delta into different drivers of subsidence. The approach also facilitates the analysis of the timing of hydraulic head decline and corresponding subsidence during the modelling period. When sufficient hydrological and geological data is available, this modelling approach can be applied to other delta systems worldwide facing groundwater-extraction related subsidence, to estimate a range of subsidence rates even when no direct subsidence measurements, such as InSAR, are available. When available, direct measurements of subsidence form valuable datasets to confine the range of groundwater extraction-induced subsidence estimates.

In case of the Vietnamese Mekong delta, the hydrogeological system of the Mekong delta has been transformed from an almost undisturbed to a human-impacted state with accelerating aquifer depletion due to increasing groundwater extraction during the past 25 years. Aquifer system compaction following dropping water pressures in the aquifers has resulted in dramatic delta subsidence over this period.

Our best estimate model suggests that a quarter-century of pumping-induced subsidence caused the MKD to sink on average by ~18 cm over the past 25 years, with areas over 30 cm. At present, the average groundwater extraction related subsidence rate in the MKD lies around 1.1 cm yr^{-1}, with local extremes over 2.5 cm yr^{-1}. For HCMC current rates are as high as ~7 cm yr^{-1}. Groundwater extraction seems to be a major subsidence driver in the MKD, as indicated by both our model and previous InSAR-measured subsidence. However, other drivers likely contribute substantially to the total subsidence experienced in the delta as well.

The alarming subsidence rates reported in this study showcase the real and urgent threat groundwater extraction related subsidence can pose to low-lying deltas like the Mekong delta, exacerbating flood vulnerability, saltwater intrusion and coastal erosion. For this reason, delta subsidence should be a priority for responsible policy makers, effective policy strategies could curtail subsidence caused by groundwater extraction. In Vietnam, this is already demonstrated for Ho Chi Minh City where the restriction on groundwater overexploitation seems to alleviate subsidence. Monitoring subsidence by measuring total surface elevation change, e.g. by InSAR, LiDAR or GPS, and in-situ, depth-dependent subsidence, e.g. by SETs, extensometers or benchmarks is essential to facilitate management decisions in subsiding deltas and should be invested in. In addition, 3D numerical models, as presented in this study, have the potential to provide highly relevant predictions of delta-wide subsidence, supporting the urgently needed decision-making in subsiding deltas.

Acknowledgements
We wish to thank the Department of Water Resources Planning and Investigation for the South of Vietnam (DWRPIS) for providing data for this study. Hans Middelkoop is thanked for comments and discussion on the manuscript; Peter Vermeulen for support on iMOD modelling procedure; Gualbert Oude Essink for discussions on hydrogeological and density-driven groundwater modelling; Ger de Lange for discussions on geotechnical parameterization. Pepijn van Elderen is acknowledged for his work on georeferencing of the InSAR images. This paper benefitted substantially from the comments and suggestions of two anonymous reviews.

6 Groundwater extraction may drown mega delta

The low-lying and populous Vietnamese Mekong delta is facing accelerating subsidence rates up to several centimeters each year that cause the delta to rapidly lose its elevation above sea level. This strongly increases the deltas vulnerability to flooding, salinization, coastal erosion and, ultimately, threatens the delta with permanent inundation. Accelerated subsidence of the delta is primarily caused by the groundwater extraction and, as the extracted volume is still increasing, projections of extraction-induced subsidence rates are urgently needed to evaluate their potential impact on future elevation loss and aid the development of sustainable delta management strategies. We developed six mitigation and non-mitigation scenarios in which the delta follows different groundwater extraction pathways until 2100. To model future groundwater flow and consequent aquifer-system compaction of the Mekong delta, we employed an updated version of a previously developed 3D hydrogeological model, coupled to a geotechnical module. Our results reveal the long-term physically response of the aquifer system and the potential of the hydrogeological system to recover. When groundwater extraction is allowed to grow continuously, as it did over the past decades, extraction-induced subsidence has to potential to drown the Mekong delta single-handedly. However, our quantifications of extraction-induced subsidence also disclose the large potential for mitigation to reduce subsidence and limit future elevation loss. As the majority of the Mekong delta plain is elevated less than 1 meter above sea level, the window for mitigation to sustain elevated above sea level is rapidly closing as large parts of the delta plain may already fall below sea level within the coming decades. Whether, when and to which degree mitigation measures, aiming to reduce the amount of groundwater extraction, are successfully implemented will determine the share of the delta that will not submerge. The future of this mega delta lies in the hands that control the groundwater pumps.

Minderhoud, P.S.J., Middelkoop, H., Erkens, G., Stouthamer, E. **Groundwater extraction may drown mega delta.** *(Submitted)*

6.1 Introduction

The world's third largest delta, the populous and low-lying Mekong delta in Vietnam (Fig. 6.1) is facing increased river flooding (Kuenzer et al., 2013), decreased sediment delivery (Darby et al., 2016; Kondolf et al., 2014; 2018; Kummi et al., 2007, Xue et al., 2011), coastal erosion (Anthony et al., 2015) and salinization (Renaud et al., 2015; Smajgl et al., 2015). On top of that, like many other deltas in the world (Syvitski et al., 2009, Nicholls and Cazenave, 2010), the Mekong delta experiences accelerating rates of relative sea-level rise, the combined effect of absolute sea-level rise and land subsidence. As the Mekong delta has one of the lowest delta plains in the world, on

average only ~80 cm above m.s.l. (Chapter 2), relative sea-level rise increasing threatens the delta's 18 million inhabitants and its important economic function as an environment for agri- and aquaculture production vital to South-East Asia's food production. Land subsidence is the main source of relative sea-level rise in the Mekong delta and is caused by various driving processes: i.e. natural processes like tectonics and natural compaction of the Holocene sediments (Zoccarato et al., 2018) and human-induced processes driven by amongst others groundwater extraction (Erban et al., 2014; Minderhoud et al., 2017), drainage of shallow sediments and loading by buildings and infrastructure (Minderhoud et al., 2018). The change of Vietnam to an open-market economy in 1986 (Seto, 2011) was the onset of large-scale groundwater extractions in the Mekong delta that triggered extraction-induced subsidence (Minderhoud et al., 2017). In the decades that followed, groundwater extraction steadily increased, providing high-quality fresh water to meet the growing agricultural, industrial and domestic demand that fueled the rapid growing economy (Wagner et al., 2012). As a result, extraction-induced subsidence has accelerated over the past decades to rates exceeding 25 mm yr^{-1} in certain areas, making it at present the main contributor of delta-wide subsidence in the Mekong delta (Chapter 5).

With its low elevation and accelerating sea-level rise, the Mekong delta is at a crossroad and delta management choices, including policy decisions on groundwater use, will shape the future of the delta. The development and implementation of integrated delta policies aimed to safeguard the delta for future generations is more important than ever before. It requires quantification of future subsidence to inform decision makers. In contrast to subsidence caused by natural processes, which cannot be mitigated, extraction-induced subsidence can be targeted for mitigation in order to reduce subsidence rate and future delta-elevation loss. Until now, future projections of extraction-induced subsidence were only based on extrapolations of past or present subsidence rates, however, these are unable to capture, for example, the influence of mitigation measures. Furthermore, as subsidence induced by groundwater extraction is a slow responding and non-linear process, it can take years until the effect of a change in hydraulic head (i.e. water level in an aquifer) in the aquifer-system, which drives extraction-induced subsidence, is fully expressed (Galloway and Burbey, 2011, Isotton et al., 2015). This means that subsidence can still happen well after groundwater extraction has stopped and hydraulic heads are rising again. It is vital to gain insights in these longer-term processes and effects to assess the impacts of future groundwater extraction on subsidence of deltas and coastal systems facing high rates of relative sea-level rise as a result of groundwater overexploitation. In this paper, we aim to study long-term, hydrogeological and geotechnical behavior of the Mekong delta's aquifer system and to provide the first process-based quantification of possible future groundwater extraction on delta-wide subsidence to support informed decision-making in the delta.

Recent research resulted in the first delta-wide 3D hydrogeological model, coupled to a geotechnical module of the Mekong delta (Minderhoud et al., 2017). This model enabled process-based modelling of groundwater flow and compaction of the delta's multi-aquifer system. To enable modeling of future groundwater extraction-induced subsidence, we advanced this model further and developed six mitigation and non-mitigation scenarios focused on hydraulic head development following different groundwater extraction pathways until 2100. These scenarios reveal the long-term physical behavior of the entire delta and provide valuable insights on recharge and recovery potential of the aquifer system. Furthermore, our results provide the first non-linear, process-based quantitative estimates of potential future extraction-induced subsidence for the Mekong delta. They show the large effect that mitigation efforts, focused on the reduction of groundwater extraction, may have on reducing future elevation loss. We found that the window for mitigation to keep the

delta elevated above sea level is rapidly closing, and show how decisions on groundwater-extraction policy will determine the future of the delta. These new insights are relevant for decision makers in the Mekong delta and demonstrate the potential impact of groundwater extraction and mitigation potential on delta subsidence for deltas and coastal plains in general.

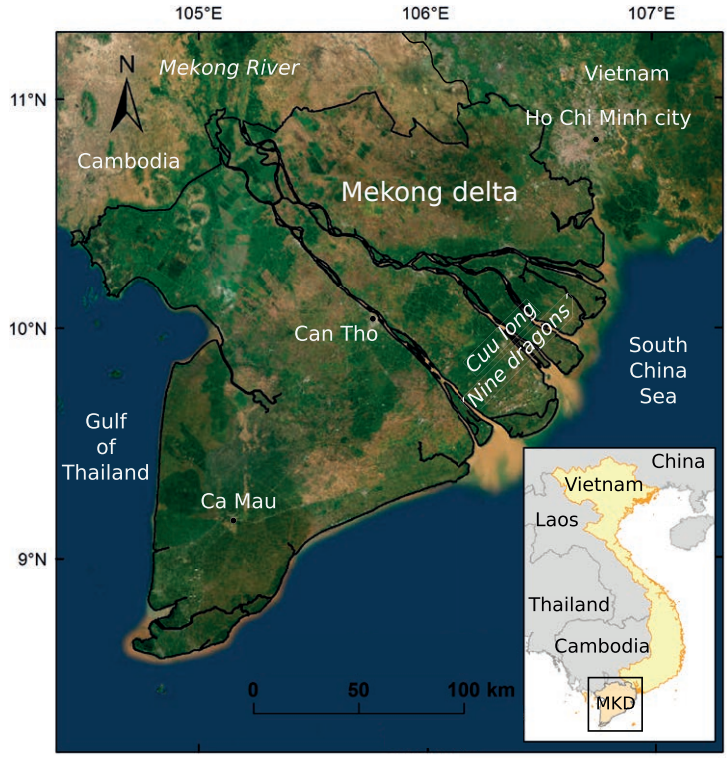

Figure 6.1 | *Location of the Vietnamese Mekong delta in South-East Asia.*

6.2 Methods

6.2.1 Groundwater and subsidence model

We used an extended and updated version of the 3D hydrogeological groundwater model of the Mekong delta developed by Minderhoud et al. (2017)(Chapter 5) to model scenarios of future groundwater extraction. Originally, this hydrogeological model was used to model groundwater flow for the period 1991-2015 using the MODFLOW-based environment iMOD (Vermeulen, 2006; Vermeulen et al., 2018). The model includes a 3D hydrogeological representation of the delta's multi-aquifer system over 500 meter depth (see Fig. 5.2 and Appendix C, Table C.1). The hydrogeological model parameters were calibrated using measurements of hydraulic head throughout the delta. Variable density groundwater flow (e.g. the effect of saline water) is not included in the model. We extended the simulation period of the model to 1991-2100 to evaluate of future groundwater extraction scenarios and corresponding extraction-induced subsidence. Furthermore, we improved the model by explicitly including the surface water network of the Mekong delta.

Adding surface water network

The surface water system of the Mekong delta consists of a dense network of natural river branches, canals and tidal creeks. In the previous version of the model the interaction with the surface water system was modeled through a constant drain at the delta surface, but the individual Mekong river channels and the extensive canal system were not explicitly included in the model. As a result, the modelled hydraulic heads in confined aquifers close to large rivers showed a mismatch with the observed hydraulic heads, as the modeled recharge at these locations was too low (also discussed in Minderhoud et al., 2017). To use the model for future predictions and simulate groundwater dynamics over more than a century, accurate modeling of groundwater recharge is essential as small mismatches cumulate to large quantities over time. Therefore, we updated the model by explicitly including the surface water system of the Mekong delta to improve modelled recharge of river water to the aquifer system. We divided input data on the surface water system into four categories which are 1) main river channels, 2) secondary river channels, 3) main canals and 4) secondary canals. Average width and depth estimates for each category were used to determine river depth and to estimate bed conductance (Appendix D, Fig. D.1). River stage measurements from 1999 to 2010 were supplied by the Division of Water Resources Planning and Investigation for the South of Vietnam (DWRPIS) from 39 locations in the main and secondary rivers (Bui et al., 2013). These measurements were interpolated to derive average annual river stage for the entire delta (Appendix D, Fig. D.1). Implementation of the surface water system into the model resulted in an improved modeling of surface water-groundwater interaction. Moreover, it increased the modeled recharge of confined aquifers in places where river channels cut through the Holocene aquitard, a phenomenon also observed in hydraulic head measurements. As a result, the overall mean correlation coefficient (r^2) between observed and modeled hydraulic heads in the Mekong delta for the period 2000-2015 improved from 0.69 to 0.73 by modeling the surface water system explicitly.

Subsidence calculations

We calculated subsidence as a result of aquifer-system compaction following decreases in hydraulic head (i.e. decreasing pressure) using a one-way coupled geotechnical subsidence module (i.e. SUB-CR). We applied the so-called *abc* model, in which *a* (recompression or swelling constant) accounts for the elastic compression, *b* (compression constant) and *c* (secondary compression constant) for the viscoplastic compression (Den Haan, 1994). This model determines natural strain (i.e. degree of compression) based on the isotach concept (Šuklje, 1957; Bjerrum, 1967) as a function of effective stress and intrinsic time using the *abc* constants. The model only considers vertical displacement and the hydrological effect of viscous compression, which tends to increase pore pressure and therefore hydraulic head, was set to zero as the model was calibrated without this budget term. The parametrization of the *abc* constants was adopted from Minderhoud et al. (2017)(Chapter 5) (Appendix C, Table C.5). Apart from the *abc* constants, the modeling of secondary compression also depends on the overconsolidation ratio (OCR) which is described as follows:

$$OCR = \sigma'_p / \sigma' \tag{6.1}$$

where σ'_p is the initial pre-consolidation stress and σ' the momentary effective stress. A lower OCR value results in higher rates of secondary compression. For the Mekong delta only limited data is available to constrain OCRs. Hoang et al. (2016) found an average OCR value of 1.6 for clayey deposits in the Mekong delta and Thoang and Giao (2015) reported a similar value for medium to stiff clays in HCMC province. Validation of modeled subsidence in the Mekong delta with InSAR-

derived subsidence rates from 2006-2010 (Erban et al., 2014) revealed an almost similar OCR value of 1.63 to provide the best fit (Chapter 5). We applied the same validation after updating the model (section 6.2.1 & 6.2.2) and the OCR value that provided the best fit with the InSAR-derived subsidence rates remains 1.63. Therefore, we also use this OCR value to calculate the best estimate subsidence values for this study. To provide a range of subsidence calculations from least conservative (very weak sediments) to most conservative estimates (rigid sediment properties), we varying the OCR value by 0.1 (i.e. 1.53-1.73). We selected a slightly narrower OCR range than used by Minderhoud et al. (2017)(Chapter 5), as it provides modeling results that were better supported by the InSAR-based subsidence rate observations providing assumably a more realistic range (see Appendix D, section D.2). The presented results of average modeled cumulative subsidence and subsidence rates for the different extraction scenarios are based on the best estimate model (OCR = 1.63) and specifically calculated for the Mekong delta (delineated in Fig. 6.1). Furthermore, as the extraction data does not cover the entire Mekong delta, results of average delta-wide subsidence presented in this paper were calculated based on areas in the Mekong delta within a 5 km radius of a modeled extraction (Appendix C, Fig. C.5).

6.2.2 Updating past groundwater extraction

In the previous model version the growth of unregistered extraction volume was estimated to be similar to the growth of the registered wells volume (Minderhoud et al., 2017). The hydrogeological modeling results showed that throughout the delta the modeled hydraulic head decline during the start of the modeling period slightly underestimated measured hydraulic head declines and overestimated hydraulic head declines at the end of the original modeling period towards the present. For modelling future development of hydraulic head declines and subsidence, especially the overestimation of hydraulic head decline at the end of the modeling period (~2010-2015) is problematic as extrapolation into the future increases such initially small overestimations further. To improve this for this study, we based the annual growth in unregistered extraction volume directly on measured hydraulic head decline in the confined aquifers. This alternative approach follows the assumption that an increase in measured hydraulic head drop in an aquifer is linked to an increase in extracted volume. It was applied for all unregistered extractions in the Mekong delta and Ho Chi Minh city (HCMC) province during the modeling period 1991-2011 (Appendix, D, Section D.4 for a detailed description of the approach and modelled annual groundwater extraction). For the period of 2011-2018, an annual growth of 2.5% was simulated for the Mekong delta based on estimates of extraction increase by the DWRPIS. For HCMC province, extraction gradually stabilized following the water act in 2007 (HCMC, 2007). The update of the annual growth of unregistered extractions resulted in an improved fit with the model and the observed hydraulic head decline (Appendix D, Fig. D.4) and the model no longer overestimates the decline towards the present. Compared to the previous model version, the overall mean correlation coefficient (r^2) between observed and modeled hydraulic heads in the Mekong delta for the period 2000-2015 improved from 0.69 to 0.75. When combined with implementing the surface water system in the model (section 6.2.1), the performance of the model increased further ($r^2 = 0.78$). By improving the modeled extraction volume for the past, the modeled extracted volume provides a more realistic starting value for the modeling of future extraction pathways.

6.2.3 Groundwater extraction scenarios

The updated and extended model enables to evaluate the future hydraulic head evolution and consequent aquifer-system compaction of the Mekong delta. We developed six scenarios to

simulate different possible pathways of future evolution of total extracted volume in the Mekong delta from 2019 to 2100 under various decrees of mitigation (Table 6.1, Fig. 6.2). The pathways were developed either focused directly on the amount of groundwater extracted in the delta or, indirectly, on the effect of extractions, i.e. hydraulic head development over time. This second pathway type was developed because maintaining certain hydraulic heads can be implemented as mitigation measure. This is, for example, the case in HCMC where, following the water act in 2007, groundwater extraction is no longer allowed when hydraulic head in an aquifer falls below a certain predetermined level (HCMC, 2007).

Table 6.1 | *Modeled scenarios of groundwater extraction pathways from 2018 until 2100. The percentual annual change in extracted volume was applied to all wells included in the model.*

Scenario		Extraction pathways
Non-mitigation	*B2: Extreme extraction increase*	*Steady annual increase: 4% of the 2018 volume*
	B1: Moderate extraction increase	*Steady annual increase: 2% of the 2018 volume*
Mitigation	*M1: Stable extraction*	*Stabilizing extraction, no increase after 2020: 2019: 1.5%; 2020: 0.5%; after 2020: stable extraction*
	M2: Stable groundwater levels	*Gradual reduction of extracted volume to 50% of the 2018 volume: 2018-2028: Annual reduction of 5%. After 2028: Stable extraction*
	M3: Recovery of groundwater levels	*Gradual reduction of extracted volume to 25% of the 2018 volume: 2018-2033: Annual reduction of 5%. After 2033: stable*
	M4: Full extraction stop	*Complete stop of all extractions after 2018*

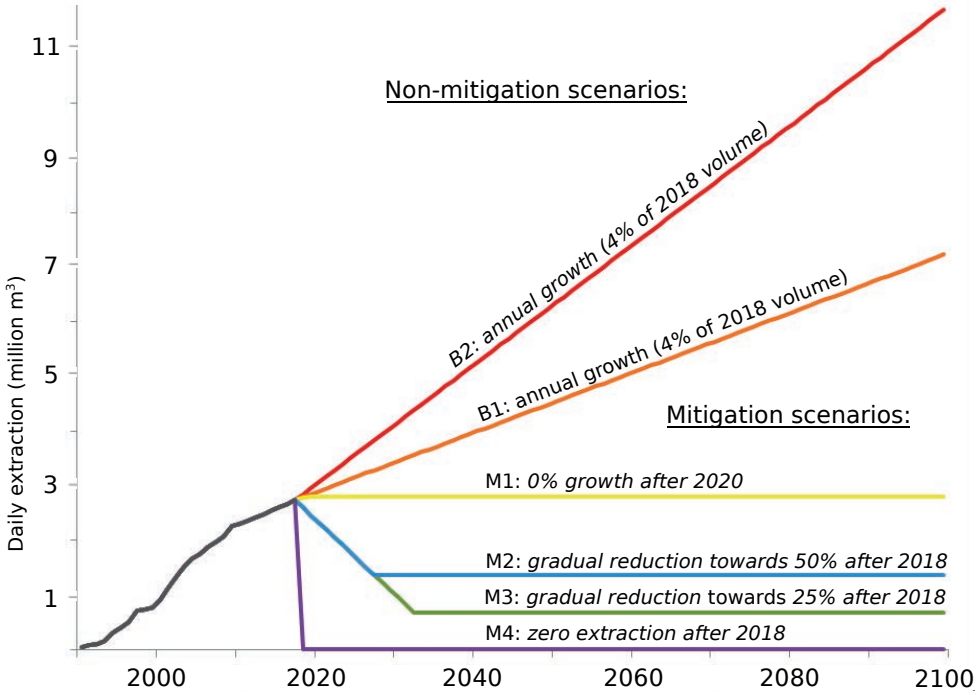

Figure 6.2 | *Total modeled daily groundwater extraction (million m^3) from 1991 to 2100 in the Mekong delta for each pathway after 2018 following the non- and mitigation scenarios.*

Two non-mitigation scenarios follow pathways in which the amount of groundwater extraction continues to grow: Scenario B1 represents a future in which groundwater extraction continues to increase moderately (annual increase of 2% of the 2018 volume; 55 x 10^3 m^3 daily extraction per year) and scenario B2 represents a worst case scenario in which extraction increases double this amount (annual increase of 4% of the 2018 volume; 110 x 10^3 m^3 daily extraction per year).

Four mitigation scenarios follow groundwater extraction pathways aiming to limit extraction growth and /or reduce total extracted volume. Scenario M1, M2 and M3 have been developed in a way that they could represent realistic cases by incorporating a transition period during which the extracted volume is gradually stabilized or reduced. This period is needed to reduce groundwater use and to create the infrastructure needed to provide for alternative fresh water sources to meet the fresh water demand. Mitigation scenario M1 represents a stabilization of the extracted volume, allowing limited volume growth until 2020 to realistically incorporate the effects of new wells that are already licensed and currently being constructed. After 2020 there is no further increase and the total extracted volume (~2.8 million m^3 daily) remains stable until 2100. Mitigation scenario M2 focuses on the stabilization of hydraulic heads and aims to maintain present hydraulic heads until 2100. In this scenario the modeled natural recharge of the delta system equals the amount of groundwater extracted from the subsurface and this requires a reduction of groundwater extraction to 50% of the 2018 volume (~1.4 million m^3 daily). Scenario M3 investigates a situation in which the recovery of groundwater levels is the main focus but groundwater is still extracted in small quantities. In this scenarios groundwater extraction is reduced to 25% of the 2018 volume (~0.7 million m^3 daily), to allow recovery of the hydraulic head through natural recharge. Scenario M4 is a theoretical case to investigate the response of the Mekong delta system after an abrupt stop of all extractions after 2018. This scenario was developed to quantify the maximum recovery rate of the hydraulic heads in the aquifer system and the minimum amount of future subsidence that will inevitably happen as inheritance of three decades of hydraulic head lowering.

In each scenario the groundwater extraction pathway was described as a percentual change in total extraction volume compared to the total volume of groundwater extraction of 2018 (Table 6.1). This annual change was simulated in all existing wells in the model located in both the Mekong delta and HCMC province. No new wells were added nor was there spatial variability in extraction growth included. For each scenario, the hydrogeological response of the groundwater system was modeled and the amount of extraction-induced subsidence quantified until 2100.

6.3 Results

6.3.1 Hydrogeological evolution

Future average delta-wide hydraulic head evolution for each scenario is presented in Fig. 6.3. The average hydraulic head is an equally weighted average of the six confined aquifers (Upper Pleistocene to Upper Miocene) in the subsurface. For both non-mitigation scenarios (B1 and B2), in which groundwater extraction continues to increase, the average hydraulic head in the Mekong delta continues to drop throughout the modelling period to -30 m in scenario B1 and to almost -50 m in scenario B2 by 2100. When the extraction volume stabilizes after 2020 (scenario M1), the average hydraulic head continues to drop until it gradually stabilizes towards the end of the century at a level twice the present-day hydraulic head level below 0 meter (-13.5 m). Scenario M2 and M3 show both a short decreasing drop in average hydraulic head, after 2018 followed by a recovery of the heads in the decades afterwards. Scenario M2 represents the extraction pathway aiming to

stabilize the average hydraulic head at its 2018 level of -6.5 m, which it does after a short dip and recovery. In the recovery scenario (M3), the hydraulic heads recover towards a level half the average hydraulic head in 2018 (-3.2 m in 2100, Appendix D, Table D.1). The full extraction stop scenario (M4) shows a recovery of the head to levels slightly above mean sea level by the end of the modeling period, comparable to the hydrogeological situation in the delta at the end of the 20th century before the excessive exploitation of the groundwater system had started. The average hydraulic head recovered to 0 meter by the year 2077, comparable to the situation in the delta in 1997.

The above hydraulic head values are delta-wide, multi-aquifer averages. Hydraulic head evolution in each separate aquifer is dependent on its specific balance between extraction and recharge, which is also spatially variable. The maps of average hydraulic head evolution for the different extraction pathways (Fig. 6.4) show the spatial variability in the Mekong delta. In general, aquifer recharge is higher in the central and northern part of the Mekong delta, where the presence of large rivers in combination with a thinner Holocene aquitard (less low-permeable clays at the delta surface) enable more recharge when compared to the southern part of the delta. This becomes especially visible in scenario M2 as hydraulic heads in the central and northern part of the delta slightly increase towards the end of the century, while in the Ca Mau peninsula in the south, the heads slightly decrease compared to the 2018 levels.

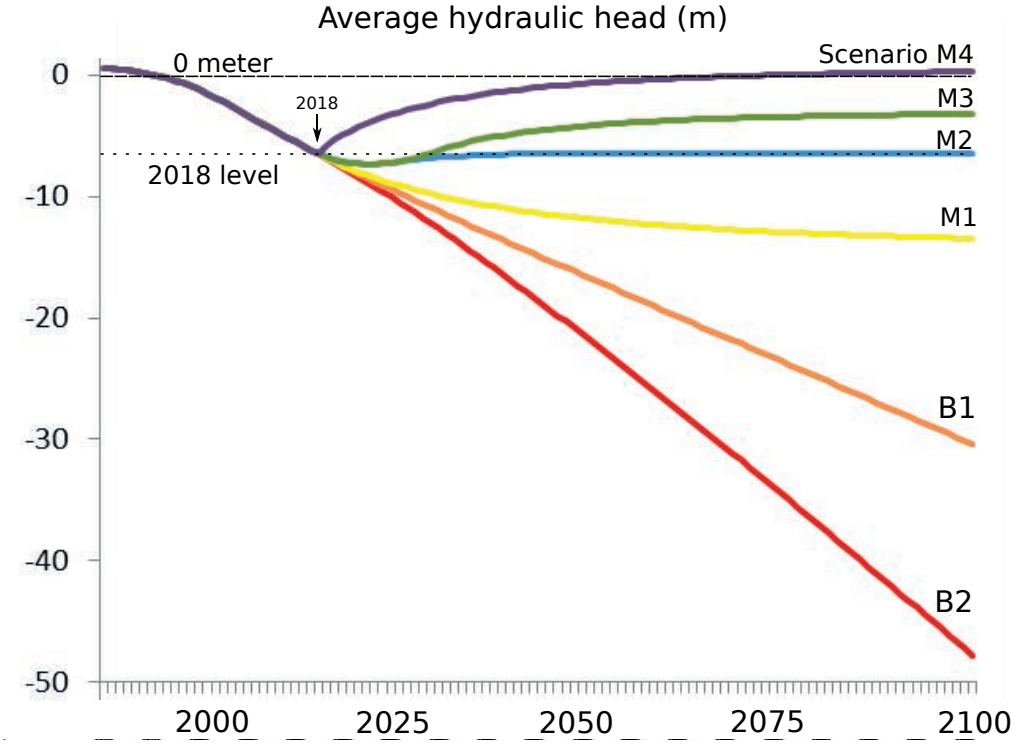

Figure 6.3 | *Average hydraulic head evolution in the Mekong delta under different groundwater extraction scenarios. The hydraulic heads are equally weighted averages of all confined aquifers.*

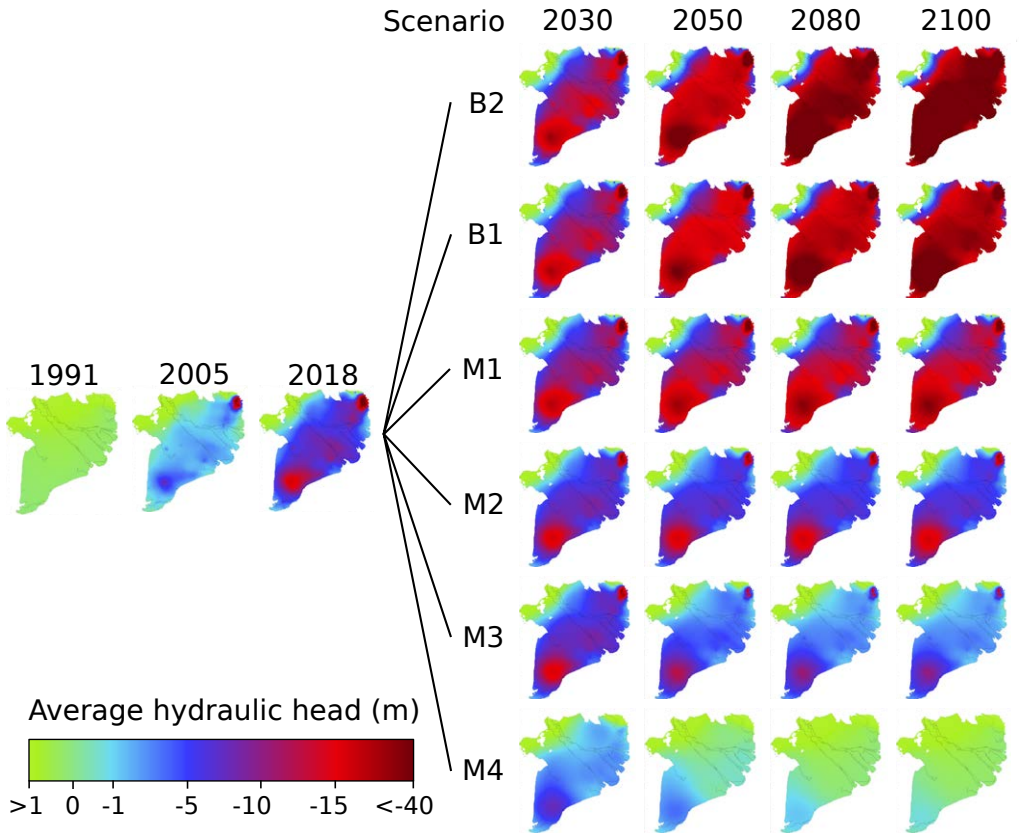

Figure 6.4 | *Modeled average hydraulic head of the confined aquifers under different groundwater extraction scenarios for the Mekong delta.*

6.3.2 Modeled extraction-induced subsidence

Present subsidence rates

The updated model, including an explicit modeled surface water system and an alternative approach to determine past extracted volume, slightly changed the simulated hydraulic head evolution compared to the previous model version (Chapter 5). The hydraulic head drop was simulated more gradually and dropped less in absolute values from 1991 to present, creating a better fit with the observed hydraulic heads (Appendix D, Fig. D.3). As a result, the modeled extraction-induced subsidence rates by the updated model are slightly lower compared to the previous model version (Appendix D, section D.4), but their values remain well within the earlier reported uncertainty range .

Future extraction-induced subsidence

The evolution of subsidence rates and cumulative subsidence since 2018 is modeled until the end of the 21th century following the six groundwater extraction pathways. Fig. 6.5 shows the spatial subsidence patterns of the best estimate model projections for the Mekong delta and HCMC province. The development of the average Mekong delta-wide subsidence rates and cumulative subsidence for each scenario during the period 2000-2100 are shown respectively, in Fig. 6.6 and Fig. 6.7.

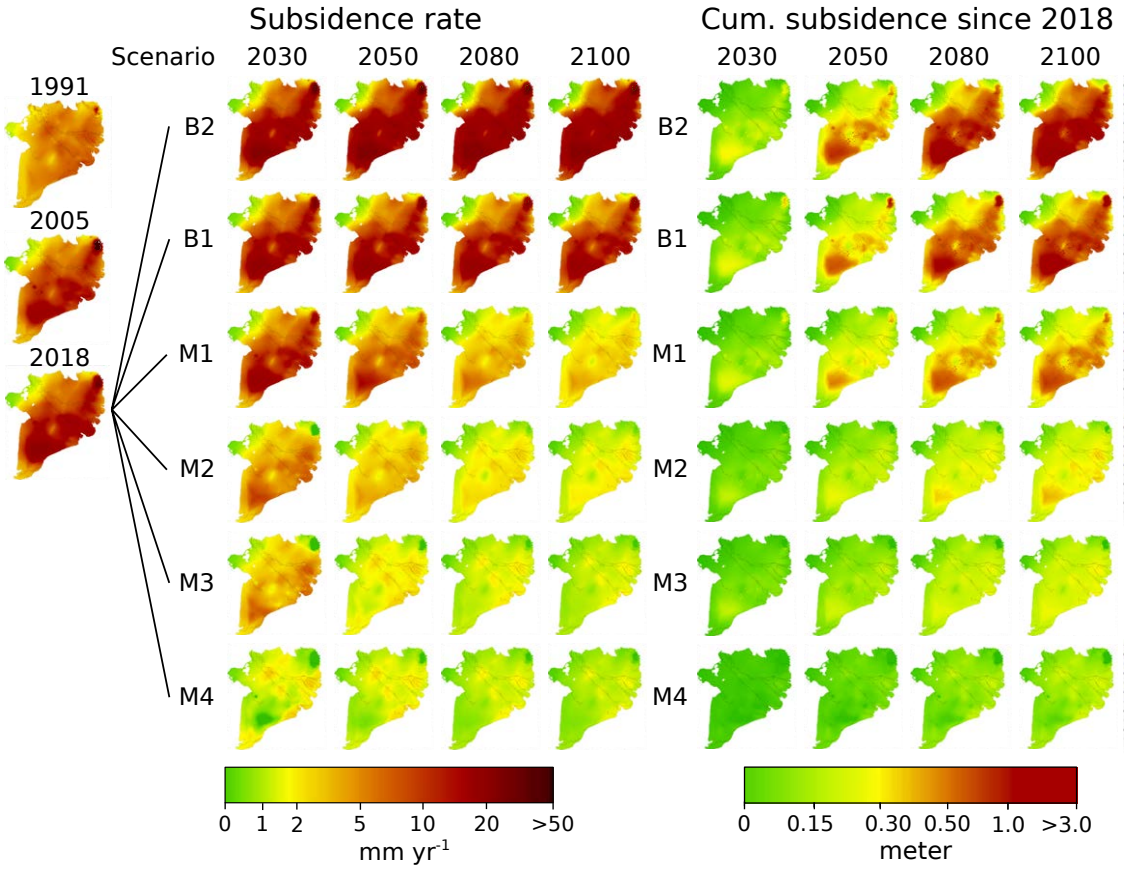

Figure 6.5 | *The evolution of subsidence rate (left) and cumulative subsidence (right) in the Mekong delta until 2100 following different groundwater extraction pathways. Cumulative subsidence is calculated from 2018 onwards. The quantifications are based on the best estimate model.*

In the two non-mitigation scenarios the total volume of groundwater extraction continues to increase and as a result subsidence rates remain high throughout the 21th century. In scenario B2, the delta-wide average subsidence rate keeps increasing until 2078 till 13.1 (12.1-13.6) mm yr^{-1} for the best estimate (most conservative and least conservative) model (Fig. 6.6). At the end of the century, the average delta-wide subsidence rate is 12.9 (12.3-13.1) mm yr^{-1} with certain areas in the delta experiencing rates exceeding 25 mm yr^{-1}. Cumulatively, the delta subsides on average 100 (86-110) cm during the period 2018-2100 in scenario B2 (Fig. 6.7). In scenario B1, the average delta-wide subsidence rate increases from 2018 towards 2023 to 8.9 (5.84-11.9) mm yr^{-1} followed by a gradual decline in rate towards 7.6 (7.0-7.9) mm yr^{-1} in 2100. In scenario B1, during the 21th century following 2018, the delta subsides on average a total of 68 (55-70) cm.

In all four mitigation scenarios in which groundwater extraction is kept stable or decreases in the future, the subsidence rates also decrease. The largest differences between the mitigation scenarios in term of subsidence rates can be observed in the coming first decades (Fig. 6.6). The largest abrupt change in subsidence rate happens in scenario M4, where subsidence rates drop sharply from 8.9 (5.5-12.5) to 1.6 (-1.3-4.9) mm yr^{-1} as a result of the abrupt stop of all groundwater extractions. In 2050 average modeled subsidence rates of the Mekong delta for scenario M1 to M4 are, 5.0 (3.5-5.9) mm yr^{-1}, 2.9 (1.7-3.7) mm yr^{-1}, 1.9 (1.0-2.7) mm yr^{-1}, 1.6 (0.7-2.3) mm yr^{-1}.

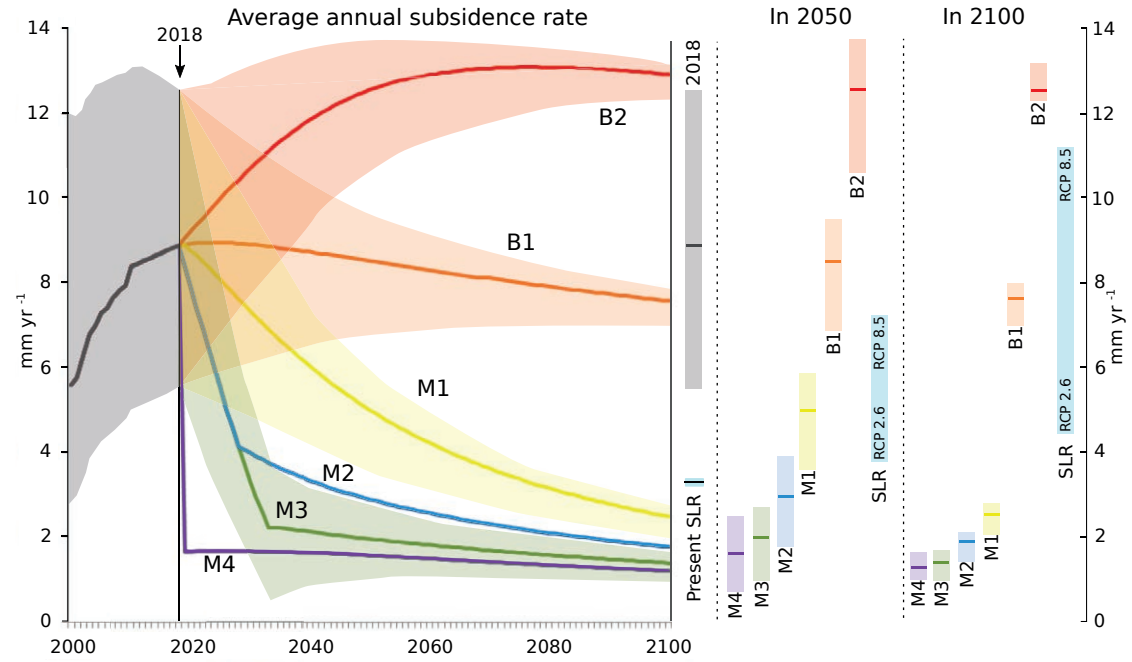

Figure 6.6 | *Annual subsidence rates under different extraction scenarios. Lines gives the best estimate model result and the uncertainty bandwidth shows the modeling results of the least and most conservative models. For a clear visualization, the range of M2 and M4 is not shown on the left panel. The range of sea-level rise (SLR) is based on the RCP 2.6 and 8.5 climate change scenarios (Church et al., 2013).*

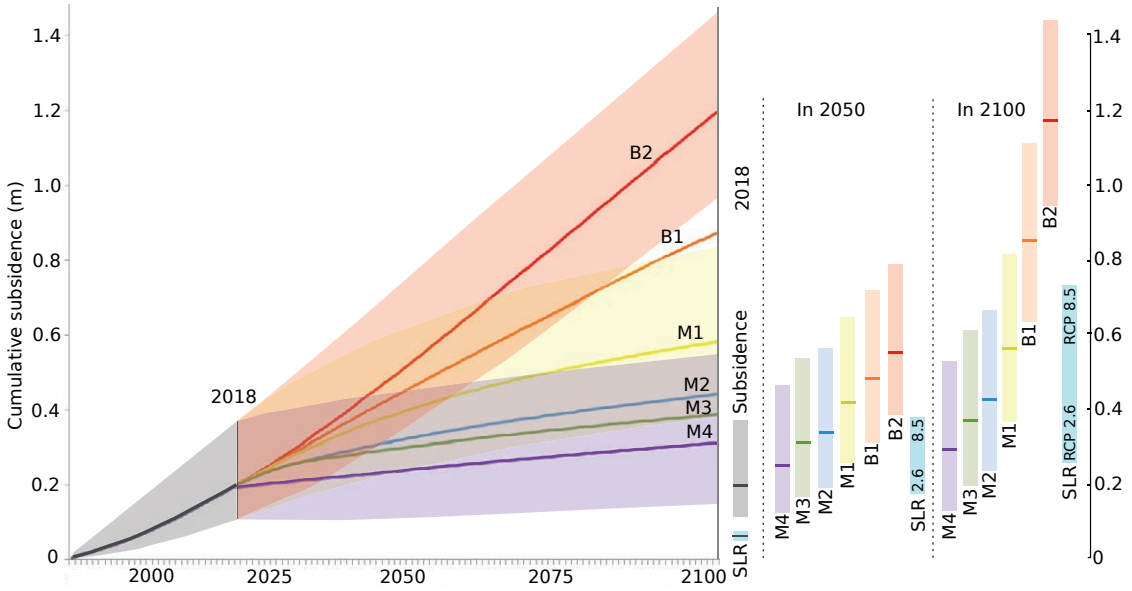

Figure 6.7 | *Average cumulative subsidence of the Mekong delta for different groundwater extraction pathways. Colored lines give the best estimate model result and the uncertainty range shows the modeling results of the least and most conservative models. For visualization purpose, the range of B1, M2 and M3 is not shown on the left panel. The range of cumulative absolute sea-level rise (SLR) in the right panel is based on the RCP 2.6 and 8.5 climate change scenarios (Church et al., 2013).*

Towards the end of the century, the subsidence rates all gradually converge towards each other and rates in 2100 range from 1.2-2.5 (0.7-2.7) mm yr^{-1} for all mitigation scenarios. Cumulatively, the mitigation scenarios result in relatively large differences. By 2100, the Mekong delta experiences, in respectively scenario M1 to M4, on average a cumulative subsidence of 39 (28-48) cm, 25 (15-33) cm, 19 (10-27) and 12 (4-18) cm since 2018. Spatially, subsidence rates vary considerably over the Mekong delta (Fig. 6.5).

Fig. 6.6 and Fig 6.7 also show the range in projections of absolute sea-level rise, caused by accelerated thermal expansion of seawater and melting of ice sheets as a result of global warming, using the RCP 2.6 and 8.5 climate change scenarios (Church et al., 2013). At present, extraction induced subsidence rates are much larger than rates of present absolute sea-level rise. During this century, when groundwater extraction continues to increase, scenario B1 and B2, the extraction-induced subsidence rates will remain higher or, at some point, equal to rates of absolute sea-level rise. In case of mitigation (scenario M1-M3) rates will gradually decrease and at some point become less than absolute sea-level rise.

6.4 Discussion

6.4.1 Limitations on modeling the hydrology and subsidence of the Mekong delta aquifer system

Future change in total groundwater extraction volume was modeled based on the delta-wide extraction database of the DWRPIS which is, at present, the best available data on groundwater extraction available for the delta. Uncertainties in extracted volume and missing extractions may affect the modeled spatial patterns of hydraulic head in the aquifers (discussed in Chapter 5). We modeled the changes in extracted volume of each extraction pathway uniformly over the delta with the aim to investigate the potential future behavior of the aquifer system. In reality, we expect changes in future extraction to be much more location-specific and temporal variable, as they are influenced by a complex interaction between groundwater governance, legislation and law enforcement which can vary locally in the delta (Ha et al., 2018). Furthermore, also local differences in access to good quality surface water, socio-economical situation, technical capability and land-use practices, which, in turn, may be influenced by physical processes and feedback-mechanisms, e.g. ongoing subsidence increasing salinization, will determine future groundwater use. Our modelling approach paves the road to investigate more complex and realistic scenarios that include abovementioned factors.

Modeled extraction-induced subsidence is affected by uncertainties in the hydrogeological model and geotechnical parameterization (discussed in Chapter 5). The difference between modeled subsidence rates for the most and least conservative geotechnical parameterization becomes smaller towards the end of the modeling period (Fig. 6.6), which shows relative influence of initial overconsolidation ratio uncertainty becomes smaller with time. While geotechnical model uncertainty decreases, the influence on modeled subsidence of the groundwater extraction pathways increases. Even though locally uncertainties in modeled extraction-induced subsidence may be considerable, on the scale of the entire delta our results do provide a first indicative, process-based quantification on how the aquifer-system may respond to different groundwater extraction pathways in the 21th century.

6.4.2 Response of the aquifer system to future groundwater extraction

The evolution of the hydrogeological situation in the aquifer system of the Mekong delta will be determined by the extraction pathway followed. When the amount of groundwater extraction in the Mekong delta remains stable after 2020 (scenario M1) or continues to increase further into the future (scenario B1 and B2), aquifer system depletion will continue as well, resulting in continuous hydraulic head drop. In scenario B2 the average hydraulic head in the delta will drop almost to -50 m by the end of the century. Although we consider this as a most extreme scenario, drawdowns of this magnitude in confined aquifers are not uncommon and have been reported throughout the world, a.o. Bangkok (40-50 m; Phien-Wej et al., 2006), Mexico city (25 m, Ortiz-Zamora et al., 2010), San Joaquin Valley, USA (up to 45 m, Sneed et al., 2013), Shanghai (30 m, Ye et al., 2016) and Tokio (40 m, Sato et al., 2006). Moreover, also nearby Ho Chi Minh city drawdowns more than 30 meter have been measured between 1994 and 2015. Although drawdowns are site-specific and depend on many factors like aquifer size and storage capacity, groundwater extraction and recharge rate, physically the hydrogeological situation modeled in scenario B2 is possible.

The modeling results of the mitigation scenarios show the potential of the Mekong delta's aquifer system to recover from past and future hydraulic head drops when extraction is reduced or stopped. They also reveal the amount of present overexploitation. Currently, the amount of groundwater extraction in the delta more or less is twice the amount of recharge. A reduction of extractions by 50% will result in a stabilization of average hydraulic head at its present level (scenario M2), indicating that the extracted volume equals the amount of aquifer recharge by infiltration of precipitation, surface water and intrusion of sea water. Maximum recovery of the hydraulic heads in the Mekong delta's aquifer system is achieved when extractions are completely stopped (scenario M4). Under these optimal circumstances, it will take the aquifer system of the Mekong delta three times the amount of time (~60 years) to recover from the hydraulic head drop caused by groundwater extraction during the past ~20 years. This demonstrates the low recharge rate of the delta's aquifer system which is likely caused by the low permeable Holocene deposits at the delta surface (Chapter 5). This means that even after a complete extraction stop, past groundwater overexploitation will still have a continued effect on the hydrogeological situation of the aquifer system for many future decades.

Past hydraulic head declines in the aquifer system have triggered aquifer-system compaction which led to subsidence of the delta surface (Chapter 5). This process of aquifer-system compaction is sluggish and, once triggered, can continue for a long time. Combined with the slow recharge rate of the delta's aquifer system, this means that even when extractions are completely stopped (scenario M4), the delta will continue to subside, amounting to an average cumulative extraction-induced subsidence of 12 (4-18) cm by the end of the 21th century. This amount of subsidence is the inevitable inheritance of past groundwater overexploitation. In reality groundwater extraction will not stop after 2018, therefore the true amount of future extraction-induced subsidence will be higher. How much higher will be determined by the extraction pathway the delta will follow in the end.

6.4.3 Future of the Mekong delta

Consequences for delta elevation and relative sea level rise

Extraction-induced subsidence results in absolute elevation loss at the delta surface. The magnitude of the impact of elevation loss on a delta's future sustainability and the livelihood of its inhabitants depends, to a large extent, by its elevation above sea level. Fig. 6.8 shows the area of the Mekong delta plain that will experience a certain amount of cumulative subsidence for each extraction pathway in 2050 and 2100 and the average delta plain elevation of the Mekong delta (0.82 m a.m.s.l., Chapter 2). It becomes evident that if groundwater extraction continues to increase in the future (scenario B1 and B2), extraction-induced subsidence alone may cause large parts of the delta to lose all elevation a.m.s.l. before the end of the century. In case of groundwater extraction mitigation, cumulative extraction-induced subsidence will cause less but still considerable amounts of elevation loss. The minimum elevation loss that the delta will experience by the end of the century, as a result of inevitable aquifer-system compaction (scenario M4), equals ~15% (5%-22%) of the present average Mekong delta plain elevation above mean sea level.

Beside extraction-induced subsidence, the delta will also lose elevation a.m.s.l. as the sea level itself is rising. When we correct future delta elevation a.m.s.l. with projections of absolute sea-level rise (Church et al., 2013), the percentual area that loses on average all elevation above sea level by extraction-induced subsidence becomes much larger (Fig. 6.8). Only when future extraction-induced subsidence is mitigated by strongly reducing groundwater extraction and rates of absolute sea-level rise follow a moderate pathway, the majority of the delta may still be elevated above sea level by the end of the century.

Beside extraction-induced subsidence and absolute sea-level rise, relative sea-level rise in the delta is also determined by other subsidence processes, like tectonics, natural compaction of Holocene sediments, which can amount up to rates of several cm yr^{-1} in the Mekong delta (Chapter 3), drainage of surface water and loading by buildings and infrastructure (Chapter 4). Whether and when a certain part of the delta will fall below sea level is location-specific and dependent on local conditions of relative sea-level rise and surface elevation. On top of that, sedimentation of clastic and organic sediments on the delta surface is the natural mechanism of a delta to keep up with relative sea-level rise and can even result in elevation gain. This is the case in some areas along the Mekong delta's coastline, hosting pristine mangrove forests with abundant sediment availability (Lovelock et al., 2015), however not for other areas in the delta. The sediment supply to the Mekong delta is declining by upstream dam construction (Kummi et al., 2007; Kondolf et al., 2018) and sand mining (Anthony et al., 2015; Brunier et al., 2014) and improved flood control in the delta itself hampers the propagation of flood water and therefore decreases the delivery of new sediments even further (Dang et al., 2016; Tran et al., 2018). This general lack of sediment-deposition at the deltas surface makes it very unlikely that sedimentation in the delta can keep up with the high rates of relative sea-level rise, but recent policy plans to restore controlled seasonal flooding (Staveren et al., 2018) may again increase sedimentation and contribute to surface elevation gain in the future.

Time for mitigation, mitigation to create time

Given its lowly elevated topography, ongoing subsidence, absolute sea-level rise and decreased sedimentation, the Mekong delta is heading for a tipping point towards a 'collapsed' state (Renaud et al., 2013). As the delta is progressively losing elevation, the window for mitigation is closing rapidly. Although relative sea-level rise for the Mekong delta is caused by more than groundwater extraction-induced subsidence, it is, at present, the most dominant factor. When and whether or not

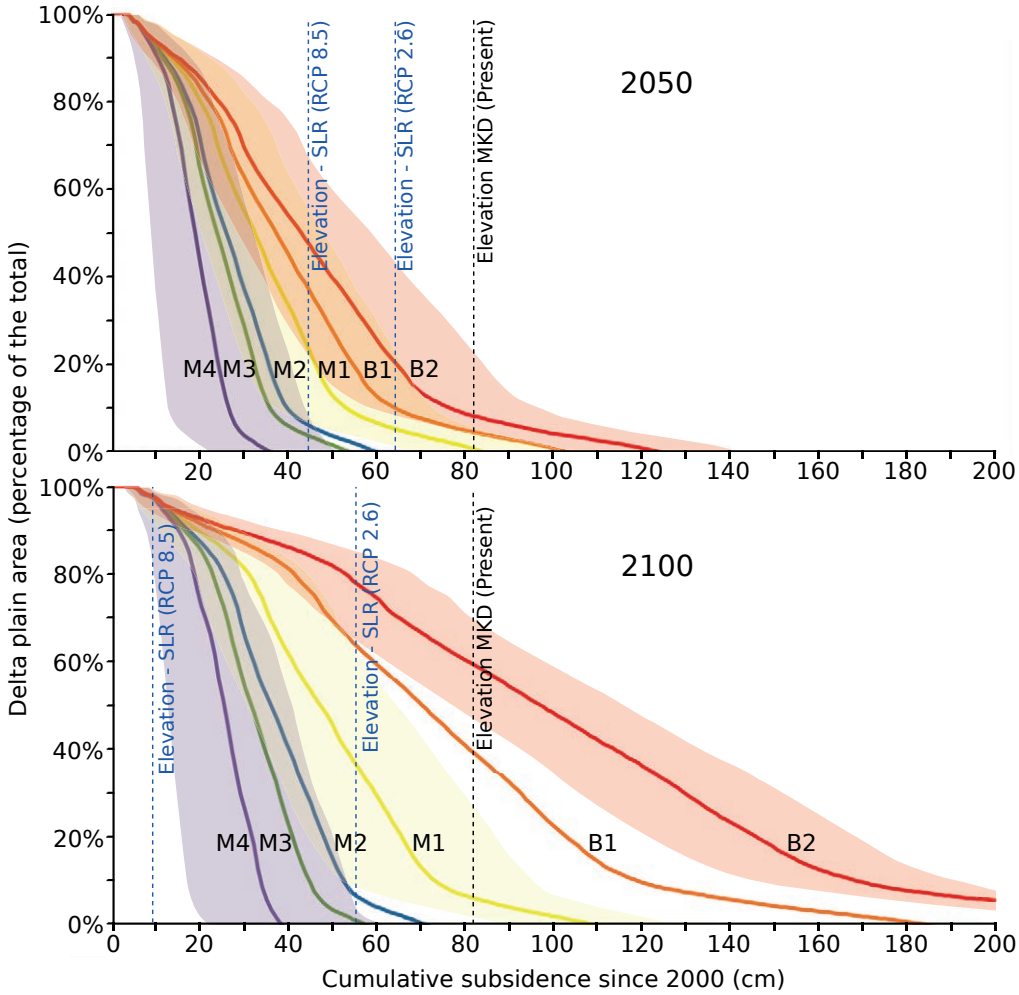

Figure 6.8 | *Area of the delta plain (in % of the total) that will experience a given amount of cumulative subsidence (in m) in the years 2050 and 2100 for different groundwater extraction pathways. The colored lines give the best estimate model results and colored band shows the uncertainty range based on the modeling results of the least and most conservative models for scenario M4, M1 and B2. Average Mekong delta (MKD) plain elevation is shown in cm by the black dotted line. The blue dotted lines give the average delta plain elevation corrected for absolute sea-level rise (SLR) projections by 2050 and 2100 based on RCP scenarios 2.6 and 8.5 (Church et al., 2013).*

mitigation strategies to reduce extraction-induced subsidence are successfully implemented, will determine, for a large extent, how long the delta will stay elevated above sea level. Although part of the future extraction-induced subsidence in inevitable (Scenario M4), a large part still can. Our results show the large potential of groundwater extraction mitigation to reduce the rate of relative sea level in the delta. Besides, a strong reduction in groundwater extraction would not only allow the aquifer system to recharge, and subsequently decrease aquifer system compaction, it would also reduce other water-related issues, such as salt water intrusion in the aquifer system (Renaud et

al., 2015; Smajgl et al., 2015). Although the best solution to reduce extraction-induced subsidence is to immediately stop all groundwater extractions as soon as possible, this is realistically not an option, as people in the delta rely on groundwater for their freshwater supply. Until alternative water sources are available, such as a piped water supply or high quality surface water, the use of groundwater will continue to meet the fresh water demand.

But also in the meantime, while investments are being made and infrastructure is being developed to provide an alternative fresh water supply, implementation of smart extraction strategies can already reduce extraction-induced subsidence while supplying fresh groundwater. For example, extractions can be relocated to areas that are less exploited, experience higher natural recharge rates (e.g. close to rivers) or are geologically less sensitive to subsidence. Additionally, extractions could be concentrated in higher elevated parts of the delta, by tolerating subsidence where it is relatively less harmful. However, such strategies only provide temporal solutions and cannot substitute the reduction in overall groundwater use. Furthermore, managed aquifer recharge (MAR) also provides opportunities to stimulate the aquifer system recharge, battling salt water intrusion and simultaneously creating strategic freshwater reserves in the subsurface.

All the above mentioned solutions will require fundamental changes in groundwater management and law enforcement, availability of alternative water sources, changes in agricultural practices less reliant on fresh water and investments in infrastructure to distribute fresh water over the delta. In November 2017, the Vietnamese Government issued 'resolution 120' which describes the ambition for a prosperous, sustainable and climate-resilient future of the Mekong delta, including the aspiration to end groundwater use by the year 2100. While these intentions provide an optimistic outlook for the delta, our results reveal that the horizon to implement the required changes and reduce groundwater extraction is far more limited. Any delay in implementation will cause the delta to lose more of its valuable elevation above sea level and increases the vulnerability of the delta and its 18 million inhabitants to flooding, storm surges, salinization and will increase the costs of flood protection to prevent permanent submersion of the delta.

Acknowledgements
We like to thank Mara Meggiorin (Deltares, University of Padova), Gualbert Oude Essink (Deltares, Utrecht University) and Hung Van Pham (Division of Water Resources Planning and Investigation in South Vietnam, Utrecht University) for collecting and processing the model input for the surface water network.

7 Synthesis

This research aimed to enhance the understanding of present and future subsidence in the Mekong delta in Vietnam, one of the largest deltas on Earth. The delta functions as an exemplar delta system for densely populated and urbanizing delta systems worldwide under increasing human and natural pressure. The main objective of this research was:

- *To understand and quantify the main natural and human-induced drivers and processes causing subsidence, and its impact on current and future surface elevation of the Vietnamese Mekong delta.*

To reach this objective, I combined data and methods from different scientific disciplines. I analyzed datasets of ground measurements of elevation and elevation change, and satellite-derived datasets on surface deformation, subsidence rate and land use. Furthermore, I developed hydrogeological and geotechnical numerical models based on geological, hydrological and geotechnical field observations and datasets. Field visits provided additional observational data that served as validation of remote sensing and modeling results.

7.1 Research questions and main conclusions

The results presented in the preceding chapters answered the following research questions:

1. *How high is the Mekong delta surface presently elevated above local mean sea level?*

The Topo DEM created using topographical elevation data revealed that, on average, the Mekong delta is elevated about ~80 cm above Vietnam's local Hon Dau geodetic datum, and its surface has an extremely low gradient (to ~6.7 mm km^{-1}). This is ~2 meters lower than previously concluded by global assessment studies based on the global, spaceborne STRM DEM. This mismatch is caused by not accounting for vertical inaccuracy of spaceborne elevation models, elevation differences between vertical datum used in global elevation models and local geodetic datum, and potential difference between zero datum and local MSL in Vietnam. This implies that the delta is more prone to relative sea-level rise: the combination between absolute sea-level rise and land subsidence. (**Chapter 2**).

2. *How much natural compaction occurs at present in the Holocene deposits of the Mekong delta following delta progradation?*

Natural compaction rates of young, Late Holocene deposits in the coastal zone go up to ~35 mm per year. These rates arise from natural sediment loading of the shallow subsurface during the development of the delta, which caused an ongoing pore-water pressure dissipation from the low-permeable, fine-grained sediments (**Chapter 3**).

3. *Is land subsidence related to land use in the Mekong delta? Is there a spatial correlation, and which are the causal mechanisms?*

Evaluation of InSAR-derived estimates of subsidence rate and land use revealed lowest subsidence rates in areas where natural delta vegetation has been preserved (6-7 mm yr^{-1} in marshland and wetland forest) but significantly higher rates in those areas where the delta has been used for agriculture (8-18 mm yr^{-1}), with highest subsidence rates (18-20 mm yr^{-1}) in urban areas. Anthropogenic land use and land-use changes enhance delta subsidence in the Mekong delta by increasing load at delta surface and altering the hydrogeological system. Likely, such relationships exist in other deltas as well (**Chapter 4**).

4. *How much land subsidence in the Mekong delta has been caused by increased groundwater extraction during the past decades?*

The steady increase in groundwater extraction during the past decades has altered the hydrogeological situation in Mekong delta's aquifer system from an almost undisturbed state with artesian conditions to a situation with ongoing aquifer depletion. Extraction-related subsidence following aquifer-system compaction in the Mekong delta started around three decades ago and has accelerated towards the present. Consequently, extraction-induced subsidence accelerated during the past decades, and the delta is presently experiencing its highest extraction-induced subsidence rates to date (**Chapter 5**). For 2018 the modeled delta-wide extraction-induced subsidence rate is 9 (5-13) mm yr^{-1} and cumulative subsidence since 1991 is 17 (9-33) cm. Locally, present-day rates go up to several cm yr^{-1} (**Chapter 6**).

5. *By how much may the Mekong delta subside in the coming century in response to groundwater extraction, and how much can be mitigated through groundwater extraction management?*

The amount and rate of extraction-induced subsidence in the future will depend on the annual amount of groundwater extraction and the rate of aquifer recharge. Model simulations for a range of groundwater extraction pathways revealed a bandwidth for future delta subsidence. The lower end projection is obtained under a complete stop of groundwater extraction after 2018, but still may result in a delta-wide subsidence by the end of the 21th century of 12 (4-18) cm. An upper estimate of 100 (86-110) cm is expected to result under conditions of continuously increasing groundwater extraction. In the latter situation delta-average rates of extraction subsidence will remain significantly higher throughout the 21th century than the rate of absolute sea-level rise. Reducing groundwater extraction indeed decreases delta-average subsidence rates; however, part of future extraction-induced subsidence is inevitable, as subsidence processes continuous to happen after a decrease in extraction, as demonstrated by the ongoing subsidence after completely stopping extractions (**Chapter 6**).

Three research questions remain to be answered:

6. *Which drivers and processes are predominantly causing present-day subsidence in the Mekong delta?*
7. *Can restoring natural deposition of Mekong river sediment compensate the elevation loss by subsidence of the delta?*
8. *When will certain parts of the delta fall below sea level in the coming century?*

In this synthesis these questions will be answered by building upon the insights and results from the previous chapters.

7.2 Individual contribution of subsidence drivers and processes in the Mekong delta

In this section the various drivers and processes that cause present-day subsidence are evaluated and their relative contribution to total subsidence is assessed to determine which are predominantly causing subsidence in the Mekong delta. After obtaining the quantitative estimates of the effects of natural compaction (Chapter 3) and extraction-induced subsidence (Chapter 5 and 6) in the delta, the next step in identifying possible additional drivers and mechanisms is to spatially 'unravel' the InSAR-derived subsidence rates that represent the total delta subsidence (Erban et al. 2014). The difference between the InSAR-derived rates and those resulting from natural compaction and groundwater extraction should reveal such other drivers or mechanisms.

This analysis requires delta-wide estimates of subsidence rate matching the InSAR-measurement period (2006-2010). These were obtained for extraction-induced subsidence (Chapter 2), but natural compaction was only calculated for a single transect (Chapter 3). Therefore, these results were spatially extrapolated to a first delta-wide estimate of natural compaction of Holocene sediments. Furthermore, the InSAR-derived subsidence estimates by Erban et al. (2014) for the years 2006-2010 were resampled from their original resolution (~57 x 57 m) to match the resolution of the hydrogeological model (1 x 1 km). Subsequently, the resulting delta-wide subsidence estimates were subtracted from the InSAR data to detect possible locations with additional subsidence not due to the two main drivers.

7.2.1 Delta-wide natural compaction of Holocene clays

A Mekong delta-wide estimate of present natural compaction of Holocene clays following their loading history by accumulating sediments during Holocene delta evolution was created using the model results from the 2D transect in Chapter 3. The 100-yr-averaged (21th century) natural compaction rate of the 18 m Holocene clay cover in the transect was calculated an taken as best-estimate for present annual natural compaction rates of this clay cover (Chapter 3, Scenario B). With these, a delta-wide map of natural compaction in the Mekong delta was created, in combination with Holocene coastline progradation estimates that quantify the age of the delta surface (Fig 3.1; Nguyen et al., 2000; Ta et al., 2002; Tamura et al., 2012), for the situation in which the entire Holocene delta existed of a homogeneous clay layer of 18 m thickness (Fig 7.1A). By dividing the natural compaction rates by 18 m, the average natural compaction per meter Holocene clay in the Mekong delta was then obtained. The actual thickness of Holocene fine-grained sediments was determined based on 524 geological and 719 lithological borehole descriptions from sediment cores in the Mekong delta (Van Laarhoven, 2016; data provided by the DWRPIS). These datasets were used to determine 1) the boundary between Holocene and much older Pleistocene deposits, and 2) the cumulative thickness of the lithological classes: 'clay', 'very soft clay' and 'soft silty clay' (excluding the classes: 'silty sand', 'silty clay' and 'sand'). This resulted in a map of the total clay thickness in the soft Holocene sediments of the delta (Fig 7.1B). By multiplying the average natural compaction rate of 1 m clay with the actual Holocene clay thickness, the first map of estimates on the annual natural compaction rate of Holocene clays based on their depositional age was created for the entire Mekong delta (Fig. 7.1C).

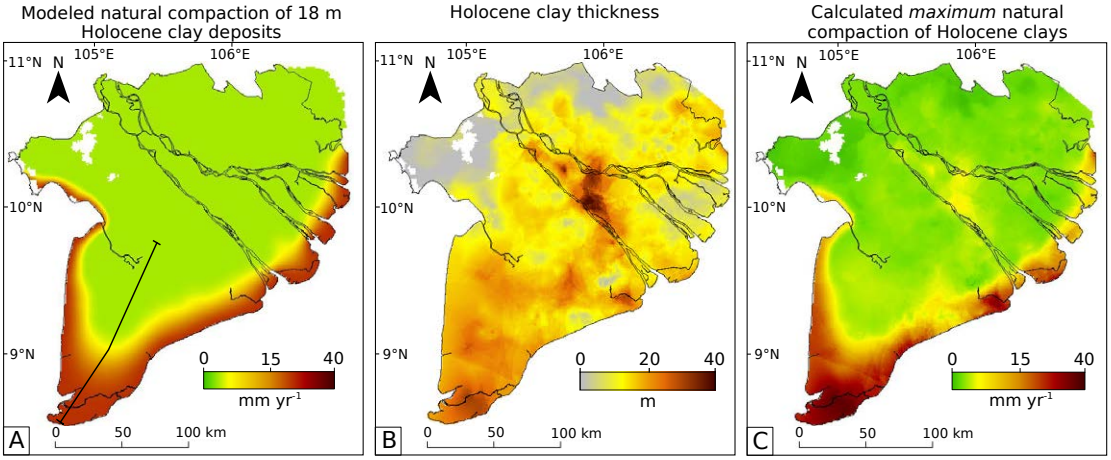

Fig. 7.1 | *Estimation of delta-wide natural compaction of Holocene clays as a function of delta evolution and delayed overpressure dissipation. A) Delta-wide extrapolation of 100-yrs average modeled natural compaction of an 18 meter thick clay deposit, based on the age of Holocene delta progradation (Figure 3.6, scenario B) and the results of a 2D numerical model of the transect shown by the black line (Chapter 3). B) Total thickness of Holocene soft clay deposits (lithological classes: 'clay', 'very soft clay' and 'soft silty clay') based on 524 geological and 719 lithological borehole descriptions (Van Laarhoven, 2016). C) Estimation of cumulative natural compaction based on average calculated natural compaction rate per m Holocene clay (A) and actual Holocene clay thickness (B). The estimates show maximum values of potential natural compaction. Calculated average delta-wide natural compaction rate is 4.4 mm yr^{-1}.*

The results of this delta-wide estimate of natural compaction of Holocene clays should be regarded with some reservations. A main reason is that the 'interpolation' of natural compaction rates is based on model simulations for homogeneous clay deposits. This results in relatively high overpressures in comparison with a situation in which sandy layers alternate with clay layers, as excess pore-water dissipates much faster in coarser-grained deposits, decreasing present-day remaining overpressure. Indeed, the Holocene deposits in the majority of the Mekong delta comprise several sequences of fine-grained (silt and clay) and coarser grained (sand and gravel) deposits. Consequently, the resulting delta-wide subsidence rates due to natural compaction of Holocene deposits given in Fig. 7.1C should be considered as an educated estimate of the maximum potential natural compaction rate that may be expected in the Mekong delta. The spatial pattern of higher shallow compaction rates near the coast with decreasing rates in landward direction corresponds to observations in both the Mississippi (Meckel et al., 2007; Törnqvist et al., 2008; Jankowski et al., 2017) and the Po delta (Teatini et al., 2011; Tosi et al., 2016). In the Mekong delta, this spatial patterns is also confirmed by high SET measurements of shallow compaction at the coast (Lovelock et al., 2015) and lower rates for SET sites with a more inland position: 5.5 - 7.8 mm yr^{-1} (Nguyen et al., 2015).

7.2.2 Explaining InSAR-derived subsidence estimates

In this section, the InSAR-derived subsidence estimates by Erban et al. (2014) are unraveled into different driving mechanisms and processes, using the delta-wide process-based quantitative estimates of natural compaction and extraction-induced subsidence (Fig. 7.2).

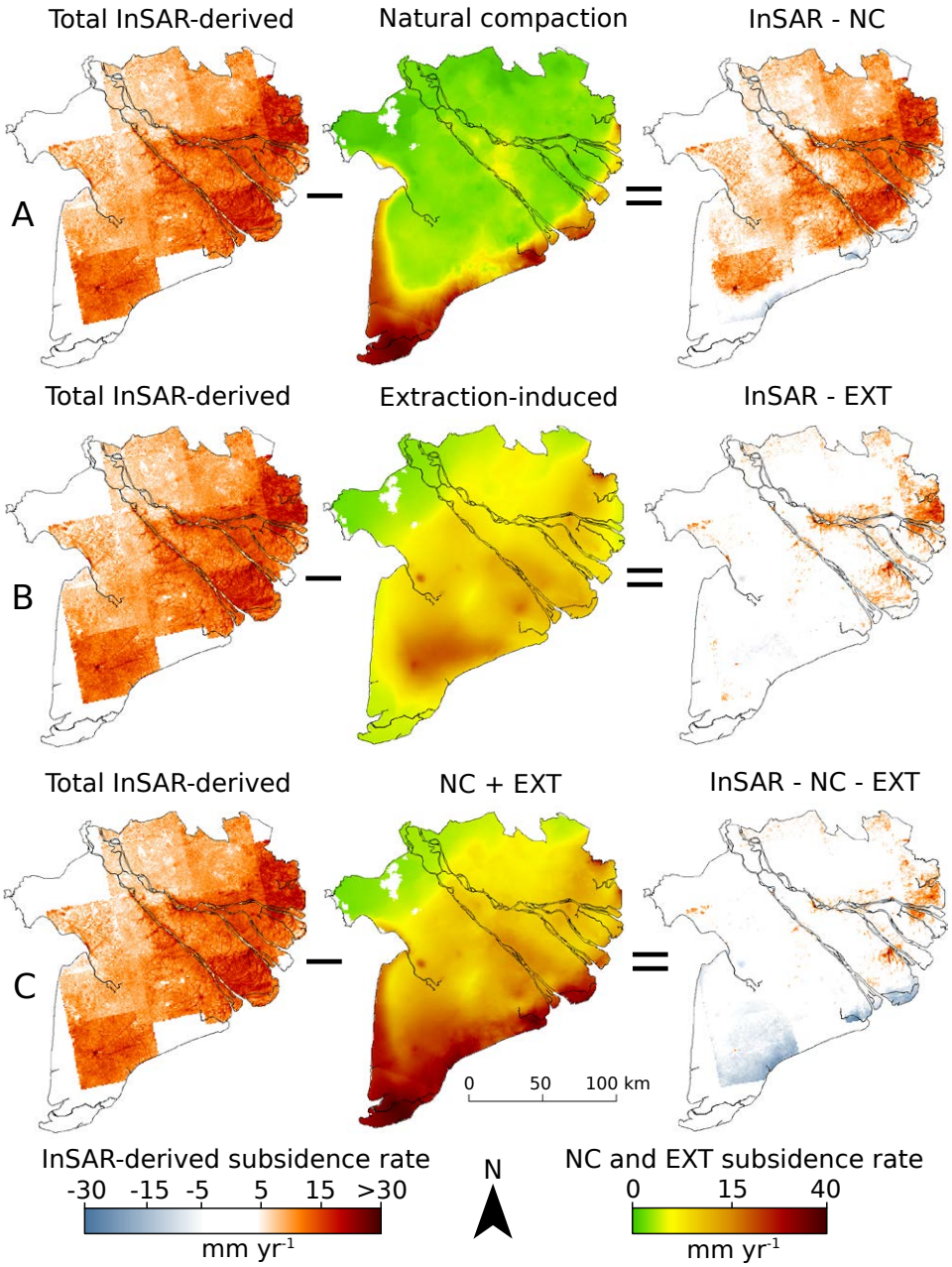

Fig. 7.2 | *Unraveling InSAR-derived estimates of subsidence rate in the Mekong delta using modeled quantifications of maximum natural compaction (NC) of Holocene clays and groundwater extraction-induced (EXT) subsidence rates. The InSAR-derived subsidence estimates are based on the raster dataset of Erban et al. (2014) and upscaled (mean value) from their original resolution of ~57x57 m to 1x1 km to match the resolution of the subsidence quantifications. The residuals of the InSAR-derived subsidence estimates reveal the spatial patterns of unexplained InSAR observations. The minimal uncertainty associated with the InSAR-derived estimates (5 mm) is made white. Individually, natural compaction may explain up to 29% of the total subsidence rate and extract-induced subsidence up to 73%. Combined NC and EXT explain 84% of the total subsidence signal.*

Contribution of natural compaction of Holocene clays to total subsidence

The InSAR-residuals after subtraction of the estimated (maximum) natural compaction of Holocene clays clearly show that in a large part of the delta, the InSAR-derived subsidence estimates exceed the amount of potential natural compaction. Total natural compaction can explain up to 29% of the total delta-wide InSAR-derived subsidence estimates for the Mekong delta (71% of the InSAR-derived subsidence remain after substracting natural compaction (Fig. 7.2A)). The remaining part of the subsidence in the delta must therefore be caused by other mechanisms than natural compaction, which confirms the conclusion that human activities in the delta cause subsidence rates exceeding rates of natural compaction (Chapter 4). In the coastal zone, natural compaction of Holocene clays may explain the entire InSAR signal. Moreover, some areas show negative residuals (Fig. 7.2A, in blue), which means that the amount of estimated natural compaction exceeds the amount of the InSAR estimated subsidence. This can have two reasons: 1) as the estimated amount of natural compaction of Holocene clays is a maximum potential rate, the present-day amount of natural compaction may actually be less, 2) the InSAR-derived subsidence rates underestimate the amount of natural compaction, as they are partially derived from reflectors that are founded well below the delta surface and do not register shallow compaction. In the coastal zone, with thick layers of young, Holocene fine-grained material, shallow compaction as a result of natural compaction can be the dominant cause of local subsidence in the delta. More inland, natural compaction may partly contribute to the total subsidence signal, but cannot explain the bulk of the InSAR-derived signal.

Contribution of groundwater extraction to total subsidence

Subtracting the modeled groundwater extraction-induced subsidence of the best estimate model for 2006-2010 from the InSAR-derived signal shows relatively few and small residuals (Fig. 7.2B). Modeled extraction-induced subsidence can explain up to 73% of the total InSAR-derived signal (27% of the InSAR-derived subsidence are unexplained after substracting extraction-induced subsidence). This indicates that groundwater extraction indeed is a major driver of observed contemporary delta subsidence, underscoring similar presumptions made in previous studies (Erban et al., 2013; 2014). Nevertheless, there are areas, mainly in the central and the western part of the delta, where the total InSAR-derived signal could not be entirely explained by the modeled extraction-induced subsidence. As there are no areas in the delta where the InSAR residuals become negative, there is no evidence that the best estimate extraction-induced subsidence quantifications overestimate the total amount of subsidence in a location.

Contribution of other subsidence drivers: anthropogenic loading and phreatic water table lowering

When maximal natural compaction of Holocene clays and extraction-induced subsidence are both subtracted from the InSAR-derived subsidence signal, 84% of the total InSAR-derived signal can be explained. Leaving 16% of the InSAR signal unexplained and residuals are located in specific areas in the delta (Fig. 7.2C). Apart from being the product of InSAR-related uncertainties or potential errors in allocated stable points (assumed to have zero vertical movement) to transform relative deformation values in individuals InSAR image tiles to absolute deformation values, these residuals show locations where the combined effect of maximal natural compaction and best-estimate extraction-induced subsidence are not enough to explain the observed subsidence estimates. Thus, should be the result of additional subsidence drivers and mechanisms.

The remaining subsidence rates clearly resemble a local signature which seems to be associated with specific land use (Chapter 4). For example, quite some of the InSAR residuals with larger subsidence rates are located in cities (Fig. 7.3). The higher subsidence rates in these cities may be due to the following local drivers: 1) loading of the surface by buildings and infrastructure, 2) lowering of the phreatic water table. Beside these, it is also possible that in these cities groundwater extraction is more intensive than assumed in the hydrogeological model simulations. In rural areas in the central part of the delta near the main Mekong river branches InSAR-derived subsidence rates are also remarkably large. These areas mainly host orchards intermingled with open urban areas (Land-use maps from 2006-2009, Chapter 4). Here, enhanced shallow subsoil compaction may occur as a result of phreatic water table lowering, possibly in combination with larger – undocumented - groundwater extraction. The residuals located in the area in the coastal zone towards to northeast may be the result of recent urbanization of the previously agriculture area dominated by rice farming (Fig. 7.3). The land-use change analysis in Chapter 4 clearly shows that such land-use changes typically result in a significant increase in subsidence rates, both by accelerating shallow compaction and increased aquifer-system compaction following the intensifications of human activities.

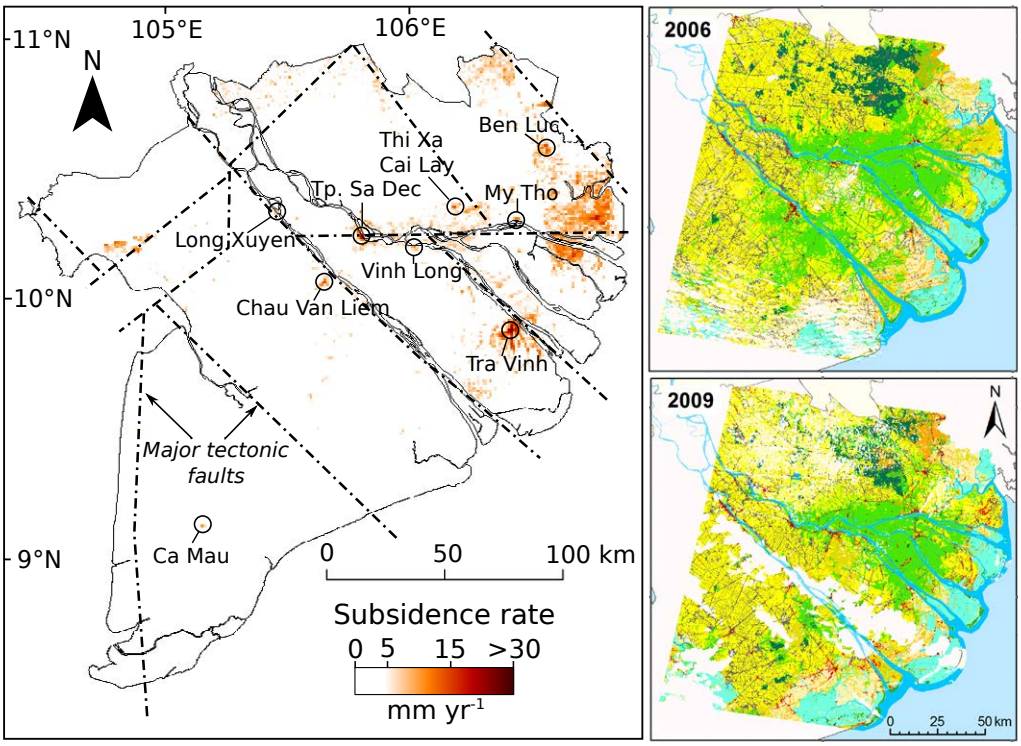

Fig. 7.3 | *InSAR-derived subsidence estimates unexplainable by estimated maximum natural compaction of Holocene clays and modeled groundwater extraction-induced (best-estimate model) and land-use maps of 2006 and 2009. Major tectonic faults in the Mekong delta are indicated by the dot-dash line (Geological survey of Vietnam; Do et al., 2015). Land-use map classes: orchards in light green, Rice agriculture in yellow, urban areas in red. For full legend see Fig. 4.2.*

The residuals of the InSAR-derived signal do not show local spatial trends corresponding with major tectonic faults in the Mekong delta (Fig. 7.3). Apparently, the inferred subsidence signal does not reflect neotectonic movement in the deeper subsurface. This does not rule out the existence of neotectonics, but it means that the rates are not high enough to be registered by InSAR, which suggests that they are at least smaller than the minimal InSAR measurement error (5 mm yr^{-1}, Erban et al., 2013).

Based on the unraveling of the InSAR-derived signal, there are two dominant subsidence mechanisms that cause subsidence and subsequent elevation loss at the scale of the entire delta: 1) compaction of shallow Holocene sediments by natural sediment loading (Chapter 3), enhanced by human loading and drainage (Chapter 4), and 2) aquifer-system compaction following delta-wide hydraulic head drawdowns as a result of groundwater overexploitation from deeper subsurface (Chapter 5). Locally, other human-induced drivers, such as loading, and increased drainage or additional groundwater exploitation, cause additional subsidence. Though these last mechanisms may locally result in damage to infrastructure and increase nuasance floodings in urban areas, they do not have a large impact on the overall elevation of the delta plain. Tectonics, natural compaction of pre-Holocene deposits and isotatic adjustment do not seem to play a major role in the present subsidence rates of the Mekong delta, which agrees with suggestions of other studies in the delta (Hanebuth et al., 2011; Nguyen et al., 2000).

7.3 The impact of subsidence on the future elevation of the Mekong delta

Subsidence will cause accelerating rates of relative sea-level rise in the Mekong delta. The impacts of relative sea-level rise on the livability and sustainability of the delta is determined by its future elevation to local sea level, which is besides subsidence also determined by sediment accretion, resulting in elevation gain. In this section, first the sedimentation potential of the Mekong river is compared to present rates of elevation loss. Secondly, the impact of future subsidence on the elevation of the Mekong delta in the 21th century is assessed using projections of relative sea-level rise (combined effect of subsidence and absolute sea-level rise) and potential elevation gain through sedimentation.

7.3.1 Can restoring sedimentation counterbalance accelerated relative sea-level rise?

Sediment starvation is widely recognized as the major cause of delta drowning (Syvitski et al., 2009; Tessler et al., 2017) and restoring sedimentation as measure to cope with future relative sea-level rise (Giosan et al., 2014). Recently, in the Mekong delta, the local delta policy has the tendency of reversing hydro-engineering developments to a more natural delta system and allowing seasonal flooding to increase the amount of sediment deposition on the delta plain to counterbalance subsidence and bring new natural nutrients to the system (Van Staveren et al., 2018). A lot of effort by both the scientific and the delta management community is put into quantifying the exact amount of suspended sediment in the Mekong river and re-allowing flood water onto the delta plain to enable sedimentation. However, as almost the entire Mekong delta is presently experiencing accelerated relative sea-level rise (this thesis), it is the question whether restoring sedimentation can actually counterbalance this. To determine whether accretion of Mekong river sediments has the potential to compensate the amount of elevation loss that the Mekong delta is experiencing, a new sediment balance of the Mekong delta is calculated based on the results from this thesis.

Many studies focused on the amount of sediment transported by the Mekong River and impact of upstream dam construction (a.o. Kummi and Varis, 2007; Kondolf et al., 2014, 2018; Manh et al., 2015; Allison et al., 2017,) and decreased hurricane activity (Darby et al., 2016). Beside decreases in suspended sediment in the Mekong River, the construction of an increasingly effective embankment system has resulted in a decrease in seasonal flooding (Triet et al., 2017; Tran et al., 2018), in turn decreasing the sediment delivery from the river to the delta plain. Yet, only few studies determined present-day amount of sedimentation on the delta plain and reported rates show large variations across the delta. Hung et al., 2014 found an average annual sedimentation of ~6 mm on Mekong delta floodplain after seasonal flooding events in an upstream area, while another delta-wide study, measuring delta plain sediment accretion during the flood season of 2013-2014, found much lower accretion rates, for many places less than 1 mm yr^{-1}, throughout the Mekong delta (Do et al., 2015).

At pristine mangrove forests along the coast, SET monitoring sites using marker horizons registered high sedimentation rates (36.8 +/- 3.1 mm yr^{-1} for Dat Mui at the southern tip of Ca Mau and 67.8 +/- 6.6 mm yr^{-1} near the mouth of the Bessac river). These rates show the high sediment accretion in mangroves forests where enough sediment is available and which is crucial for the mangroves to sustain elevated above sea level given the high rates of shallow compaction in these areas. However, such high sedimentation rates are not representative for the rest of the Mekong delta plain. Presumably a portion of the sediment that is deposited in the pristine mangrove forests consists of reworked sediments from other parts along the coast that are currently suffering high rates of coastal erosion. In recent years coastline retreats up to 100 m yr^{-1} have occurred in the Mekong delta (Anthony et al., 2015; Li et al., 2017).

Despite the attention given to re-allowing sedimentation through flooding, budget calculations to determine whether there is actually sufficient sediment available in the system to counterbalance the present-day accelerated rates of relative sea-level rise (including the effect of accelerated subsidence) have yet to be made, with the exception of Schmitt et al. (2017). They used data from literature and estimates for a first quantification, suggesting a large sediment deficit for the Mekong delta. The results from the previous chapters of this thesis enable to build the present-day sediment balance for the Mekong delta using the process-based numerical model quantifications of extraction-induced subsidence and natural compaction, in combination with quantifications of suspended sediment amounts in the Mekong river and rates of absolute sea-level rise from literature (Fig. 7.4).

The range of total amount of suspended sediment of the Mekong river is based on quantifications by Milliman & Meade (1983); Ta et al., (2002); Liu et al., (2013); Manh et al. (2014); Darby et al., (2016); Wang et al., (2011); Kummi & Varis (2007); Lu et al (2014). The amount of accommodation space created annually by extraction-induced subsidence is calculated for the least, best and most conservative model estimates for 2015 (Chapter 5) using the area of the Mekong delta (38.8 x 103 km^2) and the average weight of Mekong delta sediment (1.2 ton m-3, Xue et al., 2010). Maximum natural compaction is calculated using the quantifications in Fig. 7.1C. Potential organic sediment production is estimated by Schmitt et al. (2017) and the range of local absolute sea-level rise is based on global estimates of sea-level rise (Church et al., 2013) and local quantifications (Hak et al., 2016; Tagaki et al., 2016).

The sediment balance of the Mekong delta clearly reveals the present-day sediment deficit of this mega delta (Fig. 7.4). In a pristine natural state, the delta may have been able to compensate for the amount of elevation loss due to natural compaction or keep up with moderate projections of sea-level rise through the input of suspended river sediment and organic production. However, with the present-day accelerating rates of extraction-induced subsidence in the delta there is far too little sediment available to counterbalance the accelerating elevation loss of the delta plain. In the best-case scenario, with maximal sedimentation, half the amount of maximum natural compaction, and minimal extraction-induced subsidence and sea-level rise, 35% of total elevation loss could potentially be compensated through sedimentation. In the worst-case scenario however, sedimentation can potentially only compensate for 6% of the total elevation loss. Consequently, the Mekong delta will inevitably experience considerable relative sea-level rise in the coming century, as there is simply not enough sediment available in the system.

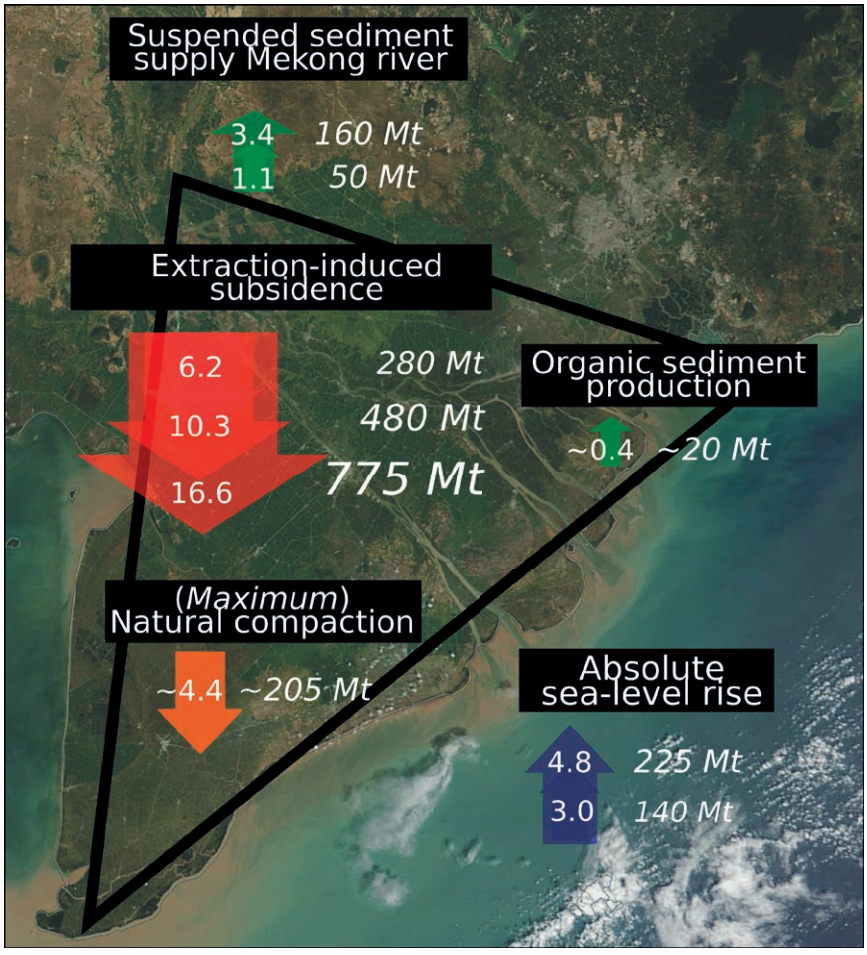

Fig. 7.4 | *Sediment balance of the Mekong delta. Arrows show potential annual delta-averaged elevation change in mm yr^{-1} that equal the amount of sediment (in Mt yr^{-1})(Italicized).*

The sediment balance also shows that extraction-induced subsidence in the Mekong delta is the dominant factor to determine future relative sea-level rise in the coming century. The fact that subsidence as a result of local processes within a delta is the main driver of relative sea-level is often underexposed in well-known global studies that assess whether deltas can cope with absolute sea-level rise by comparing it to sediment supply, and reduction in it through dam construction (e.g. Syvitski et al., 2009; Giosan et al., 2014, Tessler et al., 2017). One reason for this is the difficulty to quantify local rates of subsidence for a delta – let alone for deltas on a global scale - without extensive data collection and process-based analyses as done in this thesis.

7.3.2 Delta elevation above sea level is time

Elevation of a delta above sea level, in combination with rates of relative sea-level rise, is a measure of how much time is left for implementation of mitigation and adaptation measures before a delta's surface falls below sea level. In case of the Mekong delta, the lower southern part of the delta (Chapter 2) might have least time left, depending on local rates of relative sea-level rise. The results of the previous chapters and this synthesis enable establishing a detailed assessment of the timing when certain areas of the Mekong will fall below sea level, and whether this already might happen within this century. This is done as follows: For this evaluation we took the Topo DEM described in Chapter 2, which we consider the best available representation of the actual elevation of the Mekong delta above mean sea level, with we assumed zero level in the Topo DEM to represent current mean sea level. The Topo DEM was rescaled to 1x1 km to match the resolution of the hydrogeological model. The absolute sea-level rise varies along with the RCP scenarios (Representative Concentration Pathway, Moss et al., 2010); the median of the mid-range RCP 4.5 projects an absolute sea-level rise of 53 cm by the end of this century (Jevrejeva et al., 2016; Jackson and Jevrejeva, 2016), and is used here. For extraction-induced subsidence, different scenarios can be identified (Chapter 6), from which we here consider three possible realistic scenarios of future groundwater extraction: 1) moderate extraction increase (B1), 2) stabilized groundwater extraction (M1) and 3) strongly reduced groundwater extraction (M3). The amount of delta-average estimated, maximum natural compaction of Holocene deposits (4.4 mm yr^{-1}) almost equals the maximum amount of possible fluvial sedimentation (~160 Mt yr^{-1} = 3.4 mm yr^{-1}) and autogenic organic material production in the delta (~20 Mt yr^{-1} = 0.4 mm yr^{-1}). Hence, in an 'ideal', fully natural situation, sedimentation may counterbalance natural compaction. Therefore, two assessments are made: 1) a best-case sedimentation scenario in which all natural compaction is assumed to be completely compensated through sedimentation, and 2) a sediment-depleted scenario in which the Mekong delta is fully embanked and there is no new sediment deposition to compensate for natural compaction. In this latter scenario, natural compaction also contributes to relative sea-level rise in the 21th century.

The results of these assessments (Fig. 7.5 and 7.6) reveal that large parts of the Mekong delta will inevitably fall below sea level during the coming century, regardless whether or not there is sedimentation to compensate for natural compaction, and even under a scenario of strong reduction of groundwater extraction. In particular the low-lying SW part of the delta falls below sea level already in the course of this century, regardless the considered scenario. The extent of those parts of the delta that remain above sea level by the end of the century varies considerably among the different groundwater extraction scenarios, and whether sedimentation is able to counterbalance part of the natural compaction.

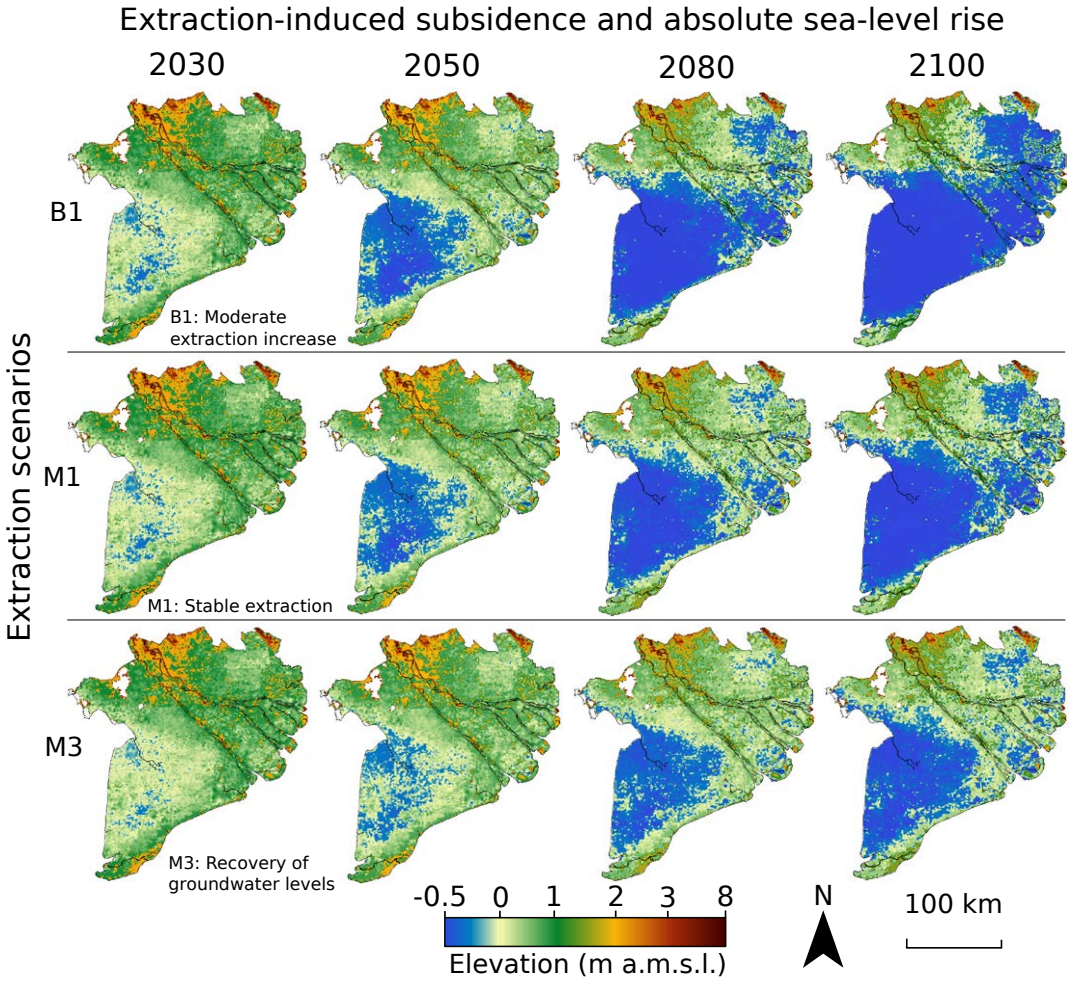

Fig. 7.5 *| Projections of future elevation assuming sedimentation counterbalances natural compaction of Holocene sediments. Elevation is in meter above mean sea-level with extraction-induced subsidence following different extraction scenarios and absolute sea-level rise according to the mid-range projections of SLR (median) of RCP 4.5. Subsidence as a result of natural compaction is assumed to be compensated by sedimentation. Blueish areas are below projected local mean sea level.*

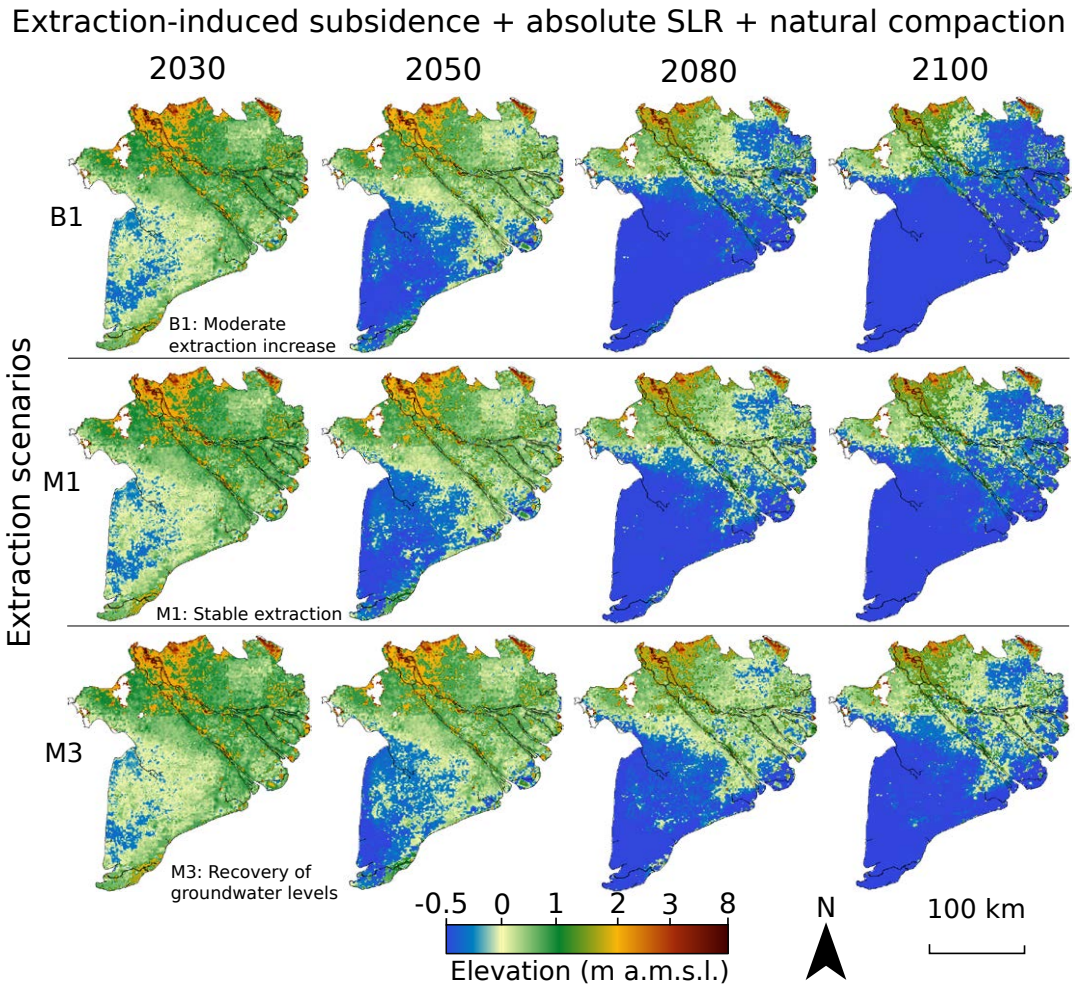

***Fig. 7.6** | Projections of future elevation without sedimentation. Elevation is in meter above mean sea-level with extraction-induced subsidence following different extraction scenarios, subsidence following natural compaction of Holocene sediments and absolute sea-level rise according to the mid-range projections of SLR (median) of RCP 4.5. Blueish areas are below projected local mean sea level.*

7.4 Future of the Mekong delta

With this thesis, I have built a knowledge base on land subsidence in the Mekong delta by advancing our understanding from measurements to process-based predictions and impact assessments. The results of this thesis provide the first quantitative estimates of present and potential future delta subsidence and relative sea-level rise for the mega Mekong delta. In spite of the uncertainties, the trend for the Mekong delta is clear: already in the coming century most of the low-lying delta plain will inevitably sink below sea level. The new insights from this thesis may serve to 1) increase awareness on the urgency of the topic and 2) catalyze information-based decision-making. They imply that drastic delta management decisions lie ahead in the near future, both to mitigate further land subsidence, and to find adaptation strategies to prepare the delta and its inhabitants for the impacts of subsidence. This step requires willingness and cooperation of national and local governments, NGOs such as the Mekong River Committee, loan agencies such as the World Bank and local delta residents.

Mitigation and adaptation challenges

The question is not whether or not there will be relative sea-level rise in the Mekong delta, but how fast it will happen. This thesis identifies groundwater extraction as the main - anthropogenic - driver of present-day accelerated subsidence in the Mekong delta. Conversely, changes in future human action might decrease subsidence rates. The rate of relative sea-level rise in the coming century will be determined by the effectiveness of mitigation measures to reduce groundwater extraction and to allow recharging of the aquifer system. This will not just be determined by the willingness to reduce groundwater use, but more so by the availability of alternative fresh water sources to meet the freshwater demand. Providing alternative sources for fresh and good quality water will be a challenge, especially for provinces located further away from the Mekong river branches. Smart extraction strategies, e.g. relocating extraction to areas that are higher elevated or less sensitive to subside may decrease the impact of extraction-induced subsidence. This requires detailed knowledge on local subsurface architecture and groundwater flow and recharge. Managed aquifer recharge may help to speed up the recovery of the hydraulic heads in the aquifer system and to mitigate further extraction-induced subsidence. Another mitigation measure to reduce relative sea-level rise in the delta is to re-enable sedimentation on the delta plain by allowing seasonal flooding; however, this can only compensate the loss in relative elevation to a certain extent.

Traditionally, the construction of embankments has been the strategy in the Mekong delta to adapt to sea-level rise and mitigate its effects such as increased flood risk and salinity intrusion. However, as the Mekong delta is a mega delta, it is physically and certainly economically almost impossible to protect the entire delta using hard measures (e.g. by building a sea dyke along the present coastline). Specifically, when considering the high natural compaction rates near the coast (Chapter 3). Moreover, the construction of a sea dyke (which is in places already has been completed) will cut off the marine sediment supply to the coastal hinterland, blocking sediments that are highly needed to compensate for the high compaction rates. The effect of a sea dyke is more or less shown by the assessments of Fig. 7.5 and 7.6. Fig. 7.5 shows the future of the delta with a natural coast (e.g. mangroves) allowing sedimentation, while Fig. 7.6 demonstrates the situation in case the whole Mekong delta coast would be embanked and sedimentation has ceased. Besides the above mention effects, when constructed, a sea dyke will also experience high rates of subsidence due to shallow compaction of underlying sediments, enhanced further by the weight of the construction. This will considerably shorten the dyke's service life and increase maintenance costs.

Scientific research recommends a shift from only 'hard' adaptation measures, such as embankments, to a combination with 'soft' adaptation measures like land-use change (Smajgl et al., 2015; Wesselink et al., 2016). Adaptation measures in the increasingly saline coastal zone such as a land-use transition to shrimp farms at the expense of rice agriculture and mangrove forest have already been implemented during the past several decades (Wilder & Phuong, 2002; Käkönen, 2008; Renaud & Kuenzer 2012; Chapter 4). Although this is an effective way to maintain agricultural production and to provide for peoples livelihood under salinization, the fresh (or brackish) groundwater use to maintain the optimal salinity levels in the shrimp ponds is notorious for creating accelerated rates of land subsidence (e.g. Higgins et al., 2013; Chapter 5). While in the Mekong delta groundwater use for rice irrigation is strictly prohibited, this is officially also the case for shrimp ponds, but it is not enforced and (unofficially) tolerated, in the absence of alternative fresh-water sources. As a result, this adaptation measure may lead to increased relative sea-level rise and accelerate degradation of the agricultural potential of the delta. Recent research has shown that mixed shrimp-mangrove farming systems provide a much more sustainable way of cultivating shrimps in a saline coastal zone. Besides maintaining a dynamic coastal zone of natural mangrove vegetation, rather than a 'hard' sea dyke, the production yields of the shrimps can be very profitable (Truong and Do, 2018).

As the Mekong delta has always been a low-lying delta affected by seasonal flooding, people living in the delta - especially in the rural parts in the south - have learnt to cope with high water levels and seasonal inundation of the delta plain. As a result, when looking at the present day self-organized, spatial planning in the low-lying parts of the delta, people build their houses on higher locations, such as natural ridges or along man-made dykes and road embankments. New houses, sometimes built next to old ones that were abandoned as they have sunk below local water level and are now permanently inundated, are constructed on stilts, sometimes even meters above the delta surface. Cities in the delta have much less flexibility compared to the rural communities to make infrastructure and buildings flood-proof. Therefore, cities have to rely much more on the development of hydro-engineering infrastructure (hard measures) for flood protection.

Elevation as exploitable natural resource

Elevation above sea level should be considered a natural resource, which can be exploited. The lower the Mekong delta surface is elevated above sea level, the more it is vulnerable to natural hazards and the more expensive it is to inhabit and exploit the area economically. As the delta increasingly loses elevation through accelerated subsidence caused by human intervention in the natural system, the natural resource 'elevation' is progressively and exhaustively exploited. This concept also applies to other coastal-deltaic systems in the world that lose elevation due to human-induced subsidence. In my opinion this view on elevation should become part of the cost-benefits analyses included in delta planning. For example, the use of groundwater is often considered as a 'free' natural resource, but when overexploited, the price for this water is paid by loss of another resource, which is the area's elevation above sea level. Expressing subsidence in a delta as a result of groundwater extraction not in units of length, but for example in percentage of delta elevation loss to mean sea level (Fig. 6.8) makes this relation explicit. Changing the view on delta elevation and valuating it as a precious natural resource which is exploitable, will help to integrate the effects of human-induced subsidence and relative sea-level rise in strategic delta planning. As a result, exploiting delta elevation by extraction-induced subsidence becomes a conscious choice rather than an unfortunate and uncontrolled effect of delta development.

Outlook for the Mekong delta

When compared to other deltas in the world, the Mekong delta is in a critical position due to its low elevation and accelerating rate of relative sea-level rise. The best chance for the Mekong delta to sustain itself in the future is through mitigation measures to reduce groundwater use, stimulate groundwater recharge, re-enable sedimentation on the delta plain, and to implement a smart combination of both hard and soft adaptive measures. The political preparedness to act is there, as demonstrated by the adoption of the Mekong delta plan vision (MKD, 2013) and in September 2017, the Vietnamese government issued 'Resolution 120', titled: *On sustainable and climate-resilient development of the Mekong delta*. Research in this thesis (Chapter 5) was used to inform government officials that were responsible for drafting this resolution. This resolution explicitly mentions the negative effects of land subsidence and groundwater level decline, and demonstrates the ambition to reduce and stop groundwater use in the future.

7.5 Research recommendations

This research presented in this thesis helped to increase our understanding on subsidence in the Mekong delta. However, there are still considerable uncertainties in the research results connected to e.g. delta elevation, subsidence monitoring, geological understanding and geotechnical behavior of the subsurface, and delta plain sedimentation. Some of the most important recommendations to improve subsidence research in the Mekong delta and in likewise deltas elsewhere in the world are listed below.

1. *Delta elevation*. The relative impact of delta subsidence is determined by future subsidence rates in combination with the delta's present elevation above local mean sea level. As deltas are low-lying and flat landforms, accurate quantitative data of land surface elevation above local mean sea level is crucial. Data errors of only a few decimeters can already strongly affect sea-level rise assessments. As this thesis shows, our global spaceborne DEMs do not have sufficiently high vertical accuracy, and local geodetic datum referenced to local sea level can deviate much from global earth gravitational models. High-resolution elevation models, e.g. by LiDAR or local geodetic surveys, remain highly needed for measuring and monitoring delta elevation, and should be made publically available to the research community.

2. S*ubsidence monitoring.* Additional measurements of present total and depth-specific subsidence are required to improve subsidence observations in the delta, and to validate and advance modeling quantification as presented in this thesis. Subsidence monitoring can be improved by: 1) performing regular surveys of the existing network of national elevation benchmarks and analyze these time series to reveal spatial and temporal changes in absolute elevation; 2) expansion of the Surface Elevation Table network throughout the delta, not just in natural areas, but also in agricultural areas, to measure shallow subsidence and sediment accretion; 3) installing an extensometer network to measure subsidence at larger depths and quantify consolidation of individual aquitards; 4) installing strategically-placed, permanent GPS measurement stations; 5) installing corner reflectors to enable accurate measurement of local total subsidence using InSAR; 6) additional InSAR analyses on recent satellite imagery of the delta, such as Sentinel-1 data, by using persistent scatterer interferometry (Ferretti et al., 2000, Hanssen, 2001) in combination with field data on the measured objects, e.g. foundation depth of the object, to improve the interpretation of the InSAR signal (Van der Horst, 2018).

3. *Geological understanding of the subsurface*. As subsurface composition of a delta determines its sensitivity for subsidence, calculations of present and future subsidence can be improved by further advancing the geological and lithological models of the delta. Subsurface models can be improved by increasing the amount of geological and lithological data on the delta subsurface and by utilizing the full potential of the available data, e.g. through sophisticated 3D probabilistic surface mapping (e.g. following the example of GeoTOP by TNO-Geological Survey of the Netherlands, Stafleu et al., 2011). This will increase understanding on the occurrence and thickness of aquitards and clayey interbeds and aquifer connectivity; such subsurface characteristics are essential for groundwater flow and geotechnical modeling. Furthermore, dating Holocene sediment deposition, especially in the southern part of the Mekong delta, will improve the chronology of past delta progradation. This enables to quantify of past Holocene sediment compaction, using age and present depth, and improves the numerical modelling of future shallow compaction.

4. *Geotechnical behavior*. We need a better understanding of time-dependent subsidence processes, and more specifically the interplay between delayed overpressure dissipation and viscous compression (i.e. creep). Current models that do not compute creep mimic its effect by increasing the computed delayed overpressure dissipation. The novel application of the isotache method on aquifer-system compaction (Chapter 5 and 6) in this thesis enables modeling of viscous compression besides delayed overpressure dissipation. Improving the modeling of aquifer-systems using the isotache method requires further understanding of overconsolidation, and its quantification at greater depths.

5. *Delta plain sedimentation*. For many parts of the Mekong delta plain little data exists on natural rates of sediment accretion under present-day conditions. Installing and extending measurement networks to measure sediment accretion will improve model quantifications of sediment delivery to the delta plain. This will increase the understanding of the present role of sedimentation to relative sea-level rise and to what extent it could be enhanced by reintroducing sedimentation.

6. *Present and future groundwater use.* Model simulation results of present and future extraction-induced subsidence will improve when more complete and well-quantified data on actual groundwater extraction are available. This requires additional surveys to identify undocumented groundwater use and integration of existing (provincial-local) databases. To provide more realistic future scenarios of groundwater extraction, and consequent subsidence rates, the next step is to develop higher-detailed and spatially variable scenarios for future groundwater extraction. These should be based on understanding and future projections of the complex interaction between groundwater governance, legislation and law enforcement (Ha et al., 2018), access to good quality surface water, socio-economical situation, technical capability and land-use practices. Some of these drivers may change in response to a changing physical environment, such as changes in land-use following ongoing subsidence or salinization. Therefore, socio-economic impact assessments of land subsidence should consider these interactions between the natural and social systems in the course of time.


83-P1
018.37
83-H7
2900
83-F5
8757

Appendix A

Supplement to chapter 2

This is part of the manuscript: Minderhoud, P.S.J., Coumou, L., Erkens, G., Middelkoop, H., Stouthamer, E. **What is the elevation of the Mekong delta? Accurate elevation data crucial to sea-level rise impact assessments in deltas.** *(in review)*

A.1 Root mean square map of the interpolated Topo DEM

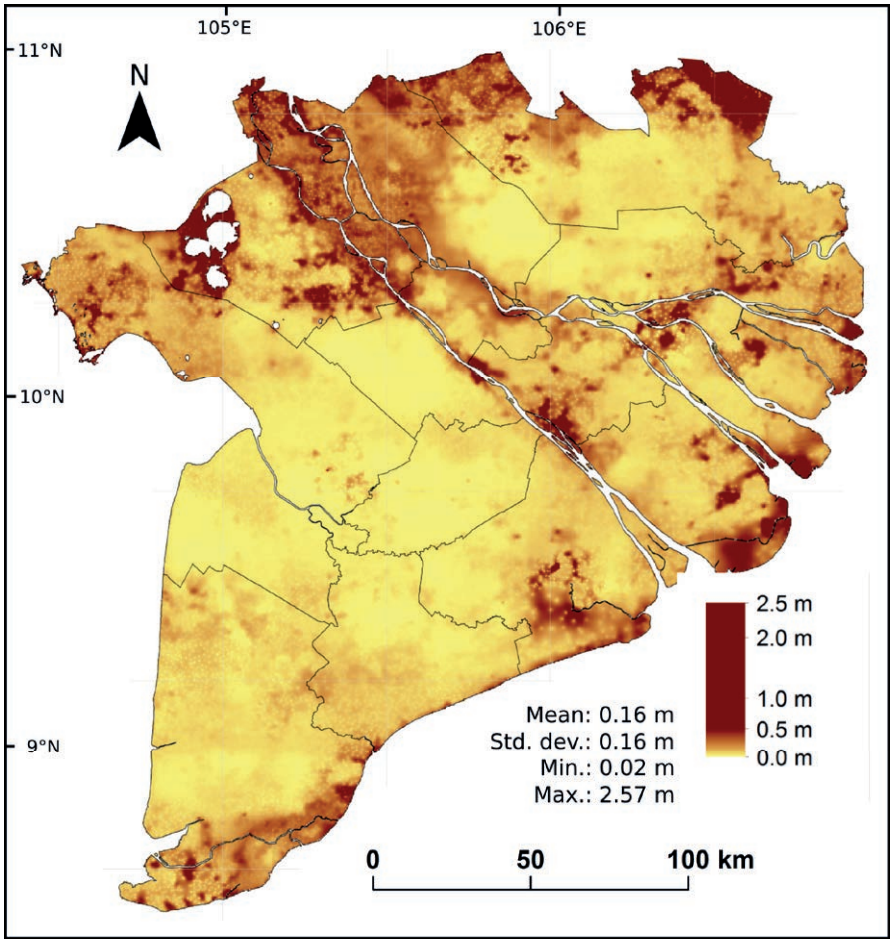

Figure A.1 | *Root mean square error (RMSE) map of the interpolated Topo DEM (Fig. 2.6). Mean RMSE and standard deviation are both 0.16 m. The RMSE increases with decreasing point density.*

A.2 Elevation anomalies

Both the SRTM, MERIT and the Topo DEMs contain an elevation anomaly which a likely the result of a measurement or data processing error. In the SW corner of the Ca Mau peninsula, an elevation anomaly is visible in the SRTM and the MERIT DEM (Fig. A.2a), also clearly visible in the elevation profile (Fig. 2.3, profile B-B'). Here, elevation values change with a sharp, geomorphological unrelated boundary to several meters below sea level. Although in absolute value much smaller, the Topo DEM also contains an elevation inconsistency. In the southern part of the delta along a horizontal line the elevation abruptly changes ~30 cm (Fig. A.2B). This sudden change in elevation is also present in the topographical elevation point dataset on which the Topo DEM is based and it may stem from a measurement error. It seems to be a local error, as the systematic offset is not present in the eastern part of the delta plain on the same latitude.

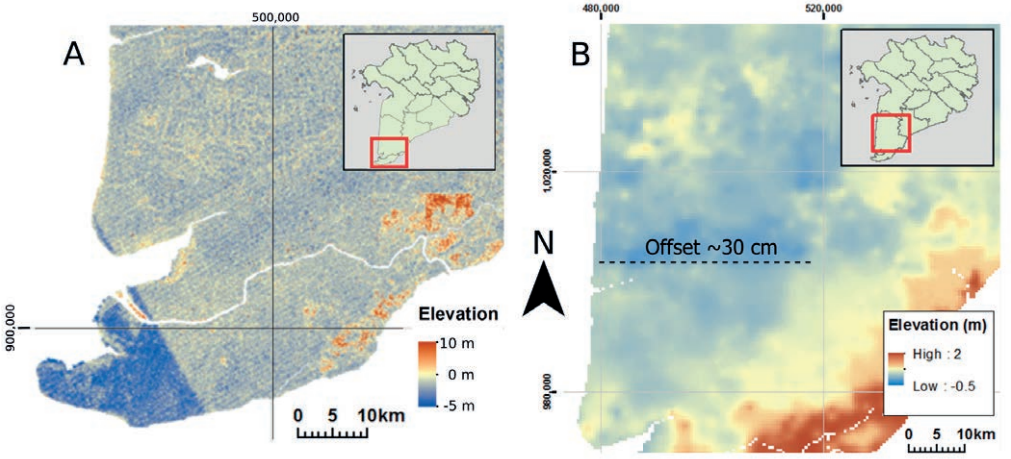

Figure A.2 | *Elevation anomalies present in the SRTM, MERIT and the Topo DEM. A) In the southwest corner of Ca Mau a sharp and unrealistic elevation change of multiple meters is visible in the SRTM and the MERIT DEM). B) An abrupt elevation change of about ~30 cm is visible along a horizontal line in the Topo DEM.*

A.3 National benchmarks used for absolute elevation validation

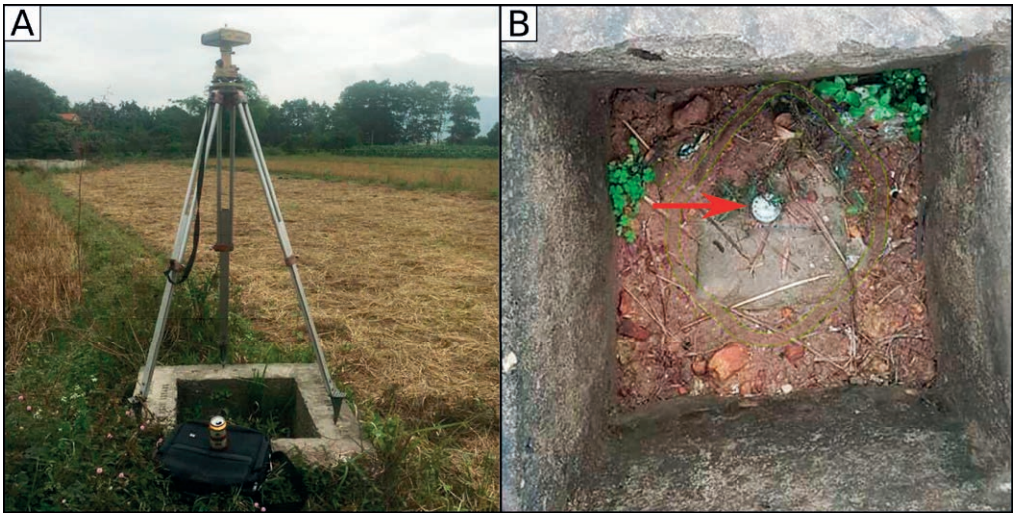

Figure A.3 | *Photographs of national benchmarks in Vietnam. A) Leveling survey in practice to measure the position of a benchmark showing the concrete structure protecting the benchmark. B) Benchmark marker. The markers are installed reportedly 30 cm below the surrounding surface elevation and a larger concrete structure is constructed around the marker for protection.*

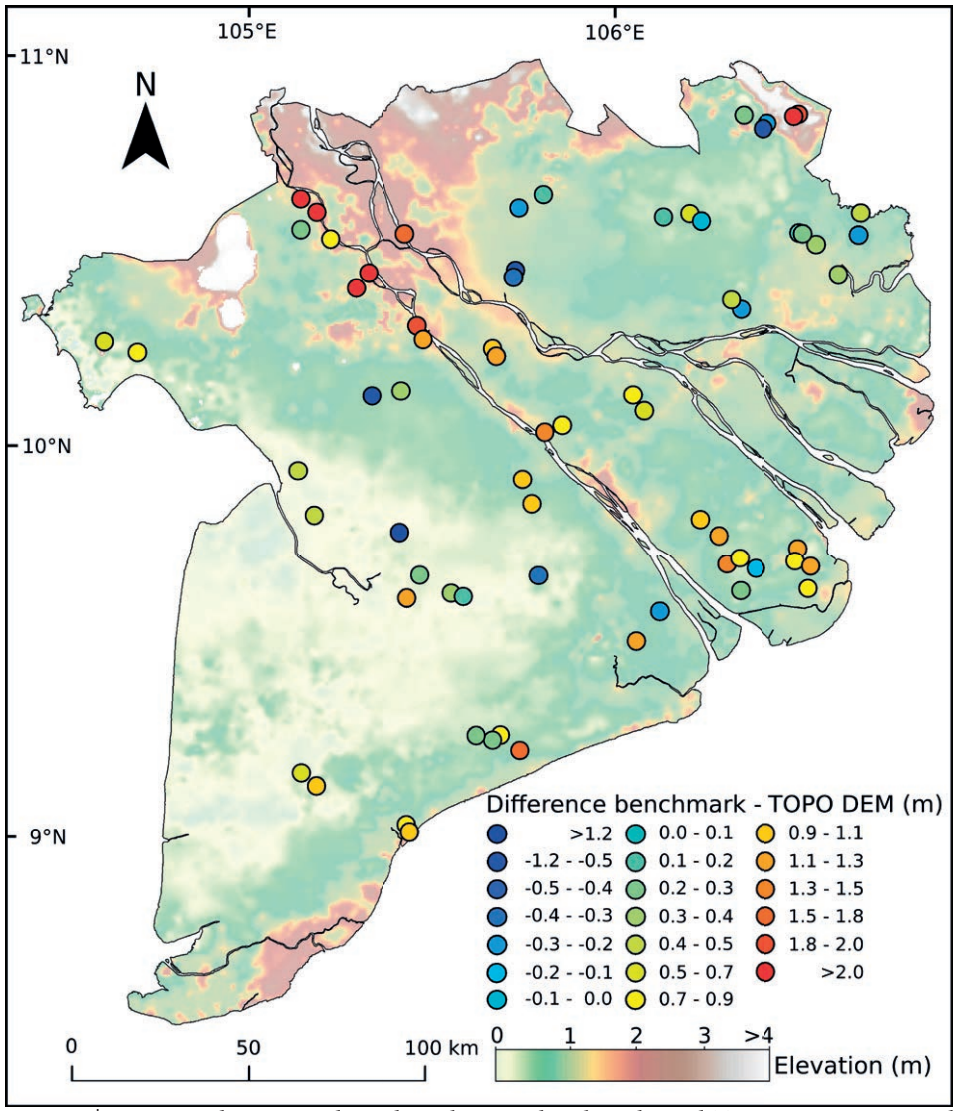

Figure A.4 | *Deviation between independent elevation benchmarks and Topo DEM. Positive values indicate that the benchmark elevation is larger than the Topo DEM elevation.*

Table A.1 | *List of national benchmarks used for absolute elevation validation. Coordinates are in VN-2000 and vertically referenced to Hon Dau datum. The national benchmark system in Vietnam is governed by the Department of Survey and Mapping of Vietnam, part of Vietnam's Ministry of Natural Resources and Environment.*

National benchmark number	Name of benchmark point	X-coordinate	Y-coordinate	Elevation (m)
657415	*Kênh Nam Lộ*	*627507*	*1176084*	*0.660*
658439	*Thuận Lợi*	*669678*	*1158808*	*0.321*
693404	*Chắc Tưng*	*612416*	*1054971*	*1.134*

National benchmark number	Name of benchmark point	X-coordinate	Y-coordinate	Elevation (m)
693518	*Tân Quy A*	*619041*	*1063319*	*-0.285*
657423	*Kênh Kè*	*630810*	*1174045*	*-0.064*
657457	*Tấn Đức*	*663288*	*1167284*	*0.375*
657417	*Ấp 2 Thuỷ Tây*	*620028*	*1175109*	*0.153*
681527	*Nô Công*	*658229*	*1081230*	*1.262*
681535	*Sóc Giụp*	*657528*	*1077655*	*0.874*
681536	*ấp Chợ*	*661848*	*1076181*	*1.120*
681529	*Chợ Tập Sơn*	*638001*	*1076824*	*1.492*
681524	*Chòm Chuối*	*641702*	*1078533*	*0.709*
681431	*ấp Tân Đại*	*630465*	*1089604*	*0.960*
681458	*Ngãi Hoà*	*635855*	*1084992*	*1.196*
669571	*Thạnh An*	*614592*	*1120402*	*0.682*
669542	*An Phú A*	*611432*	*1124804*	*0.858*
668526	*Kinh Mới*	*591426*	*1116280*	*0.827*
668528	*Vườn Ba Ngoặc*	*586585*	*1114258*	*1.330*
680413	*Nhà anh Minh*	*580295*	*1100890*	*0.928*
680436	*Trường Khánh*	*582986*	*1094121*	*0.977*
692401	*ấp 8*	*560201*	*1068475*	*0.301*
692402	*ấp 4*	*563582*	*1067544*	*0.200*
704408	*Trường Học*	*574047*	*1028463*	*0.768*
704417	*ấp Kinh Tế Mới*	*579479*	*1024004*	*1.534*
703407	*Khóm IV*	*517556*	*1017633*	*0.699*
703416	*Khóm 7*	*521765*	*1014021*	*0.998*
679434	*Hoà Thạnh*	*521116*	*1090743*	*0.468*
679506	*Phước Hoà*	*516503*	*1103392*	*0.444*
666407	*Kinh 1*	*461989*	*1139831*	*0.656*
666410	*Kinh Hạt*	*471193*	*1136886*	*0.712*
643437	*Mỹ Phó*	*517423*	*1180234*	*2.259*
655413	*Mỹ Thiện*	*521838*	*1176403*	*3.515*
655450	*Bình An II*	*536672*	*1159292*	*2.673*
655455	*Phú An*	*533075*	*1154965*	*2.229*
655499	*Phường Mỹ Thới*	*550364*	*1144340*	*1.954*
667502	*Khóm Thới Thạnh*	*552205*	*1140501*	*1.242*
668581	*Khóm 4*	*571832*	*1137922*	*1.042*
668590	*Long Hội*	*572846*	*1135765*	*1.297*
655427	*ấp 1*	*546857*	*1170395*	*1.711*
693512	*Trà Tro A*	*641941*	*1069227*	*0.276*
667431	*Tân Lợi*	*545830*	*1125843*	*0.364*
667433	*Phụng Thạnh*	*537481*	*1124494*	*-0.534*
656454	*Ấp 4*	*578346*	*1160047*	*-0.564*
656463	*Hoà Dân*	*577710*	*1158078*	*-0.381*
657452	*Bình Tây*	*658548*	*1170595*	*0.122*
657453	*Bình Đông*	*659546*	*1170372*	*0.234*
645440	*Hóc Thơm 2*	*649407*	*1201527*	*-0.279*
645465	*Ấp Thơm 2*	*648320*	*1200071*	*-0.526*
681533	*Long Trường*	*646314*	*1075599*	*-0.125*
681502	*Nghĩa Địa*	*661187*	*1069833*	*0.892*
655431	*Mỹ Phước*	*517429*	*1171578*	*0.212*

National benchmark number	Name of benchmark point	X-coordinate	Y-coordinate	Elevation (m)
655475	*Vĩnh Quới*	*525743*	*1168909*	*0.722*
657556	*Ấp Thạnh Hưng*	*642161*	*1149011*	*-0.223*
657447	*Ấp 3*	*639379*	*1151656*	*0.403*
680576	*Phú Thành B*	*551205*	*1073548*	*0.273*
692502	*Giồng Chùa*	*547642*	*1067170*	*1.236*
645416	*Kênh Rừng Sến*	*658489*	*1204078*	*1.768*
645428	*Ấp 3 Nghĩa Trang*	*642902*	*1203834*	*0.295*
645431	*Hậu Hoà*	*657106*	*1203456*	*2.567*
703493	*Ấp Thanh Hải*	*547450*	*1003072*	*0.861*
704411	*Cái Tràm A2-1*	*571888*	*1026933*	*0.239*
704409	*Hàng Bần*	*567153*	*1028257*	*0.224*
703497	*Kênh Ba*	*548363*	*1001048*	*0.905*
658407	*Ấp Phước Hậu Ngoài*	*675906*	*1176178*	*0.49*
658414	*Ấp Thuận Tây*	*675337*	*1169947*	*-0.237*
679442	*Hoà Lợi*	*545476*	*1085891*	*-1.172*
680523	*Ấp Tân Thành*	*584768*	*1073450*	*-0.305*
646405	*Tân Bửu*	*586175*	*1181420*	*0.153*
II-34	*Nghĩa Trang*	*579247*	*1177640*	*-0.266*

A.4 Areal and population statistics per province

Table A.2 | *Area and population numbers of the provinces in the Vietnamese Mekong delta (VMD). Total area and provincial population data from the General Statistics Office of Vietnam, available at www.gso.gov.vn. Area Mekong delta plain excludes bedrock, islands and rivers.*

Province	Area (km^2)			Population in 2016 (persons)	Population density in 2016 (persons * km^2)
	Total area in 2016	Main features excluded from total area	Mekong delta plain only		
An Giang	*3 537*	*Bedrock (202 km^2)*	*3 213*	*2 159 900*	*611*
Bạc Liêu	*2 669*	*-*	*2 465*	*886 200*	*332*
Bến Tre	*2 395*	*Rivers*	*2 068*	*1 265 200*	*528*
Cà Mau	*5 221*	*Rivers*	*5 138*	*1 222 600*	*234*
Cần Thơ	*1 439*	*-*	*1 400*	*1 257 900*	*874*
Đồng Tháp	*3 384*	*Rivers*	*3 242*	*1 687 300*	*499*
Hậu Giang	*1 622*	*-*	*1 622*	*772 500*	*476*
Kiên Giang	*6 349*	*Islands, bedrock (35 km^2)*	*5 607*	*1 776 700*	*280*
Long An	*4 495*	*-*	*4 458*	*1 490 600*	*332*
Sóc Trăng	*3 312*	*Rivers*	*3 148*	*1 312 500*	*396*
Tiền Giang	*2 511*	*Rivers*	*2 265*	*1 740 200*	*693*
Trà Vinh	*2 358*	*Rivers*	*2 110*	*1 040 500*	*441*
Vĩnh Long	*1 526*	*Rivers*	*1 446*	*1 048 600*	*687*
Entire VMD	*40 816*	*Rivers, islands*	*38 181*	*17 660 700*	*433*

A.5 Elevation per province for the Topo, SRTM and MERIT DEM

Table A.3 | *Basic statistics of delta plain elevation for each province and the entire Mekong delta for the Topo and the SRTM DEM. Area Mekong delta plain excludWes bedrock, islands and rivers (Table A.2).*

	Topo DEM				SRTM DEM				MERIT DEM			
Province	**Mean (m)**	**Min. (m)**	**Max. (m)**	**SD (mW)**	**Mean (m)**	**Min. (m)**	**Max. (m)**	**SD (m)**	**Mean (m)**	**Min. (m)**	**Max. (m)**	**SD (m)**
An Giang	*1.4*	*0.5*	*7.8*	*0.8*	*3.3*	*-51*	*88*	*3.4*	*3,8*	*-13,0*	*84,1*	*2,1*
Bạc Liêu	*0.5*	*0.1*	*2.0*	*0.3*	*2.0*	*-21*	*28*	*2.3*	*2,9*	*-3,6*	*9,6*	*0,6*
Bến Tre	*0.9*	*0.5*	*2.6*	*0.3*	*2.6*	*-59*	*63*	*2.8*	*3,1*	*-7,5*	*39,5*	*1,4*
Cà Mau	*0.6*	*-0.2*	*2.6*	*0.5*	*2.3*	*-25*	*71*	*2.4*	*2,4*	*-11,4*	*15,8*	*0,9*
Cần Thơ	*0.7*	*0.4*	*1.8*	*0.2*	*2.9*	*-56*	*54*	*3.4*	*3,9*	*-23,8*	*15,2*	*1,2*
Đồng Tháp	*1.4*	*0.7*	*4.0*	*0.6*	*3.7*	*-34*	*84*	*3.0*	*4,4*	*-9,2*	*24,5*	*1,3*
Hậu Giang	*0.4*	*0.1*	*1.0*	*0.2*	*1.9*	*-82*	*53*	*3.2*	*3,4*	*-12,6*	*12,9*	*0,7*
Kiên Giang	*0.4*	*-0.5*	*5.1*	*0.3*	*2.5*	*-60*	*107*	*2.6*	*3,1*	*-14,6*	*57,0*	*1,0*
Long An	*1.1*	*0.2*	*7.2*	*0.7*	*2.4*	*-46*	*51*	*2.3*	*3,9*	*-18,0*	*23,5*	*0,9*
Sóc Trăng	*0.7*	*0.2*	*2.5*	*0.3*	*2.0*	*-42*	*42*	*3.1*	*3,5*	*-7,2*	*17,5*	*1,0*
Tiền Giang	*0.9*	*0.3*	*1.9*	*0.2*	*2.8*	*-44*	*40*	*2.2*	*3,6*	*-3,9*	*14,1*	*1,0*
Trà Vinh	*0.8*	*0.3*	*2.7*	*0.2*	*2.5*	*-29*	*37*	*2.6*	*2,8*	*-8,0*	*16,9*	*1,1*
Vĩnh Long	*0.9*	*0.5*	*2.1*	*0.2*	*2.1*	*-31*	*40*	*2.8*	*2,6*	*-6,1*	*16,4*	*1,1*
VMD total	*0.8*	*-0.5*	*7.8*	*0.6*	*2.6*	*-82*	*107*	*2.8*	*3,3*	*-10,7*	*26,7*	*1,1*

A.6 Elevation statistics of geomorphological units in the Mekong delta

Table A.4 | *Elevation statistics for each geomorphological unit based on the Topo DEM (Fig. 2.2, main manuscript) and the geomorphological map of Nguyen et al., 2000 (Fig. 2.10, main manuscript).*

Geomorphological unit	**Mean (m)**	**SD (m)**	**Area (km^2)**
Abandoned channel belt	*0.91*	*0.45*	*1699*
Alluvial apron	*1.38*	*0.77*	*401*
Back swamp	*0.66*	*0.33*	*1614*
Bank: natural levee and crevasse splay	*1.38*	*0.55*	*1034*
Bank: Tidal inlet	*0.28*	*0.16*	*200*
Basement rock	*1.20*	*1.19*	*24*
Channel bar	*1.41*	*0.60*	*408*
Coastal plain	*0.53*	*0.32*	*7877*
Flood basin	*0.85*	*0.46*	*8205*
Flood plain	*0.74*	*0.29*	*339*
Mangrove marsh	*0.97*	*0.48*	*2123*
Marsh	*0.34*	*0.18*	*2085*
Relict beach ridge or sand dune	*0.84*	*0.28*	*953*
Salt marsh	*0.83*	*0.23*	*1164*
Sand spit	*1.14*	*0.20*	*45*
Swamp	*0.85*	*0.50*	*3006*
Tidal Flat	*0.99*	*0.42*	*151*
Undef. dep. of late Pleistocene age	*1.84*	*0.76*	*511*
Weathered land	*3.27*	*1.70*	*110*

Table A.5 | *Elevation statistics for each geomorphological unit based on the SRTM elevation model.*

Geomorphological unit	Mean (m)	SD (m)	Area (km^2)
Abandoned channel belt	*2.65*	*2.38*	*1699*
Alluvial apron	*2.84*	*2.09*	*401*
Back swamp	*2.44*	*3.00*	*1614*
Bank: natural levee and crevasse splay	*4.11*	*3.31*	*1034*
Bank: Tidal inlet	*2.29*	*2.26*	*200*
Basement rock	*4.49*	*4.50*	*24*
Channel bar	*3.17*	*4.11*	*408*
Coastal plain	*2.15*	*2.62*	*7877*
Flood basin	*2.83*	*3.02*	*8205*
Flood plain	*2.15*	*2.41*	*339*
Mangrove marsh	*2.35*	*2.22*	*2007*
Marsh	*2.28*	*2.53*	*2085*
Relict beach ridge or sand dune	*2.19*	*2.83*	*953*
Salt marsh	*2.14*	*2.66*	*1164*
Sand spit	*2.67*	*2.78*	*35*
Swamp	*2.57*	*2.09*	*3006*
Tidal Flat	*2.20*	*2.26*	*104*
Undef. dep. of late Pleistocene age	*3.11*	*1.81*	*511*
Weathered land	*6.37*	*5.19*	*110*

Table A.6 | *Elevation statistics for each geomorphological unit based on the MERIT elevation model and the geomorphological map of Nguyen et al., 2000 (Fig. 2.10)*

Geomorphological unit	Mean (m)	SD (m)	Area (km^2)
Abandoned channel belt	*3.48*	*0.96*	*1699*
Alluvial apron	*4.19*	*1.02*	*401*
Back swamp	*3.49*	*0.91*	*1614*
Bank: natural levee and crevasse splay	*4.67*	*1.87*	*1034*
Bank: Tidal inlet	*2.68*	*0.54*	*200*
Basement rock	*4.17*	*4.20*	*24*
Channel bar	*5.06*	*2.39*	*408*
Coastal plain	*2.87*	*0.94*	*7877*
Flood basin	*3.54*	*1.03*	*8205*
Flood plain	*3.66*	*0.57*	*339*
Mangrove marsh	*2.29*	*1.13*	*2007*
Marsh	*2.69*	*0.70*	*2085*
Relict beach ridge or sand dune	*2.78*	*1.24*	*953*
Salt marsh	*3.13*	*1.04*	*1164*
Sand spit	*1.58*	*1.59*	*35*
Swamp	*3.73*	*0.83*	*3006*
Tidal Flat	*1.47*	*1.71*	*104*
Undef. dep. of late Pleistocene age	*4.67*	*0.79*	*511*
Weathered land	*6.87*	*4.77*	*110*

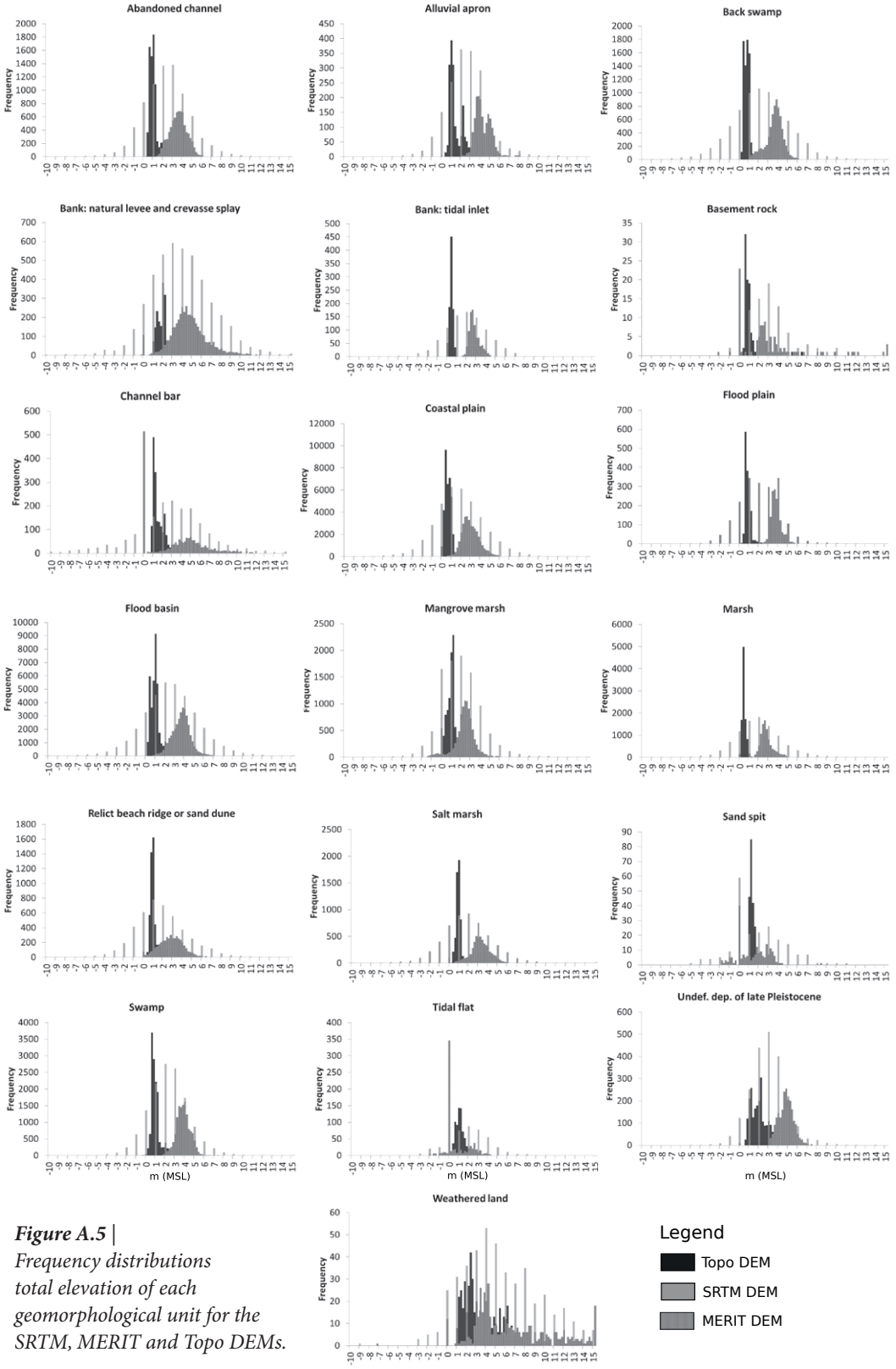

Figure A.5 |
Frequency distributions total elevation of each geomorphological unit for the SRTM, MERIT and Topo DEMs.

A.7 Tide-dominated inundation occurrences

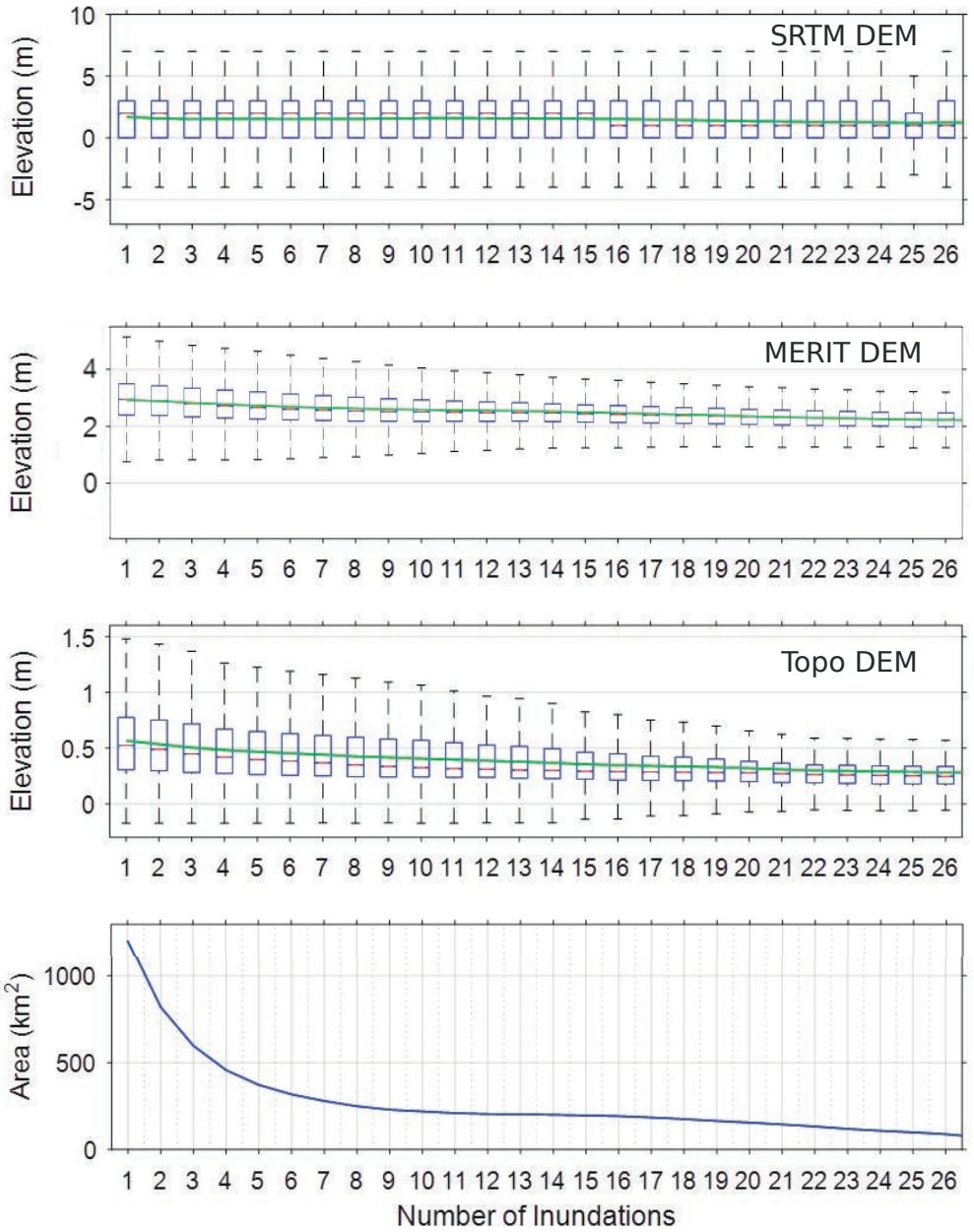

Figure A.6 | *Boxplots showing elevation of the SRTM, MERIT and Topo DEMs for areas with different inundation occurrences in the coastal zone of the Mekong delta. Blue box indicates 25 and 75 percentile, red lines the median, black whiskers the maximum within the 1.5x interquartile range (IQR), green line the average. Extremes are not displayed. Inundation occurrences were derived from 128 satellite images by Kuenzer et al. (2013) between 2007 and 2013 (Fig. 2.12).*

Appendix B

Supplement to chapter 4

This is part of the publication: Minderhoud, P.S.J., Coumou, L., Erban, L.E., Middelkoop, H., Stouthamer, E., Addink, E.A. (2018). **The relation between land use and subsidence in the Vietnamese Mekong delta.** *Science of the Total Environment*, 634, 715 – 726. doi:10.1016/j.scitotenv.2018.03.372

B.1 Land-use maps time series

B.1.1 Satellite imagery

Satellite images of the Landsat 5 Thematic Mapper (TM) sensor were used to build a time series of consistent land-use (LU) maps. Reasons for choosing images of this satellite sensor were: 1) a single tile covers a large part of the Vietnamese Mekong delta, 2) images of the same sensor are available with a high 16-days repeat interval over a long period (1984-2013), 3) the images have a wide range of available spectral bands, 4) the ground resolution of the images is sufficient for classifying LU and 5) the images are freely available. Four Landsat 5 TM images (Figure B.1) were selected based on the following criteria: 1) acquisition date, to create a relevant time series, 2) limited cloud cover, 3) acquired during dry season (preferably February) to be able to distinguish dry-season irrigation.

Table B.1 | *Landsat 5 TM surface reflectance images (WRS path 134, row 053). The images were selected via the online LandsatLook Viewer (USGS, 2016a) and the Earth Explorer application (USGS, 2016b) and downloaded by bulk order, including several spectral indices (NDVI, EVI and NDMI) (USGS, 2010).*

Date (yyyy-mm-dd)	Julian day	Landsat scene identifier
1988-01-30	*030*	*LT51250531988030*
1996-02-21	*052*	*LT51250531996052*
2006-03-04	*063*	*LT51250532006063*
2009-02-08	*039*	*LT51250532009039*

B.1.2 Land-use classification and change detection

The main steps for the pre-processing, classification and post-processing the Landsat 5 imagery are shown in Figure B.1.

Pre-processing: Extent clipping and masking clouds and cloud shadows

During the pre-processing, the satellite image was clipped to the extent of the study area (Fig. 4.1) and clouds and their shadows were classified and removed from the image (Step 1 & 2, Fig. B.1). The clouds were classified using object-based image analysis (see Table B.2 for segmentation settings). We used the randomForest package v. 4.6-12 in R v 3.3.2 (Breiman & Cutler, 2003). A manually built decision tree was used to control the cloud and cloud-shadow classification. The rules corresponding to each node in the decision tree were based on 1) the high reflection of clouds in (especially) the optical bands compared to the land surface, 2) the shape and size of the clouds, and 3) the low cloud temperature. After classification, a 60 m buffer around the clouds was applied. The outlines of the buffered clouds were manually shifted to encompass corresponding cloud shadows. Some clouds and respective shadows that were missed by the automated procedure were manually added to the cloud mask. Furthermore, areas misclassified as clouds were removed from the mask. A final shapefile of the clouds and cloud shadows was used to mask these areas in each corresponding Landsat 5 image.

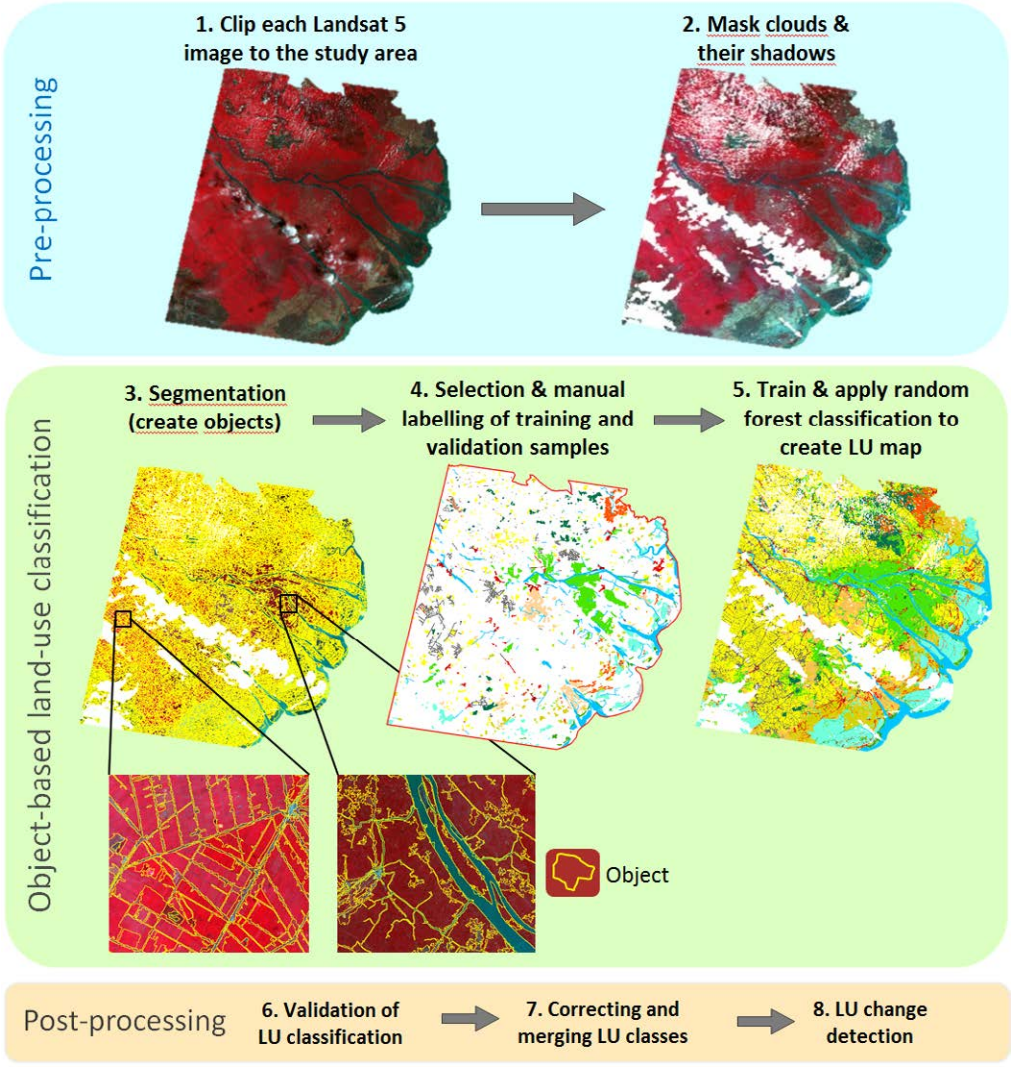

Figure B.1 | *Overview of all steps to create a land use (LU) map from a Landsat 5 satellite image, including pre- and post-processing steps. Satellite image visualization: RGB = NIR-Red-Green (false color).*

Table B.2 | *Multi-resolution segmentation settings used for cloud classification.*

Setting	Value
Scale parameter	*100, 200 and 500*
Shape parameter	*0*
Layers: Landsat 5 TM bands & indices	*Blue, green, red, NIR, SWIR1, SWIR2, TIR, EVI (500), NDMI (500) and NDVI (100, 200)*

Object-based land-use classification

Land-use classification was done using an object-based approach combined with a random-forest machine-learning algorithm (Breiman, 2001). The cloud-masked images were segmented into objects based on similar spectral characteristics of pixels (Step 3, Fig. B.1). The optimal segmentation settings for the LU classes (Table B.3) were determined such that each object representing a continuous area of a single land-use class was as large as possible. For example, an object comprises an individual field or group of fields with the same crop or a (large part of a) road, river or channel. The final segments were exported with the values for 55 selected spectral and spatial features as shape- and text file (Table B.3).

Table B.3 | *Segmentation settings used for land-use classification of each image. The Landsat TM 5 Thermal infra-red (TIR) layer was not used for this segmentation because of its coarser resolution and its limited relevance for land-use differentiation.*

Segmentation	Setting	Value
Multi-resolution	*Scale parameter*	*200*
	Shape parameter	*0*
Spectral difference	*Maximum spectral difference parameter*	*200 (100 for TM 5 image of 2009)*
Both	*Layers: Landsat 5 TM bands & indices*	*Blue, green, red, NIR, SWIR1, SWIR2, EVI and NDMI*

Subsequently, a random selection of the objects (1100 samples, about 4.5% of the total number of objects) was manually labeled to the corresponding LU classes using existing land cover and LU maps (GSO, 2017), Google Earth imagery and expert knowledge (tep 4, Fig. B.1). The randomly selected segments that were too uncertain to be attributed to a certain LU class were not labeled. The labeled dataset of segments was split into a training and validation dataset for the random-forest algorithm. To ensure each LU class had enough training segments, some additional segments were added to the selection. Lastly, the training dataset was used to train a random forest with 55 spectral and spatial feature values as input X-variables and the LU classes as output Y-value. In addition, derivatives of shapefiles of the ocean ('Ocean area around the Mekong Delta') and of the main river branches ('Main Mekong River Course Lower Mekong Basin') were also used as X-variable (WISDOM, 2014). The number of decision trees in the 'forest' was set to 10,000. The number of X-variables used to find the best rule at each tree node was set to the square of the number of variables. The training sample size for each tree was set to 2/3 of the samples per LU class without replacement. This ensures that each class is represented in each tree and a proper randomness of the trees. The remaining samples (1/3) are so called out-of-bag (OOB) samples. Furthermore, to safeguard a fully independent accuracy assessment, again only 2/3 of the total training samples were used for creating the random forest, while 1/3 were reserved as independent validation segments.

The resulting random forest was used to classify all segments in the image based on their spectral and spatial characteristics (Appendix 5, Step 5, Fig. B.1).

Table B.3 | *Spectral and spatial segment features used for land-use classification. Trimble (2015) for explanation.*

Layer values	*Mean*	*Blue* *Green* *Red* *NIR* *SWIR1* *SWIR2* *TIR* *EVI* *NDVI*
	Mode	*Blue* *Green* *Red* *EVI*
	Standard deviation	*NIR* *SWIR1* *EVI*
	Quantile	*50th EVI quantile* *5th NDVI quantile*
	Pixel-based	*Max. red pixel value* *Max. SWIR1 pixel value*
	To neighbors	*Mean difference to neighbors: NDVI* *Mean difference to darker neighbors: NDVI* *Mean difference to darker neighbors: red* *Mean difference to brighter neighbors: EVI* *Mean difference to brighter neighbors: NDVI*
Geometry	*Extent*	*Area (pixels)* *Border length (pixels)* *Length (pixels)* *Length/width (pixels)* *Width (pixels)*
	Shape	*Asymmetry* *Border index* *Compactness* *Density* *Elliptic fit* *Radius of largest enclosed ellipse* *Radius of smallest enclosing ellipse* *Rectangular fit* *Roundness*

		Shape index
Geometry	*Based on skeletons*	*Curvature/length (only main line)* *Length of main line (no cycles) (pixels)* *Length/width (only main line)* *Maximum branch length (pixels)* *Standard deviation curvature (only main line)* *Width (only main line) (pixels)*
Position	*Distance to vectors*	*Distance to Ocean (outline) (pixels)* *Distance to Rivers (centroid) (pixels)*
Thematic attributes	*Minimum overlap (%) with thematic polygons*	*Ocean* *Rivers*
Customized		*(2*width+2*length)/border length* *Area/border length* *Mean difference to neighbors: 5% quantile of NDVI* *Mean of neighboring mean NDVI* *Standard deviation EVI divided by mean EVI*

Post-processing land-use classification

The accuracy calculations of the resulting LU map (Step 6, Figure B.1) were performed internally in the training of the random-forest algorithm using the area of the OOB samples and, subsequently, after the training phase using the independent validation segments. The overall accuracies of the LU maps are respectively 77%, 94%, 92% and 89% for the LU maps of 1988, 1996, 2006 and 2009. Table B.5 shows the reliability (user's accuracy) and accuracy (producer's accuracy) and Kappa (κ) coefficient of each LU class and the total accuracy or each LU map. The Kappa coefficient is an index which corrects the accuracy for the chance that a class is correctly classified: a value of 0 indicates that a random classification is as good as the performed classification, while a value of 1 indicates that the classification is perfect (Lillesand et al., 2008). The lowest accuracy for the LU map of 1988 can be explained by the highest lack of LU reference data for this period. Inaccuracies related to specific LU classes can be related to high confusion values between LU classes (i.e. similar spectral and/or spatial characteristics), the sparse presence of cloud- shadows remnants not captured well by the initial mask and influence the spectral characteristics of the objects.

After the validation, a number of LU classes was merged (Step 7, Fig. B.1): two water classes were merged into one water class, the 'Dry-season harvested rice' class was merged with 'dry-season rice' into 'dry-season rice' and the cloud remnants were set to No Data. Fig. B.2 shows the total area for the resulting LU classes for each classified image (Fig. 4.2).

Table B.5 | *Validation statistics based on the total area of the independent validation segments. All percentages below 50% are colored red, percentages of 95% or higher are colored green. For land-use-class acronyms see Table B.2.*

Land-use class	1988		1996		2006		2009	
	Reliability	Accuracy	Reliability	Accuracy	Reliability	Accuracy	Reliability	Accuracy
Aquaculture	*90%*	*100%*	*93%*	*96%*	*99%*	*100%*	*99%*	*100%*
Dry-S Rice	*76%*	*66%*	*99%*	*100%*	*93%*	*64%*	*92%*	*97%*
Dry-S P Rice	*94%*	*88%*	*44%*	*17%*	*54%*	*72%*	*72%*	*80%*
Dry-S Harvested Rice	*0%*	*0%*	*52%*	*44%*	*91%*	*98%*	*82%*	*49%*
Dry-S Bare	*83%*	*84%*	*95%*	*95%*	*91%*	*95%*	*80%*	*79%*
Mixed Crops - No Rice	*74%*	*86%*	*97%*	*89%*	*99%*	*79%*	*82%*	*81%*
Mangroves	*98%*	*96%*	*92%*	*74%*	*100%*	*100%*	*100%*	*72%*
Wet. Forest	*74%*	*94%*	*94%*	*98%*	*97%*	*97%*	*86%*	*92%*
Orchard	*69%*	*88%*	*86%*	*98%*	*56%*	*83%*	*85%*	*65%*
Urban Dense	*95%*	*49%*	*88%*	*89%*	*91%*	*95%*	*66%*	*66%*
Urban Open	*60%*	*69%*	*77%*	*38%*	*-*	*0%*	*46%*	*37%*
Linear Settlements	*72%*	*44%*	*99%*	*99%*	*93%*	*94%*	*90%*	*97%*
Water	*100%*	*50%*	*93%*	*100%*	*100%*	*100%*	*96%*	*100%*
Water channels	*8%*	*88%*	*100%*	*94%*	*100%*	*95%*	*100%*	*100%*
Marshland	*99%*	*98%*	*98%*	*96%*	*100%*	*88%*	*100%*	*100%*
Cloud remnants	*100%*	*33%*	*67%*	*87%*	*82%*	*85%*	*93%*	*91%*
Overall accuracy		**77%**		**94%**		**92%**		**89%**
κ - coefficient		**0.74**		**0.93**		**0.90**		**0.88**

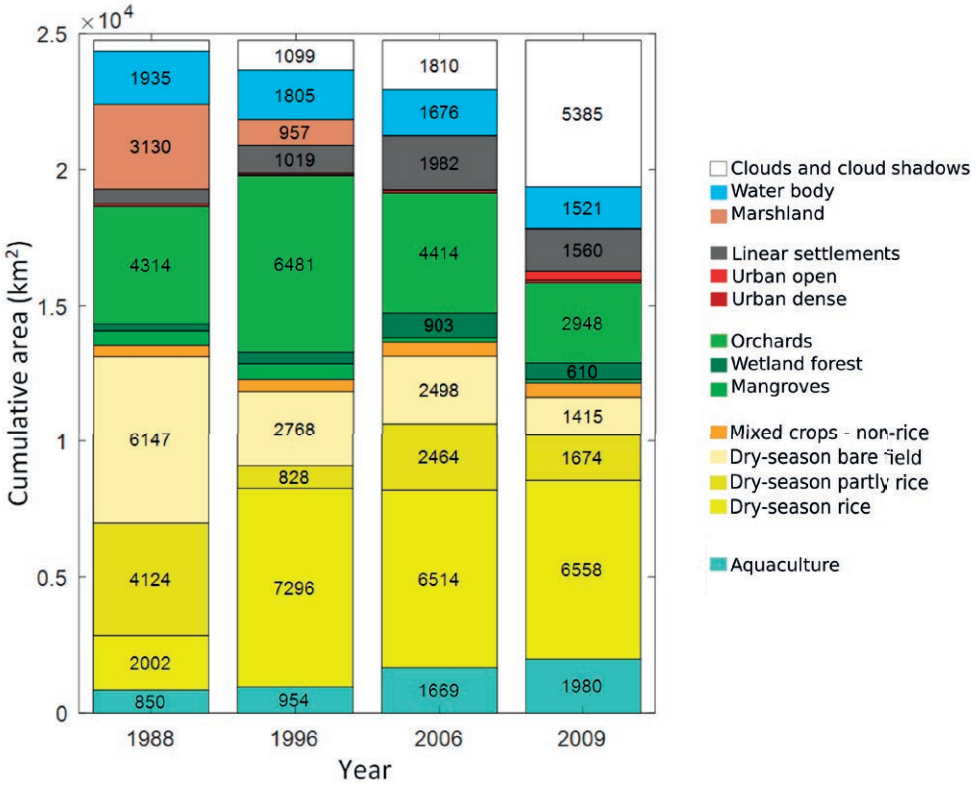

Figure B.2 | *Area (km²) per land use class for each classified Landsat TM 5 satellite image. Note that the clouds and cloud shadows have different positions in each year, affecting the estimated area of land-use classes.*

Land-use change detection

As a final step (Step 8, Figure B.1), land-use change maps were created using post-classification change detection. The land-use map of 2009 was excluded from the land-use change analysis for its large cloud-covered area. Subsequently, a LU change map was created for each combination of the LU maps of 1988, 1996 and 2006. Furthermore, the different land-use maps were compared to each other and some obvious classification errors were adjusted (e.g. areas which were classified as water in 1996, but have an identical non-water class in 1988 and 2006, have been classified as that non-water class in 1996). Areas covered by clouds in any of the maps were masked.

B.1.3 Land-use changes

LU change maps for respectively '88-'96, '88-'06, '96-'06 were created. The following tables list the total area and percentage of the total area for each period.

Table B.6 | *Area of land-use changes between 1988 and 1996 (in km²). 42% of the total area did not change (in italic).*

Land-use class in 1988 \ Land-use class in 1996	Aqua-culture	Dry-s. rice	Dry-s. p. rice	Dry-s. b. field	Mix c. no rice	Mangroves	Wet. Forest	Orchard	Urban dense	Urban open	Linear Settle.	Water	Marsh-land	Total 1988
Aquaculture	*526*	3	4	30	6	130		17	3		3	12	1	735
Dry-season rice	2	*1539*	24	21		1	8	264		1	105	4.7	5	1974.7
Dry-season partly rice	13	1419	*151*	139	35	21	37	1675	4	12	215	28	38	3787
Dry-season bare field	78	1867	317	*1597*	117	57	8	761	15	11	174	20	29	5051
Mix crops - non-rice	11	31	21	42	*129*	15	3	60			18	3	13	346
Mangroves	129	10	7	20	9	*231*		41			2	7		456
Wetland forest	1	35	3	3	1		*90*	31			14	1	69	248
Orchard	15	837	88	70	34	55	59	*2496*	1	5	164	33	16	3873
Urban dense		1	1					1	*5*	3	2	1		14
Urban open	1	7	6	7	3			30	4	*6*	2	3	1	70
Linear settlement	3	153	17	51	14	2	2	91	2	3	*100*	7	1	446
Water	78	15	4	11	2	24	2	71	2	2	17	*1575*	1	1804
Marshland	9	1188	96	113	69	3	204	355	2	4	153	21	*748*	2965
Total 1996	866	7105	739	2104	419	539	413	5893	38	47	969	1715.7	922	21770

Table B.7 | *Area of land-use changes between 1988 and 2006 (in km²). 34% of the total area did not change (in italic).*

Land-use class in 1988 \ Land-use class in 2006	Aqua-culture	Dry-s. rice	Dry-s. p. rice	Dry-s. b. field	Mix c. no rice	Mangroves	Wet. Forest	Orchard	Urban dense	Urban open	Linear Settle.	Water	Marsh-land	Total 1988
Aquaculture	*637*				14	27	1	29	1		20	12		741
Dry-season rice	6	*1080*	240	174	8	1	12	243	6	1	205	6		1982
Dry-season partly rice	45	1129	*554*	292	42	4	52	1225	22	5	409	19	1	3799
Dry-season bare field	239	1698	733	*1370*	105	6	10	459	23	1	399	7	2	5052
Mix crops - non-rice	35	33	75	41	*95*	1		32	2		33	2		349
Mangroves	313	11	35	8	17	*52*		11	1		7	8		463
Wetland forest	7	56	5	3	3		*118*	29			24	1	1	247
Orchard	61	684	479	165	74	20	58	*1927*	17	4	368	36	1	3894
Urban dense		1	1	1					*7*		3	1		14
Urban open	3	9	14	6	1			15	12	*1*	8	3		72
Linear settlement	16	135	68	57	12		1	35	3		*119*	4		450
Water	103	33	18	5	5	44	1	46	3		37	*1511*		1806
Marshland	39	1444	114	112	102		623	246	2		266	6	*17*	2971
Total 2006	1504	6313	2336	2234	478	155	876	4297	99	12	1898	1616	22	21840

Table B.8 | *Area of land-use changes between 1996 and 2006 (in km²). 53% of the total area did not change (in italic.*

Land-use class in 1996 \ Land-use class in 2006	Aquaculture	Dry-s. rice	Dry-s. p. rice	Dry-s. b. field	Mix c. no rice	Mangroves	Wet. Forest	Orchard	Urban dense	Urban open	Linear Settle.	Water	Marsh-land	Total 1996
Aquaculture	*758*				11	39		21			14	28		872
Dry-season rice	7	*4221*	844	645	14	3	103	706	9	2	553	8		7115
Dry-season partly rice	20	212	*155*	127	19	2	11	100	11	1	81	2		742
Dry-season bare field	167	359	210	*1072*	64	2	14	79	10		124	3	1	2105
Mix crops - non-rice	20	17	86	51	*159*		6	57	3	1	19	1		421
Mangroves	322	18	33	14	33	*70*		35	1		12	8		546
Wetland forest	2	122	9	3	6		*169*	55			45	1	2	414
Orchard	134	873	841	234	88	22	91	*3017*	30	7	542	43	1	5923
Urban dense	8	2	2	5	1		1	1	*15*		5	0		40
Urban open		3	9	4	1		2	4	12	*2*	9	1		48
Linear settlement	5	281	114	45	8		46	83	4		*382*	7	1	976
Water	58	24	16	5	7	19	4	28	4		44	*1508*		1716
Marshland	3	182	16	26	67		428	113			68	1	*17*	921
Total 2006	1504	6313	2336	2233	478	156	876	4298	99	14	1897	1614	22	21839

Table B.9 | *Area of land-use changes between 1988 and 2006 (in % of the total study area). 34% of the total area did not change (in italic). 1% corresponds to an area of 200 km².*

Land-use class in 1988 \ Land-use class in 2006	Aqua-culture	Dry-s. rice	Dry-s. p. rice	Dry-s. b. field	Mix c. no rice	Mangroves	Wet. Forest	Orchard	Urban dense	Urban open	Linear Settle.	Water	Marsh-land	Total in 1988
Aquaculture	*2.9*				0.1	0.1	0.0	0.1	0.0	0.0	0.1	0.1		3.4
Dry-season rice	0.0	*4.9*	1.1	0.8	0.0	0.0	0.1	1.1	0.0	0.0	0.9	0.0	0.0	9.1
Dry-season partly rice	0.2	5.2	*2.5*	1.3	0.2	0.0	0.2	5.6	0.1	0.0	1.9	0.1	0.0	17.4
Dry-season bare field	1.1	7.8	3.4	*6.3*	0.5	0.0	0.0	2.1	0.1	0.0	1.8	0.0	0.0	23.1
Mix crops - non-rice	0.2	0.2	0.3	0.2	*0.4*	0.0	0.0	0.1	0.0		0.2	0.0	0.0	1.6
Mangroves	1.4	0.0	0.2	0.0	0.1	*0.2*	0.0	0.0	0.0	0.0	0.0	0.0		2.1
Wetland forest	0.0	0.3	0.0	0.0	0.0	0.0	*0.5*	0.1			0.1	0.0	0.0	1.1
Orchard	0.3	3.1	2.2	0.8	0.3	0.1	0.3	*8.8*	0.1	0.0	1.7	0.2	0.0	17.8
Urban dense	0.0	0.0	0.0	0.0	0.0		0.0	0.0	*0.0*	0.0	0.0	0.0	0.0	0.1
Urban open	0.0	0.0	0.1	0.0	0.0	0.0		0.1	0.1	*0.0*	0.0	0.0		0.3
Linear settlement	0.1	0.6	0.3	0.3	0.1	0.0	0.0	0.2	0.0	0.0	*0.5*	0.0	0.0	2.1
Water	0.5	0.2	0.1	0.0	0.0	0.2	0.0	0.2	0.0	0.0	0.2	*6.9*		8.3
Marshland	0.2	6.6	0.5	0.5	0.5	0.0	2.9	1.1	0.0	0.0	1.2	0.0	*0.1*	13.6
Total in 2006	6.9	28.9	10.7	10.2	2.2	0.7	4.0	19.7	0.5	0.1	8.7	7.4	0.1	100.0

B.2 Subsidence per land-use class

B.2.1 Subsidence rate per unchanged land-use class.

Table B.10 | *Statistics of InSAR-based subsidence rates for the period 2006-2010 for areas with unchanged land-use.*

Land-use class	Mean (mm yr^{-1})	Median (mm yr^{-1})	Std.dev. (mm yr^{-1})	Coefficient of variation (-)	Total unchanged area (km^2)
Marshland	*6*	*5.8*	*4*	*7*	*10*
Wetland forest	*7.4*	*7.4*	*4*	*5*	*53*
Mangroves	*12.9*	*13.1*	*7*	*5*	*14*
Dry-season rice	*7.8*	*7.8*	*5*	*6*	*489*
Dry-season partly rice	*13.5*	*13.3*	*7*	*5*	*31*
Dry-season bare field	*12.9*	*12.6*	*7*	*6*	*360*
Mixed crops – non-rice	*18.4*	*18.2*	*7*	*4*	*47*
Orchards	*13.5*	*13.6*	*5*	*4*	*1187*
Aquaculture	*11.1*	*11.2*	*7*	*6*	*267*
Linear settlements	*8.5*	*8.3*	*5*	*6*	*59*
Urban open	*17.6*	*17.8*	*5*	*3*	*1*
Urban dense	*20.4*	*20.7*	*5*	*2*	*7*

B.2.2 Significance of subsidence-rate differences between land-use classes.

The significance of the differences between both the median and the mean subsidence rates experienced by the unchanged-LU classes was tested. The boxplot notches (Fig. 4.3) were used to test the null hypothesis that two *medians* truly differ at the 0.05 level. The notches around the median represent the 95% confidence interval of the median. If they do not overlap, the null hypothesis can be rejected and the medians differ significantly (Chambers et al., 1983). The advantage of this method is that boxplots do not require the assumption of a certain statistical distribution. To determine whether one or more *mean* values of the land-use classes differ significantly from the others at the 95% confidence level and assuming the probability density of the subsidence rate for each land-use class were approximately normally distributed, a one-way analysis of variance (ANOVA) was applied to the dataset. If there was a significant difference, multiple-comparison using the Tukey-Kramer method (Toothaker, 1993) was applied to determine which combinations of LU classes are significantly different. The analyses revealed that all class combinations with differences larger than 1 mm yr^{-1} are significantly different based on both analyses (Fig. B.3).

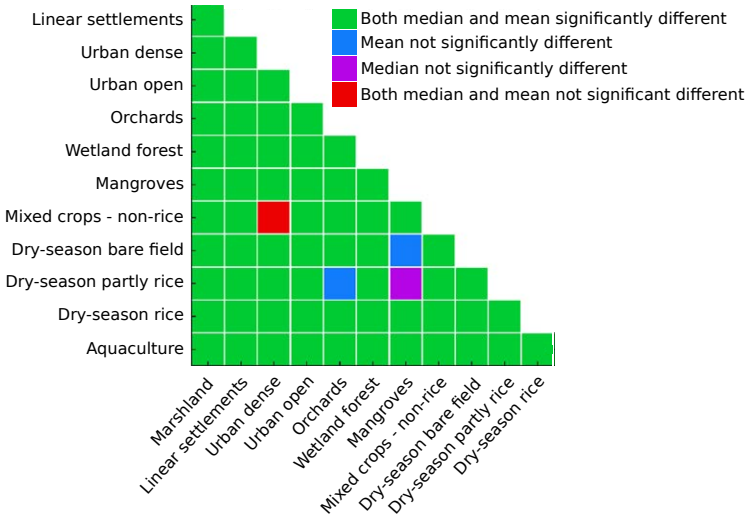

Figure B.3 | *Matrix showing which combination of mean or median land-subsidence rates per LU class is significantly different. Analysis is based on 95% confidence level based on boxplot notches (median) and/or multiple-comparison (mean).*

B.3 Performance of land-use-based predictions of subsidence rates

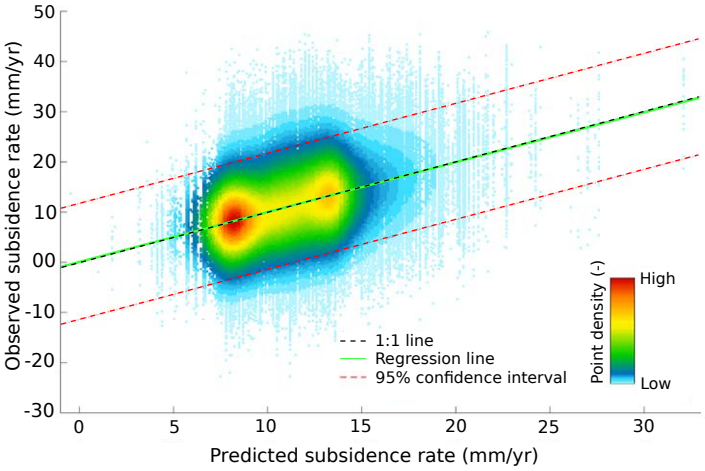

Figure B.4 | *Density scatter plot and linear regression of observed InSAR-based land-subsidence rates versus predicted subsidence rates for the period 2006-2010. Predictions based on the land-use history. Number of points >900k. The regression equation is Observed = 0.996 Predicted + 0.016, close to the 1:1 line (slope = 1, intercept = 0), showing consistent estimates and minimal bias. RMSE = 5.8 mm* yr^{-1}*. Note the different scales of the axes. The estimated subsidence shows a bimodal distribution, and the peaks correspond to dominant land-use trajectories. The peak at 8 mm* yr^{-1} *corresponds to rice cultivation and the peak at 13.5 mm* yr^{-1} *to orchards. The predicted values are discontinuous as they represent median values for specific land-use sequences.*

Appendix C

Supplement to chapter 5

This is part of the publication: Minderhoud, P.S.J., Erkens, G., Pham, H.V., Bui, V.T., Erban, L., Kooi, H., Stouthamer, E. (2017). **Impacts of 25 years of groundwater extraction on subsidence in the Mekong delta, Vietnam.** *Environmental Research Letters* 12. doi:10.1088/1748-9326/aa7146

C.1 Subsurface model

We adopt the geological subsurface schematization of the Mekong delta (MKD) and the Saigon delta made by the Division for Geological Mapping for the South of Vietnam (DGMS, 2004). As these two delta systems share the same depositional basin, their deposits and groundwater systems are inter-connected. Ten hydrogeological cross-sections based on 95 linearly interpolated, geological borehole logs were used to construct the 3D subsurface model of MKD using a linear interpolation of iMOD SolidTool (Vermeulen *et al* 2016). The deepest confined aquifer (Upper-Middle Miocene age) was not represented in the model due to data paucity. This aquifer is less relevant for this study, as no groundwater extraction is reported for it. Surface elevation was based on a detailed digital elevation model of the Mekong delta supplemented with Shuttle Radar Topography Mission (SRTM) elevation data for areas outside the delta. This resulted in a 15 layered, subsurface model, representing 7 aquifers, 7 aquitards and a phreatic top layer (Table C.1). The minimum layer thickness was set to two meters, as required for numerical functioning of the current build of the subsidence module in iMOD (SUB-CR). Furthermore, an adjustment was made in Soc Trang province: an incorrectly interpreted aquitard thickness in a geological borehole log was manually corrected to a minimum thickness of 5 meters. In the current subsurface model, ~60% of the total volume is represented as aquitard (clay and silt) and ~40% as aquifer (sand). A lithological analysis of over 700 core logs revealed a sand versus silt and clay presence for the Mekong delta of respectively 60% and 40%. This implies that about 1/3 of the aquitards in the current subsurface model actually consist of sand, which is reflected by the abundant sand lenses present in the core logs. This is taken into account in the subsidence calculations to avoid overestimation of subsidence.

Table C.1 | *Geological and hydrogeological units of the MKD and corresponding model discretization. In total ~40% of the subsurface presented in the model is aquifer and ~60% is aquitard. Model layer 1 is not shown in this table, as it is not based on a specific geological formation, but represents the phreatic top layer at the delta surface.*

Age	Subseries	Geological unit	Hydrogeological unit	Model Layer	Hydrogeological unit	Average depth below surface (m)	Average layer thickness (m)
Holocene	*Upper*	Q_{II}^{3}	qh_3	*2*	*Aquitard 1*	*9*	*18*
	Middle/Lower	Q_{II}^{2-3}/Q_{II}^{1}	qh_{2-3}/qh_1	*3*	*Aquifer 1*	*29*	*24*
Pleistocene	*Upper*	Q_{I}^{3}		*4*	*Aquitard 2*	*53*	*22*
			qp_3	*5*	*Aquifer 2*	*70*	*14*
	Middle	Q_{I}^{2-3}		*6*	*Aquitard 3*	*97*	*39*
			qp_{2-3}	*7*	*Aquifer 3*	*123*	*13*
	Lower	Q_{I}^{1}		*8*	*Aquitard 4*	*149*	*39*
			qp_1	*9*	*Aquifer 4*	*180*	*21*
Pliocene	*Upper/Middle*	N_2^3/N_2^2		*10*	*Aquitard 5*	*212*	*44*
			n_2^2	*11*	*Aquifer 5*	*242*	*18*
	Lower	N_2^1		*12*	*Aquitard 6*	*271*	*38*
			n_2^1	*13*	*Aquifer 6*	*302*	*21*
Miocene	*Upper*	N_1^3		*14*	*Aquitard 7*	*332*	*41*
			n_1^3	*15*	*Aquifer 7*	*382*	*59*

C.2 Hydrogeological model setup

Table C.2 *Description of the hydrogeological model setup*

Simulation setup	Description
Boundary conditions	
Recharge	*Measured precipitation (1991-2010); average values used (20 11-2015)*
Evaporation	*Measured evaporation (1999-2010); average values used (1991-1998/20 11-2015)*
Drainage	*-0.5m below surface elevation*
Constant head boundary (sea)	*Boundary is set 50 km off-shore with a constant head for layer 1 and 2 equal to mean sea level*
No flow boundary (bedrock)	*Boundary set at bedrock outcrops at the surface and 20 km across the Cambodian border*
Initial conditions	
Hydraulic head	*Steady-state simulation without extraction*
Start transient simulation	*January 15th, 1991*
End transient simulation	*December 15th, 2015*
Solution	
Absolute convergence criteria	*0.01*
Maximum iteration	*15*
Time step	*30 days (sensitivity to time step discretization was tested and found negligible)*
Groundwater extraction	
	Registered daily amount starting at year of registration combined with estimated of household extractions (see section C.3)

C.3 Extraction wells

C.3.1 Mekong delta

For the MKD two data sets of past groundwater are used, reporting well location (x- and y-coordinates), exploited aquifer and daily extracted volume (DWRPIS, 2010). The first dataset reports on large, industrial extraction wells with an extraction permit (>200 m^3 day^{-1}) covering the start of the modelling period until 2011. The year of registration is assumed to be the starting point of the extraction, and the permitted volume to be the actual daily extraction value. The second dataset is based on a large delta-wide survey held in 2010 using household density and interviews to estimate well depth and daily extraction by the Division of Water Resources Planning and Investigation of South Vietnam (DWRPIS). The outcomes of the survey were grouped in fictive well locations randomly distributed over freshwater zones for each province with extraction rates to match total reported provincial extractions for each aquifer (Table C.3). We assumed that the unregistered household groundwater equally grew with the industrial demand. Therefore, the growth recorded in the registered industrial extractions was used to extrapolate the 2010 survey results back to 1991. Following 2011, an annual increase of 2.5% was assumed. This results in a total extraction in the MKD approaching 2.5 million m^3 day^{-1} at the end of the modelling period (Fig. 5.3). The Lower Pleistocene (48% of the total volume) and the Lower Pliocene (26% of the total volume) aquifers are the most heavily-exploited in the MKD (Figure C.1).

C.3.2 Ho Chi Minh province

Three datasets were combined to determine the extraction of groundwater in the HCMC province. The first dataset reports small extractions (<10 m^3 day^{-1}) per aquifer but lacked location information. The second dataset documented larger extractions (>10 m^3 day^{-1}) per aquifer including well coordinates. Subsequently, assuming similar extraction patterns, these well locations were adopted for the first dataset (Fig. C.2). The year of commissioning for both datasets was unknown. The third dataset discloses registered extractions in the Holocene and Lower Pleistocene aquifer including location and year of construction until 2015. Combined extraction reported by the three datasets (until 2008) nearly matches the total groundwater exploitation reported for 2008 by Thoang and Giao (2015) and Trung *et al* (2010) in Minh *et al* (2015) (Fig. 5.3). For this reason, the reported extractions were attributed to 2015 and subsequently extrapolated over the modelling period, adopting the volumetric growth captured in the MKD wells (1991-2007) and described in the registered extraction for HCMC (2008-2015). Total extraction modelled for HCMC exceeded 800.000 m^3 day^{-1} in the year 2010 (Table C.3).

Table C.3 | *Total modelled groundwater extraction volumes from each aquifer per province in 2010 after integration of several datasets. For HCMC the reported values are for 2008.*

Aquifer	q_h	qp_3	qp_{2-3}	qp_1	n_{22}	n_{21}	n_{13}	Total m^3 day^{-1}
An Giang	*8911*	*55,319*	*37,789*	*368*	*34,185*	*864*	*0*	*137,436*
Bac Lieu	*0*	*338*	*174,319*	*61,838*	*12,465*	*0*	*0*	*248,961*
Ben Tre	*6,859*	*6,817*	*5341*	*0*	*0*	*14,961*	*8,100*	*42,078*
Ca Mau	*0*	*160*	*265,371*	*49,859*	*52,570*	*5,532*	*0*	*373,492*
Can Tho	*0*	*2,628*	*146,872*	*0*	*41,972*	*0*	*100*	*191,573*
Dong Thap	*0*	*242*	*1,426*	*0*	*114,743*	*0*	*0*	*116,411*
Hau Giang	*0*	*11,995*	*43,234*	*7,328*	*0*	*0*	*0*	*62,557*
Kien Gian	*414*	*34,046*	*149,032*	*5,232*	*6,835*	*3,500*	*0*	*199,060*
Long An	*0*	*431*	*0*	*11,491*	*146,745*	*35,609*	*3,869*	*198,146*
Soc Trang	*1,869*	*25,306*	*189,241*	*17,186*	*0*	*0*	*11,314*	*244,916*
Tien Giang	*0*	*3,541*	*0*	*0*	*17,376*	*23,536*	*99,752*	*144,205*
Tra Vinh	*4,698*	*22*	*220,175*	*0*	*0*	*0*	*0*	*224,896*
Vinh Long	*3,461*	*42*	*18,923*	*0*	*73,525*	*21,304*	*1,669*	*118,925*
Total MKD	**26,212**	**140,889**	**1,251,723**	**153,302**	**500,416**	**105,306**	**124,804**	**2,302,654**
HCMC	*3,155*	*25,699*	*148,733*	*219,368*	*386,247*	*22,935*	*4,742*	*810,880*

C.3.3 Uncertainty in extraction data

We identify four caused of uncertainty in the developed extraction database: 1) The spatial coverage of well data is not all-inclusive (Fig. C.2). Several areas where groundwater extraction is suspected are not described in the dataset, e.g. Vinh Long city. 2) Extracted volumes over time are unknown and could be the reason for a possible underestimation of extracted volume during the 90's, resulting in the observed lag of the modelled drawdown with the measured drawdown for that period (Fig. 5.7). The large increase in documented extracted volume between the year 1999 and 2000 might also be indicative of this underestimation and might be of administrative origin (Fig. 5.3). For HCMC the mismatch at the start of the modelling period between our dataset and the volumes published by Trung *et al* (2010), in Minh *et al* (2015) potentially indicate a similar underestimation of actual extraction (Fig. 5.3). 3) Brackish groundwater extraction, e.g. for shrimp

farming, is currently not reported while it is known to potentially cause strong drawdowns and consequent subsidence (Higgins *et al* 2013). The absence of brackish groundwater extraction might explain the underestimation of the modelled hydraulic head in saline, coastal areas such as in Ben Tre and Ca Mau province. 4) Seasonal variation in extracted volume is not documented but is likely the case considering the distinct dry and wet season combined with year-round agricultural practices. This could alter the cumulative annual extracted volume, depending on what season the extraction estimates are based, as actual extraction volumes during the dry season are likely higher than during the wet season.

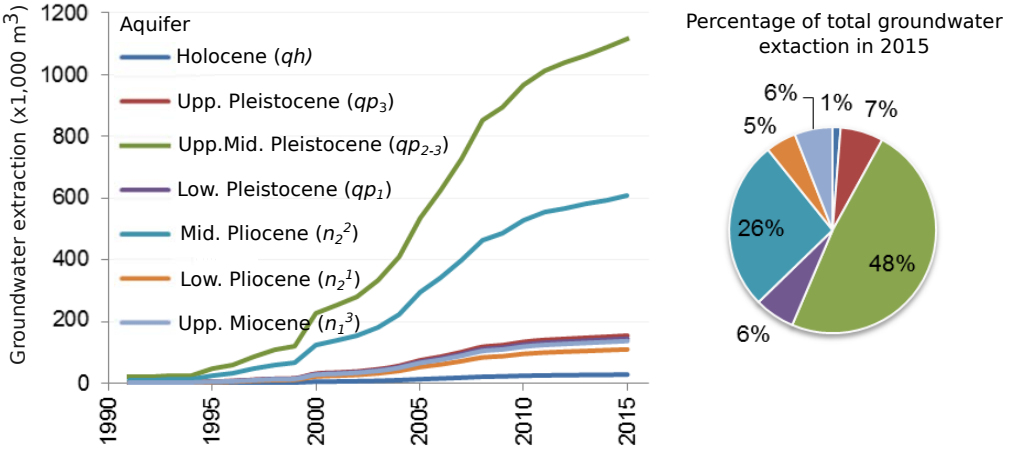

Figure C.1 | *Extracted volume for each aquifer in the MKD. The Middle Pleistocene (qp_{2-3}) aquifer is by far most exploited, followed by the Lower Pliocene aquifer (n_2^2).*

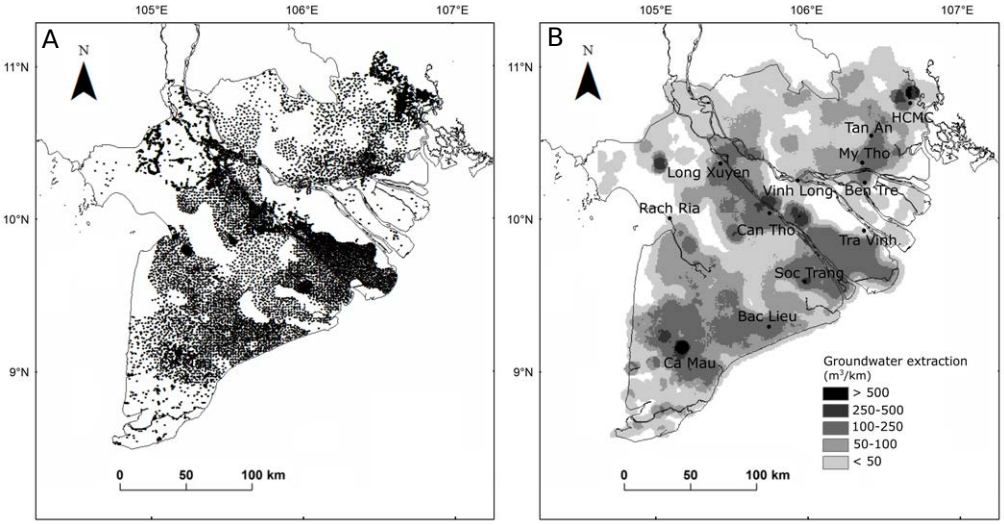

Figure C.2 | *A) Modelled extraction wells and B extracted volume adopting a 5 km radius around a single well for the year 2015. White areas depict areas with no groundwater extraction reported.*

A potential solution for the above-mentioned data deficits is to include extracted volume in the model calibration process, link extraction volume to land use practice and well locations to population density and growth over time. However, adjusting the dataset in this manner would introduce different errors and uncertainties, and requires a lot of detailed local data, as, for example, the main pumping stations producing fresh water for the city of Tra Vinh are located many kilometres away from the city.

C.4 Hydrological model parameterization

C.4.1 Initial parameterization prior to calibration

Initial values of horizontal hydraulic conductivity (K_h) for the aquifers range from 8.0 to 22.8 m day^{-1} and were derived from 999 pumping tests throughout the Mekong and the Saigon delta (DWRPIS, 2010). Aquitard layers were initially parameterized with a K_h value of 0.001 m day^{-1}. No measured data was available on the vertical anisotropy of hydraulic conductivity (K_h/K_v). We assumed a vertical anisotropy of 3, as general values of vertical anisotropy for aquifers range between the 1 and 3, with outliers up to 8 (Carlson, 2000). Initial specific storage coefficient (SS_c in m^{-1}) values for individual aquifers (ranging from 1.4×10^{-3} to 5.6×10^{-3} m^{-1}) and aquitards (ranging from 3.8×10^{-5} to 2.2×10^{-3} m^{-1}) are taken from reported values by Haskoning *et al* (1999) and Giao *et al* (2015).

C.4.2 Parameter optimisation

The automated parameter estimation in iMOD (i.e. *iPEST,* see Vermeulen *et al* 2016 for a full description of the method) was applied using piezometric head measurements from 91 monitoring wells using ten pilot points (Fig. C.3). At every pilot point, K_h and SS_c were systematically adjusted during the PEST procedure (when total model sensitivity to the parameter > 0.5%) and interpolated (simple kriging) over the entire model extend. This was done for each model layer. The maximal multiplication factor allowed for initial values for K_h and SS_c was set to 200 and 1000 for respectively the aquifer and aquitard layers to ensure realistic values. The parameter set creating the smallest error between modelled hydraulic head with measured head time series between 1995-2015 was determined through numerous iterations with each measured time series equally weighted (see also Fig. C.5 and C.6). Calibrated parameter values are within range of realistic parameter values for the expected sediments (Table C.4).

Table C.4 | *Calibrated values for horizontal hydraulic conductivity and specific storage coefficient following the automated parameter estimation.*

Model layer	Description	Calibrated horizontal hydraulic conductivity (K_h in m day^{-1}) Median *(mean)*	Calibrated specific storage coefficient (SSc in 1 m^{-1}) Median *(mean)*
Layer 1	*Phreatic top layer*	*5.0 (5.6)*	*3.0×10^{-2} (2.9×10^{-2})*
Layer 2	*Aquitard 1*	*3.3×10^{-4} (3.2×10^{-2})*	*2.6×10^{-3} (4.1×10^{-3})*
Layer 3	*Aquifer 1*	*8.2 (6.7)*	*1.1×10^{-4} (1.4×10^{-4})*
Layer 4	*Aquitard 2*	*1.1×10^{-3} (3.7×10^{-2})*	*3.8×10^{-4} (5.0×10^{-4})*
Layer 5	*Aquifer 2*	*46.8 (499.8)*	*1.2×10^{-4} (1.9×10^{-4})*
Layer 6	*Aquitard 3*	*180×10^{-2} (3.8×10^{-2})*	*1.6×10^{-4} (1.9×10^{-4})*

Layer 7	*Aquifer 3*	*59.5 (164.4)*	*5.8×10^{-5} (1.0×10^{-4})*
Layer 8	*Aquitard 4*	*5.7×10^{-4} (7.1×10^{-3})*	*1.0×10^{-4} (1.6×10^{-4})*
Layer 9	*Aquifer 4*	*11.3 (10.8)*	*5.3×10^{-5} (8.4×10^{-5})*
Layer 10	*Aquitard 5*	*3.7×10^{-3} (8.1×10^{-3})*	*7.1×10^{-5} (1.7×10^{-4})*
Layer 11	*Aquifer 5*	*67.5 (148.6)*	*5.4×10^{-5} (1.1×10^{-4})*
Layer 12	*Aquitard 6*	*2.6×10^{-3} (2.9×10^{-3})*	*5.9×10^{-5} (2.1×10^{-4})*
Layer 13	*Aquifer 6*	*39.5 (43.0)*	*5.7×10^{-5} (1.3×10^{-4})*
Layer 14	*Aquitard 7*	*1.1×10^{-3} (1.1×10^{-3})*	*5.3×10^{-5} (2.1×10^{-4})*
Layer 15	*Aquifer 7*	*6.8 (7.3)*	*8.6×10^{-5} (5.5×10^{-4})*

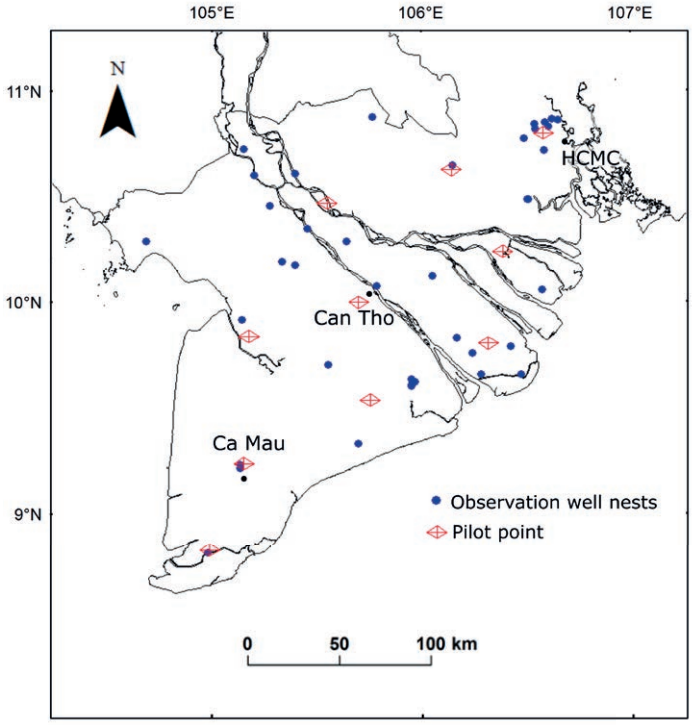

Figure C.3 | *Locations of observation wells and pilot points used during the automated parameter estimation (iPEST).*

C.5 Geotechnical parameterization

C.5.1 Determining the geotechnical parameters

The geotechnical parameterization for the *abc* model of the MKD subsurface was based on general relationships existing among compression parameters, combined with local geotechnical data. The following section explains the steps taken to determine model parameters. A summary of the used parameters is given in table C.5.

As void ratio generally decreases with depth, we empirically derived a depth-dependent void ratio relationship based on a bulk analysis of almost 40,000 geotechnical samples from HCMC province (Bakr *et al* 2013):

$$e_0 = 0.2214 * \ln(z) + 1.5248 \quad \text{(C.1)}$$

Where e_0 is void ratio and z is depth below surface (m). Through this relation, an estimate of e_0 was made for each model layer, using its average depth. The primary compression index (C_c) can be successfully estimated using correlations based on e_0 (Widodo and Ibrahim, 2012). Hence, we determined the C_c for each model layer using the following correlation (Higashi *et al* 2002 in Ohtsubo *et al* 2006):

$$C_c = 0.343 * e_0^{1.328} \quad \text{(C.2)}$$

As sand is on average 20 times less compressible than clays and silts (Table 2.b in NNI, 2012), the for the sandy aquifers was subsequently corrected for this factor.

The recompression index (C_r) was determined using local geotechnical data, following the linear relationship existing between the C_c and C_r indices (Gunduz and Arman, 2007). For the clayey aquitards, we found a C_c/C_r ratio of 5 based on the analysis of Mekong delta clays (Toan and Nu, 2013) and for the sandy aquifers a C_c/C_r ratio of 3, based on data from HCMC (Thoang and Giao, 2015).

Subsequently, the primary compression ratios, *CR* (compression ratio) and *RR* (recompression ratio), were derived from the C_c and C_r indices and the void ratio by:

$$CR = \frac{C_c}{1+e_o} \;,\; RR = \frac{C_r}{1+e_o} \quad \text{(C.3)}$$

In principle, for a specific sediment, both compression ratios are independent of depth, however, the above approach introduces a decreasing trend with depth. Physically, this can be explained by a successive coarsening trend in lithology, which is the case for the Mekong delta (Fig. C.4). The derived compression ratios for the shallow aquitards correspond to typical values associated with pure clays, and gradually decrease towards characteristic values for respectively weak sandy clay, sandy clay/loam and sandy loam for the deeper aquitards (Table 2.b in NNI, 2012).

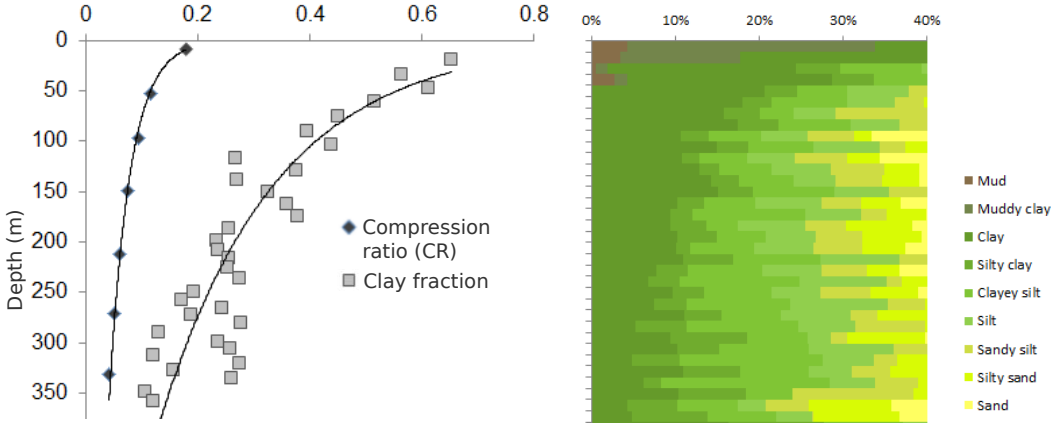

Figure C.4 *| Left: Depth-dependent compression ratio (CR) for aquitards in-line with a decreasing clay fraction with depth. Right: Lithoclass distribution of the 40% finest grained deposits in the Mekong delta, corresponding to the viscoplastic active part of the aquitards in the subsurface model. The coarsening trend in the lithoclasses with depth is clearly visible.*

The coefficient of secondary compression (C_a) for the aquitards was determined using a C_a/CR ratio of 0.04 (Mesri and Godlewski, 1977; Ladd *et al* 1977). We assume no secondary compression taking place in the sandy aquifers, therefore C_a is set to zero. For a similar reason, the sandy part in the aquitard layers (1/3 of the total layer thickness) was excluded from compression calculations.

As the *abc* model is based on natural (or Hencky) strain, the final step was to convert the *CR*, *RR* and C_a to, respectively, the *a, b* and *c*. For low strain levels, which is the case in the model, the following relationships apply:

$$\begin{aligned} a &= RR / \ln(10) \approx 0.434\,\mathrm{RR} \\ b &= CR / \ln(10) \\ c &= C_a / \ln(10) \end{aligned} \qquad \text{(C.4)}$$

Table C.5 | *Parameterization used for subsidence modelling. The top phreatic layer and the bottom aquifer layer in the model were excluded from the subsidence calculations.*

Model layer	Description	RR	CR	C_a	*a*	*b*	*c*
Layer 2	*Aquitard 1*	*3.6E-02*	*1.8E-01*	*7.1E-03*	*1.6E-02*	*7.8E-02*	*3.1E-03*
Layer 3	*Aquifer 1*	*2.3E-03*	*6.9E-03*	*0.0E+00*	*1.0E-03*	*3.0E-03*	*0.0E+00*
Layer 4	*Aquitard 2*	*2.3E-02*	*1.2E-01*	*4.7E-03*	*1.0E-02*	*5.1E-02*	*2.0E-03*
Layer 5	*Aquifer 2*	*1.8E-03*	*5.3E-03*	*0.0E+00*	*7.7E-04*	*2.3E-03*	*0.0E+00*
Layer 6	*Aquitard 3*	*1.9E-02*	*9.3E-02*	*3.7E-03*	*8.1E-03*	*4.0E-02*	*1.6E-03*
Layer 7	*Aquifer 3*	*1.4E-03*	*4.2E-03*	*0.0E+00*	*6.1E-04*	*1.8E-03*	*0.0E+00*
Layer 8	*Aquitard 4*	*1.5E-02*	*7.6E-02*	*3.0E-03*	*6.6E-03*	*3.3E-02*	*1.3E-03*
Layer 9	*Aquifer 4*	*1.1E-03*	*3.4E-03*	*0.0E+00*	*4.9E-04*	*1.5E-03*	*0.0E+00*
Layer 10	*Aquitard 5*	*1.2E-02*	*6.1E-02*	*2.4E-03*	*5.3E-03*	*2.6E-02*	*1.1E-03*
Layer 11	*Aquifer 5*	*9.2E-04*	*2.8E-03*	*0.0E+00*	*4.0E-04*	*1.2E-03*	*0.0E+00*
Layer 12	*Aquitard 6*	*1.0E-02*	*5.0E-02*	*2.0E-03*	*4.4E-03*	*2.2E-02*	*8.7E-04*
Layer 13	*Aquifer 6*	*7.6E-04*	*2.3E-03*	*0.0E+00*	*3.3E-04*	*9.9E-04*	*0.0E+00*
Layer 14	*Aquitard 7*	*8.3E-03*	*4.1E-02*	*1.7E-03*	*3.6E-03*	*1.8E-02*	*7.2E-04*

C.5.2 Implication of the simplified groundwater-subsidence modelling approach

We used a one-way coupling approach to relate hydraulic head development and subsidence in the sense that we first model hydraulic head development with a conventional groundwater model, and then use the hydraulic heads as a function of space and time to drive the subsidence module. However, ideally or formally, a fully (two-way) coupled solution is required to ensure consistency between the strain (or compression) rates in the subsidence module on the one hand, and the storage rates in the groundwater model on the other. The simplified one-way approach was adopted because calibration of the fully-coupled model would demand excessive computation time.

To check the consistency between the independently calibrated specific storage values of the groundwater model and the compression behaviour of the subsidence module, we calculated elastic and 'virgin' specific storage values for the model aquitards from the compression (*a* or C_r or *RR* and *b* or C_c or *CR*) parameter values and estimates of the effective stress. The calculated elastic values were found to differ from the calibrated values by a factor ranging between 0.05 and 0.4, and the calculated 'virgin' values by a factor ranging between 0.3 and 2.2. The fact that these values are reasonably close to 1 indicates fair consistency. A model run in which the calibrated specific storage values of the aquitards were replaced by the compression-parameter based specific storage values

(taking the mean value of the elastic and 'virgin' values) yielded slightly higher subsidence values (average value of cumulative delta-wide subsidence was ~2% higher). Thus although the parameters in the groundwater and subsidence model are not fully coupled, the potential impact on the modelled subsidence values falls well within the reported range of modelled subsidence associated with uncertainty in model parameters in general.

Another uncertainty arises from the current aquitard discretization, which might not be refined enough in a vertical direction to correctly represent the delayed propagation of pressure decline in the less permeable layers. The majority of the model is behaving quasi-steady with very limited delays in pressure decline propagation. This implies that the current layer-discretization is sufficient for this delta-wide model, however it is not the case everywhere in the model and could still contribute to model uncertainty.

C.6 Modelled versus measured hydraulic head

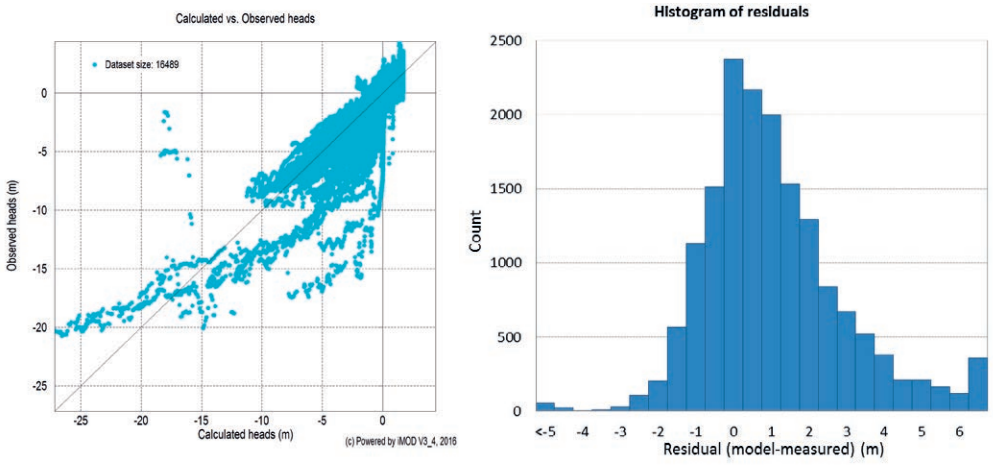

Figure C.5 | *Left: Scatterplot of measured versus modelled hydraulic heads for the MKD. Every point represent a monthly measurement of absolute head versus modelled head for the same month (average r2 = 0.73; median cross-correlation (r) = 0.94). Right: Histogram of residuals for the MKD. Of the modelled heads, >75% are within 2 meters of observed heads. Largest residuals are from monitoring wells around Ca Mau city. Residuals are positive when modelled head > observed head.*

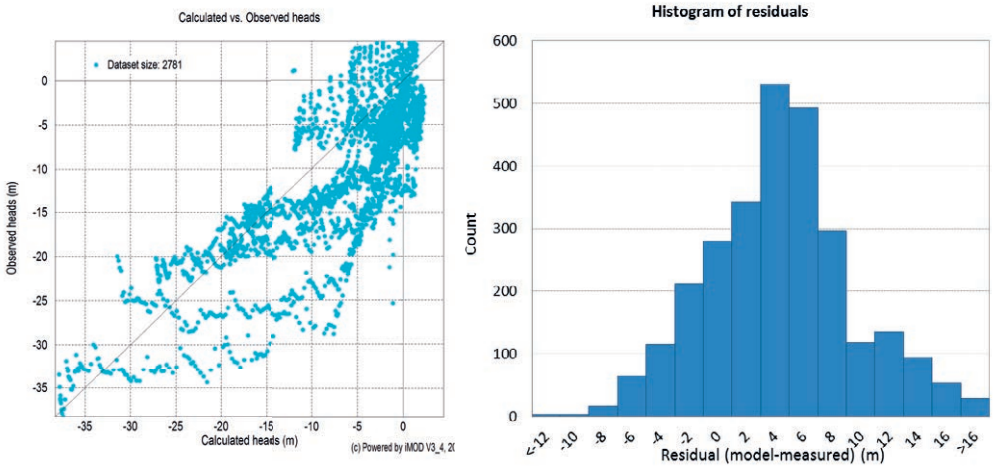

Figure C.6 | *Left: Scatterplot and residual graph of the HCMC wells. Clearly, the observed head increasingly exceeds the calculated head with increased drawdown. Right: Histogram of residuals for HCMC province, showing the structural underestimation of observed heads by the model. Residuals are positive when modelled head > observed head.*

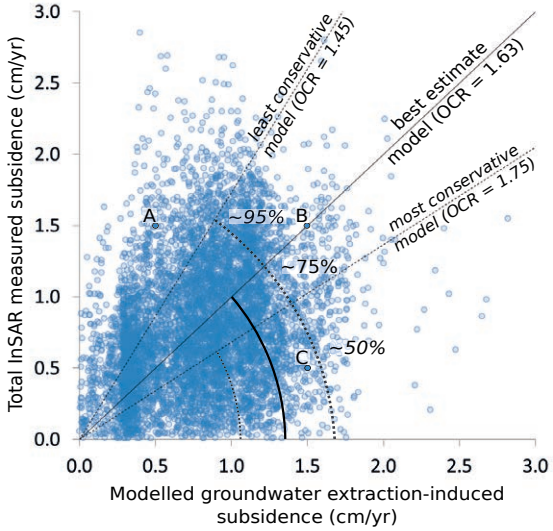

Figure C.7 | *Fit between modelled groundwater extraction-induced subsidence and InSAR-measured subsidence for the MKD (Erban et al 2014) upscaled to model resolution for the best estimate model. Linear fits (y=1x; modelled equals measured subsidence) is shown for the best estimate model (overconsolidation ratio (OCR) of 1.63) and, respectively, for the least and most conservative models with OCRs of 1.45 and 1.75 (data is not shown in this figure). The best estimate model has a rather low cross-correlation (r) of 0.28 which is to be expected as total InSAR measured subsidence and groundwater extraction induced subsidence do not correlate in absolute values (discussed in the main manuscript section: Subsidence in the Mekong Delta). A relative correlation between the two is present, shown by a Spearman's rank-order correlation (ρ) of 0.73. Subsidence rates are in average annual rates over the period 2006-2010.*

C.7 Modelled versus measured subsidence

A direct cell-by-cell comparison between upscaled InSAR-measured subsidence (Erban et al., 2014) (see Section C.8 on upscaling) and modelled groundwater extraction-induced subsidence is shown in Fig. C.7. The percentages give the part of the total InSAR-measured subsidence reproduced by modelled groundwater extraction-induced subsidence. The calculation is illustrated by the following example for Fig. C.7. Point A: 1.5/0.5 cm yr^{-1}, measured > modelled subsidence = 33% explained by the model; Point B: 1.5/1.5 cm yr^{-1} = measured equals modelled subsidence = 100% explained by the model; Point C: 0.5/1.5 cm yr^{-1}, measured < modelled subsidence = 100% explained by the model. The percentages in the figure are the average values of all cells.

C.8 Data resampling and calculating statistics

C.8.1 Resampling InSAR-measured subsidence rates

The spatial resolution of the InSAR-measured subsidence rates as presented by Erban *et al* (2014) (300 m^2) differs from the modelled subsidence cell size (1 km^2). To enable direct comparison, the InSAR-measured subsidence rates were resampled using a median bilinear interpolation creating a weighted value to match the model cell size and raster position.

C.8.2 Calculation of spatial statistics on model results

When MKD is explicitly mentioned in the text, this means that model and InSAR measurements outside of the MKD, i.e. HCMC province and Cambodia, are not included in the analysis. As the extraction database does not provide a full spatial coverage of the delta, values of reported average subsidence caused by groundwater extraction are calculated only for parts of the MKD inside a 5 km radius of an extraction with extraction amounts exceeding 5 m^3 km^2 day^{-1} (Fig C.4b). Average subsidence values reported for HCMC were calculated over the area for which >50 cm of total subsidence in the best estimate model was calculated (Fig. 5.6).

Appendix D

Supplement to chapter 6

This is part of the publication: Minderhoud, P.S.J., Middelkoop, H., Erkens, G., Stouthamer, E. . **Groundwater extraction may drown the Mekong delta.** *(Submitted)*

D.1 Model update: surface water network

The surface water system of the Mekong delta was explicitly included in the model. The input data on the surface water system was created by dividing the surface water network into four categories, i.e. main river channels, secondary river channels, main canals and secondary canals. Average width and depth estimates for each category were used to determine river depth (Fig. D.1). River stage measurement time series from 1999 to 2010 from 39 locations in the main and secondary rivers (Bui et al., 2013) were interpolated to derive average annual river stage for the entire delta (Fig. D.1 right.).

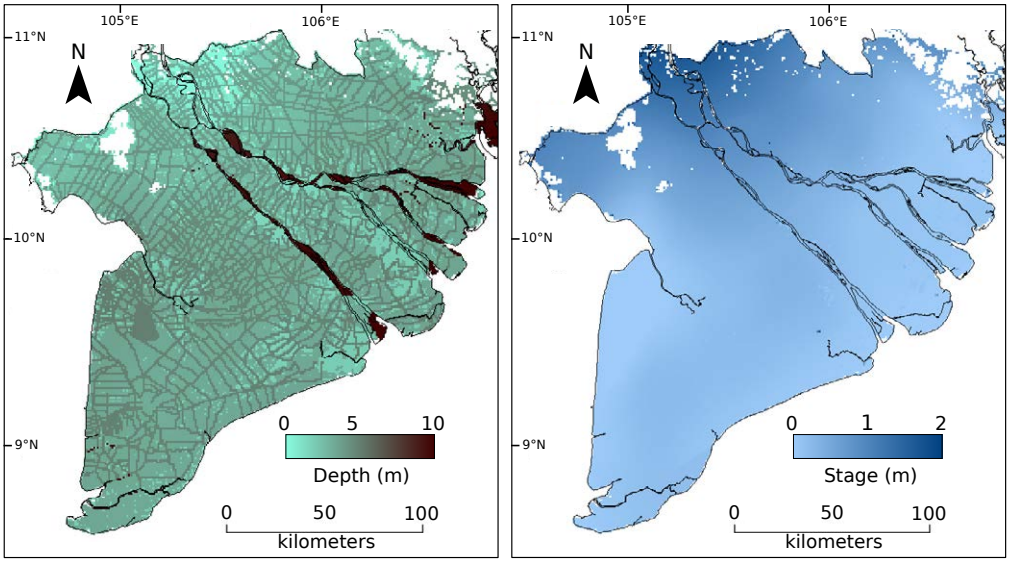

Figure D.1 | *Depth (left) and stage (right) of the modeled surface water system of the Mekong delta. Depth in meter below the surface elevation and based on average values for each of the four surface water categories. Surface water level was determined by interpolating the average river stage from measurements between 1999-2010 at 39 locations in the delta.*

D.2 Overconsolidation ratios used for subsidence modeling

Previous overconsolidation ratio (OCRs) values for the least and most conservative model used in Chapter 5 covered a relatively wide range. The result of this is that the least and most conservative models were only supported by specific observations in the delta. Therefore, we decided to narrow the difference between the least and most conservative model down to a 0.1 deviation of the OCR value of the best estimate model (1.53-1.73 instead of 1.45-1.75 used in the previous model) which seems to provide a more realistic range of average OCR values better matching the observed subsidence rates (Fig. D.2).

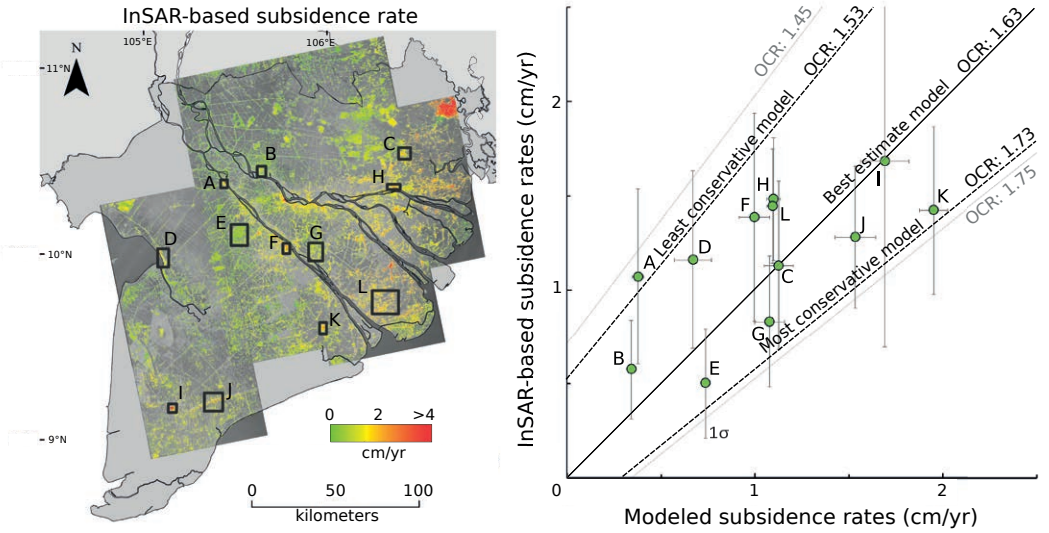

Figure D.2 | *InSAR-based subsidence rates (left) and comparison with modeled subsidence rates in the delta for different overconsolidation ratios (OCR). The OCR ratios from 1.53 to 1.73 provide a narrower and more supported range for the least to the most conservative model.*

D.3 Modeled groundwater extraction

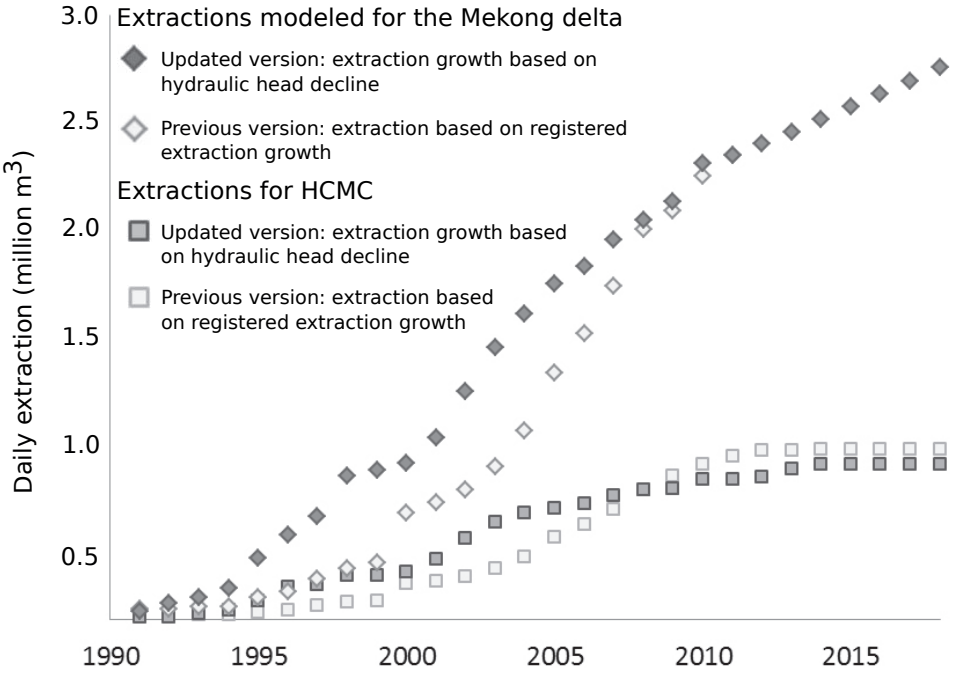

Figure D.3 | *Annual modeled groundwater extraction in the Mekong delta and HCMC province of the previous model version of Chapter 5 and the updated version (Chapter 6).*

D.4 Model update: modeled past groundwater extraction

The volumetric growth of unregistered groundwater extraction in the Mekong delta and Ho Chi Minh city (HCMC) province was updated and based on hydraulic head decline in confined aquifers instead of registered extraction wells, as was the case in the previous version. This was done by calculating the *annual* average hydraulic head drop for each aquifer as a percentage of the total hydraulic head drop during the period 1991 – 2011. Only observation wells were included that were located in areas with extraction showing hydraulic head decline. For years in which individual time series of hydraulic head show negative head change, a zero percent growth was adopted. Measurements from the semi-confined Holocene aquifer were not included as their signal was dominated by seasonality rather than groundwater extraction. Eventually, the adopted percentual growth of extraction volume between 1991 and 2011 was based on the average percentual hydraulic head decline of the six confined aquifers. This was done for both the Mekong delta as HCMC province separately. After 2011 the extractions have increased annually 2.5% according to estimates by the Division of Water Resources Planning and Investigation for the South of Vietnam (DWRPIS). For HCMC the amount of extractions stabilized following a Water act in 2007. Fig. D.3 shows the updated annual extraction volume compared to previous version of Chapter 5.

Apparently, the assumption in the previous model version that the registered groundwater extraction volume growth was also representative for the unregistered extractions created a bias that resulted in a too low extraction volume at the start of the modeling period (1991-2000) and an overestimation towards the end (2005-2015). The hydraulic heads in the updated model showed less underestimation of hydraulic head drop at the start of the calibration period (1991-2000) and less overestimation towards the end (2005-2015) compared to the previous version of the hydrogeological model of the Mekong delta (Fig. D.4). The cross-correlation (r^2) between modeled and measured hydraulic head for this location also improved from 0.94 to 0.97 for the updated model.

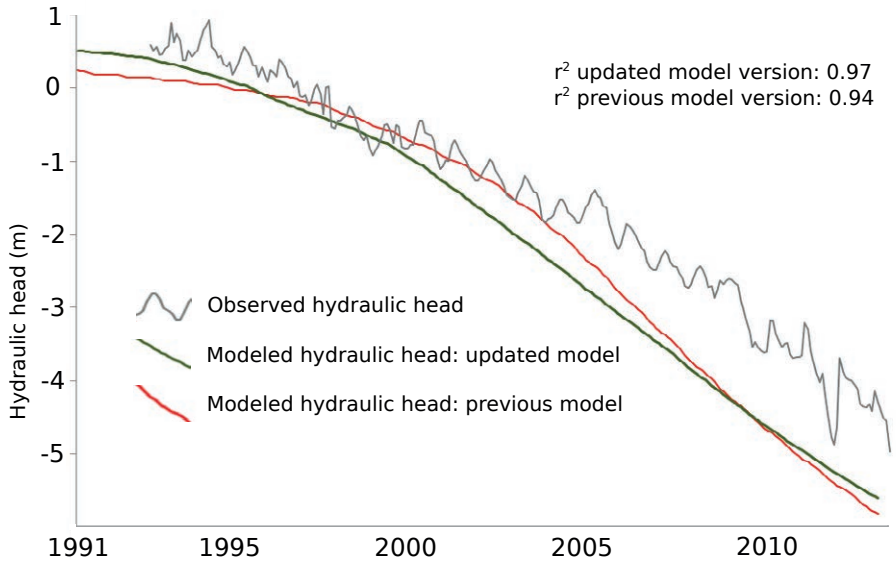

Figure D.4 *| Example of modeled hydraulic head of both the updated and previous model compared to measured hydraulic head of the Middle Pleistocene aquifer near Can Tho city.*

Both updates significantly increase the overall performance of the model. In the previous version the correlation coefficient (r^2) between all observed and the modeled hydraulic heads in the confined aquifers was 0.69. Modeling the surface water system explicitly improved the overall r^2 to 0.73 and linking the growth in extraction volume on hydraulic head decline improved the r^2 to 0.75. Combined, the r^2 of the observed and the modelled heads of the updated model became 0.78.

D.5 Model update: effects on modeled subsidence rates

In the updated version of the model, the hydraulic head drop was simulated more gradually and dropped less in absolute values from 1991 to present, creating a better fit with the observed hydraulic heads (section D.4). As a result, the modeled extraction-induced subsidence rates by the updated model are slightly lower compared to the previous model version. The previous model version quantified an average delta-wide subsidence rate of 11 *(7-18)* mm yr^{-1} (best estimate – *most* and *least conservative* – model*)* and a total average cumulative subsidence of ~18 *(9-53)* cm of the Mekong delta plain for 2015. The updated model provides slightly lower extraction-induced subsidence quantifications, namely an average delta-wide subsidence rate of 9 *(5-13)* mm yr^{-1} and a total average cumulative subsidence of ~17 *(9-33)* cm. Note also that the range between the most and least conservative model is smaller due to a narrower OCR range. Although the subsidence quantifications for 2015 have changed somewhat, they are still well within the previously reported uncertainty range.

D.6 Supplementary modeling results

Table D.1 | *Average hydraulic head of the aquifer system for different scenarios at given time intervals.*

	Average hydraulic head (m)				
Scenario	**2018**	**2025**	**2050**	**2075**	**2100**
B2 Extreme extraction increase (4% annual growth)	*-6.5*	*-9.2*	*-20.8*	*-33.9*	*-47.8*
B1 Moderate extraction increase (2% annual growth)		*-8.8*	*-16.2*	*-23.3*	*-30.4*
M1 Stable extraction (0% growth after 2020)		*-8.5*	*-11.7*	*-12.9*	*-13.5*
M2 Stable groundwater levels (50% volume reduction)		*-7.3*	*-6.5*	*-6.5*	*-6.5*
M3 Recovery of groundwater levels (75% volume reduction)		*-7.3*	*-4.3*	*-3.5*	*-3.2*
M4 Full extraction stop (zero extraction after 2018)		*-3.8*	*-0.8*	*0.0*	*0.2*

Table D.2 | *Average subsidence rates under different extraction scenarios for the Mekong delta.*

	Subsidence rate (mm yr^{-1})			
Scenario	**2025**	**2050**	**2075**	**2100**
B2 Extreme extraction increase (4% annual growth)	*10.0 (6.9-12.8)*	*12.5 (10.5-13.7)*	*13.1 (12.0-13.6)*	*12.9 (12.3-13.1)*
B1 Moderate extraction increase (2% annual growth)	*8.9 (5.9-11.7)*	*8.5 (6.7-9.6)*	*8.0 (7.0-8.5)*	*7.6 (7.0-7.9)*
M1 Stable extraction (0% growth after 2020)	*8.1 (5.2-10.7)*	*5.0 (3.5-5.9)*	*3.4 (2.6-3.8)*	*2.5 (2.0-2.7)*
M2 Stable groundwater levels (50% volume reduction)	*5.5 (2.9-7.9)*	*2.9 (1.7-3.7)*	*2.2 (1.5-2.6)*	*1.8 (1.3-2.0)*
M3 Recovery of groundwater levels (75% volume reduction)	*5.5 (2.9-7.9)*	*1.9 (1.0-2.7)*	*1.6 (1.0-2.0)*	*1.4 (0.9-1.7)*
M4 Full extraction stop (zero extraction after 2018)	*1.7(-0.2-3.5)*	*1.6(0.7-2.3)*	*1.4(0.8-1.8)*	*1.2(0.7-1.5)*

Table D.3 | *Average cumulative subsidence under different extraction scenarios for the Mekong delta.*

	Average cumulative subsidence (cm)					
	Since 1991		After 2000		After 2018	
Scenario	**2050**	**2050**	**2050**	**2100**	**2050**	**2100**
B2	*55 (37-79)*	*120 (96-147)*	*50 (35-65)*	*114 (94-133)*	*35 (27-42)*	*100 (86-110)*
B1	*47 (31-71)*	*87 (65-114)*	*42 (29-58)*	*82 (63-100)*	*28 (20-35)*	*68 (55-77)*
M1	*41 (25-64)*	*58 (38-84)*	*36 (23-51)*	*53 (36-70)*	*22 (14-28)*	*39 (28-48)*
M2	*33 (18-56)*	*44 (25-69)*	*28 (16-42)*	*39 (23-56)*	*14 (8-19)*	*25 (15-33)*
M3	*30 (16-53)*	*39 (21-63)*	*25 (14-39)*	*34 (19-50)*	*11 (5-16)*	*19 (10-27)*
M4	*24 (11-46)*	*31 (15-55)*	*19 (9-32)*	*26 (13-41)*	*5 (1-9)*	*12 (4-18)*

D.7 Absolute sea-level rise following RCP scenarios

Table D.4 | *Projections of absolute sea-level rise based on RCP climate change scenarios (Church et al., 2013).*

	Rates (mm yr^{-1})				Cumulative since 2000 (cm)		
Climate change scenario	*2000*[1]	*2018*[2]	*2050*[2]	*2100*[1]	*2018*	*2050*	*2100*
RCP 2.6	*3.2*	*3.4*	*3.8*	*4.4*	*6.3*	*17.9*	*26.5*
RCP 8.5	*3.2*	*4.6*	*7.2*	*11.2*	*7.4*	*38.4*	*72.7*

[1] *Rates from Church et al., (2013)*
[2] *Interpolated from rates from 2000 and 2100*

References

Abidin, H.Z., Andreas, H., Gumilar, I., Fukuda, Y., Pohan, Y.E., Deguchi, T., 2011. Land subsidence of Jakarta (Indonesia) and its relation with urban development. Nat. Hazards 59, 1753–1771. doi:10.1007/s11069-011-9866-9.

Addink, E.A., Van Coillie, F.M.B., de Jong, S.M., 2012. Introduction to the GEOBIA 2010 special issue: From pixels to geographic objects in remote sensing image analysis. Int. J. Appl. Earth Obs. Geoinf. 15, 1–6. doi:10.1016/j.jag.2011.12.001.

Aguilar, F., Aguilar, M., Agüera, F., Sánchez, J., 2006. The accuracy of grid digital elevation models linearly constructed from scattered sample data. Int. J. Geogr. Inf. Sci. 20, 169–192. doi:10.1080/13658810500399670.

Allison, M.A., Nittrouer, C.A., Ogston, A.S., Mullarney, J.C., Nguyen, T.T., 2017. Sediment and survival of the Mekong Delta: A case study of decreased sediment supply and accelerating rates of relative sea level rise. Oceanography 30, 98–109. doi:10.5670/oceanog.2017.318.

Anderson, B.H.R., 1978. Hydrogeologic Reconnaissance of the Mekong Delta in. U.S. Geol. Surv. Water-Resources Water-Resources Investig. Pap. 1608-R.

Anthony, E.J., 2015. Wave influence in the construction, shaping and destruction of river deltas: A review. Mar. Geol. 361, 53–78. doi:10.1016/j.margeo.2014.12.004.

Anthony, E.J., Brunier, G., Besset, M., Goichot, M., Dussouillez, P., Nguyen, V.L., 2015. Linking rapid erosion of the Mekong River delta to human activities. Sci. Rep. 5, 14745. doi:10.1038/srep14745.

Asselen, S. Van, Stouthamer, E., Asch, T.W.J. Van, 2009. Earth-Science Reviews Effects of peat compaction on delta evolution: A review on processes , responses , measuring and modeling. Earth Sci. Rev. 92, 35–51. doi:10.1016/j.earscirev.2008.11.001.

Bakr, M., de Lange, G., Toan, D.N., 2013. Ho Chi Minh City Flood and Inundation Management - Final Report, Volume 2: IFRM Strategy, Annex 3: Land Subsidence - Royal Haskoning-DHV and Deltares.

Benner, S.G., Polizzotto, M.L., Kocar, B.D., Ganguly, S., Phan, K., Ouch, K., Sampson, M., Fendorf, S., 2008. Groundwater flow in an arsenic-contaminated aquifer, Mekong Delta, Cambodia. Appl. Geochemistry 23, 3072–3087. doi:10.1016/j.apgeochem.2008.06.013.

Biffi, C.A., Tuissi, A., 2017. Stato dell'arte sulle tecniche di produzione additiva per metalli, in: Metallurgia Italiana. pp. 5–10. doi:10.1017/CBO9781107415324.004.

Binh, T.N.K.D., Vromant, N., Hung, N.T., Hens, L., Boon, E.K., 2005. Land cover changes between 1968 and 2003 in Cai Nuoc, Ca Mau Peninsula, Vietnam. Environ. Dev. Sustain. 7, 519–536. doi:10.1007/s10668-004-6001-z.

Bjerrum, L., 1967. Engineering Geology of Norwegian Normally-Consolidated Marine Clays as Related to Settlements of Buildings. Géotechnique 17, 83–118. doi:10.1680/geot.1967.17.2.83.

Blaschke, T., 2010. Object based image analysis for remote sensing. ISPRS J. Photogramm. Remote Sens. 65, 2–16. doi:10.1016/j.isprsjprs.2009.06.004.

Bouvet, A., Le Toan, T., 2011. Use of ENVISAT/ASAR wide-swath data for timely rice fields mapping in the Mekong River Delta. Remote Sens. Environ. 115, 1090–1101. doi:10.1016/j.rse.2010.12.014.

Bozzano, F., Esposito, C., Franchi, S., Mazzanti, P., Perissin, D., Rocca, A., Romano, E., 2015. Understanding the subsidence process of a quaternary plain by combining geological and hydrogeological modelling with satellite InSAR data: The Acque Albule Plain case study. Remote Sens. Environ. 168, 219–238. doi:10.1016/j.rse.2015.07.010.

Breiman, L., 2001. Random forests. Mach. Learn. 45, 5–32. doi:10.1017/CBO9781107415324.004.

Breiman, L., Cutler, A., 2003. Random forests manual v4. Tech. report. UC Berkel.

Bridge, J.S., 2003. Rivers and Floodplains: Forms, Processes, and Sedimentary Record. Wiley-Blackwell.

Brown, S., Nicholls, R.J., 2015. Subsidence and human influences in mega deltas: The case of the Ganges–Brahmaputra–Meghna. Sci. Total Environ. 527–528, 362–374. doi:10.1016/j.scitotenv.2015.04.124.

Brunier, G., Anthony, E.J., Goichot, M., Provansal, M., Dussouillez, P., 2014. Geomorphology Recent morphological changes in the Mekong and Bassac river channels , Mekong delta : The marked impact of river-bed mining and implications for delta destabilisation. Geomorphology 224, 177–191. doi:10.1016/j.geomorph.2014.07.009.

Bui, V.T., Ngo, D.C., Le, H.N., Dang, V.T., 2013. Assessment of Climate Change on Groundwater Resources in Mekong Delta, Proposal of Adaptation Measures, Division of Water Resources and Planning Investigation for the South of Viet Nam, Archives of Dept. of Water Resources Management of Vietnam, Hanoi.

Buisman, K., 1936. Results of Long Duration Settlement Tests. Proceeding 1st Int. Conf. Soil Mech. Found. Eng. Cambridge, Massachusetts 1, 103–106.

Carew-Reid, J., 2008. Rapid Assessment of the Extent and Impact of Sea Level Rise in Viet Nam, Climate Change. ICEM - Int. Cent. Environ. Manag.

Carlson, D., 2000. Estimate of Vertical Anisotropy of Hydraulic Conductivity for Northern Louisiana Aquifers from Grain-Size Data 32–42.

Chambers, J.M., Cleveland, W.S., Kleiner, B., Tukey, P. a., 1983. Graphical methods for data analysis. Wadsworth International Group, Duxbury Press, Boston.

Chapuis, R.P., 2012. Predicting the saturated hydraulic conductivity of soils: a review. Bull Eng Geol Env. 71, 401–434. doi:10.1007/s10064-012-0418-7.

Chen, C.F., Son, N.T., Chang, L.Y., 2012. Monitoring of rice cropping intensity in the upper Mekong Delta, Vietnam using time-series MODIS data. Adv. Sp. Res. 49, 292–301. doi:10.1016/j.asr.2011.09.011.

Church, J.A., Clark, P.U., Cazenave, A., Gregory, J.M., Jevrejeva, S., Levermann, A., Merrifield, M. a., Milne, G. a., Nerem, R.., Nunn, P.D., Payne, A.J., Pfeffer, W.T., Stammer, D., Unnikrishnan, A.S., 2013. Sea level change, in: Climate Change 2013: The Physical Science Basis. Contribution of Working Group I to the Fifth Assessment Report of the Intergovernmental Panel on Climate Change. pp. 1137–1216.

Clennell, M.B., Dewhurst, D.N., Brown, K.M., Westbrook, G.K., 1999. Permeability anisotropy of consolidated clays. Muds Mudstones Phys. Fluid Flow Prop. 158, 79–96. doi:10.1144/GSL.SP.1999.158.01.07.

Coleman, J.M., Roberts, H.H., 1989. Deltaic coastal wetlands, Coastal Lowlands: Geology and Geotechnology. Springer Netherlands, Dordrecht. doi:10.1007/978-94-017-1064-0_1.

Cook, A., Merwade, V., 2009. Effect of topographic data, geometric configuration and modeling approach on flood inundation mapping. J. Hydrol. 377, 131–142. doi:10.1016/j.jhydrol.2009.08.015.

Cosslett, T.L., Cosslett, P.D., 2014. Water Resources and Food Security in the Vietnam Mekong Delta. Springer International Publishing, Cham. doi:10.1007/978-3-319-02198-0.

Dang, T.D., Cochrane, T.A., Arias, M.E., Van, P.D.T., de Vries, T., 2016. Hydrological Alterations From Water Infrastructure Development in the Mekong Floodplains. Hydrol. Process. doi:10.1002/hyp.10894.

Darby, S.E., Hackney, C.R., Leyland, J., Kummu, M., Lauri, H., Parsons, D.R., Best, J.L., Nicholas, A.P., Aalto, R., 2016. Fluvial sediment supply to a mega-delta reduced by shifting tropical-cyclone activity. Nature 539, 276–279. doi:10.1038/nature19809.

Day, J.W., Agboola, J., Chen, Z., D'Elia, C., Forbes, D.L., Giosan, L., Kemp, P., Kuenzer, C., Lane, R.R., Ramachandran, R., Syvitski, J., Yañez-Arancibia, A., 2016. Approaches to defining deltaic sustainability in the 21st century. Estuar. Coast. Shelf Sci. 183, 275–291. doi:10.1016/j.ecss.2016.06.018.

DeConto, R.M., Pollard, D., 2016. Contribution of Antarctica to past and future sea-level rise. Nature 531, 591–597. doi:10.1038/nature17145.

Den Haan, E.J., 1994. Vertical compression of soils, PhD. Dissertation, Technical University of Delft.

DGMS, 2004. Research of geological structure and classification of N-Q sediments in Mekong Delta. Nguyen H.D. (Ed.), Division of Geology and Minerals of the South of Viet Nam (DGMS)(Unpublished).

Dijk, V., Hilderink, H., Rooij, W., Rutten, M., Ashton, R., Kartikasari, K., Lan, V.C., 2013. Land-use change, food security and climate change in Vietnam: A global-to-local modelling approach, LEI report 2013-020.

Do, V.L., Nguyen, D.V., Tran, V.T., Tran, V.N., Trinh, M.P., Ma, C.C., 2015. The primary results of monitoring of present aggradation and degradation in Song Cuu Long plain during 2013-2014 stage (in Vietnamese, English summary). Tap Chi Dia Chat - Loat A 7–12, 83–94.

Douglas, B.C., 1991. Global sea level rise. J. Geophys. Res. Ocean. 96, 6981–6992.

Dung, B.V., Stattegger, K., Unverricht, D., Phach, P. Van, Thanh, N.T., 2013. Late Pleistocene–Holocene seismic stratigraphy of the Southeast Vietnam Shelf. Glob. Planet. Change 110, 156–169. doi:10.1016/j.gloplacha.2013.09.010.

Dunn, F.E., 2017. Multidecadal fluvial sediment fluxes to major deltas under environmental change scenarios: projections and their implications. PhD Dissertation. University of Southampton.

DWRPIS, 2010. Report on the results of the National Groundwater Monitoring Network for Nam Bo Plain. Division of Water Resources Planning and Investigation for the South of Vietnam (DWRPIS).

Erban, L.E., Gorelick, S.M., 2016. Closing the irrigation deficit in Cambodia: Implications for transboundary impacts on groundwater and Mekong River flow. J. Hydrol. 535, 85–92. doi:10.1016/j.jhydrol.2016.01.072.

Erban, L.E., Gorelick, S.M., Zebker, H.A., 2014. Groundwater extraction, land subsidence, and sea-level rise in the Mekong Delta, Vietnam. Environ. Res. Lett. 9. doi:10.1088/1748-9326/9/8/084010.

Erban, L.E., Gorelick, S.M., Zebker, H. A, Fendorf, S., 2013. Release of arsenic to deep groundwater in the Mekong Delta, Vietnam, linked to pumping-induced land subsidence. Proc. Natl. Acad. Sci. U. S. A. 110, 13751–6. doi:10.1073/pnas.1300503110.

Ericson, J., Vorosmarty, C., Dingman, S., Ward, L., Maybeck, M., 2006. Effective sea-level rise and deltas: Causes of change and human dimension implications. Glob. Planet. Change 50, 63–82. doi:10.1016/j.gloplacha.2005.07.004.

Erkens, G., Bucx, T., Dam, R., de Lange, G., Lambert, J., 2015. Sinking coastal cities. Proc. Int. Assoc. Hydrol. Sci. 372, 189–198. doi:10.5194/piahs-372-189-2015.

Erkens, G., van der Meulen, M.J., Middelkoop, H., 2016. Double trouble: subsidence and CO2 respiration due to 1,000 years of Dutch coastal peatlands cultivation. Hydrogeol. J. 24, 551–568. doi:10.1007/s10040-016-1380-4.

Farr, T., Rosen, P., Caro, E., Crippen, R., Duren, R., Hensley, S., Kobrick, M., Paller, M., Rodriguez, E., Roth, L., Seal, D., Shaffer, S., Shimada, J., Umland, J., Werner, M., Oskin, M., Burbank, D., Alsdorf, D., 2007. The shuttle radar topography mission. Rev. Geophys. 45, 1–33. doi:10.1029/2005RG000183.1.

Ferretti, A., Prati, C., Rocca, F., 2000. Nonlinear subsidence rate estimation using permanent scatterers in differential SAR interferometry. IEEE Trans. Geosci. Remote Sens. 38, 2202–2212. doi:10.1109/36.868878.

Ferrier, K.L., Mitrovica, J.X., Giosan, L., Clift, P.D., 2015. Sea-level responses to erosion and deposition of sediment in the Indus River basin and the Arabian Sea. Earth Planet. Sci. Lett. 416, 12–20. doi:10.1016/j.epsl.2015.01.026.

Fujihara, Y., Hoshikawa, K., Fujii, H., Kotera, A., Nagano, T., Yokoyama, S., 2016. Analysis and attribution of trends in water levels in the Vietnamese Mekong Delta. Hydrol. Process. 30, 835–845. doi:10.1002/hyp.10642.

Funkenberg, T., Thai Binh, T., Moder, F., Dech, S., 2014. The Ha Tien Plain – wetland monitoring using remote-sensing techniques The Ha Tien Plain – wetland monitoring using remote-sensing techniques. Int. J. Remote Sensing 358, 2893–2909. doi:10.1080/01431161.2014.890306.

Galloway, D.L., Burbey, T.J., 2011. Review: Regional land subsidence accompanying groundwater extraction. Hydrogeol. J. 19, 1459–1486. doi:10.1007/s10040-011-0775-5.

Galloway, D.L., Erkens, G., Kuniansky, E.L., Rowland, J.C., 2016. Preface: Land subsidence processes. Hydrogeol. J. 24, 547–550. doi:10.1007/s10040-016-1386-y.

Gambolati, G., 1973. Equation for one-dimensional vertical flow of groundwater. 1. The rigorous theory. Water Resour. Res. 9, 1022–1028.

Gambolati, G., 1973. Equation for one-dimensional vertical flow of groundwater. 2. Validity range of the diffusion equation. Water Resour. Res. 9, 1385–1395.

Gambolati, G., Teatini, P., 2015. Geomechanics of subsurface water withdrawal and injection. Water Resour. Res. 51, 3922–3955. doi:10.1002/2014WR016841.

Giang, N.V., Hoa, P.V., 2013. Presentation: Mangrove forest monitoring using multi-temporal satellite images Case Study in Ben Tre and Tra Vinh provinces. Second Annu. Coast. Forum Build. Coast. Resil. to Clim. Chang. Coast. Southeast Asia.

Giao, P.H., Thoang, T.T., Thuyen, L.X., Vu, N.H.H., 2014. Geotechnical Characterization of the Subsoil profile Underlying the Land Subsidence Monitoring Points in Southern Vietnam Delta. 9th Int. Symp. Lowl. Technol. 1, 429–436. doi:10.1017/CBO9781107415324.004.

Giosan, L., Syvitski, J.P.M., Constantinescu, S., Day, J., 2014. Protect the world's deltas. Nature 516, 5–7.

Giri, C., Defourny, P., Shrestha, S., 2003. Land cover characterization and mapping of continental Southeast Asia using multi-resolution satellite sensor data. Int. J. Remote Sens. 24, 4181–4196. doi:10.1080/0143116031000139827.

Gislason, P.O., Benediktsson, J.A., Sveinsson, J.R., 2006. Random forests for land cover classification. Pattern Recognit. Lett. 27, 294–300. doi:10.1016/j.patrec.2005.08.011.

GSO [General Statistics Office], 2017. General Statistical Office of Vietnam, http://www.gso.gov.vn/ (accessed 11-11-2016 & 02-05-2017).

Gunduz, Z., Arman, H., 2007. Possible Relationships Between Compression and Recompression Indices of a Low – Plasticity. Arab. J. Sci. Eng. 32, 179–190.

Ha, T.P., Dieperink, C., Dang Tri, V.P., Otter, H.S., Hoekstra, P., 2018. Governance conditions for adaptive freshwater management in the Vietnamese Mekong Delta. J. Hydrol. 557, 116–127. doi:10.1016/j.jhydrol.2017.12.024.

Hak, D., Nadaoka, K., Patrick Bernado, L., Le Phu, V., Hong Quan, N., Quang Toan, T., Hieu Trung, N., Van Ni, D., Pham Dang Tri, V., 2016. Spatio-temporal variations of sea level around the Mekong Delta: their causes and consequences on the coastal environment. Hydrol. Res. Lett. 10, 60–66. doi:10.3178/hrl.10.60.

Hanebuth, T.J.J., Voris, H.K., Yokoyama, Y., Saito, Y., Okuno, J., 2011. Formation and fate of sedimentary depocentres on Southeast Asia's Sunda Shelf over the past sea-level cycle and biogeographic implications. Earth-Sci. Rev. 104, 92–110. doi:10.1016/j.earscirev.2010.09.006.

Hanssen, R.F., 2001. Radar Interferometry, Remote Sensing and Digital Image Processing, vol. 2. Springer Netherlands, Dordrecht. doi:10.1007/0-306-47633-9.

Haskoning, Boehmer, W., Kootstra, J., 1999. Groundwater study Mekong delta. Determination of aquifer charcteristics from aquifer tests and well tests in the Mekong delta. Unpublished report.

HCMC, 2007. Ho Chi Minh city Water Act 2007 (visited on 23-11-2016) [WWW Document]. URL http://thuvienphapluat.vn/van-ban/Tai-nguyen-Moi-truong/Quyet-dinh-69-2007-QD-UBND-Quy-dinh-han-che-cam-khai-thac-nuoc-duoi-dat-thanh-pho-Ho-Chi-Minh-19230.aspx.

Higashi, T., Ohtsubo, M., Hiyama, H., Kanayama, M., Akaboshi, K., 2002. A consideration on the compression index of Ariake clay (in Japanese), in: 83th Congr. Kyushu Branch, Japanese Soc. Irrig. Drain. Reclam. Eng. pp. 215–216.

Higgins, S.A., Overeem, I., Steckler, M.S., Syvitski, J.P.M., Seeber, L., Akhter, S.H., 2014. InSAR Measurements of Compaction and Subsidence in the Ganges-Brahmaputra Delta, Bangladesh. J. Geophys. Res. Earth Surf. 119, 1310–1321. doi:10.1002/2014JF003117.

Higgins, S.A., 2016. Review: Advances in delta-subsidence research using satellite methods. Hydrogeol. J. 587–600. doi:10.1007/s10040-015-1330-6.

Higgins, S., Overeem, I., Tanaka, A., Syvitski, J.P.M., 2013. Land subsidence at aquaculture facilities in the Yellow River delta, China. Geophys. Res. Lett. 40, 3898–3902. doi:10.1002/grl.50758.

Ho, L.P., Nguyen, T., Chau, N.X.Q., Nguyen, K.D., 2014. Integrated urban flood risk management approach in context of uncertainties: case study Ho Chi Minh city. Houille Blanche-Revue Int. L Eau 2007, 26–33. doi:10.1051/1hb/2014059.

Hoang, T.M., van Lap, N., Oanh, T.T.K., Jiro, T., 2016. The influence of delta formation mechanism on geotechnical property sequence of the late Pleistocene–Holocene sediments in the Mekong River Delta. Heliyon 2. doi:10.1016/j.heliyon.2016.e00165.

Holzer, T.L., Johnson, A.I., 1985. Land subsidence caused by ground water withdrawal in urban areas. GeoJournal 11, 245–255. doi:10.1007/BF00186338.

Hooijer, A., Page, S., Jauhiainen, J., Lee, W.A., Lu, X.X., Idris, A., Anshari, G., 2012. Subsidence and carbon loss in drained tropical peatlands. Biogeosciences 9, 1053–1071. doi:10.5194/bg-9-1053-2012.

Hung, N.N., Delgado, J.M., Guntner, A., Merz, B., Bardossy, A., Apel, H., 2014. Sedimentation in the floodplains of the Mekong Delta, Vietnam Part II: Deposition and erosion. Hydrol. Process. 28, 3145–3160. doi:10.1002/hyp.9855.

Hung, N.N., Delgado, J.M., Tri, V.K., Hung, L.M., Merz, B., Bárdossy, A., Apel, H., 2012. Floodplain hydrology of the mekong delta, Vietnam. Hydrol. Process. 26, 674–686. doi:10.1002/hyp.8183.

Hung, W.C., Hwang, C., Liou, J.C., Lin, Y.S., Yang, H.L., 2012. Modeling aquifer-system compaction and predicting land subsidence in central Taiwan. Eng. Geol. 147–148, 78–90. doi:10.1016/j.enggeo.2012.07.018.

Huong, H.T.L., Pathirana, A., 2013. Urbanization and climate change impacts on future urban flooding in Can Tho city, Vietnam. Hydrol. Earth Syst. Sci. 17, 379–394. doi:10.5194/hess-17-379-2013.

Huth, J., Kuenzer, C., Wehrmann, T., Gebhardt, S., Tuan, V.Q., Dech, S., 2012. Land cover and land use classification with TWOPAC: Towards automated processing for pixel- and object-based image classification. Remote Sens. 4, 2530–2553. doi:10.3390/rs4092530.

Hwang, C., Hung, W.C., Liu, C.H., 2008. Results of geodetic and geotechnical monitoring of subsidence for Taiwan High Speed Rail operation. Nat. Hazards 47, 1–16. doi:10.1007/s11069-007-9211-5.

Ingebritsen, S.E., Galloway, D.L., 2014. Coastal subsidence and relative sea level rise. Environ. Res. Lett. 9, 091002. doi:10.1088/1748-9326/9/9/091002.

Irvin, G., 1995. Vietnam: Assessing the achievements of Doi Moi. J. Dev. Stud. doi:10.1080/00220389508422387.

Isotton, G., Ferronato, M., Gambolati, G., Teatini, P., 2015. On the possible contribution of clayey inter-layers to delayed land subsidence above producing aquifers. Proc. Int. Assoc. Hydrol. Sci. 372, 519–523. doi:10.5194/piahs-372-519-2015.

Jackson, L.P., Jevrejeva, S., 2016. A probabilistic approach to 21st century regional sea-level projections using RCP and High-end scenarios. Glob. Planet. Change 146, 179–189. doi:10.1016/j.gloplacha.2016.10.006.

Jankowski, K.L., Törnqvist, T.E., Fernandes, A.M., 2017. Vulnerability of Louisiana's coastal wetlands to present-day rates of relative sea-level rise. Nat. Commun. 8, 14792. doi:10.1038/ncomms14792.

Jarihani, A.A., Callow, J.N., McVicar, T.R., Van Niel, T.G., Larsen, J.R., 2015. Satellite-derived Digital Elevation Model (DEM) selection, preparation and correction for hydrodynamic modelling in large, low-gradient and data-sparse catchments. J. Hydrol. 524, 489–506. doi:10.1016/j.jhydrol.2015.02.049.

Jevrejeva, S., Jackson, L.P., Riva, R.E.M., Grinsted, A., Moore, J.C., 2016. Coastal sea level rise with warming above 2 °C. Proc. Natl. Acad. Sci. 113, 13342–13347. doi:10.1073/pnas.1605312113.

Jouet, G., Hutton, E.W.H., Syvitski, J.P.M., Berné, S., 2008. Response of the Rhône deltaic margin to loading and subsidence during the last climatic cycle. Comput. Geosci. 34, 1338–1357. doi:10.1016/j.cageo.2008.02.003.

Käkönen, M., 2008. Mekong Delta at the Crossroads : More Control or Adaptation? Ambio 37, 205–213.

Karila, K., Nevalainen, O., Krooks, A., Karjalainen, M., Kaasalainen, S., 2014. Monitoring changes in rice cultivated area from SAR and optical satellite images in ben tre and tra vinh provinces in mekong delta, vietnam. Remote Sens. 6, 4090–4108. doi:10.3390/rs6054090.

Karlsrud, K., Vangelsten, B.V., 2017. Subsidence and land loss in the Ca Mau province - Vietnam. Causes, concequences and mitigration options. Geotech. Eng. J. SEAGS AGSSEA 48.

Kondolf, G.M., Schmitt, R.J.P., Carling, P., Darby, S., Arias, M., Bizzi, S., Castelletti, A., Cochrane, T.A., Gibson, S., Kummu, M., Oeurng, C., Rubin, Z., Wild, T., 2018. Science of the Total Environment Changing sediment budget of the Mekong : Cumulative threats and management strategies for a large river basin. Sci. Total Environ. 625, 114–134. doi:10.1016/j.scitotenv.2017.11.361.

Kondolf, G.M., Rubin, Z.K., Minear, J.T., 2014. Dams on the Mekong: Cumulative sediment starvation. Water Resour. Res. 50, 5158–5169. doi:10.1002/2013WR014651.

Kono, Y., 2001. Canal Development and Intesification of Rice Cultivation in the Mekong Delta: A Case Study in the Cantho province, Vietnam. Southeast Asian Stud. 39 70–85.

Koster, K., Stafleu, J., Cohen, K.M., Stouthamer, E., Busschers, F.S., Middelkoop, H., 2018. Three-dimensional distribution of organic matter in coastal-deltaic peat: Implications for subsidence and carbon dioxide emissions by human-induced peat oxidation. Anthropocene 22, 1–9. doi:10.1016/j.ancene.2018.03.001.

Koster, K., 2017. 3D characterization of Holocene peat in the Netherlands: Implications for coastal-deltaic subsidence (Dissertation) Utrecht Studies in Earth Sciences: 140. Utrecht University.

Koster, K., Erkens, G., Zwanenburg, C., 2016. A new soil mechanics approach to quantify and predict land subsidence by peat compression. Geophys. Res. Lett. 43, 10,792-10,799. doi:10.1002/2016GL071116.

Krieger, G., Moreira, A., Fiedler, H., Hajnsek, I., Werner, M., Younis, M., Zink, M., 2007. TanDEM-X: A Satellite Formation for High-Resolution SAR Interferometry. IEEE Trans. Geosci. Remote Sens. 45, 3317–3341. doi:10.1109/TGRS.2007.900693.

Kuenzer, C., Bluemel, A., Gebhardt, S., Quoc, T.V., Dech, S., 2011. Remote sensing of mangrove ecosystems: A review, Remote Sensing. doi:10.3390/rs3050878.

Kuenzer, C., Guo, H., Huth, J., Leinenkugel, P., Li, X., Dech, S., 2013. Flood mapping and flood dynamics of the mekong delta: ENVISAT-ASAR-WSM based time series analyses. Remote Sens. 5, 687–715. doi:10.3390/rs5020687.

Kuenzer, C., Klein, I., Ullmann, T., Georgiou, E.F., Baumhauer, R., Dech, S., 2015. Remote sensing of river delta inundation: Exploiting the potential of coarse spatial resolution, temporally-dense MODIS time series. Remote Sens. 7, 8516–8542. doi:10.3390/rs70708516.

Kuenzer, C., Knauer, K., 2013. Remote sensing of rice crop areas. Int. J. Remote Sens. 34, 2101–2139. doi:10.1080/01431161.2012.738946.

Kummu, M., Varis, O., 2007. Sediment-related impacts due to upstream reservoir trapping, the Lower Mekong River. Geomorphology 85, 275–293. doi:10.1016/j.geomorph.2006.03.024.

Ladd, C.C., 1977. Stress - deformation and strength characteristics: state of the art report. Proc. 9th ICSMFE 4, 421–494.

Li, X., Paul Liu, J., Saito, Y., Nguyen, V.L., 2017. Recent evolution of the Mekong Delta and the impacts of dams. Earth-Science Rev. doi:10.1016/j.earscirev.2017.10.008.

Liaw, A., Wiener, M., 2002. Classification and Regression by randomForest. R news 2, 18–22. doi:10.1177/154405910408300516.

Lillesand, T.M., Kiefer, R.W., Chipman, J.W., 2008. Remote Sensing and Image Interpretation (6th edition). John Wiley & Sons.

Liu, C., He, Y., Des Walling, E., Wang, J., 2013. Changes in the sediment load of the Lancang-Mekong River over the period 1965-2003. Sci. China Technol. Sci. 56, 843–852. doi:10.1007/s11431-013-5162-0.

Liu, C.-W., Zhang, S.-W., Lin, K.-H., Lin, W.-T., 2010. Comparative analysis of temporal changes of multifunctionality benefit of two major rice paddy plains in Taiwan. Paddy Water Environ. 8, 199–205.

Liu, P., DeMaster, D., Nguyen, T., Saito, Y., Nguyen, V.L., Ta, T.K.O., Li, X., 2017. Stratigraphic Formation of the Mekong River Delta and Its Recent Shoreline Changes. Oceanography 30, 72–83. doi:10.5670/oceanog.2017.316.

Lovelock, C.E., Cahoon, D.R., Friess, D.A., Guntenspergen, G.R., Krauss, K.W., Reef, R., Rogers, K., Saunders, M.L., Sidik, F., Swales, A., Saintilan, N., Thuyen, L.X., Triet, T., 2015. The vulnerability of Indo-Pacific mangrove forests to sea-level rise. Nature 526, 559–563. doi:10.1038/nature15538.

Luong, V.V., 2008. Studying the rainfall, temperature and moisture change in Mekong Delta. Scientific research - Ministry of Science and Technology.

Mahmoudpour, M., Khamehchiyan, M., Nikudel, M.R., Ghassemi, M.R., 2016. Numerical simulation and prediction of regional land subsidence caused by groundwater exploitation in the southwest plain of Tehran, Iran. Eng. Geol. 201, 6–28. doi:10.1016/j.enggeo.2015.12.004.

Manh, N. V, Dung, N. V, Hung, N.N., Kummu, M., Merz, B., Apel, H., 2015. Future sediment dynamics in the Mekong Delta : impacts of hydropower development , climate change and sea level rise. Glob. Planet. Change 127, 27. doi:10.1016/j.gloplacha.2015.01.001.

Manh, N. V., Dung, N. V., Hung, N.N., Merz, B., Apel, H., 2014. Large-scale suspended sediment transport and sediment deposition in the Mekong Delta. Hydrol. Earth Syst. Sci. 18, 3033–3053. doi:10.5194/hess-18-3033-2014.

Mbonimpa, M., Aubertin, M., Chapuis, R.P., Bussière, B., 2002. Practical pedotransfer functions for estimating the saturated hydraulic conductivity. Geotech. Geol. Eng. 20, 235–259. doi:10.1023/A:1016046214724.

MDP, 2013. Mekong Delta Plan. Long-term vision and strategy for a safe, prosperous and sustainable delta.

Meckel, T.A., ten Brink, U.S., Williams, S.J., 2006. Current subsidence rates due to compaction of Holocene sediments in southern Louisiana. Geophys. Res. Lett. 33, 1–5. doi:10.1029/2006GL026300.

Meckel, T.A., Ten Brink, U.S., Williams, S.J., 2007. Sediment compaction rates and subsidence in deltaic plains: Numerical constraints and stratigraphic influences. Basin Res. 19, 19–31. doi:10.1111/j.1365-2117.2006.00310.x.

Mesri, G., Godlewski, P.M., 1977. Time-and stress-compressibility interrelationship. J. Geotech. Geoenvironmental Eng. 103.

Michael, H.A., Voss, C.I., 2009. Controls on groundwater flow in the Bengal Basin of India and Bangladesh: Regional modeling analysis. Hydrogeol. J. 17, 1561–1577. doi:10.1007/s10040-008-0429-4.

Milliman, J.D., Farnsworth, K.L., 2011. River Discharge to the Coastal Ocean: A Global Synthesis. Cambride University Press.

Milliman, J.D., Meade, R.H., 1983. World-Wide Delivery of River Sediment to the Oceans. J. Geol. 91, 1–21.

Minderhoud, P.S.J., Coumou, L., Erban, L.E., Middelkoop, H., Stouthamer, E., Addink, E.A., 2018. The relation between land use and subsidence in the Vietnamese Mekong delta. Sci. Total Environ. 634, 715–726. doi:10.1016/j.scitotenv.2018.03.372.

Minderhoud, P.S.J., Erkens, G., Pham Van, H., Bui Tran, V., Erban, L.E., Kooi, H., Stouthamer, E., 2017. Impacts of 25 years of groundwater extraction on subsidence in the Mekong delta, Vietnam. Environ. Res. Lett. 12. doi:10.1088/1748-9326/aa7146 .

Minderhoud, P.S.J., Erkens, G., Pham, V.H., Vuong, B.T., Stouthamer, E., 2015. Assessing the potential of the multi-aquifer subsurface of the Mekong Delta (Vietnam) for land subsidence due to groundwater extraction. Proc. Int. Assoc. Hydrol. Sci. 372, 73–76. doi:10.5194/piahs-372-73-2015.

Minh, D., Van Trung, L., Toan, T., 2015. Mapping Ground Subsidence Phenomena in Ho Chi Minh City through the Radar Interferometry Technique Using ALOS PALSAR Data. Remote Sens. 7, 8543–8562. doi:10.3390/rs70708543

Miyaji, N., Kohyama, K., Otsuka, H., Kasubuchi, T., 1995. Surface subsidence of peatland in Bibai, central Hokkaido [Japan]. Japanese J. Soil Sci. Plant Nutr. 66, 465–473.

Moayed, R.Z., Kordnaeij, A., Mola-Abasi, H., 2016. Compressibility indices of saturated clays by group method of data handling and genetic algorithms. Neural Comput. Appl. doi:10.1007/s00521-016-2390-9.

MRC, 2009. Adaptation to climate change in the countries of the Lower Mekong Basin. MRC Manag. Inf. Bookl. Ser. 1–8.

MRC, 2014. Annual Mekong Flood Report 2013. Theme: Regional Impact of Tropical Storms. Mekong River Comm. 102 pp. doi:10.1017/CBO9781107415324.004.

Mukherjee, S., Joshi, P.K., Mukherjee, S., Ghosh, A., Garg, R.D., Mukhopadhyay, A., 2012. Evaluation of vertical accuracy of open source Digital Elevation Model (DEM). Int. J. Appl. Earth Obs. Geoinf. 21, 205–217. doi:10.1016/j.jag.2012.09.004.

Nguyen, Q.T., 2016. The Main Causes of Land Subsidence in Ho Chi Minh City. Procedia Eng. 142, 333–340. doi:10.1016/j.proeng.2016.02.058.

Nguyen, T.T.H., De Bie, C.A.J.M., Ali, A., Smaling, E.M.A., Chu, T.H., 2012. Mapping the irrigated rice cropping patterns of the Mekong delta, Vietnam, through hyper-temporal SPOT NDVI image analysis. Int. J. Remote Sens. 33, 415–434. doi:10.1080/01431161.2010.532826.

Nguyen, V.L., Ta, T.K.O., Tateishi, M., 2000. Late Holocene depositional environments and coastal evolution of the Mekong River Delta, Southern Vietnam. J. Asian Earth Sci. 18, 427–439. doi:10.1016/S1367-9120(99)00076-0.

Nguyen, V.K., Le, X.T., Dao, H.H., Do Van, L., 2015. Land surface subsidecne in Mekong delta - due to grhe groundwater extraction? (In Vietnamese, English summary). Tap Chi Dia Chat 105–110.

Nguyen, V., Ta, T., Tateishi, M., 2000. Late holocene depositional environments and coastal evolution of the Mekong River Delta, Southern Vietnam. J. Asian Earth Sci. 18, 427–439. doi:10.1016/S1367-9120(99)00076-0.

Nhan, D.K., Be, N.V., Trung, N.H., 2007. Water Use and Competition in the Mekong Delta, Vietnam, in: Be, T,T., Sinh, B.T., Miller, F. (Eds), Challenges to Sustainable Development in the Mekong Delta: Regional and National Policy Issues and Research Needs. p. 208. doi:10.1017/CBO9781107415324.004.

Nicholls, R.J., Cazenave, A., 2010. Sea-Level Rise and Its Impact on Coastal Zones. Science (80-.). 328, 1517–1520. doi:10.1126/science.1185782.

Nicholls, R.J., Leatherman, S.P., 1995. Global sea-level rise. As Clim. Chang. Int. Impacts Implic. Cambridge Univ. Press. Cambridge, United Kingdom 92–123.

NNI, 2012. NEN9997-1+C1: Geotechnical design of structures; Part 1: General rules (in Dutch). Nederlands Normalisatie Instituut (Dutch Normalization Institute).

Norwegian Geotechnical Institute (NGI). Technical report., 2017. Land subsidence in Ca Mau province, Vietnam.

Ogston, A.S., Allison, M.A., Mclachlan, R.L., Nowacki, D.J., Stephens, J.D., 2017. How tidal processes impact the transfer of sediment from source to sink: Mekong River collaborative studies. Oceanography 30, 22–33. doi:10.5670/oceanog.2017.311.

Ohtsubo, M., Higashi, T., Kanayama, M., 2007. Depositional geochemistry and geotechnical properties of marine clays in the Ariake Bay area , Japan, in: Characterisation and Engineering Properties of Natural Soils, Two Volume Set: Proceedings of the Second International Workshop on Characterisation and Engineering Properties of Natural Soils, Singapore, 29 November-1 December. pp. 1893–1937. doi:doi:10.1201/NOE0415426916.ch8\n10.1201/NOE0415426916.ch8.

O'Loughlin, F.E., Paiva, R.C.D., Durand, M., Alsdorf, D.E., Bates, P.D., 2016. A multi-sensor approach towards a global vegetation corrected SRTM DEM product. Remote Sens. Environ. 182, 49–59. doi:10.1016/j.rse.2016.04.018.

Ortiz-Zamora, D., Ortega-Guerrero, A., 2010. Evolution of long-term land subsidence near Mexico City: Review, field investigations, and predictive simulations. Water Resour. Res. 46, 1–15. doi:10.1029/2008WR007398.

Oude Essink, G.H.P., Van Baaren, E.S., De Louw, P.G.B., 2010. Effects of climate change on coastal groundwater systems: A modeling study in the Netherlands. Water Resour. Res. 46, 1–16. doi:10.1029/2009WR008719.

Peltier, W.R., Andrews, J.T., 1976. Glacial- isostatic adjustment—I. The forward problem. Geophys. J. R. Astron. Soc. 46, 605–646.

Phi, H.L., 2008. Impacts of Climate Changes and Urbanisation on Urban Inundation in Ho Chi Minh City. 11th Int. Conf. Urban Drain. 1–7.

Phien-wej, N., Giao, P.H., Nutalaya, P., 2006. Land subsidence in Bangkok, Thailand. Eng. Geol. 82, 187–201. doi:DOI: 10.1016/j.enggeo.2005.10.004.

Phuong, N.M., Catacutan, D., 2014. Land use change analysis in Dien Bien, Son La and Lai Chau provinces, Northwest Vietnam, for the period 2000-2010.

Poland, J.F., Davis, G.H., 1969. Land Subsidence Due to Withdrawal of Fluids*, in: Varnes, D.J., Kiersch, G. (Eds.), Reviews in Engineering Geology. Geological Society of America.

Pope, J.P., Burbey, T.J., 2004. Multiple-Aquifer Characterization from Single Borehole Extensometer Records. Ground Water 42, 45–58. doi:10.1111/j.1745-6584.2004.tb02449.x.

Post, V.E.A., Groen, J., Kooi, H., Person, M., Ge, S., Edmunds, W.M., 2013. Offshore fresh groundwater reserves as a global phenomenon. Nature 504, 71–78. doi:10.1038/nature12858.

Pratt, W.E., Johnson, D.W., 1926. Local subsidence of the Goose Creek oil field. J. Geol. 34, 577–590.

Renaud, F.G., Le, T.T.H., Lindener, C., Guong, V.T., Sebesvari, Z., 2015. Resilience and shifts in agro-ecosystems facing increasing sea-level rise and salinity intrusion in Ben Tre Province, Mekong Delta. Clim. Change 133, 69–84. doi:10.1007/s10584-014-1113-4.

Renaud, F.G., Kuenzer, C., 2012. The Mekong Delta System. Interdisciplinary analyses of a river delta. Springer Environmental Science and Engineering. doi:10.1007/978-94-007-3962-8.

Renaud, F.G., Syvitski, J.P.M., Sebesvari, Z., Werners, S.E., Kremer, H., Kuenzer, C., Ramesh, R., Jeuken, A.D., Friedrich, J., 2013. Tipping from the Holocene to the Anthropocene: How threatened are major world deltas? Curr. Opin. Environ. Sustain. 5, 644–654. doi:10.1016/j.cosust.2013.11.007.

Rodriguez-Galiano, V.F., Ghimire, B., Rogan, J., Chica-Olmo, M., Rigol-Sanchez, J.P., 2012. An assessment of the effectiveness of a random forest classifier for land-cover classification. ISPRS J. Photogramm. Remote Sens. 67, 93–104. doi:10.1016/j.isprsjprs.2011.11.002.

Sakamoto, T., Van Nguyen, N., Ohno, H., Ishitsuka, N., Yokozawa, M., 2006. Spatio-temporal distribution of rice phenology and cropping systems in the Mekong Delta with special reference to the seasonal water flow of the Mekong and Bassac rivers. Remote Sens. Environ. 100, 1–16. doi:10.1016/j.rse.2005.09.007.

Sakamoto, T., Van Phung, C., Kotera, A., Nguyen, K.D., Yokozawa, M., 2009. Analysis of rapid expansion of inland aquaculture and triple rice-cropping areas in a coastal area of the Vietnamese Mekong Delta using MODIS time-series imagery. Landsc. Urban Plan. 92, 34–46. doi:10.1016/j.landurbplan.2009.02.002.

Sato, C., Haga, M., Nishino, J., 2006. Land Subsidence and Groundwater Management in Tokyo. Int. Rev. Environ. Strateg. 6, 403 – 424. doi:10.1016/0022-1694(71)90273-3.

Schmitt, R.J.P., Rubin, Z., Kondolf, G.M., 2017. Losing ground - scenarios of land loss as consequence of shifting sediment budgets in the Mekong Delta. Geomorphology. doi:10.1016/j.geomorph.2017.04.029.

Schothorst, C.J., 1977. Subsidence of low moor peat soils in the western Netherlands. Geoderma 17, 265–291. doi:10.1016/0016-7061(77)90089-1.

Schumann, G., Matgen, P., Cutler, M.E.J., Black, A., Hoffmann, L., Pfister, L., 2008. Comparison of remotely sensed water stages from LiDAR, topographic contours and SRTM. ISPRS J. Photogramm. Remote Sens. 63, 283–296. doi:10.1016/j.isprsjprs.2007.09.004.

Schumann, G.J.-P., Bates, P.D., Neal, J.C., Andreadis, K.M., 2014. Fight floods on a global scale. Nature 507, 169.

Seto, K.C., 2011. Exploring the dynamics of migration to mega-delta cities in Asia and Africa: Contemporary drivers and future scenarios. Glob. Environ. Chang. 21, 94–107. doi:10.1016/j.gloenvcha.2011.08.005.

Smajgl, a., Toan, T.Q., Nhan, D.K., Ward, J., Trung, N.H., Tri, L.Q., Tri, V.P.D., Vu, P.T., 2015. Responding to rising sea levels in the Mekong Delta. Nat. Clim. Chang. 5, 167–174. doi:10.1038/nclimate2469.

Sneed, M., Brandt, J., Solt, M., 2013. Land subsidence along the Delta-Mendota Canal in the northern part of the San Joaquin Valley, California, 2003–10: U.S. Geological Survey Scientific Investigations Report 2013–5142. doi:http://dx.doi.org/10.3133/sir20135142.

Son, N.T., Chen, C.F., Chen, C.R., Duc, H.N., Chang, L.Y., 2014. A phenology-based classification of time-series MODIS data for rice crop monitoring in Mekong Delta, Vietnam. Remote Sens. 6, 135–156. doi:10.3390/rs6010135.

Stafleu, J., Maljers, D., Gunnink, J.L., Menkovic, A., Busschers, F.S., 2011. 3D modelling of the shallow subsurface of Zeeland, the Netherlands. Netherlands J. Geosci. 90, 293–310.

Stanley, D.J., Warne, A.G., 1994. Worldwide initiation of Holocene marine deltas by deceleration of sea-level rise. Science (80-.). 265, 228–231. doi:10.1126/science.265.5169.228.

Su, Y., Guo, Q., 2014. A practical method for SRTM DEM correction over vegetated mountain areas. ISPRS J. Photogramm. Remote Sens. 87, 216–228. doi:10.1016/j.isprsjprs.2013.11.009.

Suklje, L., 1957. The analysis of the consolidation process by the isotaches method. Proc. 4th Int. Conf. soil Mech. Found. Eng. 1, 201–206.

Syvitski, J.P.M., Kettner, A.J., Overeem, I., Hutton, E.W.H., Hannon, M.T., Brakenridge, G.R., Day, J., Vörösmarty, C., Saito, Y., Giosan, L., Nicholls, R.J., 2009. Sinking deltas due to human activities. Nat. Geosci. 2, 681–686. doi:10.1038/ngeo629.

Ta, K.T.O., Nguyen, V.L., Tateishi, M., Kobayashi, I., 2002. Holocene delta evolution and sediment discharge of the Mekong. Quat. Sci. Rev. 21, 1807–1819.

Ta, T.K.O., Nguyen, V.L., Tateishi, M., Kobayashi, I., Saito, Y., Nakamura, T., 2002. Sediment facies and Late Holocene progradation of the Mekong River Delta in Bentre Province, southern Vietnam: an example of evolution from a tide-dominated to a tide- and wave-dominated delta. Sediment. Geol. 152, 313–325. doi:10.1016/S0037-0738(02)00098-2.

Ta, T.K.O., Nguyen, V.L., Tateishi, M., KobayashiI, I., Saito, Y., 2005. Holocene delta evolution and depositional models of the Mekong river delta, Southern Vietnam. SEPM, SEPM Spec. Publ. 453–466.

Takagi, H., Thao, N.D., Anh, L.T., 2016. Sea-level rise and land subsidence: Impacts on flood projections for the Mekong Delta's largest city. Sustain. 8, 1–15. doi:10.3390/su8090959.

Teatini, P., Ferronato, M., Gambolati, G., Gonella, M., 2006. Groundwater pumping and land subsidence in the Emilia-Romagna coastland, Italy: Modeling the past occurrence and the future trend. Water Resour. Res. 42, 1–19. doi:10.1029/2005WR004242.

Teatini, P., Tosi, L., Strozzi, T., 2011. Quantitative evidence that compaction of Holocene sediments drives the present land subsidence of the Po Delta, Italy. J. Geophys. Res. - Solid Earth 116, B08407. doi:10.1029/2010JB008122.

Teatini, P., Tosi, L., Strozzi, T., Carbognin, L., Wegmüller, U., Rizzetto, F., 2005. Mapping regional land displacements in the Venice coastland by an integrated monitoring system. Remote Sens. Environ. 98, 403–413. doi:10.1016/j.rse.2005.08.002.

Tessler, Z.D., Vörösmarty, C.J., Grossberg, M., Gladkova, I., Aizenman, H., Syvitski, J.P.M., Foufoula-Georgiou, E., 2015. Profiling risk and sustainability in coastal deltas of the world. Science (80-.). 349, 638–643. doi:10.1126/science.aab3574.

Tessler, Z.D., Vörösmarty, C.J., Overeem, I., Syvitski, J.P.M., 2017. A model of water and sediment balance as determinants of relative sea level rise in contemporary and future deltas. Geomorphology. doi:https://doi.org/10.1016/j.geomorph.2017.09.040.

Thoang, T.T., Giao, P.H., 2015. Subsurface characterization and prediction of land subsidence for HCM City, Vietnam. Eng. Geol. 199, 107–124. doi:10.1016/j.enggeo.2015.10.009.

Toan, D.M., Nu, N.T., 2013. Studying on the engineering geological characteristics of Middle-Upper Holocene formation (in Vietnamese, English Summary). Tap chi GIA CHAT, loat A so 333, 47–56.

Tong, P.H.S., Auda, Y., Populus, J., Aizpuru, M., Habshi, a Al, Blasco, F., 2004. Assessment from space of mangroves evolution in the Mekong Delta, in relation to extensive shrimp farming. Int. J. Remote Sens. 25, 4795–4812. doi:10.1080/01431160412331270858.

Toothaker, L.E., 1993. Multiple comparison procedures. Quantitative Applications in the Social Sciences, No. 89. Sage Publications, Inc., Newbury Park, Calif.

Törnqvist, T.E., Wallace, D.J., Storms, J.E. a., Wallinga, J., van Dam, R.L., Blaauw, M., Derksen, M.S., Klerks, C.J.W., Meijneken, C., Snijders, E.M. a., 2008. Mississippi Delta subsidence primarily caused by compaction of Holocene strata. Nat. Geosci. 1, 173–176. doi:10.1038/ngeo129.

Tosi, L., Teatini, P., Carbognin, L., Brancolini, G., 2009. Using high resolution data to reveal depth-dependent mechanisms that drive land subsidence: The Venice coast, Italy. Tectonophysics 474, 271–284. doi:10.1016/j.tecto.2009.02.026.

Tosi, L., Da Lio, C., Strozzi, T., Teatini, P., 2016. Combining L- and X-Band SAR interferometry to assess ground displacements in heterogeneous coastal environments: The Po River Delta and Venice Lagoon, Italy. Remote Sens. 8, 1–22. doi:10.3390/rs8040308.

Tran, D.D., Van Halsema, G., Hellegers, P.J.G.J., Phi Hoang, L., Quang Tran, T., Kummu, M., Ludwig, F., 2018. Assessing impacts of dike construction on the flood dynamics of the Mekong Delta. Hydrol. Earth Syst. Sci. 22, 1875–1896. doi:10.5194/hess-22-1875-2018.

Tran, H., Tran, T., Kervyn, M., 2015. Dynamics of land cover/land use changes in the Mekong Delta, 1973-2011: A Remote sensing analysis of the Tran Van Thoi District, Ca Mau Province, Vietnam. Remote Sens. 7, 2899–2925. doi:10.3390/rs70302899.

Triet, N.V.K., Dung, N.V., Fujii, H., Kummu, M., Merz, B., Apel, H., 2017. Has dyke development in the Vietnamese Mekong Delta shifted flood hazard downstream? Hydrol. Earth Syst. Sci. Discuss. 1–27. doi:10.5194/hess-2017-123.

Trimble, 2015. eCognition ® Developer 9.1.3. Reference Book. Trimble Germany GmbH, München, Germany.

Truong, T.D., Do, L.H., 2018. Mangrove forests and aquaculture in the Mekong river delta. Land use policy 73, 20–28. doi:10.1016/j.landusepol.2018.01.029.

USGS, 2016. LandsatLook Viewer. US Geological Survey, landsatlook.usgs.gov/viewer (accessed 14-11-2016).

USGS, 2016. Earth Explorer. US Geological Survey, earthexplorer.usgs.gov (accessed 18-11-2016).

USGS, 2010. LSDS Science Research and Development (LSRD), bulk order. US Geological Survey, espa.cr.usgs.gov (accessed 14-11-2016).

Van Asselen, S., 2010. Peat compaction in deltas - Implications for Holocene delta evolution. PhD dissertation Utrecht University.

Van Asselen, S., Stouthamer, E., van Asch, T.W.J., 2009. Effects of peat compaction on delta evolution: A review on processes, responses, measuring and modeling. Earth-Sci. Rev. 92, 35–51. doi:10.1016/j.earscirev.2008.11.001.

Van der Horst, T., Rutten, M.M., van de Giesen, N.C., Hanssen, R.F., 2018. Monitoring land subsidence in Yangon, Myanmar using Sentinel-1 persistent scatterer interferometry and assessment of driving mechanisms. Remote Sens. Environ. 217, 101–110. doi:https://doi.org/10.1016/j.rse.2018.08.004.

Van Laarhoven, S., 2016. Subsidence potential of the Holocene deposits in the Mekong Delta, Vietnam. Guided research Utrecht University. Supervised by P.S.J. Minderhoud and E. Stouthamer.

Van Staveren, M.F., van Tatenhove, J.P.M., Warner, J.F., 2018. The tenth dragon: controlled seasonal flooding in long-term policy plans for the Vietnamese Mekong delta. J. Environ. Policy Plan. 20, 267–281. doi:10.1080/1523908X.2017.1348287.

Vaze, J., Teng, J., Spencer, G., 2010. Impact of DEM accuracy and resolution on topographic indices. Environ. Model. Softw. 25, 1086–1098. doi:10.1016/j.envsoft.2010.03.014.

Vermeulen, P.T.M., 2006. Model-reduced inverse modeling, PhD. Dissertation, Technical University of Delft.

Vermeulen, P.T.M., Burgering, L.M.T., Roelofsen, F.J., Minnema, B., 2018. iMOD User Manual version 4.2.1. https://oss.deltares.nl/web/imod.

Vermeulen, P., Hong, N., Dinh, N., Nam, G., 2013. Groundwater modeling for the Mekong Delta using iMOD. 20th Int. Congr. Model. anf Simultation 2499–2505.

Vo, Q.T., Oppelt, N., Leinenkugel, P., Kuenzer, C., 2013. Remote sensing in mapping mangrove ecosystems - an object-based approach. Remote Sens. 5, 183–201. doi:10.3390/rs5010183.

Vo, Q.T., Oppelt, N., Leinenkugel, P., Kuenzer, C., 2013. Remote sensing in mapping mangrove ecosystems - an object-based approach. Remote Sens. 5, 183–201. doi:10.3390/rs5010183.

Wagner, F., Tran, V.B., Renaud, F.G., 2012. Chapter 7: Groundwater Resources in the Mekong Delta: Availability, Utilization and Risks. The Mekong Delta System, in: Renaud, F.G., Kuenzer, C. (Eds.), Groundwater Resources in the Mekong Delta: Availability, Utilization and Risks., Springer Environmental Science and Engineering. Springer Netherlands, Dordrecht, pp. 201–220. doi:10.1007/978-94-007-3962-8.

Waltham, T., 2002. Sinking cities. Geol. Today 18, 95–100. doi:10.1046/j.1365-2451.2002.00341.x.

Wang, J.J., Lu, X.X., Kummu, M., 2011. Sediment load estimates and variations in the Lower Mekong River. River Res. Appl. 27, 33–46. doi:10.1002/rra.1337.

Warner, K., Hamza, M., Oliver-Smith, A., Renaud, F., Julca, A., 2010. Climate change, environmental degradation and migration. Nat. Hazards 55, 689–715. doi:10.1007/s11069-009-9419-7.

Warner, K., Ehrhart, C., Sherbinin, A. De, Adamo, S., Chai-Onn, T., 2009. "In Search of Shelter: Mapping the Effects of Climate Change on Human Migration and Displacement" A policy paper prepared for the 2009 Climate Negotiations. Bonn, Germany: United Nations University, CARE, and CIESIN-Columbia University 36.

Wassmann, R., Hien, N.X., Hoanh, C.T., Tuong, T.P., 2004. Sea level rise affecting the Vietnamese Mekong Delta: Water elevation in the flood season and implications for rice production. Clim. Change 66, 89–107. doi:10.1023/B:CLIM.0000043144.69736.b7.

Wen, L.J., 1995. Paddy field, groundwater and land subsidence. American Water Resources Association, Herndon, VA (United States).

Wesselink, A., Warner, J.F., Syed, M.A., Chan, F., Tran, D.D., Huq, H., Fredrik, H., Thuy, N. Le, Pinter, N., van Staveren, M.F., Wester, P., Zegwaard, A., 2016. Trends in flood risk management in deltas around the world: Are we going 'soft'? Int. J. Water Gov. 4, 25–46. doi:10.7564/15-IJWG90.

White, I., 2002. Water management in the Mekong Delta: changes, conflicts and opportunities. Technical report by International Hydrological Programme, UNESCO.

Widodo, S., Ibrahim, A., 2012. Estimation of primary compression index (CC) using physical properties of Pontianak soft clay. Int. J. Eng. Res. 2, 2232–2236.

Wilder, M., Phuong, N.T., 2002. The status of aquaculture in the Mekong Delta region of Vietnam: Sustainable production and combined farming systems (Proceedings of International Commemorative Symposium--70th Anniversary of The Japanese Society of Fisheries Science). Fish. Sci. 68, 847–850.

WISDOM, 2014. WISDOM information system. WISDOM project, web portal designed and maintained by the German Aerospace Center (DLR), wisdom.eoc.dlr.de/Elvis (accessed 19-09-2016).

WLE–Greater Mekong (Water, Land, and E.M., 2016. Dams in the Mekong River Basin: commissioned, Under Construction and Planned Dams in April 2016.

Wolters, M.L., Kuenzer, C., 2015. Vulnerability assessments of coastal river deltas - categorization and review. J. Coast. Conserv. 19, 345–368. doi:10.1007/s11852-015-0396-6.

Woodroffe, C., Saito, Y., Goodbred, S., 2006. Global Change and Integrated Coastal Management. Chapter 10. Springer. doi:10.1007/1-4020-3628-0.

WWF, 2009. The Greater Mekong and Climate Change: Biodiversity, Ecosystem Services and Development at Risk, World Wildlife fund.

Xiao, X., Boles, S., Frolking, S., Li, C., Babu, J.Y., Salas, W., Moore, B., 2006. Mapping paddy rice agriculture in South and Southeast Asia using multi-temporal MODIS images. Remote Sens. Environ. 100, 95–113. doi:10.1016/j.rse.2005.10.004.

Xue, Z., Liu, J.P., Ge, Q., 2011. Changes in hydrology and sediment delivery of the {M}ekong {R}iver in the last 50 years: connection to damming, monsoon, and {ENSO}. Earth Surf. Process. Landforms 36, 296–308. doi:10.1002/esp.2036.

Xue, Z., Liu, J.P., DeMaster, D., Van Nguyen, L., Ta, T.K.O., 2010. Late Holocene Evolution of the Mekong Subaqueous Delta, Southern Vietnam. Mar. Geol. 269, 46–60. doi:10.1016/j.margeo.2009.12.005.

Xue, Z., Liu, J.P., Ge, Q., 2011. Changes in hydrology and sediment delivery of the Mekong River in the last 50 years: Connection to damming, monsoon, and ENSO. Earth Surf. Process. Landforms 36, 296–308. doi:10.1002/esp.2036.

Yamazaki, D., Baugh, C.A., Bates, P.D., Kanae, S., Alsdorf, D.E., Oki, T., 2012. Adjustment of a spaceborne DEM for use in floodplain hydrodynamic modeling. J. Hydrol. 436–437, 81–91. doi:10.1016/j.jhydrol.2012.02.045.

Ye, S., Luo, Y., Wu, J., Yan, X., Wang, H., Jiao, X., Teatini, P., 2016. Three-dimensional numerical modeling of land subsidence in Shanghai, China. Hydrogeol. J. 24, 695–709. doi:10.1007/s10040-016-1382-2.

Yuill, B., Lavoie, D., Reed, D., 2009. Understanding subsidence processes in coastal Louisiana. J. Coast. Res. Sp.Issue, 23–36. doi:10.2112/SI54-012.1.intensity.

Zanello, F., Teatini, P., Putti, M., Gambolati, G., 2011. Long term peatland subsidence: experimental study and modeling scenarios in the Venice coastland. J. Geophys. Res. - Earth Surf. 116, F04002. doi:10.1029/2011JF002010.

Zhou, Y., Li, W., 2011. A review of regional groundwater flow modeling. Geosci. Front. 2, 205–214. doi:10.1016/j.gsf.2011.03.003.

Zhu, L., Gong, H., Li, X., Wang, R., Chen, B., Dai, Z., Teatini, P., 2015. Land subsidence due to groundwater withdrawal in the northern Beijing plain, China. Eng. Geol. 193, 243–255. doi:10.1016/j.enggeo.2015.04.020.

Zoccarato, C., Minderhoud, P.S.J., Teatini, P., 2018. The role of sedimentation and natural compaction in a prograding delta: insights from the mega Mekong delta, Vietnam. Sci. Rep. doi: 10.1038/s41598-018-29734-7.

Zoccarato, C., Teatini, P., 2017. Numerical simulations of Holocene salt-marsh dynamics under the hypothesis of large soil deformations. Adv. Water Resour. 110, 107–119. doi:10.1016/j.advwatres.2017.10.006.

Acknowledgements

When I started four years ago with the journey, that lead to this thesis, it felt like the beginning of a great adventure into the unknown. Looking back now, I can say that the past four years have exceeded my expectations. My journey took me to far-flung countries, let me met wonderful people from all points of the compass and brought exciting discoveries both scientific and personally. Although I found myself traveling the road by myself on many occasions, it never felt lonely as there were always people waiting around the corner. Wherever I was scaling up a mountain or wading waist-deep through a river, both as a figure of speech and literally, I could always count on the support of old friends and new ones. I wish to express my great gratitude to the many people that accompanied me on this journey, some of who traveled with me the entire way and others only for short passages, although not less valuable.

My PhD research within the Rise and Fall project gave me the opportunity to do research in Vietnam to one of the most majestic river deltas on the planet. The project brought challenges beyond the regular ones, one may expect during a PhD. Working and cooperating in an entirely different country, governmental structure and cultural context, called upon a great deal of flexibility, resourcefulness and improvisation, and although at times frustrating, it also gave me unique experiences, great fun and new friendships.

The first person I want to thank is Frans Verspaget, my high-school geography teacher. Thank you for your unorthodox way of teaching and stories on volcanoes and other great natural phenomena of the Earth sparked my interest in our beautiful planet. During my studies at University, two persons in particular were at the foundation of my development towards a scientist. Wim Hoek, during my first excursion in the Belgium Ardennes, I realized I could learn a lot from you by the way you made me look at landscapes and outcrops, the atmosphere you created and the supervisory gaps you filled. You have been a mentor for me ever since. Scientifically, by supervising both my Bachelor and Master theses and didactically, as student-assistant and later on during my time as junior Lecturer, thanks for everything! Chris Roosendaal, you transformed me from teenager with two left hands into a more skillful and practical person during my work at the FG lab. Perhaps even more valuable were the life lessons you taught me through and next to the practical work, shaping me as a person. I will carry them with me the rest of my life. Chris: "*als het niet gaat zoals het moet, dan moet het maar zoals het gaat*", bedankt!

During my PhD I had the luxury of a three-headed supervisory team in The Netherlands who complemented each other and myself. I experienced the right amount of freedom and trust, which is very important to me as person and scientist, and when I needed guidance, I could always count on your advice. Esther Stouthamer, thank you for acting as my daily supervisor and for always making time, even when there was no time. You taught me to write exactly what I wanted to say and I really valued your personal involvement and the fact that I could always walk into your office, for both scientific and personal matters. I really enjoyed our adventures in Vietnam, exploring the delta and Vietnamese food culture, in the south and the north. Hans Middelkoop, as my promotor, thank you for keeping your 'helicopter view' on me in the first part of my PhD and later on allowing yourself to be dragged into the specifics of my research. You helped me putting results in a bigger picture and create cohesion. Furthermore, thank you for supporting me to attend specific conferences and meetings. Gilles Erkens, your experience with subsidence research and pragmatism really helped narrowing down my research to concrete actions and make decisions to move forward. Thanks for introducing and facilitating me at Deltares, Team Bodemdaling and for the beautiful movies we made on the research. I really enjoyed our fieldtrips in Japan and in the Mekong delta to Mui Ca Mau, its most southern point.

Outside my supervisory team, I gratefully learned a lot over the years from many other people. In particular, Gu Oude Essink, thank you for all advices and discussions on groundwater modeling, helping me to grasp this discipline. It was really fun together, however, most memorable were our joint massage adventures in Vietnam including cucumber slices, hot stones and more. Henk Kooi, you introduced me into the wonderful world of calculating subsidence and I learned a lot from you. Thank you for our discussions on modeling subsidence processes, jointly working with SubCreep and for your support when we ran into skeptical reviewers.

My research was part of the Rise and Fall project, which over the years received, perhaps prophetically, alternative spellings such as: *Raise and Fall* and *Rice and Fail*. Piet Hoekstra, as PI with extensive experience on projects in Asia, thank you for your strategic leadership and the pleasant cooperation. Sepehr, eventhough you lack long blond Danish hair, you were all I could have wished for in a brother-of-arms PhD within this project. Thanks for our joint visits to Vietnam, explorations of the Vietnamese food culture, great diners and karaoke sessions, our morning coffees during which we discussed the wickedness of our PhD's: cultural differences, frustrations and strategies to move forward. Hung, next to being my PhD colleague, you were also my facilitator in HCMC at the DWRPIS and arranged many visits for me to numerous institutes and field sites in the Mekong delta. Thank you for your friendly welcomes every time in HCMC and your never ending positive support to my requests to your division and staff. Over the past years I recall many joyful day trips, diners, the visit your wife and you to The Netherlands and rememberable visits to each others families. Mr. Deputy Director, thanks for all those great experiences! Tri, with your extensive experience of international research projects and as postdoctoral researcher in our project you were the gateway into Vietnam. Thank you for receiving me in Can Tho multiple times, introducing me to your family and helping me getting around in the Mekong delta, maneuver the world of DONRE's and general support. Rien Dam, thank you for the introduction to Vietnam at the start of the project. Henriette, Maarten en Carol, thank you for all the constructive project meetings and the fun during our workshops in Vietnam.

During my visits to Vietnam I had the pleasure to receive the hospitality of the Vietnamese people, which are among the most friendly people on Earth. I spend a lot of time at the DWRPIS in HCMC and for most I would like to thank Dr. Bui, my Vietnamese supervisor, for your warm welcomes and the critical eye with which you reviewed my work. I am very grateful for the trust you placed in my integrity and sincerity, allowing me among your midst, inviting me to many special occasion and providing me access to invaluable data without which this research could not have taken place. Furthermore, I really enjoyed working together with various staff members from the DWRPIS, enthusiastic Dr. Nam, the always cheerful Mr. Chung, but also Mr. Sinh, Mr. Tung, Mr. Tuc, Mr. Chuong, other Mr Tung, Mr. Nam, Mr. Bang, Mr Quyen, Mr Thinh, Mr Thanh, Mr. Nha, Mrs Tuoi, many others and all members of the Driver's Club. You have thoroughly tested my appetite for exotic food and strained my liver on numerous occasions and taught me that hard work can well be combined with great fun. Thanks for your support. Mr Tung, thanks for being my guide in exploring the Mekong delta. At Can Tho University, I could always count on the friendly welcomes of Miss Hang, the other members of the project office and eager students who helped us during numerous workshops and meetings. Thank you, Hang, for showing Esther and me your family home and letting us experience some true delta life. I would also like to thank Tom Kompier and Laurent Umans from the Dutch embassy in Vietnam for their research dissemination efforts. Furthermore, thanks to my German colleagues from the BGR for hosting me at your workshops in Vietnam and Hannover. Special thanks to Armin for our cooperation and hanging out in HCMC and Can Tho. Olaf Neussner from GIZ for exchanging thoughts, data and visiting Deltares with the Vietnamese deligation. My fellow UDW-PhD Shahnour, thank you for our wonderful time together in HCMC during our coincidental overlapping fieldworks, sharing the hardships and the great fun we had to chase down those fresh coconuts! Thanks also to the sweet sisters Anh and Minh, who softened my stays in HCMC with their friendship.

I worked with a number of international researchers who provided invaluable input for the work on this thesis. Laura Erban, thanks for sharing your InSAR work on the Mekong delta, which proved to become a cornerstone of the research in this thesis. Also thanks your other contributions to my research and our continues cooperation on third-party research requests. Pietro Teatini and Claudia Zoccarato, thanks for hosting me at Padova. It was very enjoyable and inspiring to see how our research idea fastly took shape and resulted in a joint paper with exciting results. I hope we can continue this in the future. Kjell Karslrud is thanked for sharing geotechnical data of Ca Mau. Furthermore, thanks to Elisabeth Chamberlain for being my darkroom OSL cousin and Anneleen Geurts for being my international conference buddy.

Being based at both Utrecht University and Deltares was sometimes a challenging, especially with my many travels abroad, but also provided a lot of opportunities and doubled the amount of nice colleagues! Some specific thanks I

would like to give to colleagues from Utrecht University: Elisabeth for cooperation and joint student supervision and guiding several very enjoyable honors-excursions together, Tjalling, for, next of being a long time friend, being my roommate, stealing my chocolate and always willing to help, Eveline and Anne, thanks for being such nice roomies and the support with chocolate and writing challenges to finish our PhD's, Kay for our 'creepy' discussions, Harmjan for discussing delta sedimentology, Sanneke for Future Deltas cooperation and talking about subsidence, Maarten for exchanging witful thoughts, Kim, for the ad hoc brainstorm sessions, Kees for talking beach ridges and proof-reading this thesis, Marieke, Rike, Timme, together with Henk, Marcel and Arjen and the rest for transforming the basement of the Zonneveldvleugel to a pleasant place, everyone with whom I had the pleasure to supervise during the student fieldworks in Italy and France, Juul, Inge, Ruth and Briede from the secretariat. And a big thanks to all fellow colleagues and PhD's for the numerous lunch walks, trash talks during coffee breaks and drinks, sharing hardships at Gutenberg coffees and shared conference visits.

From Deltares special thanks to a number of people. Peter, thanks for helping me with your first version of a Mekong delta model and guiding me through the basics and more advanced options of iMOD. Ger, thanks for educating me on geotechnical properties. Harm and Marijn, thanks for having me as part of the GWB. Mariska, as PR-chef subsidence you greatly helped with creating exposure and creating our videos, thanks! Vince, thanks for being my PhD buddy at Deltares with whom I could always share my PhD struggles during numerous coffees meetings over the years. Thanks to Mara Meggiorin (presently at Padova University) for your work on the delta model and Liduin for providing the occasional iMOD support. Furthermore, thanks to all colleagues who offered me support and made my Deltares days pleasant. Special thanks to Young Deltares and everyone with whom I shared fun conversations, parties, multilingual diners and, of course, the annual laser tag events.

I had the pleasure to supervise and work together with a number of great students, who's contributions added to my research progress. Coen, Laura, Pepijn en Simon, thank you for your enthusiasm in the subject and your contributions to this thesis! Special thanks to Laura, your hard and precise work contributed directly to two chapters in this thesis and rightfully won you the Escherprize for best Msc thesis.

The past years wouldn't have been so pleasant as they were if I wouldn't have had such great friends and family, who accepted my absence at many occasions, but always gave me the warmest of welcome when I was arround. The FG boys, finally I can join the brotherhood of Dr. titles and handcorers. Gentlemen of the illuster JCT, '*dat onze storm maar 'lauter' mag blijven waaien*!'. Thanks to: the 'old generation' of TSGP for all the fun and games during reunions; Super Oma for being Super Oma; Maarten for the crazy last-minute activities to places, concerts and hilarious situations I would otherwise never have experienced. And together with Nicander, thanks for the bivouacs and coming all the way to Vietnam to celebrate by birthday in HCMC and experiencing Phu Quoc. Paul and André, thanks for the mental support, musical entertainment and late-night poker. Double Barrel and The Fellowship for the Islay visit. Tom, thanks for always being always ready to hit the road together and having my back when blowing of steam. Florence, special thanks to you for being my female mirror image and being there for me when needed. Nathalie, thanks for our shared guilty pleasure! Vera van R, thanks for relating on our world's travels. And thanks to everyone else I shared enjoyable freetime with during the past years.

Mom and Dad, you stimulated me since I was a child to enjoy the great outdoors and when I started to travel the world and explore it by myself, you always supported me in all my endeavors no matter how far they took me. I am very grateful for your unconditional support and the many *anything, anywhere, anytime*-actions. Thanks to my dear sisters and brother: Jantien, Marjolein and Koen, together with Pieter and Annabelle, for your support and numerous long-distant birthday wishes. My uncles Henk-Jan and Philip for serving as familiar examples of scientists, letting me enjoy the French Alpes, and Janneke for your interest in my research.

Lastly but most importantly, Vera, thank you for the way you shared this journey with me, the way we would give each other freedom to travel and do the work we both love to do, and the warm welcome whenever we were together again. I loved exploring Vietnam and sharing the worklife of a PhD there with you, together with the many other exotic destinations we visited over the years. Thanks for giving me your love and always being there for me.

List of publications

First author publications

Minderhoud, P.S.J., Middelkoop, H., Erkens, G., Stouthamer, E. (submitted). Groundwater extraction may drown mega delta (submitted).

Minderhoud, P.S.J., Coumou, L., Erkens, G., Middelkoop, H., Stouthamer, E. . Mekong delta lower than previously thought. Accurate elevation data crucial to sea-level rise impact assessments in deltas (in review).

Minderhoud, P.S.J., Coumou, L., Erban, L.E., Middelkoop, H., Stouthamer, E., Addink, E.A., 2018. The relation between land use and subsidence in the Vietnamese Mekong delta. Science of the Total Environment 634, 715–726. doi:10.1016/j.scitotenv.2018.03.372

Minderhoud, P.S.J., Erkens, G., Pham Van, H., Bui Tran, V., Erban, L.E., Kooi, H., Stouthamer, E., 2017. Impacts of 25 years of groundwater extraction on subsidence in the Mekong delta, Vietnam. Environmental Research Letters 12. doi:10.1088/1748-9326/aa7146

Minderhoud, P.S.J., Cohen, K.M., Toonen, W.H.J., Erkens, G., Hoek, W.Z., 2016. Improving age-depth models of fluvio-lacustrine deposits using sedimentary proxies for accumulation rates. Quaternary Geochronology doi:10.1016/j.quageo.2016.01.001

Minderhoud, P.S.J., Erkens, G., Pham, V.H., Vuong, B.T., Stouthamer, E., 2015. Assessing the potential of the multi-aquifer subsurface of the Mekong Delta (Vietnam) for land subsidence due to groundwater extraction. Proc. Int. Assoc. Hydrol. Sci. 372, 73–76. doi:10.5194/piahs-372-73-2015

Co-authored publications

Zoccarato, C., Minderhoud, P.S.J., Teatini, P., 2018. The role of sedimentation and natural compaction in a prograding delta: insights from the mega Mekong delta, Vietnam. Scientific Reports. doi:10.1038/s41598-018-29734-7

Nooren, K., Hoek, W., Winkels, T., Huizinga, A., Van Der Plicht, H., Van Dam, R.L., Van Heteren, S., Van Bergen, M.J., Prins, M.A., Reimann, T., Wallinga, J., Cohen, K.M., Minderhoud, P.S.J., Middelkoop, H. (2017). The Usumacinta-Grijalva beach-ridge plain in southern Mexico: A high-resolution archive of river discharge and precipitation. Earth Surface Dynamics 5, 3, p. 529-556.

Cunningham, A.C., Wallinga, J., Minderhoud, P.S.J. (2011). Expectations of scatter in equivalent-dose distributions when using multi-grain aliquots for OSL dating. Geochronometria 38-4, 424-431.

Awards

Winner People's Choice Award 3MT pitch competition. World finals at the 7th International Symposium 2018, Beijing, China. Awarded by the McDonnell International Scholars Academy.

Outstanding Student Poster and PICO Award. EGU General Assembly 2018, Vienna, Austria. Awarded by the European Geosciences Union.

Outstanding Student Paper Award. AGU Fall meeting 2017, New Orleans, United States. Awarded by the American Geophysical Union.

Paper award: 'Highlight of 2017'. Minderhoud et al., 2017. Top 30 articles of 2017. Awarded by Environmental Research Letters journal.

About the author

Philip Minderhoud (23 Oktober 1986) was born in Hengelo and grew up in Waalre, The Netherlands. In July 2005 he obtained his high school diploma at the Augustinianum in Eindhoven. Since his childhood, he had always been fascinated by his natural surroundings and the way Planet Earth worked. This made his choice to start his bachelor in Earth Sciences at Utrecht University, a decision without any doubts. He completed his Bachelor of Science with distinction in 2008 with a focus on Quaternary geology. For a year he traveled the world and applied his newly gained knowledge by working at Utrecht University in research projects and preparing and assisting BSc. fieldwork. Afterwards he continued with a Master in Earth Sciences in Physical Geography in 2009. As he was interested in a wide variety of processes of System Earth, he thrived to combine and integrate knowledge from different disciplines. This lead to his master research for which he traveled to the Usambara Mountains in Tanzania to study soil erosion processes at present and the past to distinguish between human-induced and natural soil erosion. As part of his MSc research, he dated Tanzanian samples using optical luminescence (OSL) dating during an internship at the Netherlands Centre for Luminescence dating (NCL) in Delft.

Following his cum laude Master of Science graduation, Philip became a junior lecturer at Utrecht University. For two-and-a-half years, he was assisting, managing, organizing, lecturing and developing a wide-variety of BSc and MSc courses in various disciplines within Earth Sciences. He supervised individual BSc and MSc students, BSc fieldworks and MSc excursions in the Netherlands and abroad and acted as honors-coordinator for Physical Geography. For his teaching efforts he was awarded Teacher Talent of the Year 2014 by the Faculty of Geosciences.

Philip started as a PhD Candidate in October 2014 within the Dutch-Vietnamese Rise and Fall project, on subsidence of the Mekong delta. This position ticked all his required boxes by providing multi-disciplinary research, international fieldwork and cooperation, the opportunity to pioneer and a strong link to society as it dealt with a real-world problem. In the Netherlands, he worked both at Utrecht University and Deltares, thriving to combine the strength of both institutes. Internationally he cooperated with researchers from many countries: a.o. Vietnam, Germany, Italy, United States, Norway. Philip continued to teach courses, supervising students and guiding international fieldworks and excursions. Also he actively engaged in public outreach which lead to a range of media outings on national and international television and newspapers, especially in Vietnam. In the last year of his PhD, he enjoyed competing in several scientific pitch competitions and won the world finals of the three-minute-thesis (3MT) competition in Bejijng by popular vote.

For the Mekong delta

I met this man
in Utrecht Netherlands
He was a doctor of the body and the soul
He said to me:

"Man, there's a book you have to read.
I feel your pain. It makes me cry
But these tears are yours - not mine.
…
And deep inside you
No surprise - there's a crisis.
You might have been to blame
But you can't go on this way
Must I watch and pray?"

Lyrics from
'Happiness Is The Road'
by Steve Hogarth
Marillion (2003)

Utrecht University
Faculty of Geosciences
Department of Physical Geography

ISSN 2211-4335